Volume 5
Issue 1
March 2016

ISSN 2164-6457 (print)
ISSN 2164-6473 (online)

Journal of Applied Nonlinear Dynamics

L&H

Journal of Applied Nonlinear Dynamics

Continued on back materials

Journal of Applied Nonlinear Dynamics

Volume 5, Issue 1, March 2016

Editors
J. A. Tenreiro Machado
Albert Chao-Jun Luo

L&H Scientific Publishing, LLC, USA

Publication Information

Journal of Applied Nonlinear Dynamics (ISSN 2164-6457 (print), eISSN 2164-6473 (online)) is published quarterly (March, June, September, and December) by L & H Scientific Publishing, LLC, P.O. Box 99, Glen Carbon, IL62034, USA. Subscription prices are available upon request from the publisher or from this journal website. Subscriptions are accepted on a prepaid basis only and entered on a calendar year basis. Issues are sent by standard mail (Surface in North America, air delivery outside North America). Priority rates are available upon request. Claims for missing issues should be made within six months of the date of dispatch.

Changes of Address

Send address changes to L&H Scientific Publishing, LLC, P.O. Box 99, Glen Carbon, IL62034, USA. Changes of address must be received at L&H Scientific Publishing eight weeks before they are effective.

Authors Inquiries

For inquiries relative to the submission including electronic submission where available, please visit journal website or contact journal Editors-in-Chief.

Advertising Information

If you are interested in adverting or other commercial opportunities, please email via lhscientificpublishing@gmail.com and your enquiry will be handled as soon as possible.

Printed in USA on acid-free paper.

Journal of Applied Nonlinear Dynamics

https://lhscientificpublishing.com/Journals/JAND-Default.aspx

Nonlinear Dynamics Analysis of a Continuum Rotor through Generalized Harmonic Balance Method

Haiyang Luo[1,2], Yuefang Wang[1,2†]

[1]Department of Engineering Mechanics, Dalian University of Technology, Dalian 116024, China
[2]State Key Laboratory of Structural Analysis for Industrial Equipment, Dalian 116024, China

Submission Info

Communicated by Albert C.J. Luo
Received 3 January 2015
Accepted 21 May 2015
Available online 1 April 2016

Keywords

Rotor dynamics
General Harmonic Balance
Stability
Bifurcation

Abstract

The dynamics of a continuum rotor system excited by nonlinear oil-film force and electromagnetic force is investigated through the Generalized Harmonic Balance Method. The governing differential equation of the continuum rotor system is reduced through the Galerkin's approximation method. Firstly, the motion in Y-direction is considered as the response of a planar continuum rotor. The analytical periodic motion is obtained and the bifurcation and stability is determined. Secondly, the dynamical model of a spatial continuum rotor is studied. The stability and bifurcation of the analytical periodic motion is obtained and compared to numerical results to show the accuracy of the Generalized Harmonic Balance Method.

1 Introduction

Nonlinear rotor-dynamical analysis has been a great concern of rotating machinery in the past several decades. The major adopted model in the literature is the so-called Jeffcott model which is composed of a massless shaft, a rigid wheel and multiple supportive bearings. For practical machines, however, the mass, stiffness and external loading are continuous functions of longitudinal position of the rotor cross-section. Hence, the dynamics of the rotor system should be described using a continuum model that admits spatial distributions of all forcing and material properties. The general methodology of modeling rotor systems with continuum models was presented in Yamamoto *et al.* [1], Shaw *et al.* [2] and Ishida *et al.* [3]. Luczko *et al.* used the Timoshenko beam model to analyze a continuum rotor considering the Karman non-linearity, non-linear curvature and gyroscopic effect [4]. Chasalevris *et al.* simplified a rotor as an isotropic Rayleigh beam with breathing cracks [5]. Khanlo *et al.* adopted the Euler-Bernoulli beam model to analyze chaotic motion of a flexible rotor with rub impact [6]. More recently, the coupling resonance of bimodal, principal resonance of an in-extensional shaft was studied by Khadem *et al.* [7] and later by Hosseini for its dynamic stability and bifurcation [8].

It is known that the dynamical response of modern rotors is usually nonlinear due to various sources of excitation. In the present research, the nonlinear transverse electromagnetic force and nonlinear oil-

†Corresponding author.
Email address: yfwang@dlut.edu.cn

ISSN 2164 – 6457, eISSN 2164 – 6473/$-see front materials
DOI : 10.5890/JAND.2016.03.001

film force are considered as major excitation to the rotor. Guo *et al.* derived the electromagnetic force in a three-phase generator and analyzed its inducing vibration to the rotor [9]. Wang *et al.* investigated analytical free and forced vibrations of a rotor running in a non-uniform magnetic field and determined the stability of equilibrium position through eigenvalue analysis [10]. Practically, the modeling of oil-film force should be considered since rotors of turbomachinery are generally supported by fluid-lubricated bearings. It is well known that the oil whirl and oil whip are related to self-excited vibration caused by the fluid-solid interaction in bearings [11]. Many models of oil-film force of lubricated bearing were proposed in literature to facilitate dynamical analysis for rotor systems with the action of bearing force [12]. Zhao *et al.* modeled a flexible rotor with squeeze-film-damper bearing and presented its vibration responses through numerical simulation [13]. Pagano *et al.* studied nonlinear vibration of a rigid rotor supported by tilting pad bearing [14]. Using the modified theory of short journal bearing, Adiletta *et al.* analyzed the bifurcation and chaotic motion of a rigid rotor-bearing system [15]. Zheng *et al.* derived a model for unsteady oil-film force of elliptical bearings and solved the nonlinear vibration response of a rotor-bearing system [16]. Chang-Jian *et al.* studied chaos and bifurcation of a flexible rub-impact rotor supported by long oil-film bearings with nonlinear suspension [17].

The nonlinearity in rotordynamics is usually complicated and hence, cannot be solved through linear dynamics. Various approximately analytical methods have been used in previous publications to determine steady state vibration as well as stability and bifurcation properties of rotor systems. Using the generalized polynomial expansion, Hwang *et al.* modeled a large flexible rotor with nonlinear supports and obtained solution through the harmonic balance method (HBM) and trigonometric collocation method [18]. Kim *et al.* developed a modified HBM method to obtain quasi-periodic response and its stability of a Jeffcott rotor with a bearing clearance [19]. Qin *et al.* analyzed a rotor weakened by cracks due to rub impact and showed the transform of periodic motion to chaos through grazing bifurcation [20]. Villa *et al.* used the invariant manifold approach to obtain the nonlinear normal modes of rotor bearing-system [21]. Using the zeros of the Melnikov function, Tong *et al.* investigated active magnetic bearings with the time-varying stiffness and presented global bifurcation, chaos and homoclinic tangency [22]. Ding *et al.* used the nonlinear Galerkin method to perform dimension reduction of a continuum rotor system with oil-lubricated journal bearings and hydrodynamic seal [23]. Luo *et al.* considered a continuum rotor system excited by transverse electromagnetic and oil-film forces [24]. The bifurcation and stability of the equilibrium of the rotor were analyzed with the Routh-Hurwitz criterion. Paez-Chavez *et al.* presented the fold bifurcation caused by grazing and hysteresis loop by cusp singularity of a non-smooth Jeffcott rotor [25]. Huang and Luo developed the analytical solutions for period-m motions of a buckled, nonlinear Jeffcott rotor system using the Generalized Harmonic Balance Method (GHBM) proposed by Luo [26], and presented various results of stability and bifurcation through eigenvalue analysis at fixed points of motion amplitude [27].

Despite the many previous investigations in nonlinear rotor-dynamical analysis, none of them were specifically aimed at oil-film lubricated continuum rotor systems that operate in non-uniform electromagnetic environment. In this paper, the transverse vibration of a continuum rotor system is analyzed through the GHBM. The rotor system is an assembly composed of a flexible shaft and a rigid disk that operates in a non-uniform electromagnetic field with the support of two journal bearings. The structural model of the rotor system is developed based on the theory of Euler-Bernoulli beam. The explicit functions of electromagnetic force and oil-film force are presented with respect to dynamical displacement and velocity of the rotor. The governing equation of system is derived and discretized through the Galerkin's approximation method. Analytical solutions in two cases i.e. the two dimensional planar rotor and the three dimensional spatial rotor are obtained, respectively, using the GHBM. It is pointed out that the Hopf bifurcation of periodic motions leads to new periodic motions via period-doubling, and the stability of the approximate solution of these periodic motions is determined. A numerical simulation is carried out and the result is found in good agreement with the analytical prediction in periodicity and bifurcation of motion.

2 Problem setup

The sketch of a continuum rotor composed of a flexible shaft and a rigid disc supported by two oil-lubricated journal bearings is shown in In Fig. 1 (a). The rotor shaft is excited by a longitudinally distributed electromagnetic force denoted by P_m. X_a and X_b are locations of the bearings whose oil-film forces are denoted by F_a and F_b, respectively. Figure 1 (b) shows the cross section of the shaft, where O is the center of stator, O' the center of shaft and O_c the mass center of shaft. ϕ is the angle between the minimum clearance and Y-axis. e is the dynamic displacement of O' with respect to O.

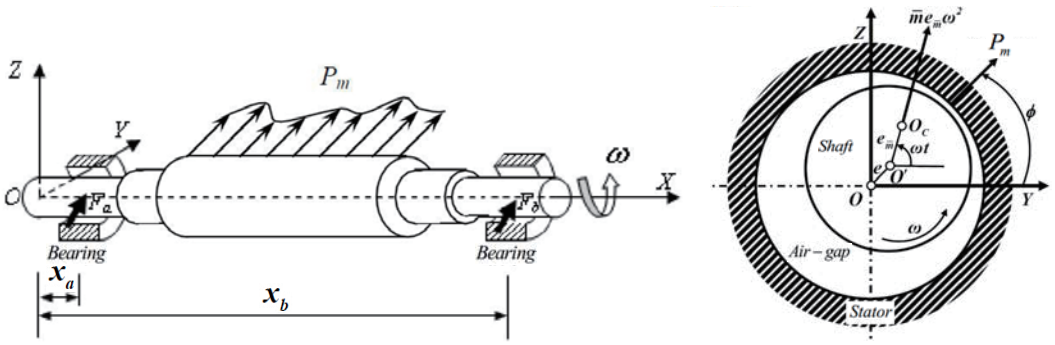

(a) (b)

Fig. 1 (a) The continuum rotor excited by nonlinear electromagnetic force; (b) The cross section of the continuum rotor.

It is assumed that the ratio of length to diameter of the shaft is more than ten so that the rotor can be modeled as a flexible Euler-Bernoulli beam [28]. The governing partial differential equation of motion is developed as follows:

$$\begin{aligned}
&\begin{bmatrix} \bar{m}(X)+\delta(X-X_c)m_c & 0 \\ 0 & \bar{m}(X)+\delta(X-X_c)m_c \end{bmatrix} \begin{Bmatrix} \partial^2 Y/\partial t^2 \\ \partial^2 Z/\partial t^2 \end{Bmatrix} \\
&\quad + \frac{\partial^2}{\partial X^2}\left[E(I(X)+\delta(X-X_c)I(X_c)) \begin{Bmatrix} \partial^2 Y/\partial X^2 \\ \partial^2 Z/\partial X^2 \end{Bmatrix} \right] \\
&= \begin{Bmatrix} \bar{m}(X)g+\delta(X-X_c)m_c g \\ 0 \end{Bmatrix} + (\bar{m}(X)e_{\bar{m}}(X)+\delta(X-X_c)m_c e_{m_c})\omega^2 \begin{Bmatrix} \cos\omega t \\ \sin\omega t \end{Bmatrix} \\
&\quad + P_m(X,t) \begin{Bmatrix} \cos\varphi \\ \sin\varphi \end{Bmatrix} + \delta(X-X_a) \begin{Bmatrix} F_{aY} \\ F_{aZ} \end{Bmatrix} + \delta(X-X_b) \begin{Bmatrix} F_{bY} \\ F_{bZ} \end{Bmatrix},
\end{aligned} \tag{1}$$

where (F_Y, F_Z) are oil-film forces in Y- and Z- directions, respectively. $\bar{m}(X) = \rho_s \pi R(X)^2$ is mass per unit length of the shaft with $\rho_s$being the density. $R(X)$ is radius of the cross-section. $Y(X,t)$ and $Z(X,t)$ represent the transverse displacement functions of X and t, respectively. $EI(X)$ is flexural rigidity and E is Young modulus, $I(X)$ is moment of inertia of cross-section of shaft. $I(X_c)$ is mass moment of inertia of disc. g is the gravitational acceleration. $e_{\bar{m}}(X)$ and e_{m_c} are mass eccentricities of the shaft and the disc, respectively. m_c is the mass of the disc positioned at $x = X_c$. ω is the rotational speed. $\delta(\cdot)$ is the Dirac-delta function.

The analytical expression of electromagnetic force by [10] is adopted in this study, which reads

$$P_m = \frac{\pi \gamma_m R (Y^2+Z^2)^{1/2}}{C_e} \left(1 - \frac{Y^2+Z^2}{C_e^2}\right)^{-3/2},$$

where $\gamma_m = B_m^2/\mu_m$. B_m is magnetic flux density. μ_m is magnetic conductivity. C_e is the mean width

of the shaft clearance in the radial direction. The oil-film forces of the oil-lubricated bearings are from [29]:

$$F_Y = \frac{-\sigma_O}{C}\{(\omega-2\dot{\psi})[d\frac{\pi}{2(1-E_{nd}^2)^{3/2}}Y+\frac{2E_{nd}}{(1-E_{nd}^2)^2}Z]+\frac{\dot{E}_{nd}}{(1-E_{nd}^2)^2}[4Y+\frac{(1+2E_{nd}^2)\pi}{E_{nd}(1-E_{nd}^2)^{1/2}}Z]\},$$
$$F_Z = \frac{\sigma_O}{C}\{(\omega-2\dot{\psi})[\frac{-2E_{nd}}{(1-E_{nd}^2)^2}Y+\frac{\pi}{2(1-E_{nd}^2)^{3/2}}Z]-\frac{\dot{E}}{(1-E_{nd}^2)^2}[\frac{(1+2E_{nd}^2)\pi}{E(1-E_{nd}^2)^{1/2}}Y-4Z]\},$$

where $\sigma_O=\mu_o RL_b^3/2C^2$. μ_o is viscosity of oil. L_b is length of the bearing, and C is the mean width of radial clearance of the bearing. $E_{nd}=\sqrt{Y^2+Z^2}/C$, $\dot{E}_{nd}=(Y\dot{Y}+Z\dot{Z})/C\sqrt{Y^2+Z^2}$, $\dot{\psi}=sgn(Z)(Y\dot{Z}-Z\dot{Y})/(Y^2+Z^2)$.

The equation of motion is expressed in a dimensionless form and is further reduced through the Galerkin's approximation method as follows

$$\begin{aligned}
H_1\ddot{\xi}_1+\kappa H_2\xi_1 =& H_7G+H_7\varepsilon_{\bar{m}}\cos\tau\\
&+\lambda_m\{A_1(H_5\xi_1^3+3H_6\xi_1\xi_2^2)+A_2[H_5\xi_1^2\eta_1+H_6(\xi_2^2\eta_1+2\xi_1\xi_2\eta_2)]\\
&+A_3[H_5\xi_1\eta_1^2+H_6(\xi_1\eta_2^2+2\xi_2\eta_1\eta_2)]+A_4(H_5\eta_1^3+3H_6\eta_1\eta_2^2)\\
&+A_5(H_3\xi_1^2+H_4\xi_2^2)+A_6(H_3\xi_1\eta_1+H_4\xi_2\eta_2)+A_7(H_3\eta_1^2+H_4\eta_2^2)\\
&+A_8H_1\xi_1+A_9H_1\eta_1+A_{10}H_7\}\\
&+\sigma\{C_1(H_{12}\xi_1^3+3H_{13}\xi_1\xi_2^2)+C_2[H_{12}\xi_1^2\eta_1+H_{13}(\xi_2^2\eta_1+2\xi_1\xi_2\eta_2)]\\
&+C_3[H_{12}\xi_1\eta_1^2+H_{13}(\xi_1\eta_2^2+2\xi_2\eta_1\eta_2)]+C_4(H_{12}\eta_1^3+3H_{13}\eta_1\eta_2^2)\\
&+C_5[H_{12}\xi_1^2\dot{\xi}_1+H_{13}(\xi_2^2\dot{\xi}_1+2\xi_1\xi_2\dot{\xi}_2)]+C_6[H_{12}\xi_1^2\dot{\eta}_1+H_{13}(\xi_2^2\dot{\eta}_1+2\xi_1\xi_2\dot{\eta}_2)]\\
&+C_7(H_{10}\xi_1^2+H_{11}\xi_2^2)+C_8[H_{12}\xi_1\eta_1\dot{\xi}_1+H_{13}(\xi_1\eta_2\dot{\xi}_2+\xi_2\eta_2\dot{\xi}_1+\xi_2\eta_1\dot{\xi}_2)]\\
&+C_9[H_{12}\xi_1\eta_1\dot{\eta}_1+H_{13}(\xi_1\eta_2\dot{\eta}_2+\xi_2\eta_2\dot{\eta}_1+\xi_2\eta_1\dot{\eta}_2)]+C_{10}(H_{10}\xi_1\eta_1+H_{11}\xi_2\eta_2)\\
&+C_{11}[H_{12}\eta_1^2\dot{\xi}_1+H_{13}(\eta_2^2\dot{\xi}_1+2\eta_1\eta_2\dot{\xi}_2)]+C_{12}[H_{12}\eta_1^2\dot{\eta}_1+H_{13}(\eta_2^2\dot{\eta}_1+2\eta_1\eta_2\dot{\eta}_2)]\\
&+C_{13}(H_{10}\eta_1^2+H_{11}\eta_2^2)+C_{14}(H_{10}\xi_1\dot{\xi}_1+H_{11}\xi_2\dot{\xi}_2)+C_{15}(H_{10}\xi_1\dot{\eta}_1+H_{11}\xi_2\dot{\eta}_2)\\
&+C_{16}H_9\xi_1+C_{17}(H_{10}\eta_1\dot{\xi}_1+H_{11}\eta_2\dot{\xi}_2)+C_{18}(H_{10}\eta_1\dot{\eta}_1+H_{11}\eta_2\dot{\eta}_2)+C_{19}H_9\eta_1\\
&+C_{20}H_9\dot{\xi}_1+C_{21}H_9\dot{\eta}_1+C_{22}H_8\},
\end{aligned}\tag{2}$$

$$\begin{aligned}
L_1\ddot{\xi}_2+\kappa L_2\xi_2 =&\lambda_m\{A_1(3L_4\xi_1^2\xi_2+L_5\xi_2^3)+A_2[L_4(2\xi_1\xi_2\eta_1+\xi_1^2\eta_2)+L_5\xi_2^2\eta_2]\\
&+A_3[L_4(2\xi_1\eta_1\eta_2+\xi_2\eta_1^2)+L_5\xi_2\eta_2^2]+A_4(3L_4\eta_1^2\eta_2+L_5\eta_2^3)\\
&+2A_5L_3\xi_1\xi_2+A_6L_3(\xi_1\eta_2+\xi_2\eta_1)+2A_7L_3\eta_1\eta_2+A_8L_1\xi_2+A_9L_1\eta_2\}\\
&+\sigma\{C_1(3L_8\xi_1^2\xi_2+L_9\xi_2^3)+C_2[L_8(\xi_1^2\eta_2+2\xi_1\xi_2\eta_1)+L_9\xi_2^2\eta_2]\\
&+C_3[L_8(2\xi_1\eta_1\eta_2+\xi_2\eta_1^2)+L_9\xi_2\eta_2^2]+C_4(3L_8\eta_1^2\eta_2+L_9\eta_2^3)\\
&+C_5[L_8(\xi_1^2\dot{\xi}_2+2\xi_1\xi_2\dot{\xi}_1)+L_9\xi_2^2\dot{\xi}_2]+C_6[L_8(\xi_1^2\dot{\eta}_2+2\xi_1\xi_2\dot{\eta}_1)+L_9\xi_2^2\dot{\eta}_2]]\\
&+2C_7L_7\xi_1\xi_2+C_8[L_8(\xi_1\eta_1\dot{\xi}_2+\xi_1\eta_2\dot{\xi}_1+\xi_2\eta_1\dot{\xi}_1)+L_9\xi_2\eta_2\dot{\xi}_2]\\
&+C_9[L_8(\xi_1\eta_1\dot{\eta}_2+\xi_1\eta_2\dot{\eta}_1+\xi_2\eta_1\dot{\eta}_1)+L_9\xi_2\eta_2\dot{\eta}_2]+C_{10}L_7(\xi_1\eta_2+\xi_2\eta_1)\\
&+C_{11}[L_8(\eta_1^2\dot{\xi}_2+2\eta_1\eta_2\dot{\xi}_1)+L_9\eta_2^2\dot{\xi}_2]+C_{12}[L_8(\eta_1^2\dot{\eta}_2+2\eta_1\eta_2\dot{\eta}_1)+L_9\eta_2^2\dot{\eta}_2]\\
&+2C_{13}L_7\eta_1\eta_2+C_{14}L_7(\xi_1\dot{\xi}_2+\xi_2\dot{\xi}_1)+C_{15}L_7(\xi_1\dot{\eta}_2+\xi_2\dot{\eta}_1)+C_{16}L_6\xi_2\\
&+C_{17}L_7(\eta_1\dot{\xi}_2+\eta_2\dot{\xi}_1)+C_{18}L_7(\eta_1\dot{\eta}_2+\eta_2\dot{\eta}_1)+C_{19}L_6\eta_2+C_{20}L_6\dot{\xi}_2+C_{21}L_6\dot{\eta}_2\},
\end{aligned}\tag{3}$$

$$
\begin{aligned}
H_1\ddot{\eta}_1+\kappa H_2\eta_1 =& H_7\varepsilon_{\bar{m}}\sin\tau\\
&+\lambda_m\{B_1(H_5\xi_1^3+3H_6\xi_1\xi_2^2)+B_2[H_5\xi_1^2\eta_1+H_6(\xi_2^2\eta_1+2\xi_1\xi_2\eta_2)]\\
&+B_3[H_5\xi_1\eta_1^2+H_6(\xi_1\eta_2^2+2\xi_2\eta_1\eta_2)]+B_4(H_5\eta_1^3+3H_6\eta_1\eta_2^2)\\
&+B_5(H_3\xi_1^2+H_4\xi_2^2)+B_6(H_3\xi_1\eta_1+H_4\xi_2\eta_2)+B_7(H_3\eta_1^2+H_4\eta_2^2)\\
&+B_8H_1\xi_1+B_9H_1\eta_1+B_{10}H_7\}\\
&+\sigma\{D_1(H_{12}\xi_1^3+3H_{13}\xi_1\xi_2^2)+D_2[H_{12}\xi_1^2\eta_1+H_{13}(\xi_2^2\eta_1+2\xi_1\xi_2\eta_2)]\\
&+D_3[H_{12}\xi_1\eta_1^2+H_{13}(\xi_1\eta_2^2+2\xi_2\eta_1\eta_2)]+D_4(H_{12}\eta_1^3+3H_{13}\eta_1\eta_2^2)\\
&+D_5[H_{12}\xi_1^2\dot{\xi}_1+H_{13}(\xi_2^2\dot{\xi}_1+2\xi_1\xi_2\dot{\xi}_2)]+D_6[H_{12}\xi_1^2\dot{\eta}_1+H_{13}(\xi_2^2\dot{\eta}_1+2\xi_1\xi_2\dot{\eta}_2)]\\
&+D_7(H_{10}\xi_1^2+H_{11}\xi_2^2)+D_8[H_{12}\xi_1\eta_1\dot{\xi}_1+H_{13}(\xi_1\eta_2\dot{\xi}_2+\xi_2\eta_2\dot{\xi}_1+\xi_2\eta_1\dot{\xi}_2)]\\
&+D_9[H_{12}\xi_1\eta_1\dot{\eta}_1+H_{13}(\xi_1\eta_2\dot{\eta}_2+\xi_2\eta_2\dot{\eta}_1+\xi_2\eta_1\dot{\eta}_2)]+D_{10}(H_{10}\xi_1\eta_1+H_{11}\xi_2\eta_2)\\
&+D_{11}[H_{12}\eta_1^2\dot{\xi}_1+H_{13}(\eta_2^2\dot{\xi}_1+2\eta_1\eta_2\dot{\xi}_2)]+D_{12}[H_{12}\eta_1^2\dot{\eta}_1+H_{13}(\eta_2^2\dot{\eta}_1+2\eta_1\eta_2\dot{\eta}_2)]\\
&+D_{13}(H_{10}\eta_1^2+H_{11}\eta_2^2)+D_{14}(H_{10}\xi_1\dot{\xi}_1+H_{11}\xi_2\dot{\xi}_2)+D_{15}(H_{10}\xi_1\dot{\eta}_1+H_{11}\xi_2\dot{\eta}_2)\\
&+D_{16}H_9\xi_1+D_{17}(H_{10}\eta_1\dot{\xi}_1+H_{11}\eta_2\dot{\xi}_2)+D_{18}(H_{10}\eta_1\dot{\eta}_1+H_{11}\eta_2\dot{\eta}_2)+D_{19}H_9\eta_1\\
&+D_{20}H_9\dot{\xi}_1+D_{21}H_9\dot{\eta}_1+D_{22}H_8\},
\end{aligned}
\tag{4}
$$

$$
\begin{aligned}
L_1\ddot{\eta}_2+\kappa L_2\eta_2 =&\lambda_m\{B_1(3L_4\xi_1^2\xi_2+L_5\xi_2^3)+B_2[L_4(2\xi_1\xi_2\eta_1+\xi_1^2\eta_2)+L_5\xi_2^2\eta_2]\\
&+B_3[L_4(2\xi_1\eta_1\eta_2+\xi_2\eta_1^2)+L_5\xi_2\eta_2^2]+B_4(3L_4\eta_1^2\eta_2+L_5\eta_2^3)+2B_5L_3\xi_1\xi_2\\
&+B_6L_3(\xi_1\eta_2+\xi_2\eta_1)+2B_7L_3\eta_1\eta_2+B_8L_1\xi_2+B_9L_1\eta_2\}\\
&+\sigma\{D_1(3L_8\xi_1^2\xi_2+L_9\xi_2^3)+D_2[L_8(\xi_1^2\eta_2+2\xi_1\xi_2\eta_1)+L_9\xi_2^2\eta_2]\\
&+D_3[L_8(2\xi_1\eta_1\eta_2+\xi_2\eta_1^2)+L_9\xi_2\eta_2^2]+D_4(3L_8\eta_1^2\eta_2+L_9\eta_2^3)\\
&+D_5[L_8(\xi_1^2\dot{\xi}_2+2\xi_1\xi_2\dot{\xi}_1)+L_9\xi_2^2\dot{\xi}_2]+D_6[L_8(\xi_1^2\dot{\eta}_2+2\xi_1\xi_2\dot{\eta}_1)+L_9\xi_2^2\dot{\eta}_2]\\
&+2D_7L_7\xi_1\xi_2+D_8[L_8(\xi_1\eta_1\dot{\xi}_2+\xi_1\eta_2\dot{\xi}_1+\xi_2\eta_1\dot{\xi}_1)+L_9\xi_2\eta_2\dot{\xi}_2]\\
&+D_9[L_8(\xi_1\eta_1\dot{\eta}_2+\xi_1\eta_2\dot{\eta}_1+\xi_2\eta_1\dot{\eta}_1)+L_9\xi_2\eta_2\dot{\eta}_2]+D_{10}L_7(\xi_1\eta_2+\xi_2\eta_1)\\
&+D_{11}[L_8(\eta_1^2\dot{\xi}_2+2\eta_1\eta_2\dot{\xi}_1)+L_9\eta_2^2\dot{\xi}_2]+D_{12}[L_8(\eta_1^2\dot{\eta}_2+2\eta_1\eta_2\dot{\eta}_1)+L_9\eta_2^2\dot{\eta}_2]\\
&+2D_{13}L_7\eta_1\eta_2+D_{14}L_7(\xi_1\dot{\xi}_2+\xi_2\dot{\xi}_1)+D_{15}L_7(\xi_1\dot{\eta}_2+\xi_2\dot{\eta}_1)+D_{16}L_6\xi_2\\
&+D_{17}L_7(\eta_1\dot{\xi}_2+\eta_2\dot{\xi}_1)+D_{18}L_7(\eta_1\dot{\eta}_2+\eta_2\dot{\eta}_1)+D_{19}L_6\eta_2+D_{20}L_6\dot{\xi}_2+D_{21}L_6\dot{\eta}_2\}
\end{aligned}
\tag{5}
$$

where coefficients $H_n(n=1,2,\ldots,8)$, $L_n(n=1,2,\ldots,7)$ are integral constants. A_n and $B_n(n=1,2,\ldots,10)$ are order coefficients in Taylor's series expansion of P_m in Y- and Z-directions, respectively. C_n and $D_n(n=1,2,\ldots,22)$ are coefficients in Taylor's series expansion of F_Y and F_Z, respectively.

3 Dynamical analysis of continuum rotor

3.1 Generalized Harmonic Balance Method

In this section, the Generalized Harmonic Balance Method (GHBM) [26] is used for analytical solution of periodic motions of the continuum rotor. Considering a nonlinear dynamical system is excited by periodic force with forcing period $T=2\pi/\Omega$, the equation of motion is expressed as

$$
\ddot{\mathbf{x}}=\mathbf{F}(\mathbf{x},\dot{\mathbf{x}},t,\mathbf{p})\in\Re^n \tag{6}
$$

where $\mathbf{F}(\mathbf{x},t,\mathbf{p})$ is a C^r-continuous ($r \geq 1$) vector of nonlinear function. The period-m flow of Eq. (6) can be expressed in the form of

$$\mathbf{x}^*(t) = \mathbf{a}_0^{(m)}(t) + \sum_{k=1}^{N} [\mathbf{b}_{k/m}(t)\cos(\frac{k}{m}\Omega t) + \mathbf{c}_{k/m}(t)\sin(\frac{k}{m}\Omega t)] \tag{7}$$

where $k = 1,2,\ldots,N$, the coefficients of harmonics are denoted by

$$\begin{aligned} \mathbf{a}_0^{(m)} &= (a_{01}^{(m)}, a_{02}^{(m)}, \ldots, a_{0n}^{(m)})^T, \\ \mathbf{b}_{k/m} &= (b_{k/m1}, b_{k/m2}, \ldots, b_{k/mn})^T, \\ \mathbf{c}_{k/m} &= (c_{k/m1}, c_{k/m2}, \ldots, c_{k/mn})^T. \end{aligned} \tag{8}$$

which are determined by the following dynamical systems

$$\begin{aligned} \ddot{\mathbf{a}}_0^{(m)} &= \mathbf{F}_0^{(m)}(\mathbf{a}_0^{(m)}, \mathbf{b}^{(m)}, \mathbf{c}^{(m)}, \dot{\mathbf{a}}_0^{(m)}, \dot{\mathbf{b}}^{(m)}, \dot{\mathbf{c}}^{(m)}), \\ \ddot{\mathbf{b}}^{(m)} &= -2\frac{\Omega}{m}\mathbf{k}_1\mathbf{c}^{(m)} + \frac{\Omega^2}{m^2}\mathbf{k}_2\mathbf{b}^{(m)} + \mathbf{F}_1^{(m)}(\mathbf{a}_0^{(m)}, \mathbf{b}^{(m)}, \mathbf{c}^{(m)}, \dot{\mathbf{a}}_0^{(m)}, \dot{\mathbf{b}}^{(m)}, \dot{\mathbf{c}}^{(m)}), \\ \ddot{\mathbf{c}}^{(m)} &= 2\frac{\Omega}{m}\mathbf{k}_1\mathbf{b}^{(m)} + \frac{\Omega^2}{m^2}\mathbf{k}_2\mathbf{c}^{(m)} + \mathbf{F}_2^{(m)}(\mathbf{a}_0^{(m)}, \mathbf{b}^{(m)}, \mathbf{c}^{(m)}, \dot{\mathbf{a}}_0^{(m)}, \dot{\mathbf{b}}^{(m)}, \dot{\mathbf{c}}^{(m)}). \end{aligned} \tag{9}$$

where

$$\begin{aligned} &\mathbf{k}_1 = diag[\mathbf{I}_{n\times n}, 2\mathbf{I}_{n\times n}, \ldots, N\mathbf{I}_{n\times n}], \\ &\mathbf{k}_2 = diag[\mathbf{I}_{n\times n}, 2^2\mathbf{I}_{n\times n}, \ldots, N^2\mathbf{I}_{n\times n}], \\ &\mathbf{b}^{(m)} = (\mathbf{b}_{1/m}, \mathbf{b}_{2/m}, \ldots, \mathbf{b}_{N/m})^T, \mathbf{c}^{(m)} = (\mathbf{c}_{1/m}, \mathbf{c}_{2/m}, \ldots, \mathbf{c}_{N/m})^T, \\ &\mathbf{F}_1^{(m)} = (\mathbf{F}_{11}^{(m)}, \mathbf{F}_{12}^{(m)}, \ldots, \mathbf{F}_{1N}^{(m)})^T, \mathbf{F}_2^{(m)} = (\mathbf{F}_{21}^{(m)}, \mathbf{F}_{22}^{(m)}, \ldots, \mathbf{F}_{2N}^{(m)})^T. \end{aligned} \tag{10}$$

and $N = 1,2,\cdots,\infty$. Further for $k = 1,2,\cdots,N$

$$\begin{aligned} \mathbf{F}_0^{(m)}(\mathbf{a}_0^{(m)}, \mathbf{b}^{(m)}, \mathbf{c}^{(m)}, \dot{\mathbf{a}}_0^{(m)}, \dot{\mathbf{b}}^{(m)}, \dot{\mathbf{c}}^{(m)}) &= \frac{1}{mT}\int_0^{mT} \mathbf{F}(\mathbf{x}, \dot{\mathbf{x}}, t, \mathbf{p})dt, \\ \mathbf{F}_{1k}^{(m)}(\mathbf{a}_0^{(m)}, \mathbf{b}^{(m)}, \mathbf{c}^{(m)}, \dot{\mathbf{a}}_0^{(m)}, \dot{\mathbf{b}}^{(m)}, \dot{\mathbf{c}}^{(m)}) &= \frac{2}{mT}\int_0^{mT} \mathbf{F}(\mathbf{x}, \dot{\mathbf{x}}, t, \mathbf{p})\cos(\frac{k}{m}\Omega t)dt, \\ \mathbf{F}_{2k}^{(m)}(\mathbf{a}_0^{(m)}, \mathbf{b}^{(m)}, \mathbf{c}^{(m)}, \dot{\mathbf{a}}_0^{(m)}, \dot{\mathbf{b}}^{(m)}, \dot{\mathbf{c}}^{(m)}) &= \frac{2}{mT}\int_0^{mT} \mathbf{F}(\mathbf{x}, \dot{\mathbf{x}}, t, \mathbf{p})\sin(\frac{k}{m}\Omega t)dt. \end{aligned} \tag{11}$$

Equation (9) can be rewritten in the state space represented by

$$\dot{\mathbf{z}}^{(m)} = \mathbf{z}_1^{(m)}, \dot{\mathbf{z}}_1^{(m)} = \mathbf{g}(\mathbf{z}^{(m)}, \mathbf{z}_1^{(m)}). \tag{12}$$

where

$$\begin{aligned} \mathbf{z}^{(m)} &= (\mathbf{a}_0^{(m)}, \mathbf{b}^{(m)}, \mathbf{c}^{(m)})^T, \\ \mathbf{g}^{(m)} &= (\mathbf{F}_0^{(m)}, -2\frac{\Omega}{m}\mathbf{k}_1\dot{\mathbf{c}}^{(m)} + \frac{\Omega^2}{m^2}\mathbf{k}_2\mathbf{b}^{(m)} + \mathbf{F}_1^{(m)}, 2\frac{\Omega}{m}\mathbf{k}_1\dot{\mathbf{b}}^{(m)} + \frac{\Omega^2}{m^2}\mathbf{k}_2\mathbf{c}^{(m)} + \mathbf{F}_2^{(m)})^T. \end{aligned} \tag{13}$$

The equivalent form of Eq. (12) can be rewritten as

$$\dot{\mathbf{y}}^{(m)} = \mathbf{f}^{(m)}(\mathbf{y}^{(m)}), \mathbf{y}^{(m)} = (\mathbf{z}^{(m)}, \mathbf{z}_1^{(m)})^T, \mathbf{f}^{(m)} = (\mathbf{z}_1^{(m)}, \mathbf{g}^{(m)})^T. \tag{14}$$

If Eq. (14) has an equilibrium point, then the analytical solution of the period-m motion in Eq. (6) exists. In the vicinity of equilibrium $\mathbf{y}^{(m)*}$, with $\mathbf{y}^{(m)} = \mathbf{y}^{(m)*} + \Delta\mathbf{y}^{(m)}$ the linearized equation of Eq. (14) is

$$\Delta\dot{\mathbf{y}}^{(m)} = D\mathbf{f}^{(m)}(\mathbf{y}^{(m)*})\Delta\mathbf{y}^{(m)} \tag{15}$$

where $D\mathbf{f}^{(m)}(\mathbf{y}^{(m)*})$represents the Jacobian of $\mathbf{f}^{(m)}$at $\mathbf{y}^{(m)}$. The eigenvalues of $D\mathbf{f}^{(m)}(\mathbf{y}^{(m)*})$ are solved through

$$|D\mathbf{f}^{(m)}(\mathbf{y}^{(m)*}) - \lambda\mathbf{I}_{2n(2N+1)\times 2n(2N+1)}| = 0 \tag{16}$$

and are then classified are classified by a set of index

$$(n_1, n_2, n_3 | n_4, n_5, n_6) \tag{17}$$

where n_1 is the total number of negative real eigenvalues; n_2 is the total number of positive real eigenvalues, n_3 is the total number of zero real eigenvalues; n_4 is the total pair number of complex eigenvalues with negative real parts; n_5 is the total pair number of complex eigenvalues with positive real parts; n_6 is the total pair number of complex eigenvalue with zero real parts. The stability of the system can be identified with indices $n_{1\sim 6}$ in Eq. (17). Further, the critical values of rotational speed for the Hopf bifurcation and period doubling bifurcation can be pinpointed based on the eigenvalue evaluation through Eq. (16).

3.2 Analytical solution of planar rotor

Equations of (2) through (5) can be rewritten as

$$\begin{aligned}
\ddot{x}_1 =& p_{\bar{m}}\varepsilon_{\bar{m}}\cos\Omega\tau + f_y + \alpha_1 x_1 + \alpha_2 x_2 + \alpha_3\dot{x}_1 + \alpha_4\dot{x}_2 + \alpha_5 x_1^2 + \alpha_6 x_1 x_2 + \alpha_7 x_1\dot{x}_1 + \alpha_8 x_1\dot{x}_2 \\
&+ \alpha_9 x_2^2 + \alpha_{10} x_2\dot{x}_1 + \alpha_{11} x_2\dot{x}_2 + \alpha_{12} x_1^3 + \alpha_{13} x_1^2 x_2 + \alpha_{14} x_1 x_2^2 + \alpha_{15} x_1^2\dot{x}_1 + \alpha_{16} x_1^2\dot{x}_2 + \alpha_{17} x_1 x_2\dot{x}_1 \\
&+ \alpha_{18} x_1 x_2\dot{x}_2 + \alpha_{19} x_2^3 + \alpha_{20} x_2^2\dot{x}_1 + \alpha_{21} x_2^2\dot{x}_2, \\
\ddot{x}_2 =& p_{\bar{m}}\varepsilon_{\bar{m}}\sin\Omega\tau + f_z + \beta_1 x_1 + \beta_2 x_2 + \beta_3\dot{x}_1 + \beta_4\dot{x}_2 + \beta_5 x_1^2 + \beta_6 x_1 x_2 + \beta_7 x_1\dot{x}_1 + \beta_8 x_1\dot{x}_2 \\
&+ \beta_9 x_2^2 + \beta_{10} x_2\dot{x}_1 + \beta_{11} x_2\dot{x}_2 + \beta_{12} x_1^3 + \beta_{13} x_1^2 x_2 + \beta_{14} x_1 x_2^2 + \beta_{15} x_1^2\dot{x}_1 + \beta_{16} x_1^2\dot{x}_2 + \beta_{17} x_1 x_2\dot{x}_1 \\
&+ \beta_{18} x_1 x_2\dot{x}_2 + \beta_{19} x_2^3 + \beta_{20} x_2^2\dot{x}_1 + \beta_{21} x_2^2\dot{x}_2.
\end{aligned} \tag{18}$$

where $\Omega = \omega/\omega_{nf}$,$\omega_{nf}$being the lowest natural frequency of the shaft. $p_{\bar{m}}$, f_y, f_z, $\alpha_{1\sim 21}$ and $\beta_{1\sim 21}$ are presented in Appendix A.

Let us first consider the case that the rotor is restricted in a planar movement. Equation (18) can be reduced to the governing equation of a y-directional motion x_1

$$\ddot{x}_1 = \alpha_1 x_1 + \alpha_3\dot{x}_1 + \alpha_5 x_1^2 + \alpha_7 x_1\dot{x}_1 + \alpha_{12} x_1^3 + \alpha_{15} x_1^2\dot{x}_1 + p_{\bar{m}}\varepsilon_{\bar{m}}\cos\Omega\tau + f_y \tag{19}$$

The standard form of Eq. (19) can be rewritten as

$$\ddot{x}_1 = f(x_1, \dot{x}_1, \tau) \tag{20}$$

where

$$f(x_1, \dot{x}_1, \tau) = \alpha_1 x_1 + \alpha_3\dot{x}_1 + \alpha_5 x_1^2 + \alpha_7 x_1\dot{x}_1 + \alpha_{12} x_1^3 + \alpha_{15} x_1^2\dot{x}_1 + p_{\bar{m}}\varepsilon_{\bar{m}}\cos\Omega\tau + f_y \tag{21}$$

The analytical solutions of arbitrary period-m motion of the continuum rotor system are expressed as

$$x_1(\tau) = a_0^{(m)}(\tau) + \sum_{k=1}^{N}\left[b_{k/m}(\tau)\cos\left(\frac{k}{m}\Omega\tau\right) + c_{k/m}(\tau)\sin\left(\frac{k}{m}\Omega\tau\right)\right] \tag{22}$$

Substituting $x_1(\tau)$ and its derivatives into Eq. (19), then averaging the coefficients gives

$$\begin{aligned}
&\ddot{a}_0^{(m)} = F_0^{(m)}(a_0^{(m)}, \mathbf{b}^{(m)}, \mathbf{c}^{(m)}, \dot{a}_0^{(m)}, \dot{\mathbf{b}}^{(m)}, \dot{\mathbf{c}}^{(m)}),\\
&\ddot{b}_{k/m} + 2\frac{k\Omega}{m}\dot{c}_{k/m} - (\frac{k\Omega}{m})^2 b_{k/m} = F_{1k}^{(m)}(a_0^{(m)}, \mathbf{b}^{(m)}, \mathbf{c}^{(m)}, \dot{a}_0^{(m)}, \dot{\mathbf{b}}^{(m)}, \dot{\mathbf{c}}^{(m)}),\\
&\ddot{c}_{k/m} - 2\frac{k\Omega}{m}\dot{b}_{k/m} - (\frac{k\Omega}{m})^2 c_{k/m} = F_{2k}^{(m)}(a_0^{(m)}, \mathbf{b}^{(m)}, \mathbf{c}^{(m)}, \dot{a}_0^{(m)}, \dot{\mathbf{b}}^{(m)}, \dot{\mathbf{c}}^{(m)}).
\end{aligned} \tag{23}$$

for $k = 1, 2, \ldots, N$, and

$$\begin{aligned}
F_0^{(m)}(a_0^{(m)}, \mathbf{b}^{(m)}, \mathbf{c}^{(m)}, \dot{a}_0^{(m)}, \dot{\mathbf{b}}^{(m)}, \dot{\mathbf{c}}^{(m)}) &= \alpha_1 a_0^{(m)} + \alpha_3 \dot{a}_0^{(m)} + \alpha_5 f_1^{(0)} + \alpha_7 f_2^{(0)} + \alpha_{12} f_3^{(0)} + \alpha_{15} f_4^{(0)} + f_y,\\
F_{1k}^{(m)}(a_0^{(m)}, \mathbf{b}^{(m)}, \mathbf{c}^{(m)}, \dot{a}_0^{(m)}, \dot{\mathbf{b}}^{(m)}, \dot{\mathbf{c}}^{(m)}) &= \alpha_1 b_{k/m} + \alpha_3(\dot{b}_{k/m} + \frac{k\Omega}{m} c_{k/m}) + \alpha_5 f_{1k}^{(c)}\\
&\quad + \alpha_7 f_{2k}^{(c)} + \alpha_{12} f_{3k}^{(c)} + \alpha_{15} f_{4k}^{(c)} + p_{\bar{m}} \varepsilon_{\bar{m}} \delta_k^m,\\
F_{2k}^{(m)}(a_0^{(m)}, \mathbf{b}^{(m)}, \mathbf{c}^{(m)}, \dot{a}_0^{(m)}, \dot{\mathbf{b}}^{(m)}, \dot{\mathbf{c}}^{(m)}) &= \alpha_1 c_{k/m} + \alpha_3(\dot{c}_{k/m} - \frac{k\Omega}{m} b_{k/m}) + \alpha_5 f_{1k}^{(s)}\\
&\quad + \alpha_7 f_{2k}^{(s)} + \alpha_{12} f_{3k}^{(s)} + \alpha_{15} f_{4k}^{(s)}.
\end{aligned} \tag{24}$$

where

$$f_1^{(0)} = (a_0^{(m)})^2 + \frac{1}{2}\sum_{l=1}^{N}\sum_{j=1}^{N}\sum_{i=1}^{N}[\frac{1}{N} b_{l/m} b_{j/m} \delta_{l-j}^0 + \frac{1}{N} c_{l/m} c_{j/m} \delta_{l-j}^0], \tag{25}$$

$$f_2^{(0)} = a_0^{(m)} \dot{a}_0^{(m)} + \frac{1}{2}\sum_{l=1}^{N}\sum_{j=1}^{N}\sum_{i=1}^{N}[\frac{1}{N} b_{l/m}(\dot{b}_{j/m} + \frac{j\Omega}{m} c_{j/m}) \delta_{l-j}^0 + \frac{1}{N} c_{l/m}(\dot{c}_{j/m} - \frac{j\Omega}{m} b_{j/m}) \delta_{l-j}^0], \tag{26}$$

$$\begin{aligned}
f_3^{(0)} =& (a_0^{(m)})^3 + \sum_{l=1}^{N}\sum_{j=1}^{N}\sum_{i=1}^{N}[\frac{3a_0^{(m)}}{2N} b_{l/m} b_{j/m} \delta_{l-j}^0 + \frac{3a_0^{(m)}}{2N} c_{l/m} c_{j/m} \delta_{l-j}^0\\
&+ \frac{1}{4} b_{l/m} b_{j/m} b_{i/m}(\delta_{i-j-l}^0 + \delta_{i-j+l}^0 + \delta_{i+j-l}^0) + \frac{3}{4} c_{l/m} c_{j/m} b_{i/m}(\delta_{i+j-l}^0 + \delta_{i-j+l}^0 - \delta_{i-j-l}^0)],
\end{aligned} \tag{27}$$

$$\begin{aligned}
f_4^{(0)} =& (a_0^{(m)})^2 \dot{a}_0^{(m)} + \sum_{l=1}^{N}\sum_{j=1}^{N}\sum_{i=1}^{N}[\frac{a_0^{(m)}}{N} b_{l/m}(\dot{b}_{j/m} + \frac{j\Omega}{m} c_{j/m}) \delta_{l-j}^0 + \frac{a_0^{(m)}}{N} c_{l/m}(\dot{c}_{j/m} - \frac{j\Omega}{m} b_{j/m}) \delta_{l-j}^0\\
&+ \frac{\dot{a}_0^{(m)}}{2N}(b_{l/m} b_{j/m} + c_{l/m} c_{j/m}) \delta_{l-j}^0 + \frac{1}{4} b_{l/m} b_{j/m}(\dot{b}_{i/m} + \frac{i\Omega}{m} c_{i/m})(\delta_{i-j-l}^0 + \delta_{i-j+l}^0 + \delta_{i+j-l}^0)\\
&+ \frac{1}{4} c_{l/m} c_{j/m}(\dot{b}_{i/m} + \frac{i\Omega}{m} c_{i/m})(\delta_{i+j-l}^0 + \delta_{i-j+l}^0 - \delta_{i-j-l}^0)\\
&+ \frac{1}{2} b_{l/m} c_{j/m}(\dot{c}_{i/m} - \frac{i\Omega}{m} b_{i/m})(-\delta_{i+j-l}^0 + \delta_{i-j+l}^0 + \delta_{i-j-l}^0)],
\end{aligned} \tag{28}$$

$$f_{1k}^{(c)} = \sum_{l=1}^{N}\sum_{j=1}^{N}\sum_{i=1}^{N}[\frac{2a_0^{(m)}}{N^2} b_{l/m} \delta_l^k + \frac{1}{2N} b_{l/m} b_{j/m}(\delta_{|l-j|}^k + \delta_{l+j}^k) + \frac{1}{2N} c_{l/m} c_{j/m}(\delta_{|l-j|}^k - \delta_{l+j}^k)], \tag{29}$$

$$\begin{aligned}
f_{2k}^{(c)} =& \sum_{l=1}^{N}\sum_{j=1}^{N}\sum_{i=1}^{N}[\frac{a_0^{(m)}}{N^2}(\dot{b}_{l/m} + \frac{l\Omega}{m} c_{l/m}) \delta_l^k + \frac{\dot{a}_0^{(m)}}{N^2} b_{l/m} \delta_l^k\\
&+ \frac{1}{2N} b_{l/m}(\dot{b}_{j/m} + \frac{j\Omega}{m} c_{j/m})(\delta_{|l-j|}^k + \delta_{l+j}^k) + \frac{1}{2N} c_{l/m}(\dot{c}_{j/m} - \frac{j\Omega}{m} b_{j/m})(\delta_{|l-j|}^k - \delta_{l+j}^k)],
\end{aligned} \tag{30}$$

$$
\begin{aligned}
f_{3k}^{(c)} =& \sum_{l=1}^{N}\sum_{j=1}^{N}\sum_{i=1}^{N}[3(\frac{a_0^{(m)}}{N})^2 b_{l/m}\delta_l^k + \frac{3a_0^{(m)}}{2N}b_{l/m}b_{j/m}(\delta_{|l-j|}^k + \delta_{l+j}^k) + \frac{3a_0^{(m)}}{2N}c_{l/m}c_{j/m}(\delta_{|l-j|}^k - \delta_{l+j}^k) \\
&+ \frac{1}{4}b_{l/m}b_{j/m}b_{i/m}(\delta_{|l-j-i|}^k + \delta_{l+j+i}^k + \delta_{|l-j+i|}^k + \delta_{|l+j-i|}^k) \\
&+ \frac{3}{4}b_{l/m}c_{j/m}c_{i/m}(-\delta_{|l-j-i|}^k - \delta_{l+j+i}^k + \delta_{|l-j+i|}^k + \delta_{|l+j-i|}^k)],
\end{aligned} \tag{31}
$$

$$
\begin{aligned}
f_{4k}^{(c)} =& \sum_{l=1}^{N}\sum_{j=1}^{N}\sum_{i=1}^{N}[(\frac{a_0^{(m)}}{N})^2(\dot{b}_{l/m} + \frac{l\Omega}{m}c_{l/m})\delta_l^k + \frac{2a_0^{(m)}\dot{a}_0^{(m)}}{N^2}b_{l/m}\delta_l^k \\
&+ \frac{a_0^{(m)}}{N}b_{l/m}(\dot{b}_{j/m} + \frac{j\Omega}{m}c_{j/m})(\delta_{|l-j|}^k + \delta_{l+j}^k) + \frac{a_0^{(m)}}{N}c_{l/m}(\dot{c}_{j/m} - \frac{j\Omega}{m}b_{j/m})(\delta_{|l-j|}^k - \delta_{l+j}^k) \\
&+ \frac{\dot{a}_0^{(m)}}{2N}b_{l/m}b_{j/m}(\delta_{|l-j|}^k + \delta_{l+j}^k) + \frac{\dot{a}_0^{(m)}}{2N}c_{l/m}c_{j/m}(\delta_{|l-j|}^k - \delta_{l+j}^k) \\
&+ \frac{1}{4}b_{l/m}b_{j/m}(\dot{b}_{i/m} + \frac{i\Omega}{m}c_{i/m})(\delta_{|l-j+i|}^k + \delta_{l+j+i}^k + \delta_{|l+j-i|}^k + \delta_{|-l+j+i|}^k) \\
&+ \frac{1}{4}c_{l/m}c_{j/m}(\dot{b}_{i/m} + \frac{i\Omega}{m}c_{i/m})(\delta_{|l-j+i|}^k - \delta_{l+j+i}^k - \delta_{|l+j-i|}^k + \delta_{|-l+j+i|}^k) \\
&+ \frac{1}{2}b_{l/m}c_{j/m}(\dot{c}_{i/m} - \frac{i\Omega}{m}b_{i/m})(\delta_{|l-j+i|}^k - \delta_{l+j+i}^k + \delta_{|l+j-i|}^k - \delta_{|-l+j+i|}^k)],
\end{aligned} \tag{32}
$$

$$
f_{1k}^{(s)} = \sum_{l=1}^{N}\sum_{j=1}^{N}\sum_{i=1}^{N}[\frac{2a_0^{(m)}}{N^2}c_{l/m}\delta_l^k + \frac{1}{N}b_{l/m}c_{j/m}[\delta_{l+j}^k - sgn(l-j)\delta_{|l-j|}^k]], \tag{33}
$$

$$
\begin{aligned}
f_{2k}^{(s)} =& \sum_{l=1}^{N}\sum_{j=1}^{N}\sum_{i=1}^{N}[\frac{a_0^{(m)}}{N^2}(\dot{c}_{l/m} - \frac{l\Omega}{m}b_{l/m})\delta_l^k + \frac{\dot{a}_0^{(m)}}{N^2}c_{l/m}\delta_l^k \\
&+ \frac{1}{2N}b_{l/m}(\dot{c}_{j/m} - \frac{j\Omega}{m}b_{j/m})[\delta_{l+j}^k - sgn(l-j)\delta_{|l-j|}^k] \\
&+ \frac{1}{2N}c_{l/m}(\dot{b}_{j/m} + \frac{j\Omega}{m}c_{j/m})[\delta_{l+j}^k + sgn(l-j)\delta_{|l-j|}^k]],
\end{aligned} \tag{34}
$$

$$
\begin{aligned}
f_{3k}^{(s)} =& \sum_{l=1}^{N}\sum_{j=1}^{N}\sum_{i=1}^{N}[3(\frac{a_0^{(m)}}{N})^2 c_{l/m}\delta_l^k + \frac{3a_0^{(m)}}{N}b_{l/m}c_{j/m}[\delta_{l+j}^k - sgn(l-j)\delta_{|l-j|}^k] \\
&+ \frac{1}{4}c_{l/m}c_{j/m}c_{i/m}[sgn(l-j+i)\delta_{|l-j+i|}^k - \delta_{l+j+i}^k + sgn(l+j-i)\delta_{|l+j-i|}^k - sgn(l-j-i)\delta_{|l-j-i|}^k] \\
&+ \frac{3}{4}b_{l/m}b_{j/m}c_{i/m}[sgn(l-j+i)\delta_{|l-j+i|}^k + \delta_{l+j+i}^k - sgn(l+j-i)\delta_{|l+j-i|}^k - sgn(l-j-i)\delta_{|l-j-i|}^k]],
\end{aligned} \tag{35}
$$

$$
\begin{aligned}
f_{4k}^{(s)} =& \sum_{l=1}^{N}\sum_{j=1}^{N}\sum_{i=1}^{N}[(\frac{a_0^{(m)}}{N})^2(\dot{c}_{l/m} - \frac{l\Omega}{m}b_{l/m})\delta_l^k + \frac{2a_0^{(m)}\dot{a}_0^{(m)}}{N^2}c_{l/m}\delta_l^k \\
&+ \frac{a_0^{(m)}}{N}b_{l/m}(\dot{c}_{j/m} - \frac{j\Omega}{m}b_{j/m})[\delta_{l+j}^k - sgn(l-j)\delta_{|l-j|}^k] \\
&+ \frac{a_0^{(m)}}{N}c_{l/m}(\dot{b}_{j/m} + \frac{j\Omega}{m}c_{j/m})[\delta_{l+j}^k + sgn(l-j)\delta_{|l-j|}^k] \\
&+ \frac{\dot{a}_0^{(m)}}{2N}b_{l/m}c_{j/m}[\delta_{l+j}^k - sgn(l-j)\delta_{|l-j|}^k] + \frac{\dot{a}_0^{(m)}}{2N}c_{l/m}b_{j/m}[\delta_{l+j}^k + sgn(l-j)\delta_{|l-j|}^k]
\end{aligned} \tag{36}
$$

$$
\begin{aligned}
&+\frac{1}{2}c_{l/m}b_{j/m}(\dot{b}_{i/m}+\frac{i\Omega}{m}c_{i/m})\\
&[sgn(l-j+i)\delta^k_{|l-j+i|}+\delta^k_{l+j+i}+sgn(l+j-i)\delta^k_{|l+j-i|}-sgn(-l+j+i)\delta^k_{|-l+j+i|}]\\
&+\frac{1}{4}b_{l/m}b_{j/m}(\dot{c}_{i/m}-\frac{i\Omega}{m}b_{i/m})\\
&[sgn(l-j+i)\delta^k_{|l-j+i|}+\delta^k_{l+j+i}-sgn(l+j-i)\delta^k_{|l+j-i|}+sgn(-l+j+i)\delta^k_{|-l+j+i|}]\\
&+\frac{1}{4}c_{l/m}c_{j/m}(\dot{c}_{i/m}-\frac{i\Omega}{m}b_{i/m})\\
&[sgn(l-j+i)\delta^k_{|l-j+i|}-\delta^k_{l+j+i}+sgn(l+j-i)\delta^k_{|l+j-i|}+sgn(-l+j+i)\delta^k_{|-l+j+i|}].
\end{aligned}
$$

Define

$$
\begin{aligned}
\mathbf{z}^{(m)} &= (a_0^{(m)},\mathbf{b}^{(m)},\mathbf{c}^{(m)})^T = (a_0^{(m)},b_{1/m}\cdots,b_{N/m},c_{1/m},\cdots,c_{N/m})^T\\
&= (z_1^{(m)},z_2^{(m)},\cdots,z_{2N}^{(m)},z_{2N+1}^{(m)})^T,\\
\mathbf{z}_1^{(m)} &= \dot{\mathbf{z}}^{(m)} = (\dot{a}_0^{(m)},\dot{\mathbf{b}}^{(m)},\dot{c}^{(m)})^T = (\dot{a}_{1,0}^{(m)},\dot{b}_{1/m},\cdots,\dot{b}_{N/m},\dot{c}_{1/m},\cdots,\dot{c}_{N/m})^T\\
&= (\dot{z}_1^{(m)},\dot{z}_2^{(m)},\cdots,\dot{z}_{2N}^{(m)},\dot{z}_{2N+1}^{(m)})^T.
\end{aligned}
\tag{37}
$$

Equation (23) can be expressed in vector field as

$$
\dot{\mathbf{z}}^{(m)} = \mathbf{z}_1^{(m)} \text{ and } \dot{\mathbf{z}}_1^{(m)} = \mathbf{g}^{(m)}(\mathbf{z}^{(m)},\mathbf{z}_1^{(m)})
\tag{38}
$$

where

$$
\mathbf{g}^{(m)}(\mathbf{z}^{(m)},\mathbf{z}_1^{(m)}) = \begin{pmatrix} F_0^{(m)}(\mathbf{z}^{(m)},\mathbf{z}_1^{(m)}) \\ -2\frac{\mathbf{k}_1\Omega}{m}\dot{\mathbf{c}}^{(m)}+\mathbf{k}_2(\frac{\Omega}{m})^2\mathbf{b}^{(m)}+\mathbf{F}_1^{(m)}(\mathbf{z}^{(m)},\mathbf{z}_1^{(m)}) \\ 2\frac{\mathbf{k}_1\Omega}{m}\dot{\mathbf{b}}^{(m)}+\mathbf{k}_2(\frac{\Omega}{m})^2\mathbf{c}^{(m)}+\mathbf{F}_2^{(m)}(\mathbf{z}^{(m)},\mathbf{z}_1^{(m)}) \end{pmatrix}
\tag{39}
$$

and

$$
\begin{aligned}
&\mathbf{k}_1 = \text{diag}(1,2,\cdots,N),\mathbf{k}_2 = \text{diag}(1,2^2,\cdots,N^2),\\
&\mathbf{F}_1^{(m)} = (F_{11}^{(m)},F_{12}^{(m)},\cdots,F_{1N}^{(m)})^T,\mathbf{F}_2^{(m)} = (F_{21}^{(m)},F_{22}^{(m)},\cdots,F_{2N}^{(m)})^T.
\end{aligned}
\tag{40}
$$

for $N = 1,2,\cdots,\infty$.

Let

$$
\mathbf{y}^{(m)} \equiv (\mathbf{z}^{(m)},\mathbf{z}_1^{(m)}),\mathbf{f}^{(m)} = (\mathbf{z}_1^{(m)},\mathbf{g}^{(m)})^T.
\tag{41}
$$

Following Section 3.1, the steady-state solution for period-m motion can be obtained by setting $\dot{\mathbf{y}}^{(m)} = 0$, i.e.,

$$
\begin{aligned}
&F_0^{(m)}(a_0^{(m)},\mathbf{b}^{(m)},\mathbf{c}^{(m)},0,\mathbf{0},\mathbf{0}) = 0,\\
&(k\Omega/m)^2 b_{k/m}+F_{1k}^{(m)}(a_0^{(m)},\mathbf{b}^{(m)},\mathbf{c}^{(m)},0,\mathbf{0},\mathbf{0}) = 0,\\
&(k\Omega/m)^2 c_{k/m}+F_{2k}^{(m)}(a_0^{(m)},\mathbf{b}^{(m)},\mathbf{c}^{(m)},0,\mathbf{0},\mathbf{0}) = 0.
\end{aligned}
\tag{42}
$$

where $k = 1,2,\ldots,N$.

The nonlinear algebraic equations in Eq. (42) can be solved by the Newton-Broyden method. The linearized system is given by Eq. (15) for which the stability of periodic motion can be identified using eigenvalue indices in Eq. (17).

To present the periodic solution of the planar motion one chooses $\rho_s = 7800\text{kg/m}^3$, $E = 206\text{GPa}$, $L = 3\text{m}$, $x_a = 0.08$, $x_b = 0.92$, $C = D/900$, $L_b = D/4$, $e_{\bar{m}} = 0.0001\text{m}$, $D = 0.3\text{m}$, $\gamma_m = 1350\text{T}^2\text{m/H}$, $\mu_o =$

0.018Pa·s, $C_e = D/1000$. The bifurcation diagram of the motion is illustrated in Fig. 2. The analytical solutions for period-m motion based on eight/sixteen harmonic terms (HB8/16) are presented herein. The black dots give the numerical solution of period-1 motion, whereas the red dots represent the numerical solution of period-2 motion. The transform of stable period-1 motion to stable period-2 motion via the Hopf bifurcation is observed. The stable period-2 motion suggests the existence of oil whirl with the frequency of one-half of rotational speed. The stable period-1 motion transform to stable period-2 motion through Hopf bifurcation can be observed as well. In Fig. 2 (a), the motion of the planar rotor marked by the black solid circles is stable and period-1 for $\omega \in (10,366) \cup (451,1000)$. In the range of $\omega \in (367,450)$, the motion becomes period-2 following a period doubling bifurcation. The frequency component of one-half rotational speed appears which is marked by red solid circles. The Hopf bifurcation is found at $\omega = 366$ and $\omega = 450$. The bifurcation diagram in the range of $\omega \in (300,500)$ is shown in Fig. 2 (b).

Table 1 Stability classification of periodic motion based on eight/sixteen harmonic terms (HB8/16).

Periodic motion	Type of eigenvalues	Rotational speed ω	Stability and Bifurcation
Period-1 motion	(0,0,0 | 17,0,0)	(300, 366), (450, 500)	Stable
	(0,0,0 | 9,8,0)	(366, 450)	Unstable
Period-2 motion	(4,0,0 | 32,0,0)	(366, 450)	Stable
Bifurcation point		366, 450	Hopf bifurcation point(HBP)

The analytical solutions for periodic motion based on eight/sixteen harmonic terms (HB8/16) are presented in Fig. 3. The constant term a_0 and integer-order harmonic terms (A_1, A_2, A_3, A_4) versus the rotational speed are shown in Fig. 3 (a), (c), (e), (g) and (i), respectively. The backbone curves of the response amplitude varying with ω are shown in Fig. 3(a)-2(i) with m=1 and m=2, respectively. Based on the eigenvalue analysis, the stability and bifurcation conditions for the analytical solutions can be determined. The black solid lines represent analytical solutions of stable period-1 and period-2 motions, whereas the red dash line is the unstable period-1 motion. In the range of $\omega \in (300,366) \cup (450,500)$, the period-1 motion is found to be stable. The speed ranges of unstable period-1 motion and stable period-2 motion are both $\omega \in (366,500)$. The type of eigenvalues of stable period-1 motion, stable period-2 motion and unstable period-1 motion are $(0,0,0|17,0,0)$, $(4,0,0|32,0,0)$ and $(0,0,0|9,8,0)$. The Hopf bifurcation points that appear at $\omega = 366$ and $\omega = 450$ are marked by empty circles and acronym HBP,

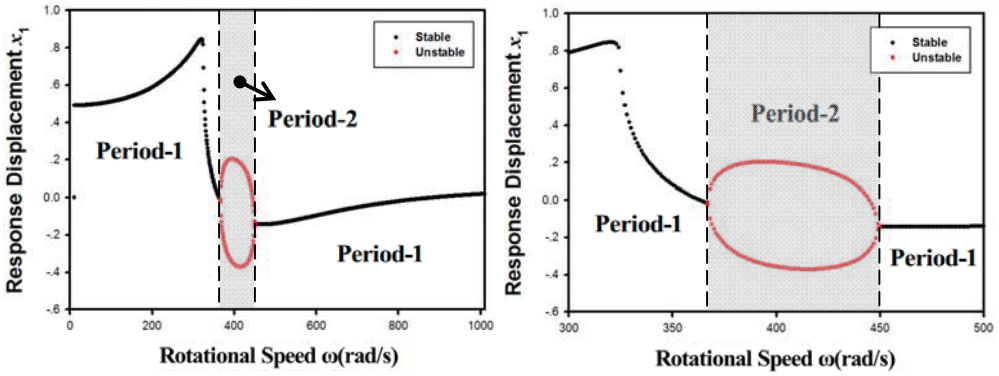

Fig. 2 Bifurcation diagram of the planar continuum rotor system. The parameters are $\rho_s = 7800\text{kg/m}^3$, $E = 206\text{GPa}$, L =3m, $x_a = 0.08$, $x_b = 0.092$, $C = D/900$, $L_b = D/4$, $e_{\bar{m}}$ =0.0001m, D =0.3m, $\gamma_m = 1350\text{T}^2\text{m/H}$, μ_o =0.0129Pa·s, $C_e = D/1000$. The black dot means that the motion is stable, and the red rot means unstable motion.

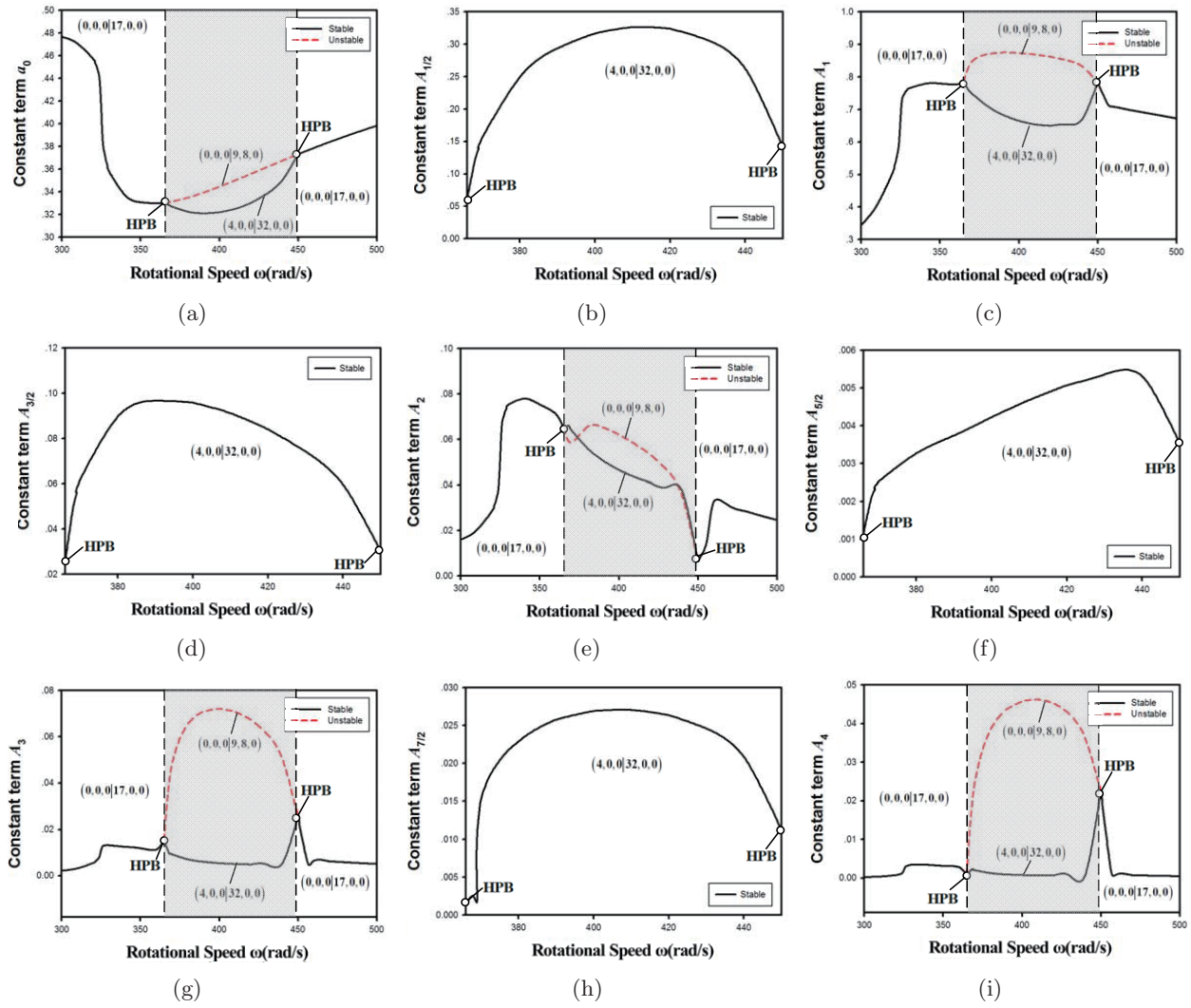

Fig. 3 Analytical prediction of periodic solutions, with $m = 1$, based on eight/sixteen harmonic terms (HB8/16): (a) constant term a_0, (b) 1/2 harmonic amplitude $A_{1/2}$, (c) first harmonic amplitude A_1, (d) 3/2 harmonic amplitude $A_{3/2}$, (e) second harmonic amplitude A_2, (f) 5/2 harmonic amplitude $A_{5/2}$, (g) third harmonic amplitude A_3, (h) 7/2 harmonic amplitude $A_{7/2}$, (i) forth harmonic amplitude A_4. The parameters of the continuum rotor system are $\rho_s = 7800\text{kg/m}^3$, $E = 206\text{GPa}$, L =3m, $x_a = 0.08$, $x_b = 0.092$, $C = D/900$, $L_b = D/4$, $e_{\bar{m}}$ =0.0001m, D =0.3m, $\gamma_m = 1350\text{T}^2\text{m/H}$, μ_o =0.0129Pa·s, $C_e = D/1000$. The black solid curve and red dot represents stable and unstable motions, respectively. HBP is the Hopf bifurcation point marked by empty circles.

as the real part of conjugated eigenvalues becomes positive. The amplitudes of the fraction harmonic terms ($A_{1/2}$,$A_{3/2}$,$A_{5/2}$,$A_{7/2}$) of the analytical of stable period-2 motion versus rotational speed are shown in Fig. 3 (b), (d), (f) and (h), respectively. The Hopf bifurcation appears when $\omega = 366$ and $\omega = 450$. The classification of eigenvalues, stability and bifurcation characteristics of continuum rotor system is tabulated in Table 1.

3.3 Analytical solution of spatial rotor

In this section, the analytical solution and stability of spatial continuum rotor system is researched, and the governing equation is Eq. (18) can be rewritten in the standard form

$$\ddot{x}_1 = f_1(x_1, x_2, \dot{x}_1, \dot{x}_2, \tau), \ddot{x}_2 = f_2(x_1, x_2, \dot{x}_1, \dot{x}_2, \tau), \tag{43}$$

where

$$\begin{cases} f_1(x_1, x_2, \dot{x}_1, \dot{x}_2, \tau) = p_{\bar{m}}\varepsilon_{\bar{m}}\cos\Omega\tau + f_y + \alpha_1 x_1 + \alpha_2 x_2 + \alpha_3\dot{x}_1 + \alpha_4\dot{x}_2 + \alpha_5 x_1^2 + \alpha_6 x_1 x_2 \\ \qquad + \alpha_7 x_1\dot{x}_1 + \alpha_8 x_1\dot{x}_2 + \alpha_9 x_2^2 + \alpha_{10} x_2\dot{x}_1 + \alpha_{11} x_2\dot{x}_2 + \alpha_{12} x_1^3 + \alpha_{13} x_1^2 x_2 + \alpha_{14} x_1 x_2^2 \\ \qquad + \alpha_{15} x_1^2\dot{x}_1 + \alpha_{16} x_1^2\dot{x}_2 + \alpha_{17} x_1 x_2\dot{x}_1 + \alpha_{18} x_1 x_2\dot{x}_2 + \alpha_{19} x_2^3 + \alpha_{20} x_2^2\dot{x}_1 + \alpha_{21} x_2^2\dot{x}_2, \\ f_2(x_1, x_2, \dot{x}_1, \dot{x}_2, \tau) = p_{\bar{m}}\varepsilon_{\bar{m}}\sin\Omega\tau + f_z + \beta_1 x_1 + \beta_2 x_2 + \beta_3\dot{x}_1 + \beta_4\dot{x}_2 + \beta_5 x_1^2 + \beta_6 x_1 x_2 \\ \qquad + \beta_7 x_1\dot{x}_1 + \beta_8 x_1\dot{x}_2 + \beta_9 x_2^2 + \beta_{10} x_2\dot{x}_1 + \beta_{11} x_2\dot{x}_2 + \beta_{12} x_1^3 + \beta_{13} x_1^2 x_2 + \beta_{14} x_1 x_2^2 \\ \qquad + \beta_{15} x_1^2\dot{x}_1 + \beta_{16} x_1^2\dot{x}_2 + \beta_{17} x_1 x_2\dot{x}_1 + \beta_{18} x_1 x_2\dot{x}_2 + \beta_{19} x_2^3 + \beta_{20} x_2^2\dot{x}_1 + \beta_{21} x_2^2\dot{x}_2. \end{cases} \tag{44}$$

The analytical solutions of period-m motion for the continuum rotor system are

$$\begin{cases} x_1(\tau) = a_{1,0}^{(m)}(\tau) + \sum_{k=1}^{N}[b_{1,k/m}(\tau)\cos(\frac{k}{m}\Omega\tau) + c_{1,k/m}(\tau)\sin(\frac{k}{m}\Omega\tau)], \\ x_2(\tau) = a_{2,0}^{(m)}(\tau) + \sum_{k=1}^{N}[b_{2,k/m}(\tau)\cos(\frac{k}{m}\Omega\tau) + c_{2,k/m}(\tau)\sin(\frac{k}{m}\Omega\tau)]. \end{cases} \tag{45}$$

The first and second order derivatives of $x_{1,2}(\tau)$ are

$$\begin{cases} \dot{x}_1(\tau) = \dot{a}_{1,0}^{(m)} + \sum_{k=1}^{N}[(\dot{b}_{1,k/m} + \frac{k\Omega}{m}c_{1,k/m})\cos(\frac{k}{m}\Omega\tau) + (\dot{c}_{1,k/m} - \frac{k\Omega}{m}b_{1,k/m})\sin(\frac{k}{m}\Omega\tau)], \\ \dot{x}_2(\tau) = \dot{a}_{2,0}^{(m)} + \sum_{k=1}^{N}[(\dot{b}_{2,k/m} + \frac{k\Omega}{m}c_{2,k/m})\cos(\frac{k}{m}\Omega\tau) + (\dot{c}_{2,k/m} - \frac{k\Omega}{m}b_{2,k/m})\sin(\frac{k}{m}\Omega\tau)]. \end{cases} \tag{46}$$

and

$$\begin{cases} \ddot{x}_1(\tau) = \ddot{a}_{1,0}^{(m)} + \sum_{k=1}^{N}[(\ddot{b}_{1,k/m} + 2\frac{k\Omega}{m}\dot{c}_{1,k/m} - (\frac{k\Omega}{m})^2 b_{1,k/m})\cos(\frac{k}{m}\Omega\tau) \\ \qquad + (\ddot{c}_{1,k/m} - 2\frac{k\Omega}{m}\dot{b}_{1,k/m} - (\frac{k\Omega}{m})^2 c_{1,k/m})\sin(\frac{k}{m}\Omega\tau)], \\ \ddot{x}_2(\tau) = \ddot{a}_{2,0}^{(m)} + \sum_{k=1}^{N}[(\ddot{b}_{2,k/m} + 2\frac{k\Omega}{m}\dot{c}_{2,k/m} - (\frac{k\Omega}{m})^2 b_{2,k/m})\cos(\frac{k}{m}\Omega\tau) \\ \qquad + (\ddot{c}_{2,k/m} - 2\frac{k\Omega}{m}\dot{b}_{2,k/m} - (\frac{k\Omega}{m})^2 c_{2,k/m})\sin(\frac{k}{m}\Omega\tau)]. \end{cases} \tag{47}$$

Substituting Eqs. (45)–(47) into Eq. (18) and averaging $\cos(k\Omega\tau/m)$ and $\sin(k\Omega\tau/m)$ gives

$$\begin{aligned}
\ddot{a}_{1,0}^{(m)} &= F_{1,0}^{(m)}(\mathbf{a}_0^{(m)},\mathbf{b}^{(m)},\mathbf{c}^{(m)},\dot{\mathbf{a}}_0^{(m)},\dot{\mathbf{b}}^{(m)},\dot{\mathbf{c}}^{(m)})\\
\ddot{a}_{2,0}^{(m)} &= F_{2,0}^{(m)}(\mathbf{a}_0^{(m)},\mathbf{b}^{(m)},\mathbf{c}^{(m)},\dot{\mathbf{a}}_0^{(m)},\dot{\mathbf{b}}^{(m)},\dot{\mathbf{c}}^{(m)})\\
\ddot{b}_{1,k/m}+2\frac{k\Omega}{m}\dot{c}_{1,k/m}-(\frac{k\Omega}{m})^2 b_{1,k/m} &= F_{1,1k}^{(m)}(\mathbf{a}_0^{(m)},\mathbf{b}^{(m)},\mathbf{c}^{(m)},\dot{\mathbf{a}}_0^{(m)},\dot{\mathbf{b}}^{(m)},\dot{\mathbf{c}}^{(m)})\\
\ddot{b}_{2,k/m}+2\frac{k\Omega}{m}\dot{c}_{2,k/m}-(\frac{k\Omega}{m})^2 b_{2,k/m} &= F_{2,1k}^{(m)}(\mathbf{a}_0^{(m)},\mathbf{b}^{(m)},\mathbf{c}^{(m)},\dot{\mathbf{a}}_0^{(m)},\dot{\mathbf{b}}^{(m)},\dot{\mathbf{c}}^{(m)})\\
\ddot{c}_{1,k/m}-2\frac{k\Omega}{m}\dot{b}_{1,k/m}-(\frac{k\Omega}{m})^2 c_{1,k/m} &= F_{1,2k}^{(m)}(\mathbf{a}_0^{(m)},\mathbf{b}^{(m)},\mathbf{c}^{(m)},\dot{\mathbf{a}}_0^{(m)},\dot{\mathbf{b}}^{(m)},\dot{\mathbf{c}}^{(m)})\\
\ddot{c}_{2,k/m}-2\frac{k\Omega}{m}\dot{b}_{2,k/m}-(\frac{k\Omega}{m})^2 c_{2,k/m} &= F_{2,2k}^{(m)}(\mathbf{a}_0^{(m)},\mathbf{b}^{(m)},\mathbf{c}^{(m)},\dot{\mathbf{a}}_0^{(m)},\dot{\mathbf{b}}^{(m)},\dot{\mathbf{c}}^{(m)})
\end{aligned} \tag{48}$$

for $k=1,2,\ldots,N$.

The coefficients of $\cos(k\Omega\tau/m)$ and $\sin(k\Omega\tau/m)$for the function of $\mathbf{f}(\mathbf{x},\dot{\mathbf{x}},\tau)$ are

$$\begin{aligned}
F_{1,0}^{(m)}(\mathbf{a}_0^{(m)},\mathbf{b}^{(m)},\mathbf{c}^{(m)},\dot{\mathbf{a}}_0^{(m)},\dot{\mathbf{b}}^{(m)},\dot{\mathbf{c}}^{(m)}) =& f_y+\alpha_1 a_{1,0}^{(m)}+\alpha_2 a_{2,0}^{(m)}+\alpha_3\dot{a}_{1,0}^{(m)}+\alpha_4\dot{a}_{2,0}^{(m)}+\alpha_5 f_{1,1}^{(0)}\\
&+\alpha_6 f_{1,2}^{(0)}+\alpha_7 f_{1,3}^{(0)}+\alpha_8 f_{1,4}^{(0)}+\alpha_9 f_{1,5}^{(0)}+\alpha_{10} f_{1,6}^{(0)}+\alpha_{11} f_{1,7}^{(0)}\\
&+\alpha_{12} f_{1,8}^{(0)}+\alpha_{13} f_{1,9}^{(0)}+\alpha_{14} f_{1,10}^{(0)}+\alpha_{15} f_{1,11}^{(0)}+\alpha_{16} f_{1,12}^{(0)}\\
&+\alpha_{17} f_{1,13}^{(0)}+\alpha_{18} f_{1,14}^{(0)}+\alpha_{19} f_{1,15}^{(0)}+\alpha_{20} f_{1,16}^{(0)}+\alpha_{21} f_{1,17}^{(0)};
\end{aligned} \tag{49}$$

$$\begin{aligned}
F_{2,0}^{(m)}(\mathbf{a}_0^{(m)},\mathbf{b}^{(m)},\mathbf{c}^{(m)},\dot{\mathbf{a}}_0^{(m)},\dot{\mathbf{b}}^{(m)},\dot{\mathbf{c}}^{(m)}) =& f_z+\beta_1 a_{1,0}^{(m)}+\beta_2 a_{2,0}^{(m)}+\beta_3\dot{a}_{1,0}^{(m)}+\beta_4\dot{a}_{2,0}^{(m)}\\
&+\beta_5 f_{2,1}^{(0)}+\beta_6 f_{2,2}^{(0)}+\beta_7 f_{2,3}^{(0)}+\beta_8 f_{2,4}^{(0)}+\beta_9 f_{2,5}^{(0)}\\
&+\beta_{10} f_{2,6}^{(0)}+\beta_{11} f_{2,7}^{(0)}+\beta_{12} f_{2,8}^{(0)}+\beta_{13} f_{2,9}^{(0)}\\
&+\beta_{14} f_{2,10}^{(0)}+\beta_{15} f_{2,11}^{(0)}+\beta_{16} f_{2,12}^{(0)}+\beta_{17} f_{2,13}^{(0)}\\
&+\beta_{18} f_{2,14}^{(0)}+\beta_{19} f_{2,15}^{(0)}+\beta_{20} f_{2,16}^{(0)}+\beta_{21} f_{2,17}^{(0)};
\end{aligned} \tag{50}$$

$$\begin{aligned}
F_{1,1k}^{(m)}(\mathbf{a}_0^{(m)},\mathbf{b}^{(m)},\mathbf{c}^{(m)},\dot{\mathbf{a}}_0^{(m)},\dot{\mathbf{b}}^{(m)},\dot{\mathbf{c}}^{(m)}) =& p_{\bar{m}}\varepsilon_{\bar{m}}\delta_k^m+\alpha_1 b_{1,k/m}+\alpha_2 b_{2,k/m}+\alpha_3(\dot{b}_{1,k/m}+\frac{k\Omega}{m}c_{1,k/m})\\
&+\alpha_4(\dot{b}_{2,k/m}+\frac{k\Omega}{m}c_{2,k/m})+\alpha_5 f_{1,1k}^{(c)}+\alpha_6 f_{1,2k}^{(c)}+\alpha_7 f_{1,3k}^{(c)}+\alpha_8 f_{1,4k}^{(c)}\\
&+\alpha_9 f_{1,5k}^{(c)}+\alpha_{10} f_{1,6k}^{(c)}+\alpha_{11} f_{1,7k}^{(c)}+\alpha_{12} f_{1,8k}^{(c)}+\alpha_{13} f_{1,9k}^{(c)}+\alpha_{14} f_{1,10k}^{(c)}\\
&+\alpha_{15} f_{1,11k}^{(c)}+\alpha_{16} f_{1,12k}^{(c)}+\alpha_{17} f_{1,13k}^{(c)}+\alpha_{18} f_{1,14k}^{(c)}+\alpha_{19} f_{1,15k}^{(c)}\\
&+\alpha_{20} f_{1,16k}^{(c)}+\alpha_{21} f_{1,17k}^{(c)};
\end{aligned} \tag{51}$$

$$\begin{aligned}
F_{2,1k}^{(m)}(\mathbf{a}_0^{(m)},\mathbf{b}^{(m)},\mathbf{c}^{(m)},\dot{\mathbf{a}}_0^{(m)},\dot{\mathbf{b}}^{(m)},\dot{\mathbf{c}}^{(m)}) =& \beta_1 b_{1,k/m}+\beta_2 b_{2,k/m}+\beta_3(\dot{b}_{1,k/m}+\frac{k\Omega}{m}c_{1,k/m})\\
&+\beta_4(\dot{b}_{2,k/m}+\frac{k\Omega}{m}c_{2,k/m})+\beta_5 f_{2,1k}^{(c)}+\beta_6 f_{2,2k}^{(c)}+\beta_7 f_{2,3k}^{(c)}+\beta_8 f_{2,4k}^{(c)}\\
&+\beta_9 f_{2,5k}^{(c)}+\beta_{10} f_{2,6k}^{(c)}+\beta_{11} f_{2,7k}^{(c)}+\beta_{12} f_{2,8k}^{(c)}+\beta_{13} f_{2,9k}^{(c)}+\beta_{14} f_{2,10k}^{(c)}\\
&+\beta_{15} f_{2,11k}^{(c)}+\beta_{16} f_{2,12k}^{(c)}+\beta_{17} f_{2,13k}^{(c)}+\beta_{18} f_{2,14k}^{(c)}\\
&+\beta_{19} f_{2,15k}^{(c)}+\beta_{20} f_{2,16k}^{(c)}+\beta_{21} f_{2,17k}^{(c)};
\end{aligned} \tag{52}$$

$$\begin{aligned}F_{1,2k}^{(m)}(\mathbf{a}_0^{(m)},\mathbf{b}^{(m)},\mathbf{c}^{(m)},\dot{\mathbf{a}}_0^{(m)},\dot{\mathbf{b}}^{(m)},\dot{\mathbf{c}}^{(m)}) =&\alpha_1 c_{1,k/m}+\alpha_2 c_{2,k/m}+\alpha_3(\dot{c}_{1,k/m}-\frac{k\Omega}{m}b_{1,k/m})\\ &+\alpha_4(\dot{c}_{2,k/m}-\frac{k\Omega}{m}b_{2,k/m})+\alpha_5 f_{1,1k}^{(s)}+\alpha_6 f_{1,2k}^{(s)}+\alpha_7 f_{1,3k}^{(s)}+\alpha_8 f_{1,4k}^{(s)}\\ &+\alpha_9 f_{1,5k}^{(s)}+\alpha_{10} f_{1,6k}^{(s)}+\alpha_{11} f_{1,7k}^{(s)}+\alpha_{12} f_{1,8k}^{(s)}+\alpha_{13} f_{1,9k}^{(s)}+\alpha_{14} f_{1,10k}^{(s)}\\ &+\alpha_{15} f_{1,11k}^{(s)}+\alpha_{16} f_{1,12k}^{(s)}+\alpha_{17} f_{1,13k}^{(s)}+\alpha_{18} f_{1,14k}^{(s)}+\alpha_{19} f_{1,15k}^{(s)}\\ &+\alpha_{20} f_{1,16k}^{(s)}+\alpha_{21} f_{1,17k}^{(s)};\end{aligned} \tag{53}$$

$$\begin{aligned}F_{2,2k}^{(m)}(\mathbf{a}_0^{(m)},\mathbf{b}^{(m)},\mathbf{c}^{(m)},\dot{\mathbf{a}}_0^{(m)},\dot{\mathbf{b}}^{(m)},\dot{\mathbf{c}}^{(m)}) =&p_{\bar{m}}\varepsilon_{\bar{m}}\delta_k^m+\beta_1 c_{1,k/m}+\beta_2 c_{2,k/m}+\beta_3(\dot{c}_{1,k/m}-\frac{k\Omega}{m}b_{1,k/m})\\ &+\beta_4(\dot{c}_{2,k/m}-\frac{k\Omega}{m}b_{2,k/m})+\beta_5 f_{2,1k}^{(s)}+\beta_6 f_{2,2k}^{(s)}+\beta_7 f_{2,3k}^{(s)}+\beta_8 f_{2,4k}^{(s)}\\ &+\beta_9 f_{2,5k}^{(s)}+\beta_{10} f_{2,6k}^{(s)}+\beta_{11} f_{2,7k}^{(s)}+\beta_{12} f_{2,8k}^{(s)}+\beta_{13} f_{2,9k}^{(s)}\\ &+\beta_{14} f_{2,10k}^{(s)}+\beta_{15} f_{2,11k}^{(s)}+\beta_{16} f_{2,12k}^{(s)}+\beta_{17} f_{2,13k}^{(s)}+\beta_{18} f_{2,14k}^{(s)}\\ &+\beta_{19} f_{2,15k}^{(s)}+\beta_{20} f_{2,16k}^{(s)}+\beta_{21} f_{2,17k}^{(s)};\end{aligned} \tag{54}$$

where $f_{1,1}^{(0)},\ldots,f_{1,17}^{(0)}$, $f_{2,1}^{(0)},\ldots,f_{2,17}^{(0)}$, $f_{1,1k}^{(c)},\ldots,f_{1,17k}^{(c)}$, $f_{2,1k}^{(c)},\ldots,f_{2,17k}^{(c)}$, $f_{1,1k}^{(s)},\ldots,f_{1,17k}^{(s)}$ and $f_{2,1k}^{(s)},\ldots,f_{2,17k}^{(s)}$ are given in Appendix B.

Following Section 3.1, the steady-state, periodic motion can be obtained by setting all derivatives in Eq. (48) to be zero, i.e.,

$$\begin{aligned}0&=F_{1,0}^{(m)}(\mathbf{a}_0^{(m)},\mathbf{b}^{(m)},\mathbf{c}^{(m)},\mathbf{0},\mathbf{0},\mathbf{0});\\ 0&=F_{2,0}^{(m)}(\mathbf{a}_0^{(m)},\mathbf{b}^{(m)},\mathbf{c}^{(m)},\mathbf{0},\mathbf{0},\mathbf{0});\\ 0&=(\frac{k\Omega}{m})^2 b_{1,k/m}+F_{1,1k}^{(m)}(\mathbf{a}_0^{(m)},\mathbf{b}^{(m)},\mathbf{c}^{(m)},\mathbf{0},\mathbf{0},\mathbf{0});\\ 0&=(\frac{k\Omega}{m})^2 b_{2,k/m}+F_{2,1k}^{(m)}(\mathbf{a}_0^{(m)},\mathbf{b}^{(m)},\mathbf{c}^{(m)},\mathbf{0},\mathbf{0},\mathbf{0});\\ 0&=(\frac{k\Omega}{m})^2 c_{1,k/m}+F_{1,2k}^{(m)}(\mathbf{a}_0^{(m)},\mathbf{b}^{(m)},\mathbf{c}^{(m)},\mathbf{0},\mathbf{0},\mathbf{0});\\ 0&=(\frac{k\Omega}{m})^2 c_{2,k/m}+F_{2,2k}^{(m)}(\mathbf{a}_0^{(m)},\mathbf{b}^{(m)},\mathbf{c}^{(m)},\mathbf{0},\mathbf{0},\mathbf{0});\end{aligned} \tag{55}$$

The stability of the periodic motion of the system can be determined again using linearization-based eigenvalue analysis expressed by Eqs.(15) through (17).

For the numerical illustration one chooses $\rho_s=7800\text{kg/m}^3$, $E=206\text{GPa}$, $L=3\text{m}$, $x_a=0.08$, $x_b=0.92$, $C=D/1000$, $L_b=D/4$, $e_{\bar{m}}=0.0001\text{m}$, $D=0.3\text{m}$, $\gamma_m=1000\text{T}^2\text{m/H}$, $\mu_o=0.018\text{Pa}\cdot\text{s}$, $C_e=D/1600$. The bifurcation diagram of the spatial continuum rotor system is illustrated in Fig. 4, and the stable period-1 motion and unstable period-1 motion (i.e. stable period-2 motion). The analytical solutions for period-1 motion based on eight harmonic terms (HB8) are presented herein. The backbone curves of response amplitude varying with rotational speed ω are shown in Fig. 5(a)-5(f) with k=1, whereas the results for k=2∼8 are not depicted. The harmonic amplitude and phase are defined by

$$\begin{aligned}A_{1,k/m}&\equiv\sqrt{b_{1,k/m}^2+c_{1,k/m}^2},\phi_{1,k/m}\equiv\arctan\frac{c_{1,k/m}}{b_{1,k/m}},\\ A_{2,k/m}&\equiv\sqrt{b_{2,k/m}^2+c_{2,k/m}^2},\phi_{2,k/m}\equiv\arctan\frac{c_{2,k/m}}{b_{2,k/m}}.\end{aligned} \tag{56}$$

and the corresponding solution in Eq. (45) is

$$\begin{aligned} x_1(t) =& a_{1,0}^{(m)} + \sum_{k=1}^{N} A_{1,k/m} \cos(\frac{k}{m}\Omega\tau - \phi_{1,k/m}), \\ x_2(t) =& a_{2,0}^{(m)} + \sum_{k=1}^{N} A_{2,k/m} \cos(\frac{k}{m}\Omega\tau - \phi_{2,k/m}). \end{aligned} \tag{57}$$

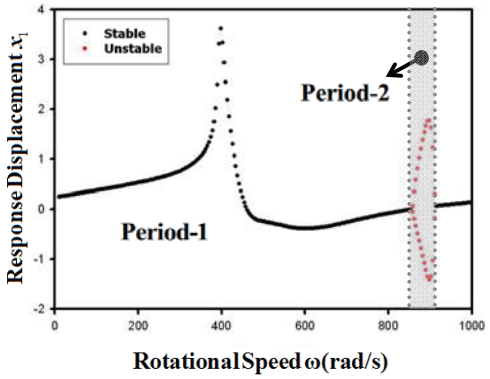

Fig. 4 Bifurcation diagram of the spatial continuum rotor system. $\rho_s = 7800\text{kg}/\text{m}^3$, $E = 206\text{GPa}$, L =3m, $x_a = 0.08$, $x_b = 0.092$, $C = D/1000$, $L_b = D/4$, $e_{\bar{m}}$ =0.0001m, D =0.3m, $\gamma_m = 1000\text{T}^2\text{m/H}$, μ_o =0.018Pa·s, $C_e = D/1600$. The parameters are The black dot means that the motion is stable, and the red rot means unstable motion.

Table 2 Stability classification of periodic motion based on eight harmonic terms (HB8). $\rho_s = 7800\text{kg}/\text{m}^3$, $E = 206\text{GPa}$, L =3m, $x_a = 0.08$, $x_b = 0.092$, $C = D/1000$, $L_b = D/4$, $e_{\bar{m}}$ =0.0001m, D =0.3m, $\gamma_m = 1000\text{T}^2\text{m/H}$, μ_o =0.018Pa·s, $C_e = D/1600$

Type of eigenvalues	Rotational speed ω	Stability and Bifurcation
(0,0,0 | 34,0,0)	(10, 385), (426, 847), (919, 1000)	Stable
(8,0,0 | 30,0,0)	(385, 396), (421, 426)	Stable
(16,0,0 | 26,0,0)	(396, 421)	Stable
(0,0,0 | 30,4,0)	(847, 919)	Unstable
	847, 919	Hopf bifurcation point(HBP)

In Fig. 4, the motion of the rotor system marked by black solid circles is stable and period-1 for $\omega \in (10, 847) \cup (919, 1000)$. For $\omega \in (847, 919)$the stability of period-1 is lost, and the motion becomes period-2 marked by red solid circles. In this case, the motion of the system is transformed to half frequency whirl at bifurcation points $\omega = 847$ and $\omega = 919$.

The analytical solutions for periodic motion based on eight harmonic terms (HB8) are presented in Fig. 5. The constant terms $(a_{1,0}, a_{2,0})$, the amplitudes of the first harmonic terms $(A_{1,1}, A_{2,1})$ and phases $(\phi_{1,1}, \phi_{2,1})$ are presented versus rotational speed in Fig. 5(a)-5(f), respectively. An eigenvalue analysis is performed to determine the stability and bifurcation conditions for the periodic motions based on the analytical solutions. The black and red solid circles represent the stable and unstable periodic solutions using harmonic terms HB8, respectively. In the range of $\omega \in (10, 847) \cup (919, 1000)$, the period-1 motion is stable. In other range of rotational speed, the motion is unstable. The Hopf bifurcation points appearing at $\omega = 847$ and $\omega = 919$ are marked by empty circles and acronym HBP

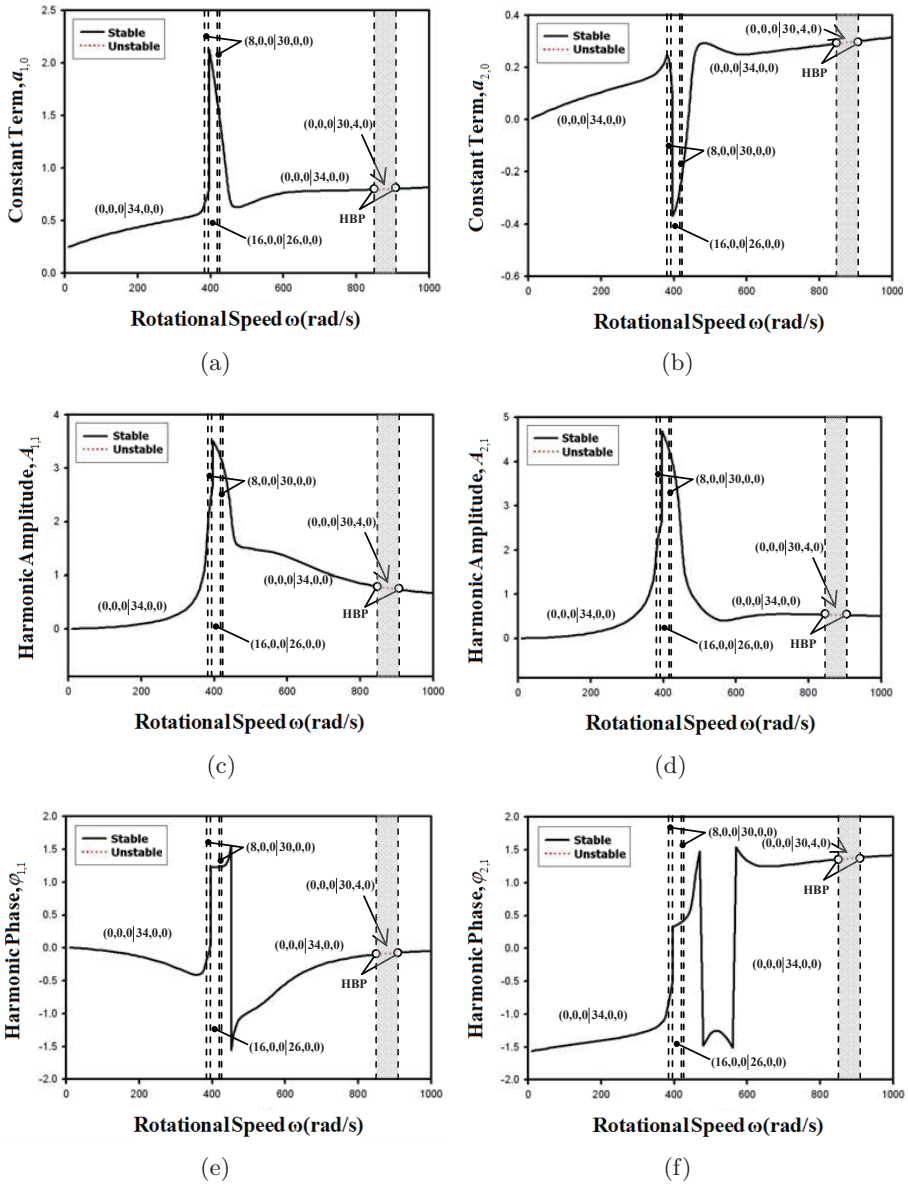

Fig. 5 Analytical prediction of periodic solutions, with $k = 1$ and $m = 1$, based on eight harmonic terms (HB8): (a) constant term in x_1-direction ($a_{1,0}$), (b) constant term in x_2-direction ($a_{2,0}$), (c) first harmonic amplitude in x_1-direction ($A_{1,1}$), (d) first harmonic amplitude in x_2-direction ($A_{2,1}$), (e) first harmonic phase in x_1-direction ($\varphi_{1,1}$), (f) first harmonic phase in x_2-direction ($\varphi_{1,1}$). The parameters of the continuum rotor system are $\rho_s = 7800\text{kg/m}^3$, $E = 206\text{GPa}$, L =3m, $x_a = 0.08$, $x_b = 0.092$, $C = D/1000$, $L_b = D/4$, $e_{\bar{m}}$ =0.0001m, D =0.3m, $\gamma_m = 1000\text{T}^2\text{m/H}$, μ_o =0.018Pa·s, $C_e = D/1600$. The black solid curve and red dot represents stable and unstable motions, respectively. HBP is Hopf bifurcation point marked by empty circles

as the real part of the conjugated eigenvalues changes from negative to positive. In addition, the eigenvalues computed with the periodic motions are classified. Based on the eigenvalues indices, the stability and bifurcation characteristics are determined and tabulated in Table 2.

It can be observed that, through the comparison of Fig. 4 and Fig. 5, the numerical solution of dynamic responses matches well with the analytical predictions of by the analytical GHBM regarding the periodicity and stability of the motion. That is, both of the two methods give period-1 motion for rotation speed$\omega \in (10, 847) \cup (919, 1000)$, and periodic-2 motion for $\omega \in (847, 919)$. For $\omega = 847$

and $\omega = 919$, bifurcation is found in both of the numerical solution and the GHBM prediction. The unstable period-1 motion will transform through the Hopf bifurcation to a stable period-2 motion with a half frequency whirl of the rotor shaft. The GHBM can be very helpful in understanding the whole onset of periodic/non-periodic motions as well as various types of bifurcation in an analytical way.

4 Conclusions

In this paper, the nonlinear dynamical response of a rotor system excited by both of the electromagnetic force and oil-film force is investigated using a continuum model of Euler-Bernoulli beam. The governing equation of the system is derived and discretized through the Galerkin's approximation method. The Generalized Harmonic Balance Method is adopted to obtain the analytical solutions of periodic motions of planar and spatial continuum rotors, respectively. In both cases the stability and bifurcations of rotor motion are presented through eigenvalue analysis. It is shown through comparison with numerical solution that the GHBM is an accurate and effective method in analyses of nonlinear rotor systems with complicated scenarios of bifurcation.

Acknowledgments

The authors are grateful for supports from Free Exploration Project of State Key Laboratory of Structural Analysis for Industrial Equipment (Grant S14204), Liaoning Provincial Program for Science and Technology (Grants 201303002, 2014028004), and the State Key Development Program for Basic Research of China (Grant 2015CB057300).

References

[1] Yamamoto, T., Ishida, Y. and Ikeda, T. (1982), Non-linear forced-oscillations of a rotating shaft carrying an unsymmetrical rotor at the major critical speed, *Bulletin of the JSME-JAPAN Society of Mechanical Engineers*, **25**(210), 1969-1976.

[2] Shaw, S. W. (1988), Chaotic dynamics of a slender beam rotating about its longitudinal axis, *Journal of Sound and Vibration*, **124**(2), 329-343.

[3] Ishida, Y. Nagasaka, I. Inoue, T. and Lee, S. W. (1996), Forced oscillations of a vertical continuous rotor with geometric nonlinearity, *Nonlinear Dynamics*, **11**(2), 107-120.

[4] Luczko, A.(2002), A geometrically non-linear model of rotating shafts with internal resonance and self-excited vibration, *Journal of Sound and Vibration*, **255**(3), 433-456.

[5] Chasalevris, A. C., Papadopoulos, C. A. (2009), A continuous model approach for cross -coupled bending vibrations of a rotor-bearing system with a transverse breathing crack, *Mechanism and Machine Theory*, **44**(6), 1176-1191.

[6] Khanlo, M., Ghayour, M. and Ziaer-Rad, S. (2011), Chaotic vibration analysis of rotating, flexible, continuous shaft-disk system with a rub-impact between the disk and the stator, *Communications in Nonlinear Science and Numerical Simulation*, **16**(1), 566-582.

[7] Khadem, S. E., Shahgholi, M. and Hosseini, S. A. A. (2011), Two-mode combination resonances of an in-extensional rotating shaft with large amplitude, *Nonlinear Dynamics*, **65**(3), 217-233.

[8] Hosseini S. A. A. (2013), Dynamic stability and bifurcation of a nonlinear in-extensional rotating shaft with internal damping, *Nonlinear Dynamics*, **74**(1-2), 345-358.

[9] Guo, D., Chu, F. and Chen, D. (2002), The unbalanced magnetic pull and its effects on vibration in a three-phase generator with eccentric rotor, *Journal of Sound and Vibration*, **254**(2), 297-312.

[10] Wang, Y. F., Huang, L. H. and Li, Y. (2007), Nonlinear vibration and stability of a Jeffcott rotor under unbalanced magnetic excitation, *International Journal of Nonlinear Sciences and Numerical Simulation*, **8**(3), 375-384.

[11] Muszynska, A. (2005), Rotordynamics, Taylor & Francis: Boca Raton.

[12] Szeri, A. (2010), Fluid film lubrication, Cambridge University Press: Cambridge, UK.

[13] Zhao, J. Y., Linnett, I. W. and Mclean, L. J. (1994), Stability and bifurcation of unbalanced response of a squeeze film damped flexible rotor, *Journal of Tribology*, **116**(2), 361-368.
[14] Pagano, S. Rocca, E. and Russo, R. (1995), Dynamic behaviour of tilting-pad journal bearings, Proceedings of the Institution of Mechanical Engineers, *Part J: Journal of Engineering Tribology*, **209**(4), 275-285.
[15] Adiletta, G., Guido, A. R. and Rossi, C. (1996), Chaotic motions of a rigid rotor in short journal bearing, *Nonlinear Dynamics*, **10**(3), 251-269.
[16] Zheng, T. and Hasebe, N. (2000), Nonlinear dynamic behaviors of a complex rotor-bearing system, *Journal of Applied Mechanics*, **67**(3), 485-495.
[17] Chang-Jian, C. W. and Chen, C. K. (2007), Chaos and bifurcation of a flexible rub-impact rotor supported by oil film bearings with nonlinear suspension, *Mechanism and Machine Theory*, **42**(3), 312-333.
[18] Hwang, J. L. and Shiau, T. N. (1991), An application of the generalized polynomial expansion method to nonlinear rotor bearing systems, *Journal of Vibration and Acoustics*, **113**(3), 299-308.
[19] Kim, Y. B. and Noah, S. T. (1996), Quasi-periodic response and stability analysis for a non-linear Jeffcott rotor, *Journal of Sound and Vibration*, **190**(2), 239-253.
[20] Qin, W. Y., Chen, G. R. and Ren, X. M. (2004), Grazing bifurcation in the response of cracked Jeffcott rotor, *Nonlinear Dynamics*, **35**(2), 147-157.
[21] Villa, C. V. S., Sinou, J. J. and Thouverez, F. (2005), The invariant manifold approach applied to nonlinear dynamics of a rotor-bearing system, *European Journal of Mechanics –A/Solids*, **24**(4), 676-689.
[22] Tong, H. Z., Yang, F. H. and Chen, L. H. (2009), Global bifurcations for a rotor-active magnetic bearings system, *Industrial Engineering and Engineering Management, 2009. IEEM 2009. IEEE International Conference on. IEEE*, 2124-2127.
[23] Ding, Q. and Zhang, K. P. (2012), Order reduction and nonlinear behaviors of a continuous rotor system, *Nonlinear Dynamics*, **67**(1), 251-262.
[24] Luo, H. Y. and Wang, Y. F. (2012), Nonlinear vibration of a continuum rotor with transverse electromagnetic and bearing excitations, *Shock and Vibration*, **19**(6), 1297-1314.
[25] Paez-Chavez, J. and Wiercigroch, M. (2013), Bifurcation analysis of periodic orbits of a non-smooth Jeffcott rotor model, *Communica in Nonlinear Science and Numerical Simulation*, **18**(9), 2571-2580.
[26] Luo, A. C. J. (2012), *Continuous dynamical systems*, Higher Education Press: Beijing.
[27] Huang, J. Z. and Luo, A. C. J. (2015), Periodic motions and bifurcation trees in a buckled, nonlinear Jeffcott rotor system, International Journal of Bifurcation and Chaos, 25(1), 155002-1-155002-34.
[28] Meirovitch, L. (2001), Fundamentals of Vibrations, McGraw-Hill: Singapore.
[29] Wan, F. Y., Xu, Q. Y. and Li, S. T. (2004), Vibration analysis of cracked rotor sliding bearing system with rotor–stator rubbing by harmonic wavelet transform, *Journal of Sound and Vibration*, **271**(3-5), 507-518.

Appendix A: Expressions of constants of Eq. (18)

$$p_{\bar{m}}=\frac{H_{12}}{H_1},f_y=\frac{H_{12}}{H_1}G+\frac{\lambda_m A_{10}H_{12}}{H_1}+\frac{\sigma C_{22}H_{13}}{H_1},f_z=\frac{\lambda_m B_{10}H_{12}}{H_1}+\frac{\sigma D_{22}H_{13}}{H_1}.$$
$$\alpha_1=-\frac{\kappa H_3}{H_1}+\lambda_m A_8+\frac{\sigma C_{16}H_{14}}{H_1},\alpha_2=\lambda_m A_9+\frac{\sigma C_{19}H_{14}}{H_1},\alpha_3=\frac{\sigma C_{20}H_{14}}{H_1},\alpha_4=\frac{\sigma C_{21}H_{14}}{H_1},$$
$$\alpha_5=\frac{\lambda_m A_5H_5}{H_1}+\frac{\sigma C_7H_{16}}{H_1},\alpha_6=\frac{\lambda_m A_6H_5}{H_1}+\frac{\sigma C_{10}H_{16}}{H_1},\alpha_7=\frac{\sigma C_{14}H_{16}}{H_1},\alpha_8=\frac{\sigma C_{15}H_{16}}{H_1},$$
$$\alpha_9=\frac{\lambda_m A_7H_5}{H_1}+\frac{\sigma C_{13}H_{16}}{H_1},\alpha_{10}=\frac{\sigma C_{17}H_{16}}{H_1},\alpha_{11}=\frac{\sigma C_{18}H_{16}}{H_1},\alpha_{12}=\frac{\lambda_m A_1H_8}{H_1}+\frac{\sigma C_1H_{19}}{H_1},$$
$$\alpha_{13}=\frac{\lambda_m A_2H_8}{H_1}+\frac{\sigma C_2H_{19}}{H_1},\alpha_{14}=\frac{\lambda_m A_3H_8}{H_1}+\frac{\sigma C_3H_{19}}{H_1},\alpha_{15}=\frac{\sigma C_5H_{19}}{H_1},\alpha_{16}=\frac{\sigma C_6H_{19}}{H_1},$$
$$\alpha_{17}=\frac{\sigma C_8H_{19}}{H_1},\alpha_{18}=\frac{\sigma C_9H_{19}}{H_1},\alpha_{19}=\frac{\lambda_m A_4H_8}{H_1}+\frac{\sigma C_4H_{19}}{H_1},\alpha_{20}=\frac{\sigma C_{11}H_{19}}{H_1},\alpha_{21}=\frac{\sigma C_{12}H_{19}}{H_1}.$$
$$\beta_1=\lambda_m B_8+\frac{\sigma D_{16}H_{14}}{H_1},\beta_2=-\frac{\kappa H_3}{H_1}+\lambda_m B_9+\frac{\sigma D_{19}H_{14}}{H_1},\beta_3=\frac{\sigma D_{20}H_{14}}{H_1},\beta_4=\frac{\sigma D_{21}H_{14}}{H_1},$$
$$\beta_5=\frac{\lambda_m B_5H_5}{H_1}+\frac{\sigma D_7H_{16}}{H_1},\beta_6=\frac{\lambda_m B_6H_5}{H_1}+\frac{\sigma D_{10}H_{16}}{H_1},\beta_7=\frac{\sigma D_{14}H_{16}}{H_1},\beta_8=\frac{\sigma D_{15}H_{16}}{H_1},$$
$$\beta_9=\frac{\lambda_m B_7H_5}{H_1}+\frac{\sigma D_{13}H_{16}}{H_1},\beta_{10}=\frac{\sigma D_{17}H_{16}}{H_1},\beta_{11}=\frac{\sigma D_{18}H_{16}}{H_1},\beta_{12}=\frac{\lambda_m B_1H_8}{H_1}+\frac{\sigma D_1H_{19}}{H_1},$$
$$\beta_{13}=\frac{\lambda_m B_2H_8}{H_1}+\frac{\sigma D_2H_{19}}{H_1},\beta_{14}=\frac{\lambda_m B_3H_8}{H_1}+\frac{\sigma D_3H_{19}}{H_1},\beta_{15}=\frac{\sigma D_5H_{19}}{H_1},\beta_{16}=\frac{\sigma D_6H_{19}}{H_1},$$
$$\beta_{17}=\frac{\sigma D_8H_{19}}{H_1},\beta_{18}=\frac{\sigma D_9H_{19}}{H_1},\beta_{19}=\frac{\lambda_m B_4H_8}{H_1}+\frac{\sigma D_4H_{19}}{H_1},\beta_{20}=\frac{\sigma D_{11}H_{19}}{H_1},\beta_{21}=\frac{\sigma D_{12}H_{19}}{H_1}.$$

Appendix B: Expressions of constants of Eqs. (49)∼(54)

$$f_{1,1}^{(0)}=f_{2,1}^{(0)}=(a_{1,0}^{(m)})^2+\sum_{l=1}^{N}\sum_{j=1}^{N}\sum_{i=1}^{N}[\frac{1}{2N}b_{1,l/m}b_{1,j/m}\delta_{l-j}^0+\frac{1}{2N}c_{1,l/m}c_{1,j/m}\delta_{l-j}^0]$$
$$f_{1,2}^{(0)}=f_{2,2}^{(0)}=a_{1,0}^{(m)}a_{2,0}^{(m)}+\sum_{l=1}^{N}\sum_{j=1}^{N}\sum_{i=1}^{N}[\frac{1}{2N}b_{1,l/m}b_{2,j/m}\delta_{l-j}^0+\frac{1}{2N}c_{1,l/m}c_{2,j/m}\delta_{l-j}^0]$$
$$f_{1,3}^{(0)}=f_{2,3}^{(0)}=a_{1,0}^{(m)}\dot{a}_{1,0}^{(m)}+\sum_{l=1}^{N}\sum_{j=1}^{N}\sum_{i=1}^{N}[\frac{1}{2N}b_{1,l/m}(\dot{b}_{1,j/m}+\frac{j\Omega}{m}c_{1,j/m})\delta_{l-j}^0+\frac{1}{2N}c_{1,l/m}(\dot{c}_{1,j/m}-\frac{j\Omega}{m}b_{1,j/m})\delta_{l-j}^0]$$
$$f_{1,4}^{(0)}=f_{2,4}^{(0)}=a_{1,0}^{(m)}\dot{a}_{2,0}^{(m)}+\sum_{l=1}^{N}\sum_{j=1}^{N}\sum_{i=1}^{N}[\frac{1}{2N}b_{1,l/m}(\dot{b}_{2,j/m}+\frac{j\Omega}{m}c_{2,j/m})\delta_{l-j}^0+\frac{1}{2N}c_{1,l/m}(\dot{c}_{2,j/m}-\frac{j\Omega}{m}b_{2,j/m})\delta_{l-j}^0]$$
$$f_{1,4}^{(0)}=f_{2,4}^{(0)}=a_{1,0}^{(m)}\dot{a}_{2,0}^{(m)}+\sum_{l=1}^{N}\sum_{j=1}^{N}\sum_{i=1}^{N}[\frac{1}{2N}b_{1,l/m}(\dot{b}_{2,j/m}+\frac{j\Omega}{m}c_{2,j/m})\delta_{l-j}^0+\frac{1}{2N}c_{1,l/m}(\dot{c}_{2,j/m}-\frac{j\Omega}{m}b_{2,j/m})\delta_{l-j}^0]$$
$$f_{1,5}^{(0)}=f_{2,5}^{(0)}=(a_{2,0}^{(m)})^2+\sum_{l=1}^{N}\sum_{j=1}^{N}\sum_{i=1}^{N}[\frac{1}{2N}b_{2,l/m}b_{2,j/m}\delta_{l-j}^0+\frac{1}{2N}c_{2,l/m}c_{2,j/m}\delta_{l-j}^0]$$
$$f_{1,5}^{(0)}=f_{2,5}^{(0)}=(a_{2,0}^{(m)})^2+\sum_{l=1}^{N}\sum_{j=1}^{N}\sum_{i=1}^{N}[\frac{1}{2N}b_{2,l/m}b_{2,j/m}\delta_{l-j}^0+\frac{1}{2N}c_{2,l/m}c_{2,j/m}\delta_{l-j}^0]$$

$$f_{1,6}^{(0)} = f_{2,6}^{(0)} = a_{2,0}^{(m)}\dot{a}_{1,0}^{(m)} + \sum_{l=1}^{N}\sum_{j=1}^{N}\sum_{i=1}^{N}[\frac{1}{2N}b_{2,l/m}(\dot{b}_{1,j/m} + \frac{j\Omega}{m}c_{1,j/m})\delta_{l-j}^{0} + \frac{1}{2N}c_{2,l/m}(\dot{c}_{1,j/m} - \frac{j\Omega}{m}b_{1,j/m})\delta_{l-j}^{0}]$$

$$f_{1,7}^{(0)} = f_{2,7}^{(0)} = a_{2,0}^{(m)}\dot{a}_{2,0}^{(m)} + \sum_{l=1}^{N}\sum_{j=1}^{N}\sum_{i=1}^{N}[\frac{1}{2N}b_{2,l/m}(\dot{b}_{2,j/m} + \frac{j\Omega}{m}c_{2,j/m})\delta_{l-j}^{0} + \frac{1}{2N}c_{2,l/m}(\dot{c}_{2,j/m} - \frac{j\Omega}{m}b_{2,j/m})\delta_{l-j}^{0}]$$

$$\begin{aligned}f_{1,8}^{(0)} = f_{2,8}^{(0)} &= (a_{1,0}^{(m)})^3 + \sum_{l=1}^{N}\sum_{j=1}^{N}\sum_{i=1}^{N}[\frac{3}{2N}a_{1,0}^{(m)}b_{1,l/m}b_{1,j/m}\delta_{l-j}^{0} + \frac{3}{2N}a_{1,0}^{(m)}c_{1,l/m}c_{1,j/m}\delta_{l-j}^{0}\\ &+\frac{1}{4}b_{1,l/m}b_{1,j/m}b_{1,i/m}(\delta_{l-j-i}^{0} + \delta_{l-j+i}^{0} + \delta_{l+j-i}^{0}) + \frac{3}{4}c_{1,l/m}c_{1,j/m}b_{1,i/m}(\delta_{l-j-i}^{0} + \delta_{l-j+i}^{0} - \delta_{l+j-i}^{0})]\end{aligned}$$

$$\begin{aligned}f_{1,9}^{(0)} = f_{2,9}^{(0)} &= (a_{1,0}^{(m)})^2 a_{2,0}^{(m)} + \sum_{l=1}^{N}\sum_{j=1}^{N}\sum_{i=1}^{N}[\frac{1}{N}a_{1,0}^{(m)}b_{1,l/m}b_{2,j/m}\delta_{l-j}^{0} + \frac{1}{N}a_{1,0}^{(m)}c_{1,l/m}c_{2,j/m}\delta_{l-j}^{0}\\ &+\frac{1}{2N}a_{2,0}^{(m)}b_{1,l/m}b_{1,j/m}\delta_{l-j}^{0} + \frac{1}{2N}a_{2,0}^{(m)}c_{1,l/m}c_{1,j/m}\delta_{l-j}^{0} + \frac{1}{4}b_{1,l/m}b_{1,j/m}b_{2,i/m}(\delta_{l-j-i}^{0} + \delta_{l-j+i}^{0} + \delta_{l+j-i}^{0})\\ &+\frac{1}{4}c_{1,l/m}c_{1,j/m}b_{2,i/m}(\delta_{l-j-i}^{0} + \delta_{l-j+i}^{0} - \delta_{l+j-i}^{0}) + \frac{1}{2}b_{1,l/m}c_{1,j/m}c_{2,i/m}(-\delta_{l-j-i}^{0} + \delta_{l-j+i}^{0} + \delta_{l+j-i}^{0})]\end{aligned}$$

$$\begin{aligned}f_{1,10}^{(0)} = f_{2,10}^{(0)} &= a_{1,0}^{(m)}(a_{2,0}^{(m)})^2 + \sum_{l=1}^{N}\sum_{j=1}^{N}\sum_{i=1}^{N}[\frac{1}{2N}a_{1,0}^{(m)}b_{2,l/m}b_{2,j/m}\delta_{l-j}^{0} + \frac{1}{2N}a_{1,0}^{(m)}c_{2,l/m}c_{2,j/m}\delta_{l-j}^{0}\\ &+\frac{1}{N}a_{2,0}^{(m)}b_{1,l/m}b_{2,j/m}\delta_{l-j}^{0} + \frac{1}{N}a_{2,0}^{(m)}c_{1,l/m}c_{2,j/m}\delta_{l-j}^{0}\\ &+\frac{1}{4}b_{1,l/m}b_{2,j/m}b_{2,i/m}(\delta_{l-j-i}^{0} + \delta_{l-j+i}^{0} + \delta_{l+j-i}^{0}) + \frac{1}{4}c_{1,l/m}c_{2,j/m}b_{2,i/m}(\delta_{l-j-i}^{0} + \delta_{l-j+i}^{0} - \delta_{l+j-i}^{0})\\ &+\frac{1}{4}b_{1,l/m}c_{2,j/m}c_{2,i/m}(-\delta_{l-j-i}^{0} + \delta_{l-j+i}^{0} + \delta_{l+j-i}^{0}) + \frac{1}{4}c_{1,l/m}b_{2,j/m}c_{2,i/m}(\delta_{l-j-i}^{0} - \delta_{l-j+i}^{0} + \delta_{l+j-i}^{0})]\end{aligned}$$

$$\begin{aligned}f_{1,11}^{(0)} = f_{2,11}^{(0)} &= (a_{1,0}^{(m)})^2\dot{a}_{1,0}^{(m)}\\ &+\sum_{l=1}^{N}\sum_{j=1}^{N}\sum_{i=1}^{N}[\frac{1}{N}a_{1,0}^{(m)}b_{1,l/m}(\dot{b}_{1,j/m} + \frac{j\Omega}{m}c_{1,j/m})\delta_{l-j}^{0} + \frac{1}{N}a_{1,0}^{(m)}c_{1,l/m}(\dot{c}_{1,j/m} - \frac{j\Omega}{m}b_{1,j/m})\delta_{l-j}^{0}\\ &+\frac{1}{2N}\dot{a}_{1,0}^{(m)}b_{1,l/m}b_{1,j/m}\delta_{l-j}^{0} + \frac{1}{2N}\dot{a}_{1,0}^{(m)}c_{1,l/m}c_{1,j/m}\delta_{l-j}^{0} + \frac{1}{4}b_{1,l/m}b_{1,j/m}(\dot{b}_{1,i/m} + \frac{i\Omega}{m}c_{1,i/m})(\delta_{l-j-i}^{0}\\ &+\delta_{l-j+i}^{0} + \delta_{l+j-i}^{0}) + \frac{1}{4}c_{1,l/m}c_{1,j/m}(\dot{b}_{1,i/m} + \frac{i\Omega}{m}c_{1,i/m})(\delta_{l-j-i}^{0} + \delta_{l-j+i}^{0} - \delta_{l+j-i}^{0})\\ &+\frac{1}{2}b_{1,l/m}c_{1,j/m}(\dot{c}_{1,i/m} - \frac{i\Omega}{m}b_{1,i/m})(-\delta_{l-j-i}^{0} + \delta_{l-j+i}^{0} + \delta_{l+j-i}^{0})]\end{aligned}$$

$$\begin{aligned}f_{1,12}^{(0)} = f_{2,12}^{(0)} &= (a_{1,0}^{(m)})^2\dot{a}_{2,0}^{(m)}\\ &+\sum_{l=1}^{N}\sum_{j=1}^{N}\sum_{i=1}^{N}[\frac{1}{N}a_{1,0}^{(m)}b_{1,l/m}(\dot{b}_{2,j/m} + \frac{j\Omega}{m}c_{2,j/m})\delta_{l-j}^{0} + \frac{1}{N}a_{1,0}^{(m)}c_{1,l/m}(\dot{c}_{2,j/m} - \frac{j\Omega}{m}b_{2,j/m})\delta_{l-j}^{0}\\ &+\frac{1}{2N}\dot{a}_{2,0}^{(m)}b_{1,l/m}b_{1,j/m}\delta_{l-j}^{0} + \frac{1}{2N}\dot{a}_{2,0}^{(m)}c_{1,l/m}c_{1,j/m}\delta_{l-j}^{0}\\ &+\frac{1}{4}b_{1,l/m}b_{1,j/m}(\dot{b}_{2,i/m} + \frac{i\Omega}{m}c_{2,i/m})(\delta_{l-j-i}^{0} + \delta_{l-j+i}^{0} + \delta_{l+j-i}^{0})\\ &+\frac{1}{4}c_{1,l/m}c_{1,j/m}(\dot{b}_{2,i/m} + \frac{i\Omega}{m}c_{2,i/m})(\delta_{l-j-i}^{0} + \delta_{l-j+i}^{0} - \delta_{l+j-i}^{0})\\ &+\frac{1}{2}b_{1,l/m}c_{1,j/m}(\dot{c}_{2,i/m} - \frac{i\Omega}{m}b_{2,i/m})(-\delta_{l-j-i}^{0} + \delta_{l-j+i}^{0} + \delta_{l+j-i}^{0})]\end{aligned}$$

$$
\begin{aligned}
f_{1,13}^{(0)} =& f_{2,13}^{(0)} = a_{1,0}^{(m)} a_{2,0}^{(m)} \dot{a}_{1,0}^{(m)} \\
&+ \sum_{l=1}^{N}\sum_{j=1}^{N}\sum_{i=1}^{N} [\frac{1}{2N} a_{1,0}^{(m)} b_{2,l/m} (\dot{b}_{1,j/m} + \frac{j\Omega}{m} c_{1,j/m}) \delta_{l-j}^{0} + \frac{1}{2N} a_{1,0}^{(m)} c_{2,l/m} (\dot{c}_{1,j/m} - \frac{j\Omega}{m} b_{1,j/m}) \delta_{l-j}^{0} \\
&+ \frac{1}{2N} a_{2,0}^{(m)} b_{1,l/m} (\dot{b}_{1,j/m} + \frac{j\Omega}{m} c_{1,j/m}) \delta_{l-j}^{0} + \frac{1}{2N} a_{2,0}^{(m)} c_{1,l/m} (\dot{c}_{1,j/m} - \frac{j\Omega}{m} b_{1,j/m}) \delta_{l-j}^{0} \\
&+ \frac{1}{2N} \dot{a}_{1,0}^{(m)} b_{1,l/m} b_{2,j/m} \delta_{l-j}^{0} + \frac{1}{2N} \dot{a}_{1,0}^{(m)} c_{1,l/m} c_{2,j/m} \delta_{l-j}^{0} \\
&+ \frac{1}{4} b_{1,l/m} b_{2,j/m} (\dot{b}_{1,i/m} + \frac{i\Omega}{m} c_{1,i/m}) (\delta_{l-j-i}^{0} + \delta_{l-j+i}^{0} + \delta_{l+j-i}^{0}) \\
&+ \frac{1}{4} c_{1,l/m} c_{2,j/m} (\dot{b}_{1,i/m} + \frac{i\Omega}{m} c_{1,i/m}) (\delta_{l-j-i}^{0} + \delta_{l-j+i}^{0} - \delta_{l+j-i}^{0}) \\
&+ \frac{1}{4} b_{1,l/m} c_{2,j/m} (\dot{c}_{1,i/m} - \frac{i\Omega}{m} b_{1,i/m}) (-\delta_{l-j-i}^{0} + \delta_{l-j+i}^{0} + \delta_{l+j-i}^{0}) \\
&+ \frac{1}{4} c_{1,l/m} b_{2,j/m} (\dot{c}_{1,i/m} - \frac{i\Omega}{m} b_{1,i/m}) (\delta_{l-j-i}^{0} - \delta_{l-j+i}^{0} + \delta_{l+j-i}^{0})] \\
f_{1,14}^{(0)} =& f_{2,14}^{(0)} = a_{1,0}^{(m)} a_{2,0}^{(m)} \dot{a}_{2,0}^{(m)} \\
&+ \sum_{l=1}^{N}\sum_{j=1}^{N}\sum_{i=1}^{N} [\frac{1}{2N} a_{1,0}^{(m)} b_{2,l/m} (\dot{b}_{2,j/m} + \frac{j\Omega}{m} c_{2,j/m}) \delta_{l-j}^{0} + \frac{1}{2N} a_{1,0}^{(m)} c_{2,l/m} (\dot{c}_{2,j/m} - \frac{j\Omega}{m} b_{2,j/m}) \delta_{l-j}^{0} \\
&+ \frac{1}{2N} a_{2,0}^{(m)} b_{1,l/m} (\dot{b}_{2,j/m} + \frac{j\Omega}{m} c_{2,j/m}) \delta_{l-j}^{0} + \frac{1}{2N} a_{2,0}^{(m)} c_{1,l/m} (\dot{c}_{2,j/m} - \frac{j\Omega}{m} b_{2,j/m}) \delta_{l-j}^{0} \\
&+ \frac{1}{2N} \dot{a}_{2,0}^{(m)} b_{1,l/m} b_{2,j/m} \delta_{l-j}^{0} + \frac{1}{2N} \dot{a}_{2,0}^{(m)} c_{1,l/m} c_{2,j/m} \delta_{l-j}^{0} \\
&+ \frac{1}{4} b_{1,l/m} b_{2,j/m} (\dot{b}_{2,i/m} + \frac{i\Omega}{m} c_{2,i/m}) (\delta_{l-j-i}^{0} + \delta_{l-j+i}^{0} + \delta_{l+j-i}^{0}) \\
&+ \frac{1}{4} c_{1,l/m} c_{2,j/m} (\dot{b}_{2,i/m} + \frac{i\Omega}{m} c_{2,i/m}) (\delta_{l-j-i}^{0} + \delta_{l-j+i}^{0} - \delta_{l+j-i}^{0}) \\
&+ \frac{1}{4} b_{1,l/m} c_{2,j/m} (\dot{c}_{2,i/m} - \frac{i\Omega}{m} b_{2,i/m}) (-\delta_{l-j-i}^{0} + \delta_{l-j+i}^{0} + \delta_{l+j-i}^{0}) \\
&+ \frac{1}{4} c_{1,l/m} b_{2,j/m} (\dot{c}_{2,i/m} - \frac{i\Omega}{m} b_{2,i/m}) (\delta_{l-j-i}^{0} - \delta_{l-j+i}^{0} + \delta_{l+j-i}^{0})] \\
f_{1,15}^{(0)} =& f_{2,15}^{(0)} = (a_{2,0}^{(m)})^3 + \sum_{l=1}^{N}\sum_{j=1}^{N}\sum_{i=1}^{N} [\frac{3}{2N} a_{2,0}^{(m)} b_{2,l/m} b_{2,j/m} \delta_{l-j}^{0} + \frac{3}{2N} a_{2,0}^{(m)} c_{2,l/m} c_{2,j/m} \delta_{l-j}^{0} \\
&+ \frac{1}{4} b_{2,l/m} b_{2,j/m} b_{2,i/m} (\delta_{l-j-i}^{0} + \delta_{l-j+i}^{0} + \delta_{l+j-i}^{0}) + \frac{3}{4} c_{2,l/m} c_{2,j/m} b_{2,i/m} (\delta_{l-j-i}^{0} + \delta_{l-j+i}^{0} - \delta_{l+j-i}^{0})] \\
f_{1,16}^{(0)} =& f_{2,16}^{(0)} = (a_{2,0}^{(m)})^2 \dot{a}_{1,0}^{(m)} \\
&+ \sum_{l=1}^{N}\sum_{j=1}^{N}\sum_{i=1}^{N} [\frac{1}{N} a_{2,0}^{(m)} b_{2,l/m} (\dot{b}_{1,j/m} + \frac{j\Omega}{m} c_{1,j/m}) \delta_{l-j}^{0} + \frac{1}{N} a_{2,0}^{(m)} c_{2,l/m} (\dot{c}_{1,j/m} - \frac{j\Omega}{m} b_{1,j/m}) \delta_{l-j}^{0} \\
&+ \frac{1}{2N} \dot{a}_{1,0}^{(m)} b_{2,l/m} b_{2,j/m} \delta_{l-j}^{0} + \frac{1}{2N} \dot{a}_{1,0}^{(m)} c_{2,l/m} c_{2,j/m} \delta_{l-j}^{0} \\
&+ \frac{1}{4} b_{2,l/m} b_{2,j/m} (\dot{b}_{1,i/m} + \frac{i\Omega}{m} c_{1,i/m}) (\delta_{l-j-i}^{0} + \delta_{l-j+i}^{0} + \delta_{l+j-i}^{0}) \\
&+ \frac{1}{4} c_{2,l/m} c_{2,j/m} (\dot{b}_{1,i/m} + \frac{i\Omega}{m} c_{1,i/m}) (\delta_{l-j-i}^{0} + \delta_{l-j+i}^{0} - \delta_{l+j-i}^{0}) \\
&+ \frac{1}{2} b_{2,l/m} c_{2,j/m} (\dot{c}_{1,i/m} - \frac{i\Omega}{m} b_{1,i/m}) (-\delta_{l-j-i}^{0} + \delta_{l-j+i}^{0} + \delta_{l+j-i}^{0})]
\end{aligned}
$$

$$
\begin{aligned}
f_{1,17}^{(0)} =& f_{2,17}^{(0)} = (a_{2,0}^{(m)})^2 \dot{a}_{2,0}^{(m)} \\
&+ \sum_{l=1}^{N}\sum_{j=1}^{N}\sum_{i=1}^{N}[\frac{1}{N}a_{2,0}^{(m)} b_{2,l/m}(\dot{b}_{2,j/m} + \frac{j\Omega}{m}c_{2,j/m})\delta_{l-j}^{0} + \frac{1}{N}a_{2,0}^{(m)} c_{2,l/m}(\dot{c}_{2,j/m} - \frac{j\Omega}{m}b_{2,j/m})\delta_{l-j}^{0} \\
&+ \frac{1}{2N}\dot{a}_{2,0}^{(m)} b_{2,l/m} b_{2,j/m}\delta_{l-j}^{0} + \frac{1}{2N}\dot{a}_{2,0}^{(m)} c_{2,l/m} c_{2,j/m}\delta_{l-j}^{0} \\
&+ \frac{1}{4}b_{2,l/m} b_{2,j/m}(\dot{b}_{2,i/m} + \frac{i\Omega}{m}c_{2,i/m})(\delta_{l-j-i}^{0} + \delta_{l-j+i}^{0} + \delta_{l+j-i}^{0}) \\
&+ \frac{1}{4}c_{2,l/m} c_{2,j/m}(\dot{b}_{2,i/m} + \frac{i\Omega}{m}c_{2,i/m})(\delta_{l-j-i}^{0} + \delta_{l-j+i}^{0} - \delta_{l+j-i}^{0}) \\
&+ \frac{1}{2}b_{2,l/m} c_{2,j/m}(\dot{c}_{2,i/m} - \frac{i\Omega}{m}b_{2,i/m})(-\delta_{l-j-i}^{0} + \delta_{l-j+i}^{0} + \delta_{l+j-i}^{0})] \\
f_{1,1k}^{(c)} =& f_{2,1k}^{(c)} = 2a_{1,0}^{(m)} b_{1,k/m} + \sum_{l=1}^{N}\sum_{j=1}^{N}\sum_{i=1}^{N}[\frac{1}{2N}b_{1,l/m} b_{1,j/m}(\delta_{l+j}^{k} + \delta_{|l-j|}^{k}) + \frac{1}{2N}c_{1,l/m} c_{1,j/m}(-\delta_{l+j}^{k} + \delta_{|l-j|}^{k})] \\
f_{1,2k}^{(c)} =& f_{2,2k}^{(c)} = a_{1,0}^{(m)} b_{2,k/m} + a_{2,0}^{(m)} b_{1,k/m} + \sum_{l=1}^{N}\sum_{j=1}^{N}\sum_{i=1}^{N}[\frac{1}{2N}b_{1,l/m} b_{2,j/m}(\delta_{l+j}^{k} + \delta_{|l-j|}^{k}) \\
&+ \frac{1}{2N}c_{1,l/m} c_{2,j/m}(-\delta_{l+j}^{k} + \delta_{|l-j|}^{k})] \\
f_{1,3k}^{(c)} =& f_{2,3k}^{(c)} = a_{1,0}^{(m)}(\dot{b}_{1,k/m} + \frac{k\Omega}{m}c_{1,k/m}) + \dot{a}_{1,0}^{(m)} b_{1,k/m} \\
&+ \sum_{l=1}^{N}\sum_{j=1}^{N}\sum_{i=1}^{N}[\frac{1}{2N}b_{1,l/m}(\dot{b}_{1,j/m} + \frac{j\Omega}{m}c_{1,j/m})(\delta_{l+j}^{k} + \delta_{|l-j|}^{k}) \\
&+ \frac{1}{2N}c_{1,l/m}(\dot{c}_{1,j/m} - \frac{j\Omega}{m}b_{1,j/m})(-\delta_{l+j}^{k} + \delta_{|l-j|}^{k})] \\
f_{1,4k}^{(c)} =& f_{2,4k}^{(c)} = a_{1,0}^{(m)}(\dot{b}_{2,k/m} + \frac{k\Omega}{m}c_{2,k/m}) + \dot{a}_{2,0}^{(m)} b_{1,k/m} \\
&+ \sum_{l=1}^{N}\sum_{j=1}^{N}\sum_{i=1}^{N}[\frac{1}{2N}b_{1,l/m}(\dot{b}_{2,j/m} + \frac{j\Omega}{m}c_{2,j/m})(\delta_{l+j}^{k} + \delta_{|l-j|}^{k}) \\
&+ \frac{1}{2N}c_{1,l/m}(\dot{c}_{2,j/m} - \frac{j\Omega}{m}b_{2,j/m})(-\delta_{l+j}^{k} + \delta_{|l-j|}^{k})] \\
f_{1,5k}^{(c)} =& f_{2,5k}^{(c)} = 2a_{2,0}^{(m)} b_{2,k/m} \\
&+ \sum_{l=1}^{N}\sum_{j=1}^{N}\sum_{i=1}^{N}[\frac{1}{2N}b_{2,l/m} b_{2,j/m}(\delta_{l+j}^{k} + \delta_{|l-j|}^{k}) + \frac{1}{2N}c_{2,l/m} c_{2,j/m}(-\delta_{l+j}^{k} + \delta_{|l-j|}^{k})] \\
f_{1,6k}^{(c)} =& f_{2,6k}^{(c)} = a_{2,0}^{(m)}(\dot{b}_{1,k/m} + \frac{k\Omega}{m}c_{1,k/m}) + \dot{a}_{1,0}^{(m)} b_{2,k/m} \\
&+ \sum_{l=1}^{N}\sum_{j=1}^{N}\sum_{i=1}^{N}[\frac{1}{2N}b_{2,l/m}(\dot{b}_{1,j/m} + \frac{j\Omega}{m}c_{1,j/m})(\delta_{l+j}^{k} + \delta_{|l-j|}^{k}) \\
&+ \frac{1}{2N}c_{2,l/m}(\dot{c}_{1,j/m} - \frac{j\Omega}{m}b_{1,j/m})(-\delta_{l+j}^{k} + \delta_{|l-j|}^{k})]
\end{aligned}
$$

$$
\begin{aligned}
f_{1,7k}^{(c)} =& f_{2,7k}^{(c)} = a_{2,0}^{(m)}(\dot{b}_{2,k/m} + \frac{k\Omega}{m}c_{2,k/m}) + \dot{a}_{2,0}^{(m)}b_{2,k/m} \\
&+ \sum_{l=1}^{N}\sum_{j=1}^{N}\sum_{i=1}^{N}[\frac{1}{2N}b_{2,l/m}(\dot{b}_{2,j/m} + \frac{j\Omega}{m}c_{2,j/m})(\delta_{l+j}^{k} + \delta_{|l-j|}^{k}) \\
&+ \frac{1}{2N}c_{2,l/m}(\dot{c}_{2,j/m} - \frac{j\Omega}{m}b_{2,j/m})(-\delta_{l+j}^{k} + \delta_{|l-j|}^{k})] \\
f_{1,8k}^{(c)} =& f_{2,8k}^{(c)} = 3(a_{1,0}^{(m)})^2 b_{1,k/m} + \sum_{l=1}^{N}\sum_{j=1}^{N}\sum_{i=1}^{N}[\frac{3}{2N}a_{1,0}^{(m)}b_{1,l/m}b_{1,j/m}(\delta_{l+j}^{k} + \delta_{|l-j|}^{k}) \\
&+ \frac{3}{2N}a_{1,0}^{(m)}c_{1,l/m}c_{1,j/m}(-\delta_{l+j}^{k} + \delta_{|l-j|}^{k}) \\
&+ \frac{1}{4}b_{1,l/m}b_{1,j/m}b_{1,i/m}(\delta_{l+j+i}^{k} + \delta_{|l-j+i|}^{k} + \delta_{|l+j-i|}^{k} + \delta_{|l-j-i|}^{k}) \\
&+ \frac{3}{4}c_{1,l/m}c_{1,j/m}b_{1,i/m}(-\delta_{l+j+i}^{k} + \delta_{|l-j+i|}^{k} - \delta_{|l+j-i|}^{k} + \delta_{|l-j-i|}^{k})] \\
f_{1,9k}^{(c)} =& f_{2,9k}^{(c)} = (a_{1,0}^{(m)})^2 b_{2,k/m} + 2a_{1,0}^{(m)}a_{2,0}^{(m)}b_{1,k/m} \\
&+ \sum_{l=1}^{N}\sum_{j=1}^{N}\sum_{i=1}^{N}[\frac{1}{N}a_{1,0}^{(m)}b_{1,l/m}b_{2,j/m}(\delta_{l+j}^{k} + \delta_{|l-j|}^{k}) + \frac{1}{N}a_{1,0}^{(m)}c_{1,l/m}c_{2,j/m}(-\delta_{l+j}^{k} + \delta_{|l-j|}^{k}) \\
&+ \frac{1}{2N}a_{2,0}^{(m)}b_{1,l/m}b_{1,j/m}(\delta_{l+j}^{k} + \delta_{|l-j|}^{k}) + \frac{1}{2N}a_{2,0}^{(m)}c_{1,l/m}c_{1,j/m}(-\delta_{l+j}^{k} + \delta_{|l-j|}^{k}) \\
&+ \frac{1}{4}b_{1,l/m}b_{1,j/m}b_{2,i/m}(\delta_{l+j+i}^{k} + \delta_{|l-j+i|}^{k} + \delta_{|l+j-i|}^{k} + \delta_{|l-j-i|}^{k}) \\
&+ \frac{1}{4}c_{1,l/m}c_{1,j/m}b_{2,i/m}(-\delta_{l+j+i}^{k} + \delta_{|l-j+i|}^{k} - \delta_{|l+j-i|}^{k} + \delta_{|l-j-i|}^{k}) \\
&+ \frac{1}{2}b_{1,l/m}c_{1,j/m}c_{2,i/m}(-\delta_{l+j+i}^{k} + \delta_{|l-j+i|}^{k} + \delta_{|l+j-i|}^{k} - \delta_{|l-j-i|}^{k})] \\
f_{1,10k}^{(c)} =& f_{2,10k}^{(c)} = 2a_{1,0}^{(m)}a_{2,0}^{(m)}b_{2,k/m} + (a_{2,0}^{(m)})^2 b_{1,k/m} \\
&+ \sum_{l=1}^{N}\sum_{j=1}^{N}\sum_{i=1}^{N}[\frac{1}{2N}a_{1,0}^{(m)}b_{2,l/m}b_{2,j/m}(\delta_{l+j}^{k} + \delta_{|l-j|}^{k}) + \frac{1}{2N}a_{1,0}^{(m)}c_{2,l/m}c_{2,j/m}(-\delta_{l+j}^{k} + \delta_{|l-j|}^{k}) \\
&+ \frac{1}{N}a_{2,0}^{(m)}b_{1,l/m}b_{2,j/m}(\delta_{l+j}^{k} + \delta_{|l-j|}^{k}) + \frac{1}{N}a_{2,0}^{(m)}c_{1,l/m}c_{2,j/m}(-\delta_{l+j}^{k} + \delta_{|l-j|}^{k}) \\
&+ \frac{1}{4}b_{1,l/m}b_{2,j/m}b_{2,i/m}(\delta_{l+j+i}^{k} + \delta_{|l-j+i|}^{k} + \delta_{|l+j-i|}^{k} + \delta_{|l-j-i|}^{k}) \\
&+ \frac{1}{4}c_{1,l/m}c_{2,j/m}b_{2,i/m}(-\delta_{l+j+i}^{k} + \delta_{|l-j+i|}^{k} - \delta_{|l+j-i|}^{k} + \delta_{|l-j-i|}^{k}) \\
&+ \frac{1}{4}b_{1,l/m}c_{2,j/m}c_{2,i/m}(-\delta_{l+j+i}^{k} + \delta_{|l-j+i|}^{k} + \delta_{|l+j-i|}^{k} - \delta_{|l-j-i|}^{k}) \\
&+ \frac{1}{4}c_{1,l/m}b_{2,j/m}c_{2,i/m}(-\delta_{l+j+i}^{k} - \delta_{|l-j+i|}^{k} + \delta_{|l+j-i|}^{k} + \delta_{|l-j-i|}^{k})] \\
f_{1,11k}^{(c)} =& f_{2,11k}^{(c)} = (a_{1,0}^{(m)})^2(\dot{b}_{1,k/m} + \frac{k\Omega}{m}c_{1,k/m}) + 2a_{1,0}^{(m)}\dot{a}_{1,0}^{(m)}b_{1,k/m} \\
&+ \sum_{l=1}^{N}\sum_{j=1}^{N}\sum_{i=1}^{N}[\frac{1}{N}a_{1,0}^{(m)}b_{1,l/m}(\dot{b}_{1,j/m} + \frac{j\Omega}{m}c_{1,j/m})(\delta_{l+j}^{k} + \delta_{|l-j|}^{k})
\end{aligned}
$$

$$
\begin{aligned}
&+\frac{1}{N}a_{1,0}^{(m)}c_{1,l/m}(\dot{c}_{1,j/m}-\frac{j\Omega}{m}b_{1,j/m})(-\delta_{l+j}^{k}+\delta_{|l-j|}^{k})\\
&+\frac{1}{2N}\dot{a}_{1,0}^{(m)}b_{1,l/m}b_{1,j/m}(\delta_{l+j}^{k}+\delta_{|l-j|}^{k})+\frac{1}{2N}\dot{a}_{1,0}^{(m)}c_{1,l/m}c_{1,j/m}(-\delta_{l+j}^{k}+\delta_{|l-j|}^{k})\\
&+\frac{1}{4}b_{1,l/m}b_{1,j/m}(\dot{b}_{1,i/m}+\frac{i\Omega}{m}c_{1,i/m})(\delta_{l+j+i}^{k}+\delta_{|l-j+i|}^{k}+\delta_{|l+j-i|}^{k}+\delta_{|l-j-i|}^{k})\\
&+\frac{1}{4}c_{1,l/m}c_{1,j/m}(\dot{b}_{1,i/m}+\frac{i\Omega}{m}c_{1,i/m})(-\delta_{l+j+i}^{k}+\delta_{|l-j+i|}^{k}-\delta_{|l+j-i|}^{k}+\delta_{|l-j-i|}^{k})\\
&+\frac{1}{2}b_{1,l/m}c_{1,j/m}(\dot{c}_{1,i/m}-\frac{i\Omega}{m}b_{1,i/m})(-\delta_{l+j+i}^{k}+\delta_{|l-j+i|}^{k}+\delta_{|l+j-i|}^{k}-\delta_{|l-j-i|}^{k})]\\
f_{1,12k}^{(c)}=&f_{2,12k}^{(c)}=(a_{1,0}^{(m)})^{2}(\dot{b}_{2,k/m}+\frac{k\Omega}{m}c_{2,k/m})+2a_{1,0}^{(m)}\dot{a}_{2,0}^{(m)}b_{1,k/m}\\
&+\sum_{l=1}^{N}\sum_{j=1}^{N}\sum_{i=1}^{N}[\frac{1}{N}a_{1,0}^{(m)}b_{1,l/m}(\dot{b}_{2,j/m}+\frac{j\Omega}{m}c_{2,j/m})(\delta_{l+j}^{k}+\delta_{|l-j|}^{k})\\
&+\frac{1}{N}a_{1,0}^{(m)}c_{1,l/m}(\dot{c}_{2,j/m}-\frac{j\Omega}{m}b_{2,j/m})(-\delta_{l+j}^{k}+\delta_{|l-j|}^{k})\\
&+\frac{1}{2N}\dot{a}_{2,0}^{(m)}b_{1,l/m}b_{1,j/m}(\delta_{l+j}^{k}+\delta_{|l-j|}^{k})+\frac{1}{2N}\dot{a}_{2,0}^{(m)}c_{1,l/m}c_{1,j/m}(-\delta_{l+j}^{k}+\delta_{|l-j|}^{k})\\
&+\frac{1}{4}b_{1,l/m}b_{1,j/m}(\dot{b}_{2,i/m}+\frac{i\Omega}{m}c_{2,i/m})(\delta_{l+j+i}^{k}+\delta_{|l-j+i|}^{k}+\delta_{|l+j-i|}^{k}+\delta_{|l-j-i|}^{k})\\
&+\frac{1}{4}c_{1,l/m}c_{1,j/m}(\dot{b}_{2,i/m}+\frac{i\Omega}{m}c_{2,i/m})(-\delta_{l+j+i}^{k}+\delta_{|l-j+i|}^{k}-\delta_{|l+j-i|}^{k}+\delta_{|l-j-i|}^{k})\\
&+\frac{1}{2}b_{1,l/m}c_{1,j/m}(\dot{c}_{2,i/m}-\frac{i\Omega}{m}b_{2,i/m})(-\delta_{l+j+i}^{k}+\delta_{|l-j+i|}^{k}+\delta_{|l+j-i|}^{k}-\delta_{|l-j-i|}^{k})]\\
f_{1,13k}^{(c)}=&f_{2,13k}^{(c)}=a_{1,0}^{(m)}a_{2,0}^{(m)}(\dot{b}_{1,k/m}+\frac{k\Omega}{m}c_{1,k/m})+a_{1,0}^{(m)}\dot{a}_{1,0}^{(m)}b_{2,k/m}+a_{2,0}^{(m)}\dot{a}_{1,0}^{(m)}b_{1,k/m}\\
&+\sum_{l=1}^{N}\sum_{j=1}^{N}\sum_{i=1}^{N}[\frac{1}{2N}a_{1,0}^{(m)}b_{2,l/m}(\dot{b}_{1,j/m}+\frac{j\Omega}{m}c_{1,j/m})(\delta_{l+j}^{k}+\delta_{|l-j|}^{k})\\
&+\frac{1}{2N}a_{1,0}^{(m)}c_{2,l/m}(\dot{c}_{1,j/m}-\frac{j\Omega}{m}b_{1,j/m})(-\delta_{l+j}^{k}+\delta_{|l-j|}^{k})\\
&+\frac{1}{2N}a_{2,0}^{(m)}b_{1,l/m}(\dot{b}_{1,j/m}+\frac{j\Omega}{m}c_{1,j/m})(\delta_{l+j}^{k}+\delta_{|l-j|}^{k})\\
&+\frac{1}{2N}a_{2,0}^{(m)}c_{1,l/m}(\dot{c}_{1,j/m}-\frac{j\Omega}{m}b_{1,j/m})(-\delta_{l+j}^{k}+\delta_{|l-j|}^{k})\\
&+\frac{1}{2N}\dot{a}_{1,0}^{(m)}b_{1,l/m}b_{2,j/m}(\delta_{l+j}^{k}+\delta_{|l-j|}^{k})+\frac{1}{2N}\dot{a}_{1,0}^{(m)}c_{1,l/m}c_{2,j/m}(-\delta_{l+j}^{k}+\delta_{|l-j|}^{k})\\
&+\frac{1}{4}b_{1,l/m}b_{2,j/m}(\dot{b}_{1,i/m}+\frac{i\Omega}{m}c_{1,i/m})(\delta_{l+j+i}^{k}+\delta_{|l-j+i|}^{k}+\delta_{|l+j-i|}^{k}+\delta_{|l-j-i|}^{k})\\
&+\frac{1}{4}c_{1,l/m}c_{2,j/m}(\dot{b}_{1,i/m}+\frac{i\Omega}{m}c_{1,i/m})(-\delta_{l+j+i}^{k}+\delta_{|l-j+i|}^{k}-\delta_{|l+j-i|}^{k}+\delta_{|l-j-i|}^{k})\\
&+\frac{1}{4}b_{1,l/m}c_{2,j/m}(\dot{c}_{1,i/m}-\frac{i\Omega}{m}b_{1,i/m})(-\delta_{l+j+i}^{k}+\delta_{|l-j+i|}^{k}+\delta_{|l+j-i|}^{k}-\delta_{|l-j-i|}^{k})\\
&+\frac{1}{4}c_{1,l/m}b_{2,j/m}(\dot{c}_{1,i/m}-\frac{i\Omega}{m}b_{1,i/m})(-\delta_{l+j+i}^{k}-\delta_{|l-j+i|}^{k}+\delta_{|l+j-i|}^{k}+\delta_{|l-j-i|}^{k})]
\end{aligned}
$$

$$
\begin{aligned}
f^{(c)}_{1,14k} =& f^{(c)}_{2,14k} = a^{(m)}_{1,0}a^{(m)}_{2,0}(\dot{b}_{2,k/m} + \frac{k\Omega}{m}c_{2,k/m}) + a^{(m)}_{1,0}\dot{a}^{(m)}_{2,0}b_{2,k/m} + a^{(m)}_{2,0}\dot{a}^{(m)}_{2,0}b_{1,k/m} \\
&+ \sum_{l=1}^{N}\sum_{j=1}^{N}\sum_{i=1}^{N}[\frac{1}{2N}a^{(m)}_{1,0}b_{2,l/m}(\dot{b}_{2,j/m} + \frac{j\Omega}{m}c_{2,j/m})(\delta^k_{l+j} + \delta^k_{|l-j|}) \\
&+ \frac{1}{2N}a^{(m)}_{1,0}c_{2,l/m}(\dot{c}_{2,j/m} - \frac{j\Omega}{m}b_{2,j/m})(-\delta^k_{l+j} + \delta^k_{|l-j|}) \\
&+ \frac{1}{2N}a^{(m)}_{2,0}b_{1,l/m}(\dot{b}_{2,j/m} + \frac{j\Omega}{m}c_{2,j/m})(\delta^k_{l+j} + \delta^k_{|l-j|}) \\
&+ \frac{1}{2N}a^{(m)}_{2,0}c_{1,l/m}(\dot{c}_{2,j/m} - \frac{j\Omega}{m}b_{2,j/m})(-\delta^k_{l+j} + \delta^k_{|l-j|}) \\
&+ \frac{1}{2N}\dot{a}^{(m)}_{2,0}b_{1,l/m}b_{2,j/m}(\delta^k_{l+j} + \delta^k_{|l-j|}) + \frac{1}{2N}\dot{a}^{(m)}_{2,0}c_{1,l/m}c_{2,j/m}(-\delta^k_{l+j} + \delta^k_{|l-j|}) \\
&+ \frac{1}{4}b_{1,l/m}b_{2,j/m}(\dot{b}_{2,i/m} + \frac{i\Omega}{m}c_{2,i/m})(\delta^k_{l+j+i} + \delta^k_{|l-j+i|} + \delta^k_{|l+j-i|} + \delta^k_{|l-j-i|}) \\
&+ \frac{1}{4}c_{1,l/m}c_{2,j/m}(\dot{b}_{2,i/m} + \frac{i\Omega}{m}c_{2,i/m})(-\delta^k_{l+j+i} + \delta^k_{|l-j+i|} - \delta^k_{|l+j-i|} + \delta^k_{|l-j-i|}) \\
&+ \frac{1}{4}b_{1,l/m}c_{2,j/m}(\dot{c}_{2,i/m} - \frac{i\Omega}{m}b_{2,i/m})(-\delta^k_{l+j+i} + \delta^k_{|l-j+i|} + \delta^k_{|l+j-i|} - \delta^k_{|l-j-i|}) \\
&+ \frac{1}{4}c_{1,l/m}b_{2,j/m}(\dot{c}_{2,i/m} - \frac{i\Omega}{m}b_{2,i/m})(-\delta^k_{l+j+i} - \delta^k_{|l-j+i|} + \delta^k_{|l+j-i|} + \delta^k_{|l-j-i|})] \\
f^{(c)}_{1,15k} =& f^{(c)}_{2,15k} = 3(a^{(m)}_{2,0})^2 b_{2,k/m} + \sum_{l=1}^{N}\sum_{j=1}^{N}\sum_{i=1}^{N}[\frac{3}{2N}a^{(m)}_{2,0}b_{2,l/m}b_{2,j/m}(\delta^k_{l+j} + \delta^k_{|l-j|}) \\
&+ \frac{3}{2N}a^{(m)}_{2,0}c_{2,l/m}c_{2,j/m}(-\delta^k_{l+j} + \delta^k_{|l-j|}) \\
&+ \frac{1}{4}b_{2,l/m}b_{2,j/m}b_{2,i/m}(\delta^k_{l+j+i} + \delta^k_{|l-j+i|} + \delta^k_{|l+j-i|} + \delta^k_{|l-j-i|}) \\
&+ \frac{3}{4}c_{2,l/m}c_{2,j/m}b_{2,i/m}(-\delta^k_{l+j+i} + \delta^k_{|l-j+i|} - \delta^k_{|l+j-i|} + \delta^k_{|l-j-i|})] \\
f^{(c)}_{1,16k} =& f^{(c)}_{2,16k} = (a^{(m)}_{2,0})^2(\dot{b}_{1,k/m} + \frac{k\Omega}{m}c_{1,k/m}) + 2a^{(m)}_{2,0}\dot{a}^{(m)}_{1,0}b_{2,k/m} \\
&+ \sum_{l=1}^{N}\sum_{j=1}^{N}\sum_{i=1}^{N}[\frac{1}{N}a^{(m)}_{2,0}b_{2,l/m}(\dot{b}_{1,j/m} + \frac{j\Omega}{m}c_{1,j/m})(\delta^k_{l+j} + \delta^k_{|l-j|}) \\
&+ \frac{1}{N}a^{(m)}_{2,0}c_{2,l/m}(\dot{c}_{1,j/m} - \frac{j\Omega}{m}b_{1,j/m})(-\delta^k_{l+j} + \delta^k_{|l-j|}) \\
&+ \frac{1}{2N}\dot{a}^{(m)}_{1,0}b_{2,l/m}b_{2,j/m}(\delta^k_{l+j} + \delta^k_{|l-j|}) + \frac{1}{2N}\dot{a}^{(m)}_{1,0}c_{2,l/m}c_{2,j/m}(-\delta^k_{l+j} + \delta^k_{|l-j|}) \\
&+ \frac{1}{4}b_{2,l/m}b_{2,j/m}(\dot{b}_{1,i/m} + \frac{i\Omega}{m}c_{1,i/m})(\delta^k_{l+j+i} + \delta^k_{|l-j+i|} + \delta^k_{|l+j-i|} + \delta^k_{|l-j-i|}) \\
&+ \frac{1}{4}c_{2,l/m}c_{2,j/m}(\dot{b}_{1,i/m} + \frac{i\Omega}{m}c_{1,i/m})(-\delta^k_{l+j+i} + \delta^k_{|l-j+i|} - \delta^k_{|l+j-i|} + \delta^k_{|l-j-i|}) \\
&+ \frac{1}{2}b_{2,l/m}c_{2,j/m}(\dot{c}_{1,i/m} - \frac{i\Omega}{m}b_{1,i/m})(-\delta^k_{l+j+i} + \delta^k_{|l-j+i|} + \delta^k_{|l+j-i|} - \delta^k_{|l-j-i|})] \\
f^{(c)}_{1,17k} =& f^{(c)}_{2,17k} = (a^{(m)}_{2,0})^2(\dot{b}_{2,k/m} + \frac{k\Omega}{m}c_{2,k/m}) + 2a^{(m)}_{2,0}\dot{a}^{(m)}_{2,0}b_{2,k/m} \\
&+ \sum_{l=1}^{N}\sum_{j=1}^{N}\sum_{i=1}^{N}[\frac{1}{N}a^{(m)}_{2,0}b_{2,l/m}(\dot{b}_{2,j/m} + \frac{j\Omega}{m}c_{2,j/m})(\delta^k_{l+j} + \delta^k_{|l-j|})
\end{aligned}
$$

$$
\begin{aligned}
&+\frac{1}{N}a_{2,0}^{(m)}c_{2,l/m}(\dot{c}_{2,j/m}-\frac{j\Omega}{m}b_{2,j/m})(-\delta_{l+j}^{k}+\delta_{|l-j|}^{k})\\
&+\frac{1}{2N}\dot{a}_{2,0}^{(m)}b_{2,l/m}b_{2,j/m}(\delta_{l+j}^{k}+\delta_{|l-j|}^{k})+\frac{1}{2N}\dot{a}_{2,0}^{(m)}c_{2,l/m}c_{2,j/m}(-\delta_{l+j}^{k}+\delta_{|l-j|}^{k})\\
&+\frac{1}{4}b_{2,l/m}b_{2,j/m}(\dot{b}_{2,i/m}+\frac{i\Omega}{m}c_{2,i/m})(\delta_{l+j+i}^{k}+\delta_{|l-j+i|}^{k}+\delta_{|l+j-i|}^{k}+\delta_{|l-j-i|}^{k})\\
&+\frac{1}{4}c_{2,l/m}c_{2,j/m}(\dot{b}_{2,i/m}+\frac{i\Omega}{m}c_{2,i/m})(-\delta_{l+j+i}^{k}+\delta_{|l-j+i|}^{k}-\delta_{|l+j-i|}^{k}+\delta_{|l-j-i|}^{k})\\
&+\frac{1}{2}b_{2,l/m}c_{2,j/m}(\dot{c}_{2,i/m}-\frac{i\Omega}{m}b_{2,i/m})(-\delta_{l+j+i}^{k}+\delta_{|l-j+i|}^{k}+\delta_{|l+j-i|}^{k}-\delta_{|l-j-i|}^{k})]\\
f_{1,1k}^{(s)}=&f_{2,1k}^{(s)}=2a_{1,0}^{(m)}c_{1,k/m}\\
&+\sum_{l=1}^{N}\sum_{j=1}^{N}\sum_{i=1}^{N}[\frac{1}{2N}b_{1,l/m}c_{1,j/m}(\delta_{l+j}^{k}-sgn(l-j)\delta_{|l-j|}^{k})+\frac{1}{2N}c_{1,l/m}b_{1,j/m}(\delta_{l+j}^{k}+sgn(l-j)\delta_{|l-j|}^{k})]\\
f_{1,2k}^{(s)}=&f_{2,2k}^{(s)}=a_{1,0}^{(m)}c_{2,k/m}+a_{2,0}^{(m)}c_{1,k/m}\\
&+\sum_{l=1}^{N}\sum_{j=1}^{N}\sum_{i=1}^{N}[\frac{1}{2N}b_{1,l/m}c_{2,j/m}(\delta_{l+j}^{k}-sgn(l-j)\delta_{|l-j|}^{k})+\frac{1}{2N}c_{1,l/m}b_{2,j/m}(\delta_{l+j}^{k}+sgn(l-j)\delta_{|l-j|}^{k})]\\
f_{1,3k}^{(s)}=&f_{2,3k}^{(s)}=a_{1,0}^{(m)}(\dot{c}_{1,k/m}-\frac{k\Omega}{m}b_{1,k/m})+\dot{a}_{1,0}^{(m)}c_{1,k/m}\\
&+\sum_{l=1}^{N}\sum_{j=1}^{N}\sum_{i=1}^{N}[\frac{1}{2N}b_{1,l/m}(\dot{c}_{1,j/m}-\frac{j\Omega}{m}b_{1,j/m})(\delta_{l+j}^{k}-sgn(l-j)\delta_{|l-j|}^{k})\\
&+\frac{1}{2N}c_{1,l/m}(\dot{b}_{1,j/m}+\frac{j\Omega}{m}c_{1,j/m})(\delta_{l+j}^{k}+sgn(l-j)\delta_{|l-j|}^{k})]\\
f_{1,4k}^{(s)}=&f_{2,4k}^{(s)}=a_{1,0}^{(m)}(\dot{c}_{2,k/m}-\frac{k\Omega}{m}b_{2,k/m})+\dot{a}_{2,0}^{(m)}c_{1,k/m}\\
&+\sum_{l=1}^{N}\sum_{j=1}^{N}\sum_{i=1}^{N}[\frac{1}{2N}b_{1,l/m}(\dot{c}_{2,j/m}-\frac{j\Omega}{m}b_{2,j/m})(\delta_{l+j}^{k}-sgn(l-j)\delta_{|l-j|}^{k})\\
&+\frac{1}{2N}c_{1,l/m}(\dot{b}_{2,j/m}+\frac{j\Omega}{m}c_{2,j/m})(\delta_{l+j}^{k}+sgn(l-j)\delta_{|l-j|}^{k})]\\
f_{1,5k}^{(s)}=&f_{2,5k}^{(s)}=2a_{2,0}^{(m)}c_{2,k/m}\\
&+\sum_{l=1}^{N}\sum_{j=1}^{N}\sum_{i=1}^{N}[\frac{1}{2N}b_{2,l/m}c_{2,j/m}(\delta_{l+j}^{k}-sgn(l-j)\delta_{|l-j|}^{k})+\frac{1}{2N}c_{2,l/m}b_{2,j/m}(\delta_{l+j}^{k}+sgn(l-j)\delta_{|l-j|}^{k})]\\
f_{1,6k}^{(s)}=&f_{2,6k}^{(s)}=a_{2,0}^{(m)}(\dot{c}_{1,k/m}-\frac{k\Omega}{m}b_{1,k/m})+\dot{a}_{1,0}^{(m)}c_{2,k/m}\\
&+\sum_{l=1}^{N}\sum_{j=1}^{N}\sum_{i=1}^{N}[\frac{1}{2N}b_{2,l/m}(\dot{c}_{1,j/m}-\frac{j\Omega}{m}b_{1,j/m})(\delta_{l+j}^{k}-sgn(l-j)\delta_{|l-j|}^{k})\\
&+\frac{1}{2N}c_{2,l/m}(\dot{b}_{1,j/m}+\frac{j\Omega}{m}c_{1,j/m})(\delta_{l+j}^{k}+sgn(l-j)\delta_{|l-j|}^{k})]\\
f_{1,7k}^{(s)}=&f_{2,7k}^{(s)}=a_{2,0}^{(m)}(\dot{c}_{2,k/m}-\frac{k\Omega}{m}b_{2,k/m})+\dot{a}_{2,0}^{(m)}c_{2,k/m}\\
&+\sum_{l=1}^{N}\sum_{j=1}^{N}\sum_{i=1}^{N}[\frac{1}{2N}b_{2,l/m}(\dot{c}_{2,j/m}-\frac{j\Omega}{m}b_{2,j/m})(\delta_{l+j}^{k}-sgn(l-j)\delta_{|l-j|}^{k})\\
&+\frac{1}{2N}c_{2,l/m}(\dot{b}_{2,j/m}+\frac{j\Omega}{m}c_{2,j/m})(\delta_{l+j}^{k}+sgn(l-j)\delta_{|l-j|}^{k})]
\end{aligned}
$$

$$
\begin{aligned}
f_{1,8k}^{(s)} =& f_{2,8k}^{(s)} = 3(a_{1,0}^{(m)})^2 c_{1,k/m} + \sum_{l=1}^{N}\sum_{j=1}^{N}\sum_{i=1}^{N}[\frac{3}{2N}a_{1,0}^{(m)} b_{1,l/m} c_{1,j/m}(\delta_{l+j}^{k} - sgn(l-j)\delta_{|l-j|}^{k}) \\
&+ \frac{3}{2N}a_{1,0}^{(m)} c_{1,l/m} b_{1,j/m}(\delta_{l+j}^{k} + sgn(l-j)\delta_{|l-j|}^{k}) \\
&+ \frac{3}{4}b_{1,l/m} c_{1,j/m} b_{1,i/m}(\delta_{l+j+i}^{k} - sgn(l-j+i)\delta_{|l-j+i|}^{k} + sgn(l+j-i)\delta_{|l+j-i|}^{k} - sgn(l-j-i)\delta_{|l-j-i|}^{k}) \\
&+ \frac{1}{4}c_{1,l/m} c_{1,j/m} c_{1,i/m}(-\delta_{l+j+i}^{k} + sgn(l-j+i)\delta_{|l-j+i|}^{k} + sgn(l+j-i)\delta_{|l+j-i|}^{k} - sgn(l-j-i)\delta_{|l-j-i|}^{k})] \\
f_{1,9k}^{(s)} =& f_{2,9k}^{(s)} = (a_{1,0}^{(m)})^2 c_{2,k/m} + 2a_{1,0}^{(m)} a_{2,0}^{(m)} c_{1,k/m} + \sum_{l=1}^{N}\sum_{j=1}^{N}\sum_{i=1}^{N}[\frac{1}{N}a_{1,0}^{(m)} b_{1,l/m} c_{2,j/m}(\delta_{l+j}^{k} - sgn(l-j)\delta_{|l-j|}^{k}) \\
&+ \frac{1}{N}a_{1,0}^{(m)} c_{1,l/m} b_{2,j/m}(\delta_{l+j}^{k} + sgn(l-j)\delta_{|l-j|}^{k}) \\
&+ \frac{1}{2N}a_{2,0}^{(m)} b_{1,l/m} c_{1,j/m}(\delta_{l+j}^{k} - sgn(l-j)\delta_{|l-j|}^{k}) + \frac{1}{2N}a_{2,0}^{(m)} c_{1,l/m} b_{1,j/m}(\delta_{l+j}^{k} + sgn(l-j)\delta_{|l-j|}^{k}) \\
&+ \frac{1}{2}b_{1,l/m} c_{1,j/m} b_{2,i/m}(\delta_{l+j+i}^{k} - sgn(l-j+i)\delta_{|l-j+i|}^{k} + sgn(l+j-i)\delta_{|l+j-i|}^{k} - sgn(l-j-i)\delta_{|l-j-i|}^{k}) \\
&+ \frac{1}{4}b_{1,l/m} b_{1,j/m} c_{2,i/m}(\delta_{l+j+i}^{k} + sgn(l-j+i)\delta_{|l-j+i|}^{k} - sgn(l+j-i)\delta_{|l+j-i|}^{k} - sgn(l-j-i)\delta_{|l-j-i|}^{k}) \\
&+ \frac{1}{4}c_{1,l/m} c_{1,j/m} c_{2,i/m}(-\delta_{l+j+i}^{k} + sgn(l-j+i)\delta_{|l-j+i|}^{k} + sgn(l+j-i)\delta_{|l+j-i|}^{k} - sgn(l-j-i)\delta_{|l-j-i|}^{k})] \\
f_{1,10k}^{(s)} =& f_{2,10k}^{(s)} = 2a_{1,0}^{(m)} a_{2,0}^{(m)} c_{2,k/m} + (a_{2,0}^{(m)})^2 c_{1,k/m} \\
&+ \sum_{l=1}^{N}\sum_{j=1}^{N}\sum_{i=1}^{N}[\frac{1}{2N}a_{1,0}^{(m)} b_{2,l/m} c_{2,j/m}(\delta_{l+j}^{k} - sgn(l-j)\delta_{|l-j|}^{k}) + \frac{1}{2N}a_{1,0}^{(m)} c_{2,l/m} b_{2,j/m}(\delta_{l+j}^{k} + sgn(l-j)\delta_{|l-j|}^{k}) \\
&+ \frac{1}{N}a_{2,0}^{(m)} b_{1,l/m} c_{2,j/m}(\delta_{l+j}^{k} - sgn(l-j)\delta_{|l-j|}^{k}) + \frac{1}{N}a_{2,0}^{(m)} c_{1,l/m} b_{2,j/m}(\delta_{l+j}^{k} + sgn(l-j)\delta_{|l-j|}^{k}) \\
&+ \frac{1}{4}b_{1,l/m} c_{2,j/m} b_{2,i/m}(\delta_{l+j+i}^{k} - sgn(l-j+i)\delta_{|l-j+i|}^{k} + sgn(l+j-i)\delta_{|l+j-i|}^{k} - sgn(l-j-i)\delta_{|l-j-i|}^{k}) \\
&+ \frac{1}{4}c_{1,l/m} b_{1,j/m} b_{2,i/m}(\delta_{l+j+i}^{k} + sgn(l-j+i)\delta_{|l-j+i|}^{k} + sgn(l+j-i)\delta_{|l+j-i|}^{k} + sgn(l-j-i)\delta_{|l-j-i|}^{k}) \\
&+ \frac{1}{4}b_{1,l/m} b_{2,j/m} c_{2,i/m}(\delta_{l+j+i}^{k} + sgn(l-j+i)\delta_{|l-j+i|}^{k} - sgn(l+j-i)\delta_{|l+j-i|}^{k} - sgn(l-j-i)\delta_{|l-j-i|}^{k}) \\
&+ \frac{1}{4}c_{1,l/m} c_{2,j/m} c_{2,i/m}(-\delta_{l+j+i}^{k} + sgn(l-j+i)\delta_{|l-j+i|}^{k} + sgn(l+j-i)\delta_{|l+j-i|}^{k} - sgn(l-j-i)\delta_{|l-j-i|}^{k})] \\
f_{1,11k}^{(s)} =& f_{2,11k}^{(s)} = (a_{1,0}^{(m)})^2(\dot{c}_{1,k/m} - \frac{k\Omega}{m}b_{1,k/m}) + 2a_{1,0}^{(m)}\dot{a}_{1,0}^{(m)} c_{1,k/m} \\
&+ \sum_{l=1}^{N}\sum_{j=1}^{N}\sum_{i=1}^{N}[\frac{1}{N}a_{1,0}^{(m)} b_{1,l/m}(\dot{c}_{1,j/m} - \frac{j\Omega}{m}b_{1,j/m})(\delta_{l+j}^{k} - sgn(l-j)\delta_{|l-j|}^{k}) \\
&+ \frac{1}{N}a_{1,0}^{(m)} c_{1,l/m}(\dot{b}_{1,j/m} + \frac{j\Omega}{m}c_{1,j/m})(\delta_{l+j}^{k} + sgn(l-j)\delta_{|l-j|}^{k}) \\
&+ \frac{1}{2N}\dot{a}_{1,0}^{(m)} b_{1,l/m} c_{1,j/m}(\delta_{l+j}^{k} - sgn(l-j)\delta_{|l-j|}^{k}) + \frac{1}{2N}\dot{a}_{1,0}^{(m)} c_{1,l/m} b_{1,j/m}(\delta_{l+j}^{k} + sgn(l-j)\delta_{|l-j|}^{k}) \\
&+ \frac{1}{2}b_{1,l/m} c_{1,j/m}(\dot{b}_{1,i/m} + \frac{i\Omega}{m}c_{1,i/m})(\delta_{l+j+i}^{k} - sgn(l-j+i)\delta_{|l-j+i|}^{k} \\
&+ sgn(l+j-i)\delta_{|l+j-i|}^{k} - sgn(l-j-i)\delta_{|l-j-i|}^{k}) \\
&+ \frac{1}{4}b_{1,l/m} b_{1,j/m}(\dot{c}_{1,i/m} - \frac{i\Omega}{m}b_{1,i/m})(\delta_{l+j+i}^{k} + sgn(l-j+i)\delta_{|l-j+i|}^{k}
\end{aligned}
$$

$$
\begin{aligned}
&- sgn(l+j-i)\delta^k_{|l+j-i|} - sgn(l-j-i)\delta^k_{|l-j-i|}) \\
&+ \frac{1}{4}c_{1,l/m}c_{1,j/m}(\dot{c}_{1,i/m} - \frac{i\Omega}{m}b_{1,i/m})(-\delta^k_{l+j+i} + sgn(l-j+i)\delta^k_{|l-j+i|} \\
&+ sgn(l+j-i)\delta^k_{|l+j-i|} - sgn(l-j-i)\delta^k_{|l-j-i|})] \\
f^{(s)}_{1,12k} =& f^{(s)}_{2,12k} = (a^{(m)}_{1,0})^2(\dot{c}_{2,k/m} - \frac{k\Omega}{m}b_{2,k/m}) + 2a^{(m)}_{1,0}\dot{a}^{(m)}_{2,0}c_{1,k/m} \\
&+ \sum_{l=1}^{N}\sum_{j=1}^{N}\sum_{i=1}^{N}[\frac{1}{N}a^{(m)}_{1,0}b_{1,l/m}(\dot{c}_{2,j/m} - \frac{j\Omega}{m}b_{2,j/m})(\delta^k_{l+j} - sgn(l-j)\delta^k_{|l-j|}) \\
&+ \frac{1}{N}a^{(m)}_{1,0}c_{1,l/m}(\dot{b}_{2,j/m} + \frac{j\Omega}{m}c_{2,j/m})(\delta^k_{l+j} + sgn(l-j)\delta^k_{|l-j|}) \\
&+ \frac{1}{2N}\dot{a}^{(m)}_{2,0}b_{1,l/m}c_{1,j/m}(\delta^k_{l+j} - sgn(l-j)\delta^k_{|l-j|}) + \frac{1}{2N}\dot{a}^{(m)}_{2,0}c_{1,l/m}b_{1,j/m}(\delta^k_{l+j} + sgn(l-j)\delta^k_{|l-j|}) \\
&+ \frac{1}{2}b_{1,l/m}c_{1,j/m}(\dot{b}_{2,i/m} + \frac{i\Omega}{m}c_{2,i/m})(\delta^k_{l+j+i} - sgn(l-j+i)\delta^k_{|l-j+i|} \\
&+ sgn(l+j-i)\delta^k_{|l+j-i|} - sgn(l-j-i)\delta^k_{|l-j-i|}) \\
&+ \frac{1}{4}b_{1,l/m}b_{1,j/m}(\dot{c}_{2,i/m} - \frac{i\Omega}{m}b_{2,i/m})(\delta^k_{l+j+i} + sgn(l-j+i)\delta^k_{|l-j+i|} \\
&- sgn(l+j-i)\delta^k_{|l+j-i|} - sgn(l-j-i)\delta^k_{|l-j-i|}) \\
&+ \frac{1}{4}c_{1,l/m}c_{1,j/m}(\dot{c}_{2,i/m} - \frac{i\Omega}{m}b_{2,i/m})(-\delta^k_{l+j+i} + sgn(l-j+i)\delta^k_{|l-j+i|} \\
&+ sgn(l+j-i)\delta^k_{|l+j-i|} - sgn(l-j-i)\delta^k_{|l-j-i|})] \\
f^{(s)}_{1,13k} =& f^{(s)}_{2,13k} = a^{(m)}_{1,0}a^{(m)}_{2,0}(\dot{c}_{1,k/m} - \frac{k\Omega}{m}b_{1,k/m}) + a^{(m)}_{1,0}\dot{a}^{(m)}_{1,0}c_{2,k/m} + a^{(m)}_{2,0}\dot{a}^{(m)}_{1,0}c_{1,k/m} \\
&+ \sum_{l=1}^{N}\sum_{j=1}^{N}\sum_{i=1}^{N}[\frac{1}{2N}a^{(m)}_{1,0}b_{2,l/m}(\dot{c}_{1,j/m} - \frac{j\Omega}{m}b_{1,j/m})(\delta^k_{l+j} - sgn(l-j)\delta^k_{|l-j|}) \\
&+ \frac{1}{2N}a^{(m)}_{1,0}c_{2,l/m}(\dot{b}_{1,j/m} + \frac{j\Omega}{m}c_{1,j/m})(\delta^k_{l+j} + sgn(l-j)\delta^k_{|l-j|}) \\
&+ \frac{1}{2N}a^{(m)}_{2,0}b_{1,l/m}(\dot{c}_{1,j/m} - \frac{j\Omega}{m}b_{1,j/m})(\delta^k_{l+j} - sgn(l-j)\delta^k_{|l-j|}) \\
&+ \frac{1}{2N}a^{(m)}_{2,0}c_{1,l/m}(\dot{b}_{1,j/m} + \frac{j\Omega}{m}c_{1,j/m})(\delta^k_{l+j} + sgn(l-j)\delta^k_{|l-j|}) \\
&+ \frac{1}{2N}\dot{a}^{(m)}_{1,0}b_{1,l/m}c_{2,j/m}(\delta^k_{l+j} - sgn(l-j)\delta^k_{|l-j|}) + \frac{1}{2N}\dot{a}^{(m)}_{1,0}c_{1,l/m}b_{2,j/m}(\delta^k_{l+j} + sgn(l-j)\delta^k_{|l-j|}) \\
&+ \frac{1}{4}b_{1,l/m}c_{2,j/m}(\dot{b}_{1,i/m} + \frac{i\Omega}{m}c_{1,i/m})(\delta^k_{l+j+i} - sgn(l-j+i)\delta^k_{|l-j+i|} \\
&+ sgn(l+j-i)\delta^k_{|l+j-i|} - sgn(l-j-i)\delta^k_{|l-j-i|}) \\
&+ \frac{1}{4}c_{1,l/m}b_{2,j/m}(\dot{b}_{1,i/m} + \frac{i\Omega}{m}c_{1,i/m})(\delta^k_{l+j+i} + sgn(l-j+i)\delta^k_{|l-j+i|} \\
&+ sgn(l+j-i)\delta^k_{|l+j-i|} + sgn(l-j-i)\delta^k_{|l-j-i|}) \\
&+ \frac{1}{4}b_{1,l/m}b_{2,j/m}(\dot{c}_{1,i/m} - \frac{i\Omega}{m}b_{1,i/m})(\delta^k_{l+j+i} + sgn(l-j+i)\delta^k_{|l-j+i|} \\
&- sgn(l+j-i)\delta^k_{|l+j-i|} - sgn(l-j-i)\delta^k_{|l-j-i|}) \\
&+ \frac{1}{4}c_{1,l/m}c_{2,j/m}(\dot{c}_{1,i/m} - \frac{i\Omega}{m}b_{1,i/m})(-\delta^k_{l+j+i} + sgn(l-j+i)\delta^k_{|l-j+i|} \\
&+ sgn(l+j-i)\delta^k_{|l+j-i|} - sgn(l-j-i)\delta^k_{|l-j-i|})]
\end{aligned}
$$

$$
\begin{aligned}
f^{(s)}_{1,14k} =& f^{(s)}_{2,14k} = a^{(m)}_{1,0}a^{(m)}_{2,0}(\dot{c}_{2,k/m} - \frac{k\Omega}{m}b_{2,k/m}) + a^{(m)}_{1,0}\dot{a}^{(m)}_{2,0}c_{2,k/m} + a^{(m)}_{2,0}\dot{a}^{(m)}_{2,0}c_{1,k/m} \\
&+ \sum_{l=1}^{N}\sum_{j=1}^{N}\sum_{i=1}^{N}[\frac{1}{2N}a^{(m)}_{1,0}b_{2,l/m}(\dot{c}_{2,j/m} - \frac{j\Omega}{m}b_{2,j/m})(\delta^k_{l+j} - sgn(l-j)\delta^k_{|l-j|}) \\
&+ \frac{1}{2N}a^{(m)}_{1,0}c_{2,l/m}(\dot{b}_{2,j/m} + \frac{j\Omega}{m}c_{2,j/m})(\delta^k_{l+j} + sgn(l-j)\delta^k_{|l-j|}) \\
&+ \frac{1}{2N}a^{(m)}_{2,0}b_{1,l/m}(\dot{c}_{2,j/m} - \frac{j\Omega}{m}b_{2,j/m})(\delta^k_{l+j} - sgn(l-j)\delta^k_{|l-j|}) \\
&+ \frac{1}{2N}a^{(m)}_{2,0}c_{1,l/m}(\dot{b}_{2,j/m} + \frac{j\Omega}{m}c_{2,j/m})(\delta^k_{l+j} + sgn(l-j)\delta^k_{|l-j|}) \\
&+ \frac{1}{2N}\dot{a}^{(m)}_{2,0}b_{1,l/m}c_{2,j/m}(\delta^k_{l+j} - sgn(l-j)\delta^k_{|l-j|}) + \frac{1}{2N}\dot{a}^{(m)}_{2,0}c_{1,l/m}b_{2,j/m}(\delta^k_{l+j} + sgn(l-j)\delta^k_{|l-j|}) \\
&+ \frac{1}{4}b_{1,l/m}c_{2,j/m}(\dot{b}_{2,i/m} + \frac{i\Omega}{m}c_{2,i/m})(\delta^k_{l+j+i} - sgn(l-j+i)\delta^k_{|l-j+i|} \\
&+ sgn(l+j-i)\delta^k_{|l+j-i|} - sgn(l-j-i)\delta^k_{|l-j-i|}) \\
&+ \frac{1}{4}c_{1,l/m}b_{2,j/m}(\dot{b}_{2,i/m} + \frac{i\Omega}{m}c_{2,i/m})(\delta^k_{l+j+i} + sgn(l-j+i)\delta^k_{|l-j+i|} \\
&+ sgn(l+j-i)\delta^k_{|l+j-i|} + sgn(l-j-i)\delta^k_{|l-j-i|}) \\
&+ \frac{1}{4}b_{1,l/m}b_{2,j/m}(\dot{c}_{2,i/m} - \frac{i\Omega}{m}b_{2,i/m})(\delta^k_{l+j+i} + sgn(l-j+i)\delta^k_{|l-j+i|} \\
&- sgn(l+j-i)\delta^k_{|l+j-i|} - sgn(l-j-i)\delta^k_{|l-j-i|}) \\
&+ \frac{1}{4}c_{1,l/m}c_{2,j/m}(\dot{c}_{2,i/m} - \frac{i\Omega}{m}b_{2,i/m})(-\delta^k_{l+j+i} + sgn(l-j+i)\delta^k_{|l-j+i|} \\
&+ sgn(l+j-i)\delta^k_{|l+j-i|} - sgn(l-j-i)\delta^k_{|l-j-i|})] \\
f^{(s)}_{1,15k} =& f^{(s)}_{2,15k} = 3(a^{(m)}_{2,0})^2c_{2,k/m} \\
&+ \sum_{l=1}^{N}\sum_{j=1}^{N}\sum_{i=1}^{N}[\frac{3}{2N}a^{(m)}_{2,0}b_{2,l/m}c_{2,j/m}(\delta^k_{l+j} - sgn(l-j)\delta^k_{|l-j|}) + \frac{3}{2N}a^{(m)}_{2,0}c_{2,l/m}b_{2,j/m}(\delta^k_{l+j} + sgn(l-j)\delta^k_{|l-j|}) \\
&+ \frac{3}{4}b_{2,l/m}c_{2,j/m}b_{2,i/m}(\delta^k_{l+j+i} - sgn(l-j+i)\delta^k_{|l-j+i|} + sgn(l+j-i)\delta^k_{|l+j-i|} - sgn(l-j-i)\delta^k_{|l-j-i|}) \\
&+ \frac{1}{4}c_{2,l/m}c_{2,j/m}c_{2,i/m}(-\delta^k_{l+j+i} + sgn(l-j+i)\delta^k_{|l-j+i|} + sgn(l+j-i)\delta^k_{|l+j-i|} - sgn(l-j-i)\delta^k_{|l-j-i|})] \\
f^{(s)}_{1,16k} =& f^{(s)}_{2,16k} = (a^{(m)}_{2,0})^2(\dot{c}_{1,k/m} - \frac{k\Omega}{m}b_{1,k/m}) + 2a^{(m)}_{2,0}\dot{a}^{(m)}_{1,0}c_{2,k/m} \\
&+ \sum_{l=1}^{N}\sum_{j=1}^{N}\sum_{i=1}^{N}[\frac{1}{N}a^{(m)}_{2,0}b_{2,l/m}(\dot{c}_{1,j/m} - \frac{j\Omega}{m}b_{1,j/m})(\delta^k_{l+j} - sgn(l-j)\delta^k_{|l-j|}) \\
&+ \frac{1}{N}a^{(m)}_{2,0}c_{2,l/m}(\dot{b}_{1,j/m} + \frac{j\Omega}{m}c_{1,j/m})(\delta^k_{l+j} + sgn(l-j)\delta^k_{|l-j|}) \\
&+ \frac{1}{2N}\dot{a}^{(m)}_{1,0}b_{2,l/m}c_{2,j/m}(\delta^k_{l+j} - sgn(l-j)\delta^k_{|l-j|}) + \frac{1}{2N}\dot{a}^{(m)}_{1,0}c_{2,l/m}b_{2,j/m}(\delta^k_{l+j} + sgn(l-j)\delta^k_{|l-j|}) \\
&+ \frac{1}{2}b_{2,l/m}c_{2,j/m}(\dot{b}_{1,i/m} + \frac{i\Omega}{m}c_{1,i/m})(\delta^k_{l+j+i} - sgn(l-j+i)\delta^k_{|l-j+i|} \\
&+ sgn(l+j-i)\delta^k_{|l+j-i|} - sgn(l-j-i)\delta^k_{|l-j-i|}) \\
&+ \frac{1}{4}b_{2,l/m}b_{2,j/m}(\dot{c}_{1,i/m} - \frac{i\Omega}{m}b_{1,i/m})(\delta^k_{l+j+i} + sgn(l-j+i)\delta^k_{|l-j+i|} \\
&- sgn(l+j-i)\delta^k_{|l+j-i|} - sgn(l-j-i)\delta^k_{|l-j-i|})
\end{aligned}
$$

$$
\begin{aligned}
&+\frac{1}{4}c_{2,l/m}c_{2,j/m}(\dot{c}_{1,i/m}-\frac{i\Omega}{m}b_{1,i/m})(-\delta^k_{l+j+i}+sgn(l-j+i)\delta^k_{|l-j+i|}\\
&+sgn(l+j-i)\delta^k_{|l+j-i|}-sgn(l-j-i)\delta^k_{|l-j-i|})]\\
f^{(s)}_{1,17k}=&f^{(s)}_{2,17k}=(a^{(m)}_{2,0})^2(\dot{c}_{2,k/m}-\frac{k\Omega}{m}b_{2,k/m})+2a^{(m)}_{2,0}\dot{a}^{(m)}_{2,0}c_{2,k/m}\\
&+\sum_{l=1}^{N}\sum_{j=1}^{N}\sum_{i=1}^{N}[\frac{1}{N}a^{(m)}_{2,0}b_{2,l/m}(\dot{c}_{2,j/m}-\frac{j\Omega}{m}b_{2,j/m})(\delta^k_{l+j}-sgn(l-j)\delta^k_{|l-j|})\\
&+\frac{1}{N}a^{(m)}_{2,0}c_{2,l/m}(\dot{b}_{2,j/m}+\frac{j\Omega}{m}c_{2,j/m})(\delta^k_{l+j}+sgn(l-j)\delta^k_{|l-j|})\\
&+\frac{1}{2N}\dot{a}^{(m)}_{2,0}b_{2,l/m}c_{2,j/m}(\delta^k_{l+j}-sgn(l-j)\delta^k_{|l-j|})+\frac{1}{2N}\dot{a}^{(m)}_{2,0}c_{2,l/m}b_{2,j/m}(\delta^k_{l+j}+sgn(l-j)\delta^k_{|l-j|})\\
&+\frac{1}{2}b_{2,l/m}c_{2,j/m}(\dot{b}_{2,i/m}+\frac{i\Omega}{m}c_{2,i/m})(\delta^k_{l+j+i}-sgn(l-j+i)\delta^k_{|l-j+i|}\\
&+sgn(l+j-i)\delta^k_{|l+j-i|}-sgn(l-j-i)\delta^k_{|l-j-i|})\\
&+\frac{1}{4}b_{2,l/m}b_{2,j/m}(\dot{c}_{2,i/m}-\frac{i\Omega}{m}b_{2,i/m})(\delta^k_{l+j+i}+sgn(l-j+i)\delta^k_{|l-j+i|}\\
&-sgn(l+j-i)\delta^k_{|l+j-i|}-sgn(l-j-i)\delta^k_{|l-j-i|})\\
&+\frac{1}{4}c_{2,l/m}c_{2,j/m}(\dot{c}_{2,i/m}-\frac{i\Omega}{m}b_{2,i/m})(-\delta^k_{l+j+i}+sgn(l-j+i)\delta^k_{|l-j+i|}\\
&+sgn(l+j-i)\delta^k_{|l+j-i|}-sgn(l-j-i)\delta^k_{|l-j-i|})]
\end{aligned}
$$

Journal of Applied Nonlinear Dynamics 5(1) (2016) 33–41

Journal of Applied Nonlinear Dynamics

https://lhscientificpublishing.com/Journals/JAND-Default.aspx

Application of the Generalized Mean Value Function for Detection of Defects in Metal Cylindrical Slugs

Raoul R. Nigmatullin[1,3], Sergey I. Osokin[1†], Victor M. Larionov[1], Yuriy V. Vankov[2], Evgeniya V. Izmajlova[2], Wei Zhang[4]

[1]Kazan (Volga region) Federal University, Institute of Physics, Kremlevskaya str., bld. 18, 420008, Kazan, Ta-tarstan, Russian Federation

[2]Kazan State Power Engineering University, Krasnoselskaya str., bld. 51, 420066, Kazan, Tatarstan, Russian Federation

[3]Kazan National Research Technical University (KNRTU-KAI), 10 Karl Marx street, 420011, Kazan, Tatarstan, Russian Federation

[4]Department of Electronic Engineering, School of Information Science and Technology, JiNan University, Guang-zhou, 510632, China

Submission Info

Communicated by J.A T. Machado
Received 26 April 2015
Accepted 20 May 2015
Available online 1 April 2016

Keywords

Fractional moments
Generalized mean value function
Free-oscillation method
Defects detection in metal cylindrical slugs

Abstract

In this paper we present a free-oscillation method for acoustic detection of defects in metal rods. For detection of normal rods from rods with defects we use a treatment procedure based on the statistics of the fractional moments. This procedure allows to extract the quanti-tative information from the acoustic signals that are propagated in cylindrical slugs after mechanical strike and having different defects. This information allows separating normal rods (without defects) from the rods having different cuts and differentiating the saw-cut defects with different depth from each other. The analysis of data obtained from this research shows that the proposed method of the fractional moments can be applied for quantitative "reading" of envelopes of different acoustic signals that are obtained by means of free-oscillation method and propagated in dense medium having local defects.

1 Introduction

Rejection of intermediates before machining is one of the main problem in production optimization. For the selection of necessary intermediates that satisfy necessary requirements/criteria one can use nondestructive testing methods. There are many different nondestructive testing methods that are used in different manufacturing: magnetic methods [1], capillary [2], eddy current [3], acoustic [4], radiation [5], optical [6] and etc. Each of them has its own range of applicability conditioned by cost,

†Corresponding author.
Email address: sergey.osokin@gmail.com

ISSN 2164 – 6457, eISSN 2164 – 6473/$-see front materials
DOI : 10.5890/JAND.2016.03.002

possibility of application, sensitivity and adaptability. Another important point in testing procedure lies in the processing and analysis of data obtained after application of nondestructive testing method. Frequently, the recorded data forms a large set and are "polluted" strongly by random fluctuations (known as a 'noise') that make difficult them for extraction of significant information that is associated, in particular, with identification of the desired defect located in the given intermediate. One of the most ancient method of acoustic monitoring is acoustic free-oscillation method [7]. The main advantages of this method are: 1) possibility of integral control of the complex high-curvature shape intermediates; 2) there is no need for preliminary control surface preparing; 3) quickness of the desired results achieved. The essential drawback of this method is sensitivity to the way of securing the intermediate and to the place and direction of the excitation force. Usually acoustic free-oscillation method is used in conjunction with the Fourier analysis [8]. Fourier analysis has its own area of applicability and some essential drawbacks. Two basic drawbacks are listed below: 1) assumption about the normal distribution of the noises; 2) uncontrollable errors injections during its application.

In this work we are trying to use another signal processing procedure that does not contain assumptions about the nature of the probability distribution function and does not create uncontrollable errors during its application. This procedure is based on the use of the generalized mean value (GMV)-function that has demonstrated its applicability for reliable selection of different probability distributions [9].

2 Experiment

The objects of investigation represent themselves 7 steel cylindrical rods with radius $R = 8$ mm and length $L = 300$ mm mounted on special supports. Six of them have transversal saw-cuts with penetration depth 1, 2, 3, 4, 5 and 6 mm, accordingly. These saw-cuts simulates different defects with different depths. The seventh rod is considered as the normal one and it does not contain this type of defect.

Experimental setup for investigation of the rods is depicted on figure 1. This setup is mounted on vibration isolating table (concrete plate with rubber dampers) and contains the following elements: base stand, rod laying device, striker assembly and microphone.

During experiment rods were fixed on H-frame supports that were made from transformer steel. These supports were fastened on vertical stands that, in turn, were fixed on vibration isolating table. Impact (strike contact) was made in the center of the rods and the proper acoustic response was registered by the use of microphone and ADC connected with personal computer.

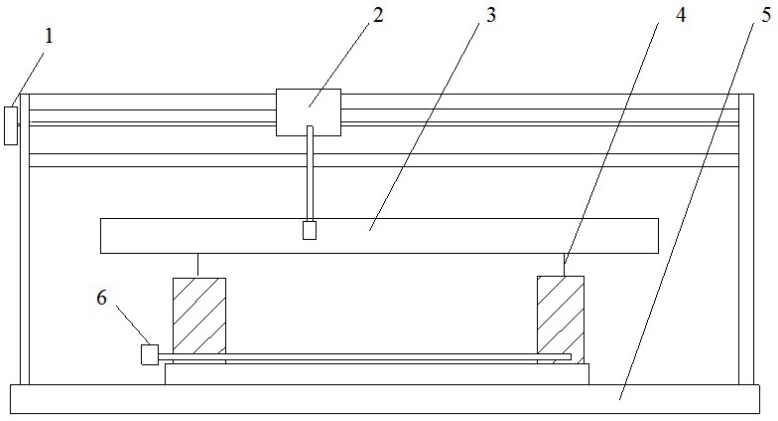

Fig. 1 Experimental setup for investigation of the rods. (1 - external screw for changing position of the striker; 2 - striker assembly; 3 - investigated rod; 4 - knife supports; 5 - base stand; 6 - screw for regulation of the distance between supports).

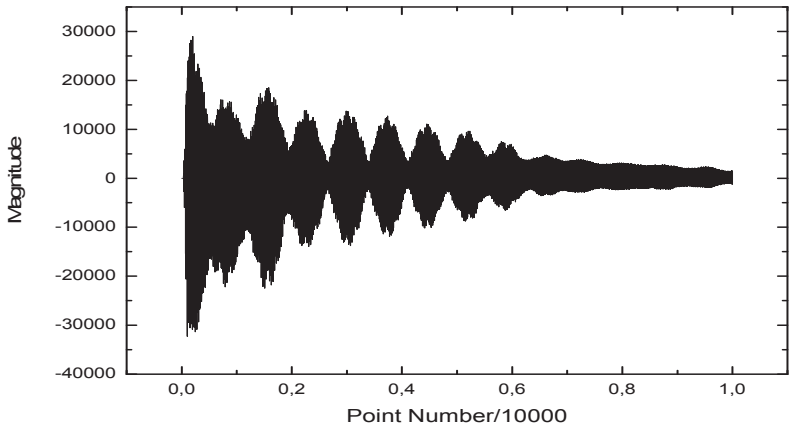

Fig. 2 Acoustic response registered from rod without defect.

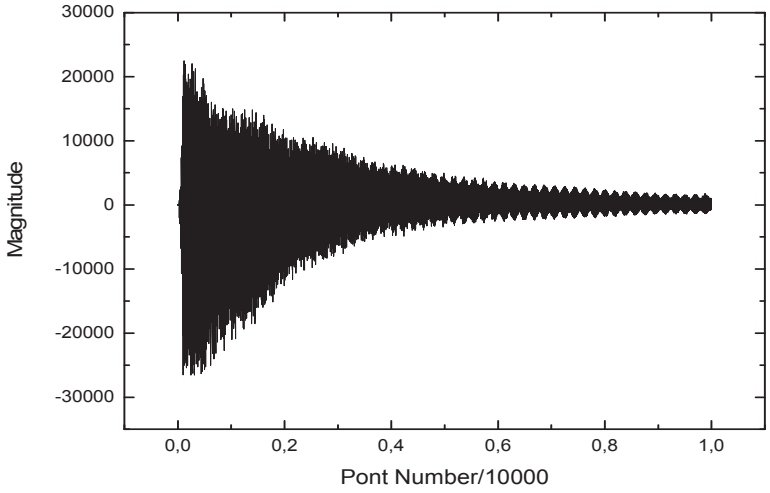

Fig. 3 Acoustic response recorded from a rod with the saw-cut defect having the depth 5 mm.

On figures 2 and 3 one can see examples of acoustic responses from rods without defect and with defect having saw-cut form and depth 5 mm.

For each rod we obtained 40 samples of acoustic data.

3 Description of the signal processing procedure

The idea of this treatment is to extract significant information that can be presented in an arbitrary form for differentiation of rods having saw-cut defects with different depth from each other and from normal rod without defect. For solution of this problem we apply the GMV- function.

This approach has been initially suggested by one of the authors (RRN) in paper [10]. It is based on idea of generalization of the arithmetic mean value and takes into consideration the total set of moments including the fractional and even complex values. The integer (or fractional) moment of the pth order is determined as:

$$\Delta_p \equiv \Delta(m_p) = \frac{1}{N}\sum_{j=1}^{N}(\tilde{y}_j)^{m_p},\ 0 \le m_p \le Mx. \tag{1}$$

where N is the number of points in the sampling considered, m signifies the order of the moment and y – values of the points in the sampling.

The GMV-function is related to the moment of the pth order by means of relationship.

$$GMV_N(m_p) = [\Delta(m_p)]^{1/m_p} \tag{2}$$

This function reproduces the harmonic mean ($m_p = -1$), geometric mean (obtained in the limit $m_p \to 0$), arithmetic mean ($m_p = 1$) as partial cases. The GMV-function is increasing (monotonous) function and at $m_p \to \infty$ GMV-function recovers the right limit of the sequence ($\tilde{y}_{\max} = ymx$) and in the opposite case (at $m_p \to -\infty$) it coincides with another limiting value $\tilde{y}_{\min} = ymn$. Mathematically, these properties are expressed by the following expressions

$$\begin{aligned} &GMV_N(m_1) > GMV_N(m_2),\ if\ m_1 > m_2, \\ &\lim_{m\to\pm\infty} GMV_N(m) = \begin{pmatrix} ymx \\ ymn \end{pmatrix}. \end{aligned} \tag{3}$$

This function has a remarkable property, viz., being presented in the plot $G2_N(m) = G1_N(m)$ it demonstrates the statistical proximity of two random sequences compared if they satisfy to the linear relationship of the type

$$GMV2_N(m) = \lambda GMV1_N(m) + b. \tag{4}$$

The linear relationship (4) can be chosen as a quantitative criterion for verification of the statistical proximity for two arbitrary random sequences compared. However, for detection of the statistical proximity it is necessary to calculate expressions (2) for two sequences and plot them with respect to each other for approximate verification of expression (4).

The normalized moments (1) can be fitted by the linear combination of the exponential functions [10] that was successfully demonstrated recently in differentiation of different 3D-video films [11]

$$\Delta_p = a_0 + \sum_{i=1}^{S} a_i \exp(\lambda_i p). \tag{5}$$

Here the upper limit S of this exponential decomposition is defined by the accuracy of the fitting procedure applied. Application of this function shows [11] that for the most cases it is sufficient to use $S = 3$. So, using the GMV- function and function (5) one can "read" quantitatively any signal (with trend or without trend) in terms of the fitting parameters a_i and λ_i figuring in expression (5).

The first step in the proposed signal processing algorithm is data preparation. Under the "data preparation" we mean extraction of the data that have informative significance for detection of the desired defects.

Let N be the total length of the considered data set $\{y_i = y(t_i)\}$ (forming in our case the considered acoustic response). This sequence can be divided into M consecutive "segments" each one lasting m samples, that is $M = [N/m]$. Now, let $\{P_i\} \equiv \{p_i(1), p_i(1), \ldots, p_i(m)\}$ be the i-th segment. Reduction of this "cloud" of points to two incident points translates into the calculation of two typical points for each segment:

$$p_i^{\mathrm{up}} = \max\{P_i\}, p_i^{\mathrm{dn}} = \min\{P_i\},\ i = 1..N. \tag{6}$$

The so obtained subsets, that is $F^{\mathrm{up}} = \{p_1^{\mathrm{up}}, p_2^{\mathrm{up}}, \ldots, p_M^{\mathrm{up}}\}$ and $F^{\mathrm{dn}} = \{p_1^{\mathrm{dn}}, p_2^{\mathrm{dn}}, \ldots, p_M^{\mathrm{dn}}\}$ form two curves, describing the data trend on a compressed time scale (with a compression factor of m). If F^{up} and F^{dn}

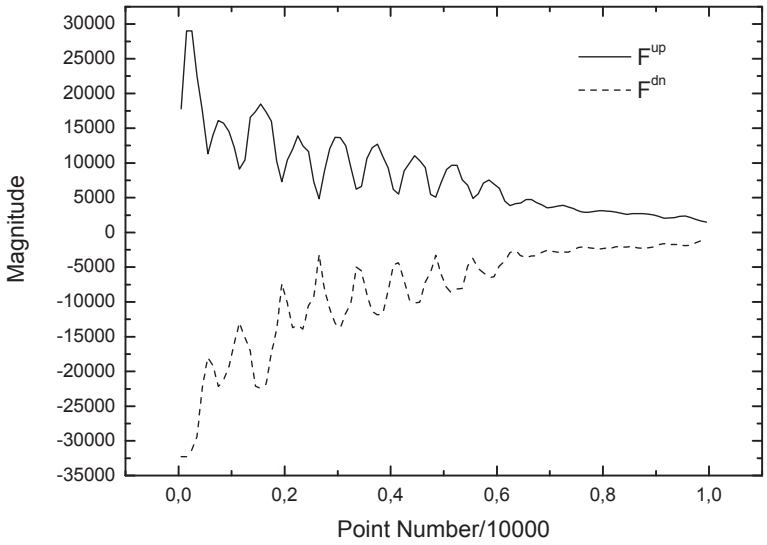

Fig. 4 Curves F^{up} and F^{dn} from rod without defect.

keep their values very close each other, then it serves as an indication of the invariance of the data set under analysis, with respect to self-similar transformations [12]. This is an advantage, because the properties of the whole set can be inferred by using much less data samples.

Please note that, if observed, this behavior is independent on the value of m, which anyway should be kept in a proper range to keep the statistical similarity of the compressed subsets. Choosing a too high value of m would translate in a lower value of M with a consequent very strong data compression and this surely destroys the possibility of detecting the data trend at a smaller time scale. On the other side, m cannot be too small, to allow capturing the low-frequency behavior of the data set under analysis. An empirical rule of thumb for a correct choice of m is based on the following compromise: the number M of the compressed data samples should be less than $N/3$ (i.e., at least three original samples per compressed sample), and at the same time it should be greater than $30 \div 40$. That is:

$$30 \div 40 \le M \le \frac{N}{3} \Rightarrow 3 \le m \le \frac{N}{40} \div \frac{N}{30}. \tag{7}$$

Application of this procedure (6) to the raw acoustic data (presented on figures 2 and 3) gives us curves Fup and Fdn presented on figures 4 and 5 ($m = 100$).

On figures 6, 7 and 8 one can see curves obtained as difference between F^{up} and F^{dn}:

$$DF = F^{\mathrm{up}} - F^{\mathrm{dn}}. \tag{8}$$

Comparing figures 6, 7 and 8 one can see that DF curves become smoother with increasing of the saw-cut depth.

The second step of our proposed signal processing algorithm is normalization procedure

$$Normalized\,DF = \frac{DF - MeanValue(DF)}{StDev(DF)} + 10, \tag{9}$$

where $MeanValue(DF)$ represents the mean value calculated from curve DF and $StDev(DF)$ represents the standard deviation value calculated from curve DF.

The third step of our proposed signal processing algorithm is calculation of the GMV functions using normalized curves (9) as input data. As it has been mentioned above for each rod we get 40 samples of acoustic data. Then after calculation of the GMV-function (2) to the normalized data expressed by

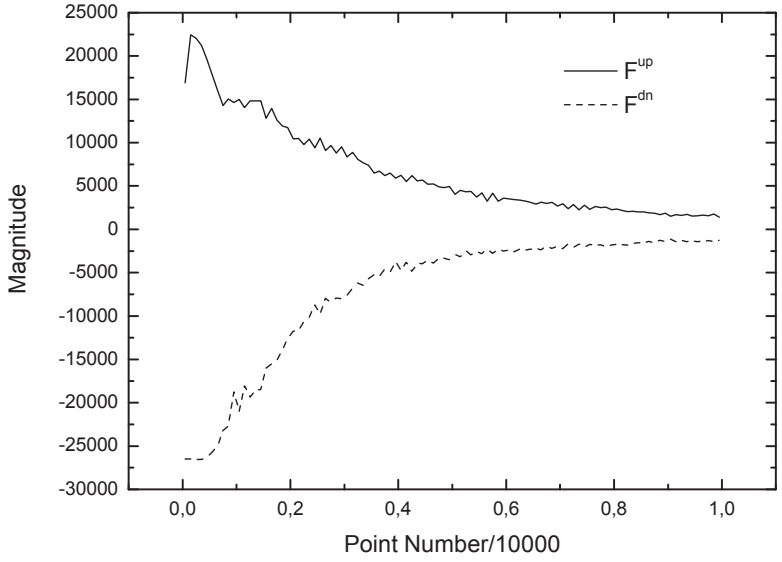

Fig. 5 Curves Fup and Fdn from rod with saw cut 5 mm.

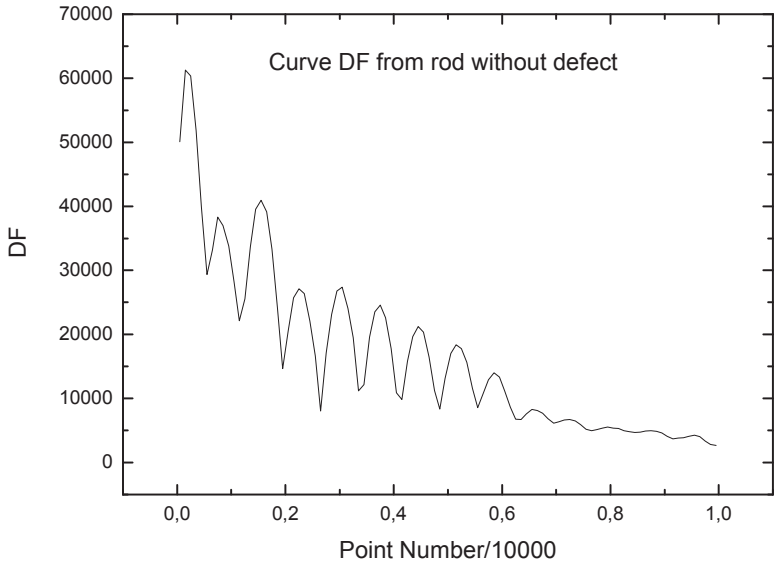

Fig. 6 Curve DF from rod without defect.

(9) we get 40 GMV-curves for each rod. After that one can get the mean function from the set of the GMV-functions corresponding to each rod. On figure 9 one can see the averaged curves obtained from each sampling of the GMV-function for seven rods (one normal rod without defect and six rods with saw-cuts with depths 1, 2, 3, 4, 5 and 6 mm, accordingly).

On the next figure 10 one can see the part of previous figure 9 for more clarity.

Here one can see the direct correlation between saw-cut depths and position of the averaged mean value function. As one can see from this plot the smallest saw-cut defect with depth 1 mm cannot be differentiated; while others starting from 2 mm can be definitely differentiated for forming of the desired calibration curve (the relative distance between the limiting values, right-hand side of figures 9 and 10) of the rods with respect to the depth of the defect:

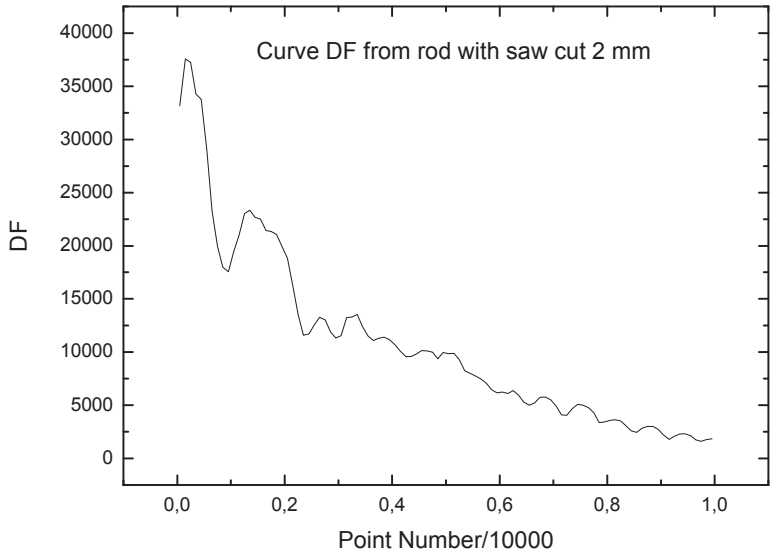

Fig. 7 Curve DF from rod with saw cut 2 mm.

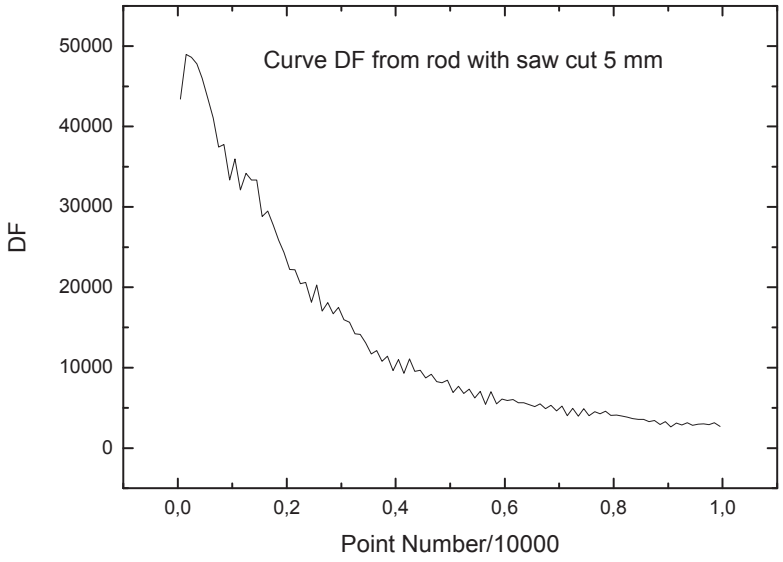

Fig. 8 Curve DF from rod with saw cut 5 mm.

$$Calibration(sawcut\ depth) = \frac{GMV(sawcut, p = 500) - GMV(normal, p = 500)}{0.5 \cdot (GMV(sawcut, p = 500) + GMV(normal, p = 500))\,.} \tag{10}$$

Below on figure 11 one can see the desired calibration curve calculated from expression (10).

4 Results and conclusions

The basic result of this work can be formulated as follows. It becomes possible to present a novel signal processing algorithm based on the specific behavior of the GMV-function. This algorithm helps to extract the significant and quantitative information from the acoustic signals that are propagated inside metal cylindrical slugs having saw-cut defects with different depths. This information allows to

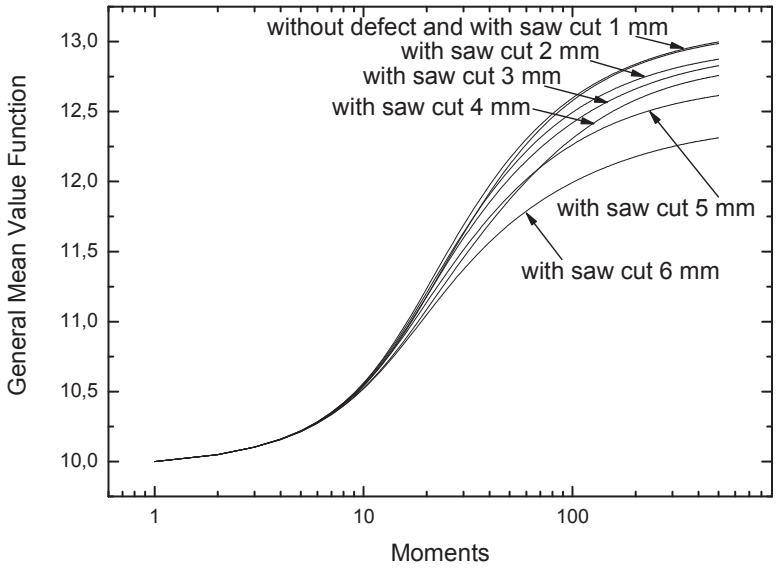

Fig. 9 Averaged general mean value functions for seven rods (one rod without defect and six rods with saw cuts with depths 1, 2, 3, 4, 5 and 6 mm).

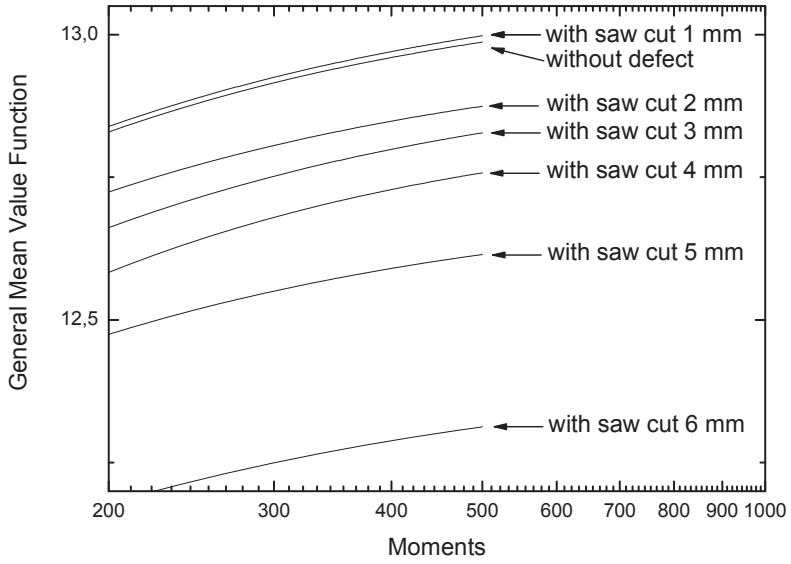

Fig. 10 The part of figure 9 - averaged general mean value functions for seven rods (one rod without defect and six rods with saw cuts with depths 1, 2, 3, 4, 5 and 6 mm).

distinguish normal rods/intermediates (without defects) from rods with saw-cut defect and construct the desired calibration curve (see figure 10) that helps to differentiate the rods with different saw-cuts depths from each other.

The conclusion of this preliminary study is that the proposed signal processing method is suited to be employed for acoustic signals acquired in frame of free-oscillation method in order to detect and evaluate defects in metal rods. We think that proposed signal processing algorithm can be used as a basic and simple procedure for development a really powerful, efficient and reliable signal processing method for detection of different defects (not only transversal saw cuts but also inner cavities) in essential improving of the free-oscillation method drawbacks.

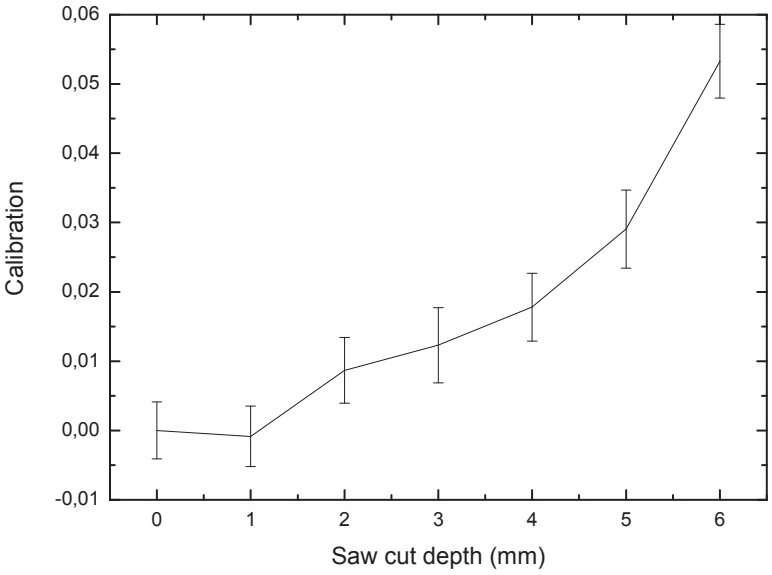

Fig. 11 Calibration curve with respect to saw cut depth.

Acknowledgements

The work is performed according to the Russian Government Program of Competitive Growth of Kazan Federal University.

References

[1] Nondestructive Testing Handbook, (2008) Vol. 8. Magnetic Testing / tech. ed.: David G. Moore; ed.: Patrick O. Moore. 3-rd ed. Columbus: ASNT.
[2] ASNT Level II Study Guide (2002), Liquid Penetrant Testing Method / William Spaulding and Mark Hermes. , 2-nd ed. Columbus: ASNT.
[3] ASNT Level III Study Guide (2007), Electromagnetic Testing / ed.: James E. Cox. 2-nd ed. Columbus: ASNT; Eddy Current Testing Theory and Practice / E. Dane Harvey. (1995) Columbus: ASNT.
[4] ASNT Level II Study Guide (2009), Ultrasonic Testing Method / William Spaulding and George C. Wheeler. (2002), 2-nd ed. Columbus: ASNT.
[5] An Introduction to Nondestructive Testing / George V. Crowe. 2-nd ed. Columbus: ASNT.
[6] Nondestructive Testing Handbook, (2010), Visual Testing / tech. eds: Michael W. Allgaier and Robert E. Cameron; ed.: Patrick O. Moore. Columbus: ASNT, Vol. **9**.
[7] Bouraou, N.I. and Gelman, L.M. (1997), Theoretical bases of the free oscillation method for acoustical nondestructive testing, *J. Acoust. Soc. Am.* **101**, 3085.
[8] Gelman, L. and Braun, S. The optimal usage of the Fourier transform for pattern recognition, *Mechanical Systems and Signal Processing*, **15**(3), 641–645.
[9] Nigmatullin, R.R., Osokin, S.I., Munther, R., Shami, Al., and Mugdadi, A.R. (2013), (December 2013)Application of the fractional moments for comparing random variables with varying probability distributions, *Applications and Applied Mathematics: An International Journal* (AMM). **8**(2), 366–390.
[10] Nigmatullin, R.R. (2006), The statistics of the fractional moments: Is there any chance to read "quantitatively" any randomness?, *Journal of Signal Processing*, **86**, 2529–2547.
[11] Nigmatullin, R., Ceglie, C., Maione, G., and Striccoli, D. (2014), "Reduced Fractional Modeling of 3-D Video Streams: the FERMA Approach", Nonlinear Dynamics, Springer, doi: 10.1007/s11071-014-1792-4
[12] Nigmatullin, R., Machado, J., and Menezes, R.(2013), Self-similarity principle: the reduced description of randomness, Central European Journal of Physics, **11**(6), 724–739.

Journal of Applied Nonlinear Dynamics 5(1) (2016) 43–58

Journal of Applied Nonlinear Dynamics

https://lhscientificpublishing.com/Journals/JAND-Default.aspx

Generalized Combination-combination Synchronization of Chaos in Identical Orders Chaotic Systems

K.S. Ojo[†,2], A.N. Njah[2], O.I. Olusola[2]

[1]Department of Physics, University of Agriculture, Abeokuta, Nigeria
[2]Department of Physics, University of Lagos, Lagos, Nigeria

Submission Info

Communicated by Albert C.J. Luo
Received 17 March 2015
Accepted 2 July 2015
Available online 1 January 2016

Keywords

GCCS
Active backstepping
Josephson junctions
Chaos

Abstract

This paper proposes a generalized combination-combination synchronization scheme (GCCS) for identical order chaotic systems. Using the active backstepping technique. Based on active backstepping technique, suitable controllers are designed to achieve GCCS for any desired scaling factor among four chaotic Josephson junctions (JJs) evolving from different initial conditions. Numerical simulations are carried out to verify the feasibility and effectiveness of the proposed GCCS via active backstepping technique. The result shows that the proposed GCCS could be used to vary the JJ signal to any desired level and provide higher security in information transmission due its complex dynamical formulation.

1 Introduction

Our world consists of artificial and natural systems that are undoubtedly nonlinear. As we understand this fact, we will realize that chaos is inevitable and inherently present in our lives, even though it may not be seen with the naked eye. It has been repeatedly demonstrated by scientists in the last recent decades that nonlinear systems, which model our real world, can display a variety of behaviors including chaos and hyperchaos [1]. Chaos is a very special nonlinear phenomenon because it possesses several properties such as bounded dynamical state trajectories and sensitivity to initial conditions, as well as an irregular and unpredictable behaviour. One of the most important subjects of nonlinear dynamical systems is that of synchronization of chaotic systems which has a lot of applications in many systems such as mechanical systems, biological systems, information processing and secure communication systems etc [2]. Following up the pioneering work of Pecora and Carroll [3], various methodologies have emerged in search of improved and effective methods for achieving stable synchronization between two identical and nonidentical chaotic systems. These include sliding mode control [4], [5], adaptive control [6], active control [7, 8], impulsive control [9], linear feedback control [10], passive control [11], backstepping control [8, 12–14].

[†]Corresponding author.
Email address: kaystephe@yahoo.com, kaojo@unilag.edu.ng

ISSN 2164 – 6457, eISSN 2164 – 6473/$-see front materials
DOI : 10.5890/JAND.2016.03.003

Over the last few decades, most of the theoretical and experimental frameworks on drive-response synchronization scheme have been devoted to one drive system and one response synchronization scheme [15–19]. Based on this drive-response synchronization scheme, other forms of synchronization scheme such as combination synchronization, combination-combination synchronization and compound synchronization were recently developed for synchronization among three and four chaotic systems [20–23]. GCCS is particularly useful in secure communication where transmitted signal can be divided into several parts, and each part loaded in different drive systems and then recombined after synchronization. GCCS can also be used to route transmitted signal to different receivers at a desired time. Thus, the transmitted signals via GCCS will have higher security than the usual transmission through one drive-one response system [24–26]

Motivated by the above discussion, the objective of this paper is to study GCCS between two drive systems and two response system with evolving from different initial conditions using the active backstepping technique. The major contribution of the GCCS proposed in this paper is that it designed in such a way that combination synchronization and the usual one drive one response synchronization are special cases of GCCS. Moreover, the GCCS proposed in this paper is generalized in such a way that an appropriate control function can be designed for a desired synchronization type such as complete synchronization, anti-synchronization, projective synchronization, hybrid synchronization etc. The rest of this paper is organized as follows. Section 2 gives the description of system. Section 3 presents generalized combination-combination synchronization scheme (GCCS). In Section 4, generalized combination-combination synchronization of four third order Josephson junctions via active backstepping technique is considered. Section 5 concludes the paper.

2 Resistive-capacitive-inductive shunted Josephson junction (RCLSJJ)

The resistive-capacitive-inductive shunted Josephson junction in dimensionless form is described by the set of first order differential equations below

$$\begin{aligned} \dot{x} &= y, \\ \dot{y} &= \frac{1}{\beta_C}(i - g(y)y - \sin x - z), \\ \dot{z} &= \frac{1}{\beta_L}(y - z), \end{aligned} \tag{1}$$

where $g(y)$ is the nonlinear damping function approximated by current-voltage relation between the junctions and is defined by

$$g(y) = \begin{cases} 0.366 & \text{if } |y| > 2.9, \\ 0.061 & \text{if } |y| \leq 2.9, \end{cases}$$

x, y and z represent the phase difference, the voltage in the junction and the inductive current respectively. β_C and β_L are capacitive and inductive constant respectively. i is the external direct current. Fig. 1 shows the chaotic attractor of the RCL shunted Josephson junction for the following set of parameters: $1 < i < 1.3$, $\beta_C = 2.6$ and $\beta_L = 0.707$ with the initial conditions $(x, y, z) = (0, 0, 0)$.

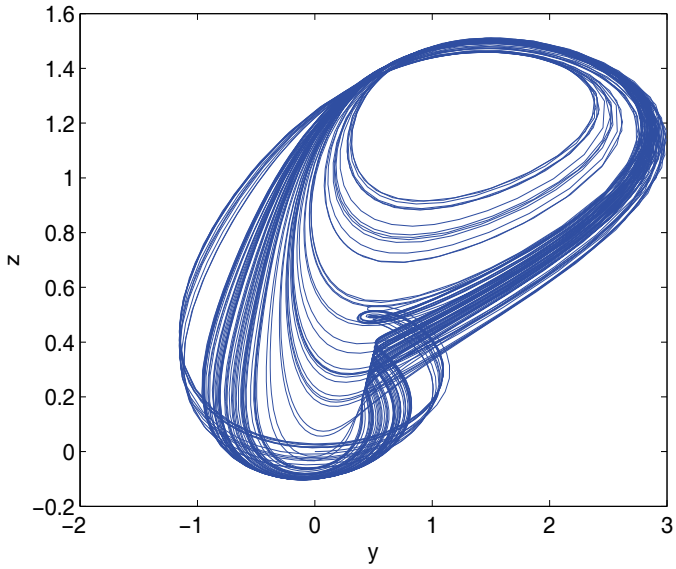

Fig. 1 Phase portrait of chaotic attractors of resistive-capacitive-inductive Josephson junction.

3 Generalized Combination-Combination Synchronization Scheme (GCCS)

Using the drive response scheme, we shall consider generalized combination-combination synchronization of four chaotic systems consisting of two drive systems and two response systems. The drive systems are

$$\dot{x} = Ax + f(x) \tag{2}$$
$$\dot{y} = By + f(y) \tag{3}$$

while the response systems are

$$\dot{z} = Cz + f(z) + u(x,y,z,w) \tag{4}$$
$$\dot{w} = Dw + f(w) + v(x,y,z,w) \tag{5}$$

where $x = (x_1, x_2, \ldots, x_n)^T \in \Re^m, y = (y_1, y_2, \ldots, y_n)^T \in \Re^n, z = (z_1, z_2, \ldots, z_n)^T \in \Re^p$ and $w = (w_1, w_2, \ldots, w_n)^T \in \Re^q$ are the state vectors of system (2)-(5) respectively. $A \in \Re^m \times \Re^m, B \in \Re^n \times \Re^n, C \in \Re^p \times \Re^p, D \in \Re^q \times \Re^q$ are the constant matrices. m, n, p, q are the order of the systems and $f(x)$, $f(y)$, $f(z)$, $f(w)$ are nonlinear functions of the systems which are continuous and differentiable. $u(x,y,z,w) = (u_1(x,y,z,w), u_2(x,y,z,w), \ldots, u_p(x,y,z,w))^T \in \Re^p$ and $v(x,y,z,w) = (v_1(x,y,z,w), v_2(x,y,z,w), \ldots, v_q(x,y,z,w))^T \in \Re^q$ are the controllers to be designed.

Definition 1. *: If the order of the drive and the response systems are the same and there exists four constant scaling matrices $M_1, M_2, M_3, M_4 \in \Re^m$ such that $\lim_{t\to\infty} \| (M_4 w + M_3 z) - (M_1 x + M_2 y) \| = 0$, where $\| \cdot \|$ represent the matrix norm. Then, the drive systems (2), (3) and the response systems (4), (5) achieve combination-combination synchronization.*

Remark 1. *: If M_3 or $M_4 = 0$ then, combination-combination synchronization scheme reduces to combination synchronization scheme. Similarly, if M_1 or $M_2 = 0$ combination-combination synchronization scheme reduces to combination synchronization scheme.*

Definition 2. *The drive systems (2), (3) and the response systems (4), (5) are said to achieve generalized increased or reduced order combination-combination synchronization if there exists four constant matrices* $M_1 \in \Re^m$, $M_2 \in \Re^n$, $M_3 \in \Re^p$ *and* $M_4 \in \Re^q$ *such that* $\lim_{t\to\infty} \| (M_4 w + M_3 z) - (M_1 x + M_2 y) \| = 0$, *where* $\| . \|$ *represent the matrix norm. For increased order combination-combination synchronization* $m,n < p,q$ *and for reduced order combination-combination synchronization scheme* $m,n > p,q$.

Remark 2. *If* M_3 *or* $M_4 = 0$ *then, increased/reduced order combination-combination synchronization scheme becomes increased/reduced order combination synchronization scheme. Similarly, if* M_1 *or* $M_2 = 0$ *increased/reduced order combination-combination synchronization scheme becomes to increased/reduced combination synchronization scheme.*

4 Generalized combination-combination synchronization of four third order Josephson junctions

In this section, Josephson junction in (6) and (7) are taken as the drive systems and Josephson junctions in (8) and (9) are taken as the response systems in order to achieve generalized combination-combination synchronization among the four chaotic third order Josephson junctions

$$\begin{aligned} \dot{x}_1 &= x_2 \\ \dot{x}_2 &= \frac{1}{\beta_C}(i - g(x_2)x_2 - \sin x_1 - x_3) \\ \dot{x}_3 &= \frac{1}{\beta_L}(x_2 - x_3) \end{aligned} \tag{6}$$

$$\begin{aligned} \dot{y}_1 &= y_2 \\ \dot{y}_2 &= \frac{1}{\beta_C}(i - g(y_2)y_2 - \sin y_1 - y_3) \\ \dot{y}_3 &= \frac{1}{\beta_L}(y_2 - y_3) \end{aligned} \tag{7}$$

$$\begin{aligned} \dot{z}_1 &= z_2 + u_1 \\ \dot{z}_2 &= \frac{1}{\beta_C}(i - g(z_2)z_2 - \sin z_1 - z_3) + u_2 \\ \dot{z}_3 &= \frac{1}{\beta_L}(z_2 - z_3) + u_3 \end{aligned} \tag{8}$$

$$\begin{aligned} \dot{w}_1 &= w_2 + u_4 \\ \dot{w}_2 &= \frac{1}{\beta_C}(i - g(w_2)w_2 - \sin w_1 - w_3) + u_5 \\ \dot{w}_3 &= \frac{1}{\beta_L}(w_2 - w_3) + u_6 \end{aligned} \tag{9}$$

where u_1, u_2, u_3, u_4, u_5 and u_6 are the controllers to be designed. We define the error systems as follows

$$\begin{aligned} e_1 &= \delta_1 w_1 + \gamma_1 z_1 - (\alpha_1 x_1 + \beta_1 y_1) \\ e_2 &= \delta_2 w_2 + \gamma_2 z_2 - (\alpha_2 x_2 + \beta_2 y_2) \\ e_3 &= \delta_3 w_3 + \gamma_3 z_3 - (\alpha_3 x_3 + \beta_3 y_3) \end{aligned} \tag{10}$$

using the error systems (10) and the systems defined in (6)-(9) we obtain the following error dynamics

$$\begin{aligned}
\dot{e}_1 &= \frac{\delta_1}{\delta_2}(e_2 - \gamma_2 z_2 + \alpha_2 x_2 + \beta_2 y_2) + \gamma_1 z_2 - \alpha_1 x_2 - \beta_1 y_2 + \delta_1 u_4 + \gamma_1 u_1 \\
\dot{e}_2 &= \frac{\delta_2}{\beta_C}(i - g(w_2)w_2 - \sin w_1) - \frac{\delta_2}{\delta_3\beta_C}(e_3 - \gamma_3 z_3 + \alpha_3 x_3 + \beta_3 y_3) \\
&\quad + \frac{\gamma_2}{\beta_C}(i - g(z_2)z_2 - \sin z_1 - z_3) - \frac{\alpha_2}{\beta_C}(i - g(x_2)x_2 - \sin x_1 - x_3) \\
&\quad - \frac{\beta_2}{\beta_C}(i - g(y_2)y_2 - \sin y_1 - y_3) + \delta_2 u_5 + \gamma_2 u_2 \\
\dot{e}_3 &= \frac{\delta_3}{\delta_2\beta_L}(e_2 - \gamma_2 z_2 + \alpha_2 x_2 + \beta_2 y_2) - \frac{\delta_3}{\delta_2\beta_L}(e_3 - \gamma_3 z_3 + \alpha_3 x_3 + \beta_3 y_3) \\
&\quad + \frac{\gamma_3}{\beta_L}(z_2 - z_3) - \frac{\alpha_3}{\beta_L}(x_2 - x_3) - \frac{\beta_3}{\beta_L}(y_2 - y_3) + \delta_3 u_6 + \gamma_3 u_3
\end{aligned} \tag{11}$$

Consequently, the error dynamics of the systems can be written as

$$\begin{aligned}
\dot{e}_1 &= \frac{\delta_1}{\delta_2}e_2 + A_1 + U_1 \\
\dot{e}_2 &= -\frac{\delta_2 e_3}{\delta_3\beta_C} + A_2 + U_2 \\
\dot{e}_3 &= \frac{\delta_3}{\delta_2\beta_L}e_2 - \frac{1}{\beta_L}e_3 + A_3 + U_3
\end{aligned} \tag{12}$$

where

$$\begin{aligned}
A_1 &= \frac{\delta_1}{\delta_2}(-\gamma_2 z_2 + \alpha_2 x_2 + \beta_2 y_2) + \gamma_1 z_2 - \alpha_1 x_2 - \beta_1 y_2 \\
A_2 &= \frac{\delta_2}{\beta_C}(i - g(w_2)w_2 - \sin w_1) - \frac{\delta_2}{\delta_3\beta_C}(-\gamma_3 z_3 + \alpha_3 x_3 + \beta_3 y_3) \\
&\quad + \frac{\gamma_2}{\beta_C}(i - g(z_2)z_2 - \sin z_1 - z_3) - \frac{\alpha_2}{\beta_C}(i - g(x_2)x_2 - \sin x_1 - x_3) \\
&\quad - \frac{\beta_2}{\beta_C}(i - g(y_2)y_2 - \sin y_1 - y_3) \\
A_3 &= \frac{\delta_3}{\delta_2\beta_L}(-\gamma_2 z_2 + \alpha_2 x_2 + \beta_2 y_2) - \frac{\delta_3}{\delta_2\beta_L}(-\gamma_3 z_3 + \alpha_3 x_3 + \beta_3 y_3) \\
&\quad + \frac{\gamma_3}{\beta_L}(z_2 - z_3) - \frac{\alpha_3}{\beta_L}(x_2 - x_3) - \frac{\beta_3}{\beta_L}(y_2 - y_3) \\
U_1 &= \delta_1 u_4 + \gamma_1 u_1 \\
U_2 &= \delta_2 u_5 + \gamma_2 u_2 \\
U_3 &= \delta_3 u_6 + \gamma_3 u_3
\end{aligned}$$

then we obtain the following results.

Theorem 1. *: If the controllers are chosen as*

$$\begin{aligned}
U_1 &= \frac{\delta_1}{\delta_2}(-\gamma_2 z_2 + \alpha_2 x_2 + \beta_2 y_2) - \gamma_1 z_2 + \alpha_1 x_2 + \beta_1 y_2 - kq_1 \\
U_2 &= \frac{\delta_2}{\delta_3 \beta_C}(\alpha_3 x_3 + \beta_3 y_3 - \gamma_3 z_3) - \frac{\delta_2}{\beta_C}(i - g(w_2)w_2 - \sin w_1) \\
&\quad - \frac{\gamma_2}{\beta_C}(i - g(z_2)z_2 - \sin z_1 - z_3) + \frac{\alpha_2}{\beta_C}(i - g(x_2)x_2 - \sin x_1 - x_3) \\
&\quad + \frac{\beta_2}{\beta_C}(i - g(y_2)y_2 - \sin y_1 - y_3) - q_1 - kq_2 \\
U_3 &= \frac{1}{\beta_C}q_2 + \frac{\delta_3}{\delta_2 \beta_L}(-\gamma_2 z_2 + \alpha_2 x_2 + \beta_2 y_2) + \frac{\delta_3}{\delta_2 \beta_L}(-\gamma_3 z_3 + \alpha_3 x_3 + \beta_3 y_3) \\
&\quad - \frac{\gamma_3}{\beta_L}(z_2 - z_3) + \frac{\alpha_3}{\beta_L}(x_2 - x_3) + \frac{\beta_3}{\beta_L}(y_2 - y_3) - \frac{1}{\beta_L}(\frac{\delta_3}{\delta_2}q_2 - q_3) - kq_3
\end{aligned} \tag{13}$$

where $q_1 = e_1, q_2 = e_2, q_3 = e_3$ and k is the positive constant then, the drive systems (6), (7) and the response systems (8),(9) will achieve generalized combination-combination synchronization.

Proof: The objective of this section is to find control functions via the active backstepping technique that would stabilize the error state dynamics (12) in order for the drive systems (6), (7) and the response systems (8), (9) to achieve generalized combination-combination synchronization. The design procedure include the following steps.

Step 1: Let $q_1 = e_1$, then we obtain its time derivative as

$$\dot{q}_1 = \dot{e}_1 = e_2 + U_1 + A_1 \tag{14}$$

Now to stabilize subsystem (14), let $e_2 = \alpha_1(q_1)$ be regarded as virtual controller and $V_1 = \frac{1}{2}q_1^2$ be a Lyapunov function with time derivative is

$$\dot{V}_1 = q_1\dot{q}_1 = q_1(\alpha_1(q_1) + A_1 + U_1) \tag{15}$$

Suppose $\alpha_1(q_1) = 0$ and the control function U_1 is chosen as

$$U_1 = -(A_1 + kq_1) \tag{16}$$

then, $\dot{V}_1 = -kq_1^2 < 0$ where k is a positive constant which represents the feedback gain. So, $\dot{V}_1$ is negative definite and the subsystem q_1 is asymptotically stable. Since, the virtual controller $\alpha_1(q_1)$ is estimative, the error between e_2 and $\alpha_1(q_1)$ can be denoted by $q_2 = e_2 - \alpha_1(q_1)$. Thus, we have the following (q_1, q_2)-subsystems

$$\begin{aligned}
\dot{q}_1 &= q_2 - kq_1 \\
\dot{q}_2 &= -\frac{1}{\beta_C}e_3 + U_2 + A_2
\end{aligned} \tag{17}$$

Step 2: In order to stabilize subsystem (17) we regard $e_3 = \alpha_2(q_1, q_2)$ as a virtual controller choose a Lyapunov function $V_2 = V_1 + \frac{1}{2}q_2^2$ and obtain its time derivative as

$$\dot{V}_2 = -kq_1^2 + q_2(q_1 - \frac{1}{\beta_C}\alpha_2(q_1, q_2) + A_2 + U_2) \tag{18}$$

If $\alpha_2(q_1, q_2) = 0$ and the control function U_2 is chosen as

$$U_2 = -A_2 - q_1 - kq_2 \tag{19}$$

then $\dot{V}_2 = -kq_1^2 - kq_2^2 < 0$ where k is a positive constant which represents the feedback gain. Then, $\dot{V}_2$ is negative definite and the subsystem (q_1, q_2) in (17) is asymptotically stable. Thus, we have the following (q_1, q_2, q_3) subsystems

$$\begin{aligned} \dot{q}_1 &= q_2 - kq_1 \\ \dot{q}_2 &= -\frac{1}{\beta_C} q_3 - q_1 - kq_2 \\ \dot{q}_3 &= \frac{1}{\beta_L}(\delta_3\delta_2 q_2 - q_3) + A_3 + U_3 \end{aligned} \tag{20}$$

Step 3: Finally, we stabilize the subsystem (q_1, q_2, q_3) by choosing an appropriate Lyapunov function $V_3 = V_2 + \frac{1}{2}q_1^2$ and obtain its time derivative as

$$\dot{V}_3 = -kq_1^2 - kq_2^2 + q_3(-\frac{1}{\beta_C} q_2 + \frac{1}{\beta_L}(\delta_3\delta_2 q_2 - q_3) + A_3 + U_3) \tag{21}$$

now if the control function the U_3 is chosen as

$$U_3 = \frac{1}{\beta_C} q_2 - \frac{1}{\beta_L}(\delta_3\delta_2 q_2 - q_3) - A_3 - kq_3 \tag{22}$$

then $\dot{V}_3 = -kq_1^2 - kq_2^2 - kq_3^2 < 0$ hence, $\dot{V}_3$ is negative definite since k is taking as a positive constant and the subsystem (q_1, q_2) in (20) is asymptotically stable. This shows that generalized combination-combination synchronization between the drive systems (6),(7) and the response systems (8)-(9) is achieved. Finally, the full (q_1, q_2, q_3) is

$$\begin{aligned} \dot{q}_1 &= q_2 - kq_1 \\ \dot{q}_2 &= -\frac{1}{\beta_C} q_3 - q_1 - kq_2 \\ \dot{q}_3 &= \frac{1}{\beta_C} q_2 - kq_3 \end{aligned} \tag{23}$$

This complete the prove.

Several Corollaries can be deduced from the above generalized combination-combination synchronization. However, we shall discuss few of them.

Suppose $\delta_1 = \delta_2 = \delta_3 = \gamma_1 = \gamma_2 = \gamma_3 = 1$, $u_1 = u_4$, $u_2 = u_5$, $u_3 = u_6$ in (13) then, we have Corollary 1.

Corollary 1. *If the controllers are chosen as*

$$\begin{aligned} u_1 = u_4 &= \frac{1}{2}(-\alpha_2 x_2 - \beta_2 y_2 + \alpha_1 x_2 + \beta_1 y_2 - kq_1) \\ u_2 = u_5 &= \frac{1}{2}(\frac{1}{\beta_C}(\alpha_3 x_3 + \beta_3 y_3 - z_3) - \frac{1}{\beta_C}(i - g(w_2)w_2 - \sin w_1) \\ &\quad - \frac{1}{\beta_C}(i - g(z_2)z_2 - \sin z_1 - z_3) + \frac{\alpha_2}{\beta_C}(i - g(x_2)x_2 - \sin x_1 - x_3) \\ &\quad + \frac{\beta_2}{\beta_C}(i - g(y_2)y_2 - \sin y_1 - y_3) - q_1 - kq_2) \\ u_3 = u_6 &= \frac{1}{2}(\frac{1}{\beta_C} q_2 - \frac{1}{\beta_L}(-z_2 + \alpha_2 x_2 + \beta_2 y_2) + \frac{1}{\beta_L}(\alpha_3 x_3 + \beta_3 y_3 - z_3) \\ &\quad - \frac{1}{\beta_L}(z_2 - z_3) + \frac{\alpha_3}{\beta_L}(x_2 - x_3) + \frac{\beta_3}{\beta_L}(y_2 - y_3) - \frac{1}{\beta_L}(q_2 - q_3) - kq_3) \end{aligned} \tag{24}$$

where $e_1 = w_1 + z_1 - \alpha_1 x_1 - \beta_1 y_1, e_2 = w_2 + z_2 - \alpha_2 x_2 - \beta_2 y_2, e_3 = w_3 + z_3 - \alpha_3 x_3 - \beta_3 y_3$ *and* k *is the positive feedback gain then, the drive systems (6) and (7) will achieve modified projective combination-combination synchronization with response systems (8) and (9).*

In order to verify the effectiveness of the designed controllers, ode45 fourth order Runge-Kutta algorithm run on Matlab is used. The system parameter values are chosen as shown in Figure 1 to ensure chaotic dynamics of the state variables and this chaotic dynamics is maintained throughout this work. Solving the drive systems (6), (7) and the response systems (8), (9) with the controllers defined in (24) using the initial conditions of the drive systems and response systems are given respectively as $(x_1, x_2, x_3) = (0,0,0)$, $(y_1, y_2, y_3) = (1,1,1)$, $(z_1, z_2, z_3) = (0.2, 0.2, 0.2)$ and $(w_1, w_2, w_3) = (0.3, 0.3, 0.3)$. The numerical results shall be considered under three special cases.

1. Projective combination-combination synchronization: Choosing the scaling parameter value as $\alpha_1 = \alpha_2 = \alpha_3 = \beta_1 = \beta_2 = \beta_3 = 2.0$, projective combination-combination synchronization of the drive systems (6), (7) and the response systems (8), (9) are achieved as indicated by the convergence of the error state variables to zero and the projection of the state variables of the drive Josephson junctions on the response Josephson junctions when the controllers are activated for $t \geq 80$ as shown in Figure 2.

2. Projective combination-combination anti-synchronization: Choosing the scaling parameter value as $\alpha_1 = \alpha_2 = \alpha_3 = \beta_1 = \beta_2 = \beta_3 = -2.0$, projective combination-combination anti-synchronization of the drive systems (6), (7) and the response systems (8), (9) are achieved as indicated by the convergence of the error state variables to zero and the projection of the state variables of the drive Josephson junctions on the response Josephson junctions when the controllers are activated for $t \geq 80$ as shown in Figure 3.

3. Hybrid projective combination-combination synchronization: Choosing the scaling parameter value as $\alpha_1 = \alpha_3 = \beta_1 = \beta_3 = 2.0, \alpha_2 = -2$, hybrid projective combination-combination synchronization of the drive systems (6), (7) and the response systems (8), (9) are achieved as indicated by the convergence of the error state variables to zero and the projection of the state variables of the drive Josephson junctions on the response Josephson junctions when the controllers are activated for $t \geq 80$ as shown in Figure 4.

Suppose $\delta_1 = \delta_2 = \delta_3 = 1$, $\gamma_1 = \gamma_2 = \gamma_3 = 0$, $u_1 = u_4$, $u_2 = u_5$, $u_3 = u_6$ in (13), we have Corollary 2.

Corollary 2. *: If the controllers are chosen as*

$$\begin{aligned}
u_1 &= \alpha_1 x_2 + \beta_1 y_2 - \alpha_2 x_2 - \beta_2 y_2 - k q_1) \\
u_2 &= \frac{1}{\beta_C}(\alpha_3 x_3 + \beta_3 y_3) - \frac{1}{\beta_C}(i - g(w_2) w_2 - \sin w_1) - q_1 - k q_2 \\
&\quad + \frac{\alpha_2}{\beta_C}(i - g(x_2) x_2 - \sin x_1 - x_3) + \frac{\beta_2}{\beta_C}(i - g(y_2) y_2 - \sin y_1 - y_3) \\
u_3 &= \frac{1}{\beta_C} q_2 - \frac{1}{\beta_L}(\alpha_2 x_2 + \beta_2 y_2) + \frac{1}{\beta_L}(\alpha_3 x_3 + \beta_3 y_3) \\
&\quad + \frac{\alpha_3}{\beta_L}(x_2 - x_3) + \frac{\beta_3}{\beta_L}(y_2 - y_3) - \frac{1}{\beta_L}(q_2 - q_3) - k q_3
\end{aligned} \tag{25}$$

where $e_1 = w_1 - \alpha_1 x_1 - \beta_1 y_1, e_2 = w_2 - \alpha_2 x_2 - \beta_2 y_2, e_3 = z_3 - \alpha_3 x_3 - \beta_3 y_3$ *and* k *is the positive feedback gain then, the drive systems (6) and(7) will achieve modified projective combination synchronization with response system (9).*

Solving the drive systems (6), (7) and the response system (9) with the controllers defined in (25) and using the initial conditions of the drive systems and response systems as $(x_1, x_2, x_3) = (0,0,0)$, $(y_1, y_2, y_3) = (1,1,1)$ and $(w_1, w_2, w_3) = (0.30.30.3)$. The numerical results are considered under three special cases.

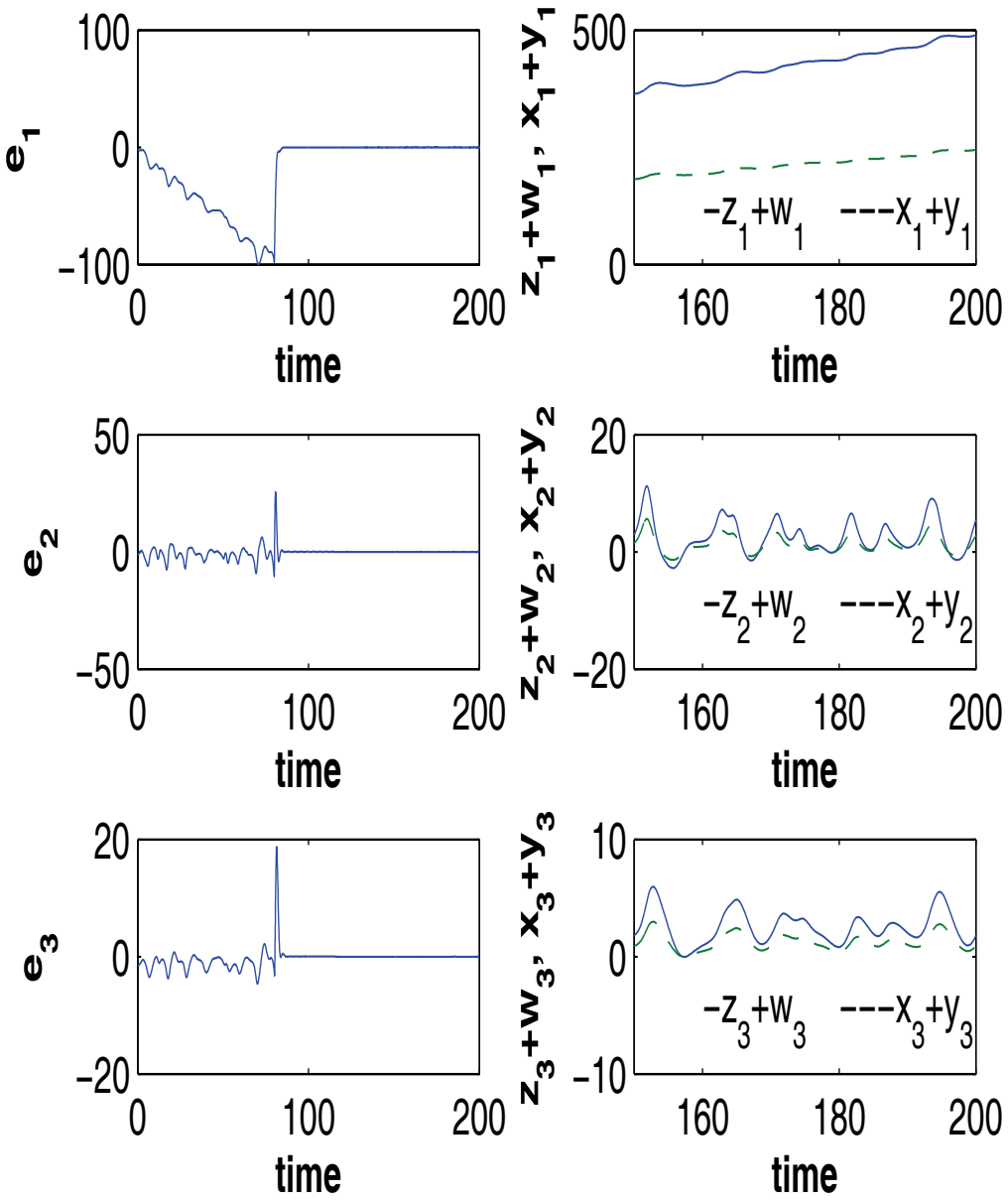

Fig. 2 Error dynamics among the drive and the response systems (column one) and the corresponding dynamics (time series) of the state variable of the drive (dashed line) and the response (solid line) variables (column two) with controllers deactivated for $0 < t < 80$ and activated for $t \geq 80$ where $e_1 = w_1 + z_1 - 2.0(x_1 + y_1)$, $e_2 = w_2 + z_2 - 2.0(x_2 + y_2)$ and $e_3 = w_3 + z_3 - 2.0(x_3 + y_3)$.

1. Projective combination synchronization: Choosing the scaling parameter values as $\alpha_1 = \alpha_2 = \alpha_3 = \beta_1 = \beta_2 = \beta_3 = 2.0$ projective combination synchronization of the drive systems (6), (7) and the response system (9) are achieved as indicated by the convergence of the error state variables to zero and the projection of the state variables of the drive Josephson junctions on the response Josephson junctions when the controllers are activated for $t \geq 80$ as shown in Figure 5.

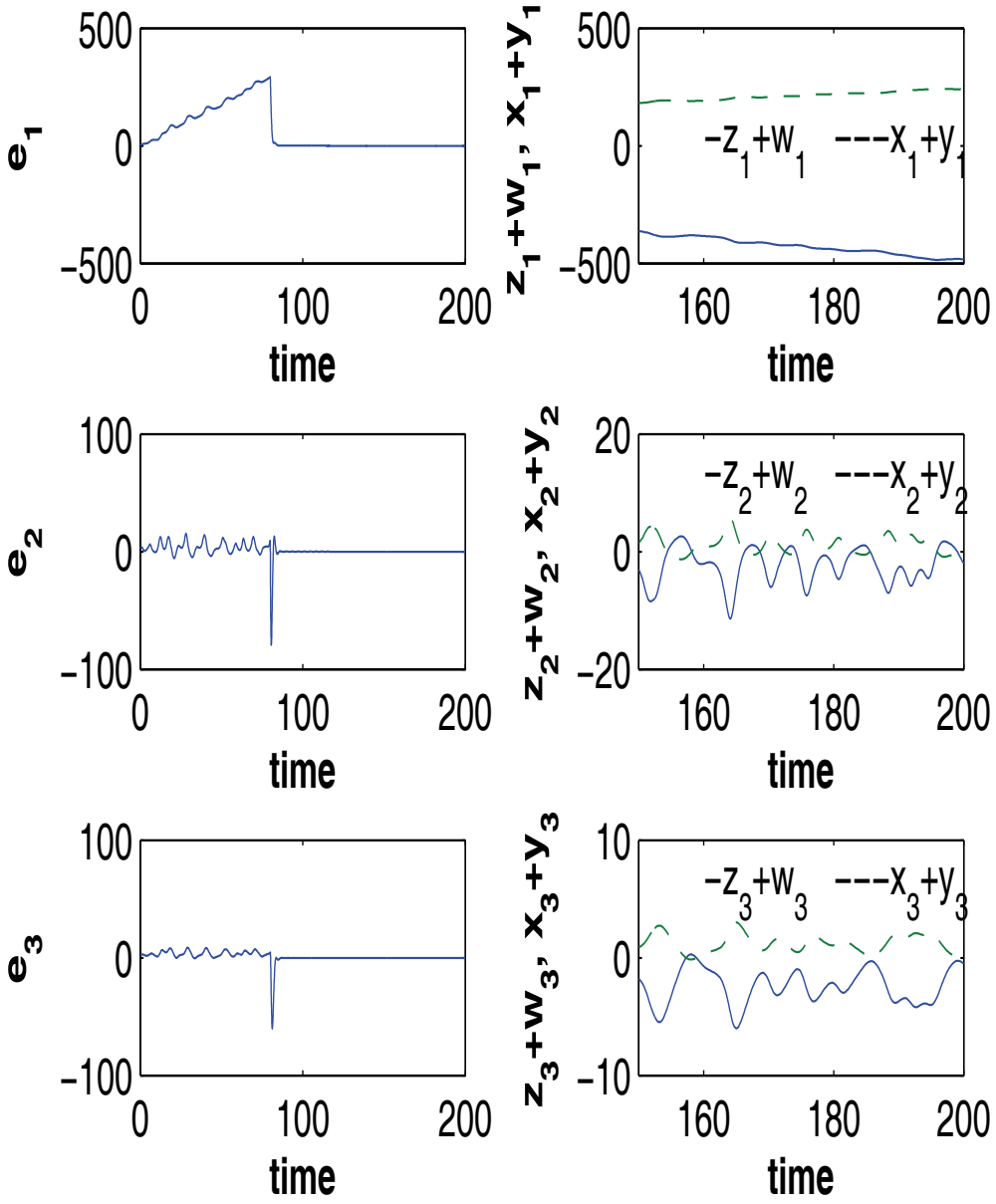

Fig. 3 Error dynamics among the drive and the response systems (column one) and the corresponding dynamics (time series) of the state variable of the drive (dashed line) and the response (solid line) variables (column two) with controllers deactivated for $0 < t < 80$ and activated for $t \geq 80$ where $e_1 = w_1 + z_1 + 2.0(x_1 + y_1)$, $e_2 = w_2 + z_2 + 2.0(x_2 + y_2)$ and $e_3 = w_3 + z_3 + 2.0(x_3 + y_3)$.

2. Projective combination anti-synchronization: Choosing the scaling parameter value as $\alpha_1 = \alpha_2 = \alpha_3 = \beta_1 = \beta_2 = \beta_3 = -2.0$ projective combination ant1-synchronization of the drive systems (6), (7) and the response system (9) are achieved as indicated by the convergence of the error state variables to zero and the projection of the state variables of the drive Josephson junctions on the response Josephson junctions when the controllers are activated for $t \geq 80$ as shown in Figure 6.

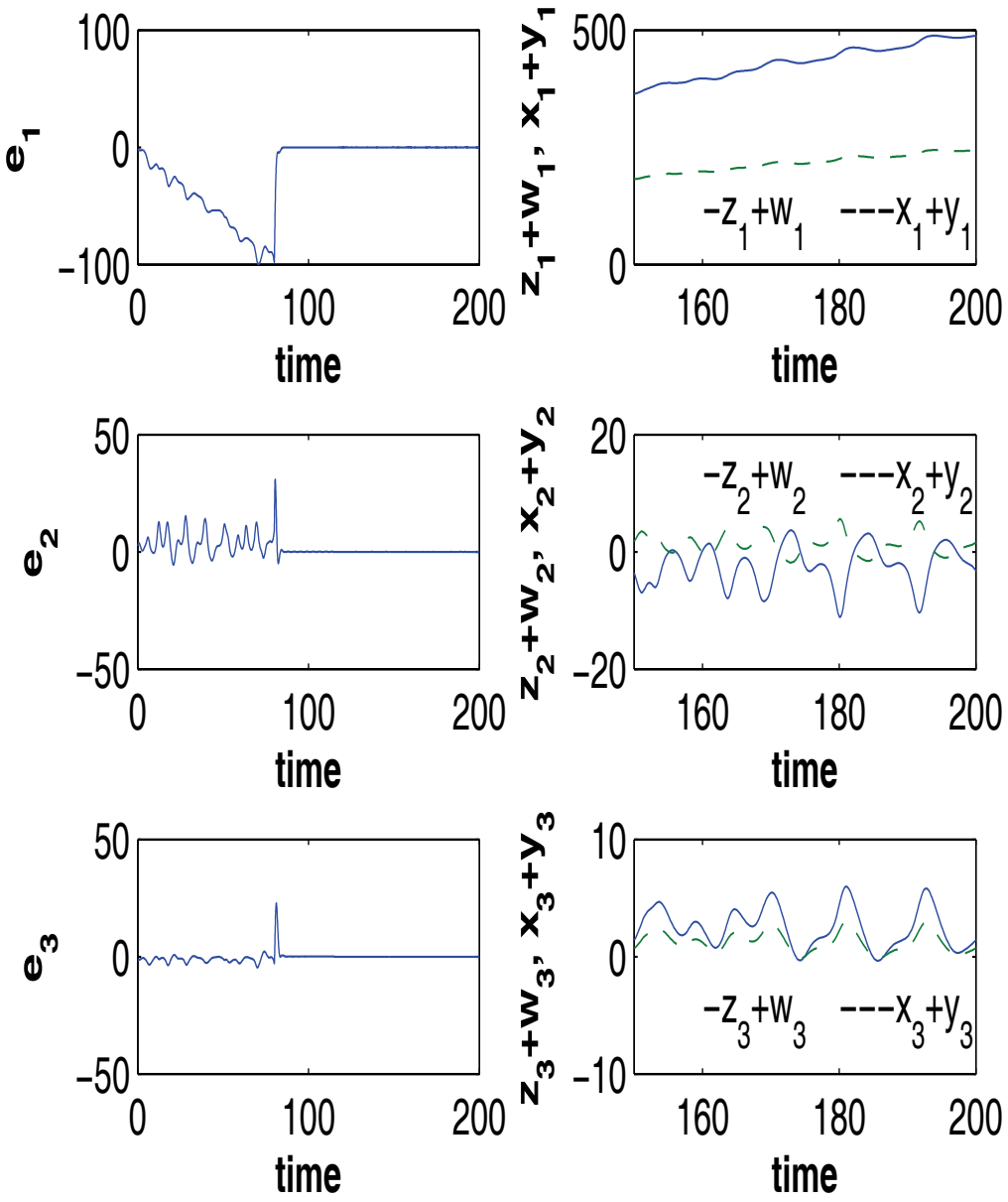

Fig. 4 Error dynamics among the drive and the response systems (column one) and the corresponding dynamics (time series) of the state variable of the drive (dashed line) and the response (solid line) variables (column two) with controllers deactivated for $0 < t < 80$ and activated for $t \geq 80$ where $e_1 = w_1 + z_1 - 2.0(x_1 + y_1)$, $e_2 = w_2 + z_2 + 2.0(x_2 + y_2)$ and $e_3 = w_3 + z_3 - 2.0(x_3 + y_3)$.

3. Hybrid projective combination synchronization: Choosing the parameter values as $\alpha_1 == \alpha_3 = \beta_1 = \beta_3 = 2.0, \alpha_2 = \beta_2 = -2.0$ hybrid projective combination synchronization of the drive systems (6), (7) and the response system (9) are achieved as indicated by the convergence of the error state variables to zero and the projection of the state variables of the drive Josephson junctions on the response Josephson junctions when the controllers are activated for $t \geq 80$ as shown in Figure 7.

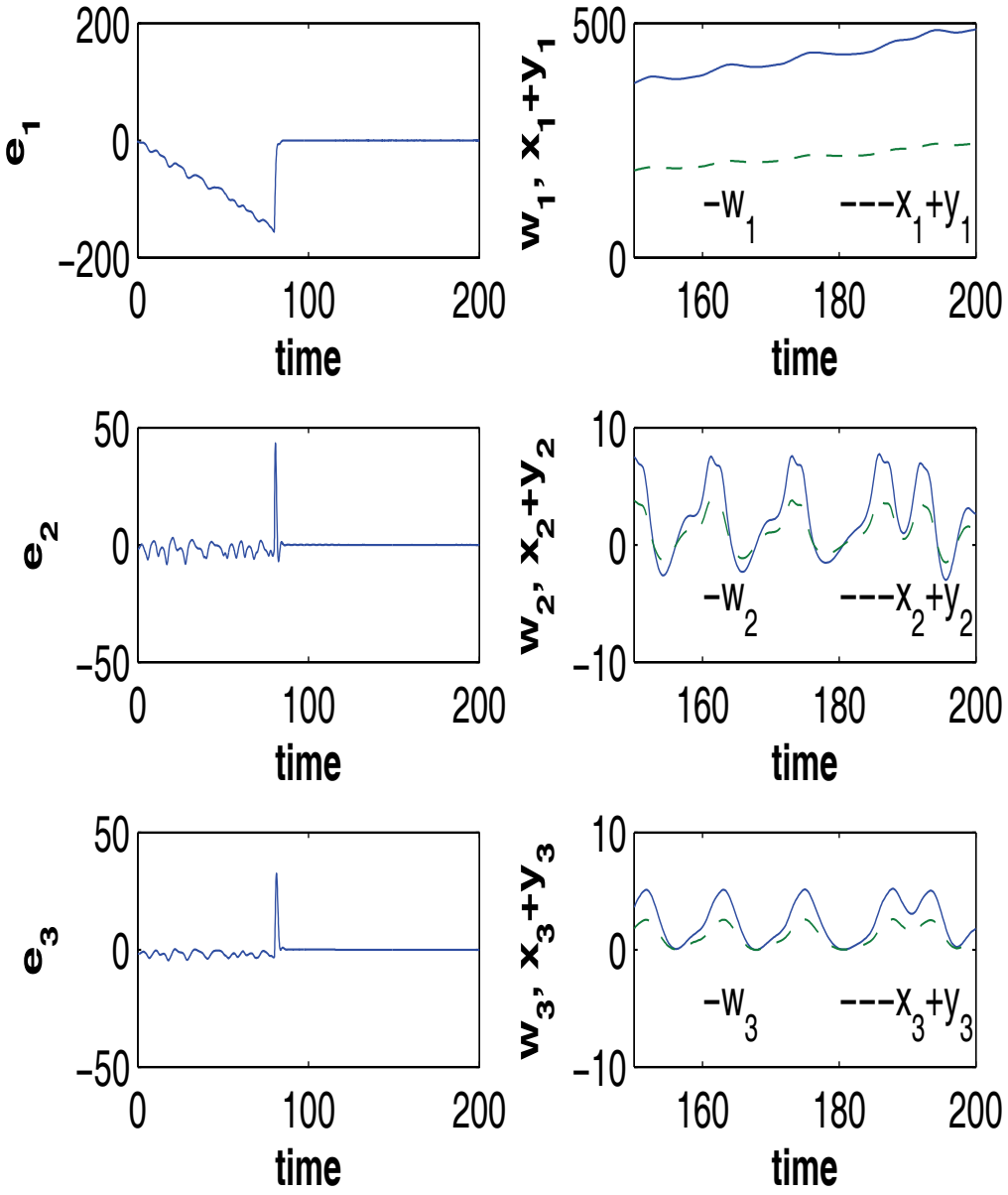

Fig. 5 Error dynamics among the drive and the response systems (column one) and the corresponding dynamics (time series) of the state variable of the drive (dashed line) and the response (solid line) variables (column two) with controllers deactivated for $0 < t < 80$ and activated for $t \geq 80$ where $e_1 = w_1 - 2.0(x_1 + y_1)$, $e_2 = w_2 - 2.0(x_2 + y_2)$ and $e_3 = w_3 - 2.0(x_3 + y_3)$.

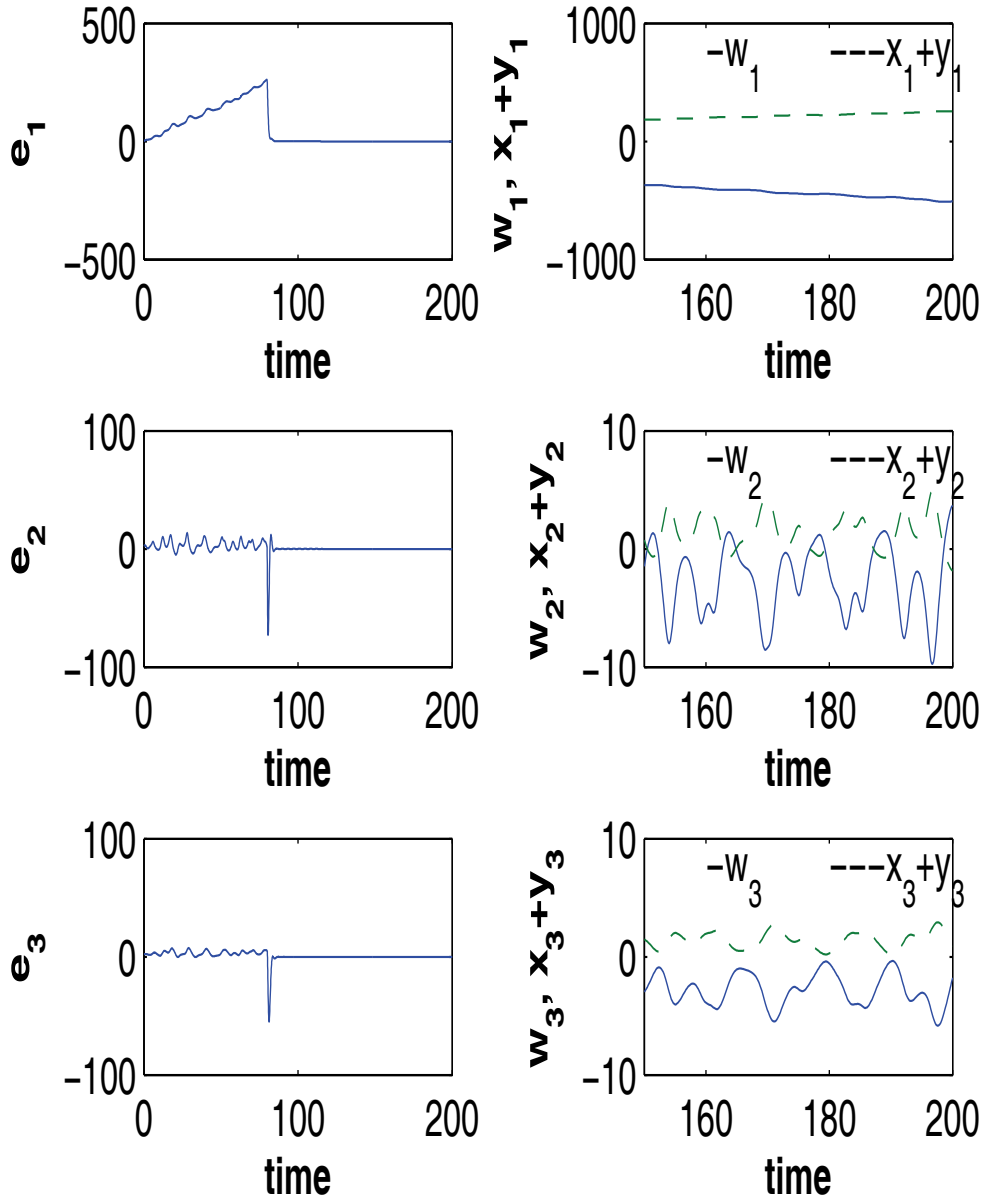

Fig. 6 Error dynamics among the drive and the response systems (column one) and the corresponding dynamics (time series) of the state variable of the drive (dashed line) and the response (solid line) variables (column two) with controllers deactivated for $0 < t < 80$ and activated for $t \geq 80$ where $e_1 = w_1 + 2.0(x_1 + y_1)$, $e_2 = w_2 + 2.0(x_2 + y_2)$ and $e_3 = w_3 + 2.0(x_3 + y_3)$.

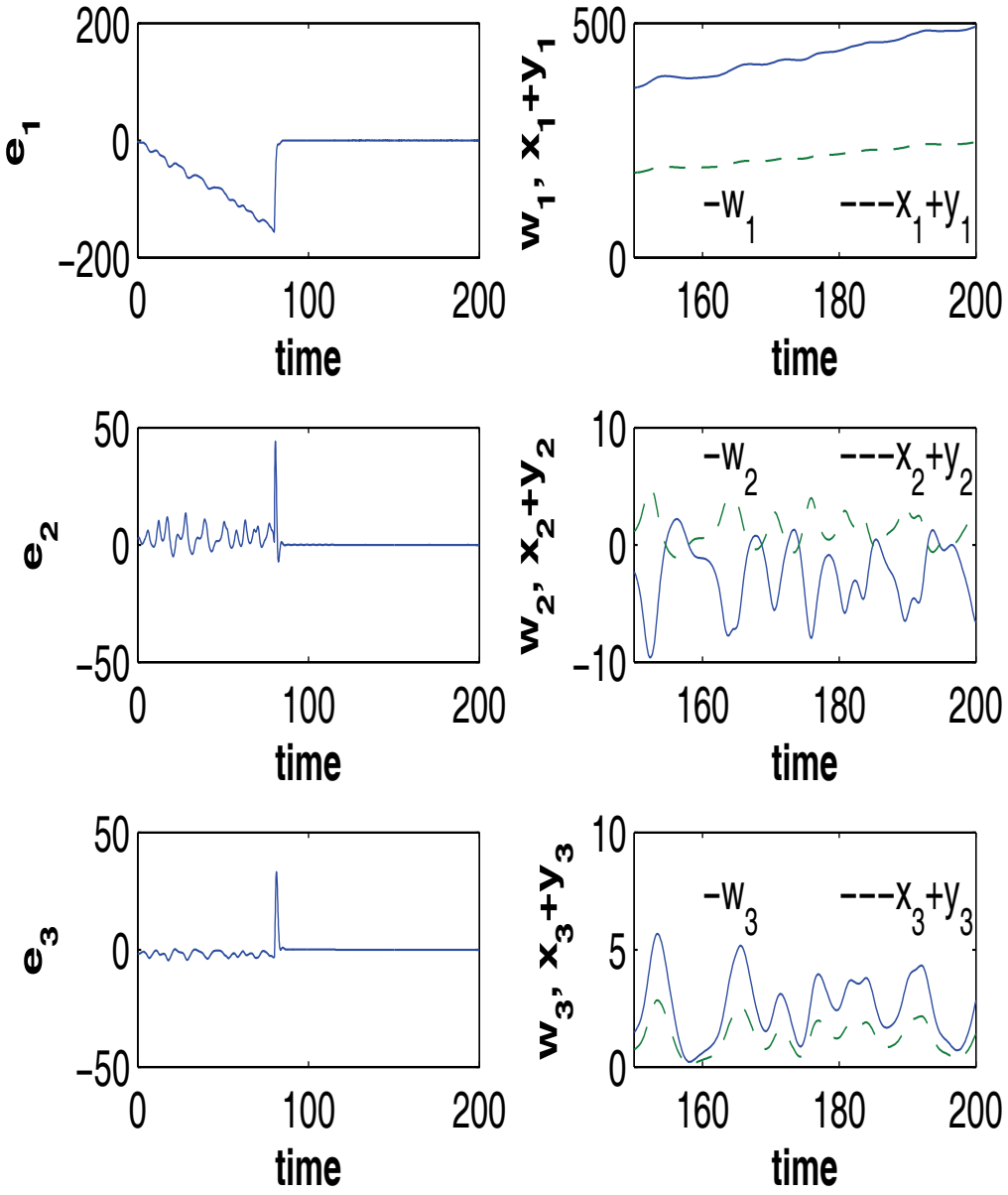

Fig. 7 Error dynamics among the drive and the response systems (column one) and the corresponding dynamics (time series) of the state variable of the drive (dashed line) and the response (solid line) variables (column two) with controllers deactivated for $0 < t < 80$ and activated for $t \geq 80$ where $e_1 = w_1 - 2.0(x_1 + y_1)$, $e_2 = w_2 + 2.0(x_2 + y_2)$ and $e_3 = w_3 - 2.0(x_3 + y_3)$.

5 Conclusion

GCCS of four chaotic systems consisting of two third order chaotic Josephson junctions as drives and two third order chaotic Josephson junctions as response systems via active backstepping technique has

been achieved. We showed from the theoretical analyze that various controllers which is suitable for different types of synchronization scheme can be obtained from the general results. We also showed that combination synchronization and the usual one drive system to one response system synchronization scheme are special cases of the GCCS. Furthermore, the GCCS discussed in this paper can be used to improve security in communication sector in two ways: (1) signal $A\sin\omega t$ can be splited up into two different signals say, $\frac{A}{2}\sin\omega t$ and $\frac{A}{2}\sin\omega t$. Each signal $\frac{A}{2}\sin\omega t$ is loaded into each drive systems and, after synchronization has taken place between the two response systems and the two drive systems then, the message can be retrieved; (2) another way is to load the split up signals $\frac{A}{2}\sin\omega t$ into the first drive system at time t_1 and load the second signal $\frac{A}{2}\sin\omega t$ into the second drive system at another time t_2 and after each of the drive system has undergone GCCS with the response system then the message can retrieved and recombined. So, from this point of view GCCS can offer higher and better security to transmitted information.

References

[1] Alsawalha, M.M. and Noorani, M.S.M. (2012), Chaos reduced-order anti-synchronization of chaotic systems with fully unknown parameters, *Communication in Nonlinear Science and Numerical Simulation*, **17**, 1908–1920.

[2] Yang, C.C. (2012), Robust synchronization and anti-synchronization of identical ϕ^6 oscillators via adaptive sliding mode control, *Journal of Sound and Vibration*, **331**, 501–509.

[3] Pecora, L.M. and Carroll, T.L. (1990), Synchronization of chaotic systems, *Physica Review Letters*, **64**, 821–824.

[4] Jianwen, F., Ling, H., Chen, X., Austin, F., and Geng, W. (2010), Synchronizing the noise perturbed genesio chaotic system by adaptive sliding mode control, *Communications in Nonlinear Science and Numerical Simulation*, **15**, 2546–2551.

[5] Zribi, M., Smaoui, N., and Salim, H. (2010), Synchronization of the unified chaotic systems using active sliding mode controller, *Chaos Solitons and Fractals*, **42**, 3197–3209.

[6] Yang, C.C. (2011), Adaptive synchronization of l$\ddot{u}$ hyperchaotic system with uncertain with parameters based on single-input controller, *Nonlinear Dynamics*, **63**, 447–454.

[7] Njah, A.N. (2011), Synchronization via active control of parametrically and externally excited ϕ^6 van der pol and duffing oscillators and application to secure communications. *Journal of Sound and Vibration*, **17**, 493–504.

[8] Ojo, K.S., Njah, A.N., and Ogunjo, S.T. (2013), Comparison of backstepping and modified active control in projective synchronization of chaos in an extended bonh$\ddot{o}$ffer- van der pol oscillator, *Pramana*, **80**(5), 825–835.

[9] Lu, J., Ho, D.W.C., Cao, J., and Kurth, J. (2013), Single impulsive controller for globally exponential synchronization of dynamical networks, *Nonlinear Analysis: Real World Application*, **14**, 581–593.

[10] Ma, M., Zhou, J., and Cai, J. (2012), Practical synchronization of non autonomous systems with uncertain parameter mismatch via a single state feedback control, *International Journal of Modern Physics C*, **23**(11), 12500731–(14pp).

[11] Sangpet, T. and Kuntanapreeda, S. (2010), Adaptive control of hyperchaotic systems via passitivity feedback control with time-varying gains, *Journal of Sound and Vibration*, **329**, 2490–2496.

[12] Idowu, B.A., Vincent, U.E., and Njah, A.N. (2009), Generalized adaptive backstepping synchronization for non-identical parametrically excited systems, *Nonlinear Analysis: Modelling and Control*, **14**, 165–176.

[13] Njah, A.N., Ojo, K.S.,Adebayo, G.A., and Obawole, A.O. (2010), Generalized control and synchronization of chaos in rcl-shunted josephson junction using ,backstepping design, *Physica C*, **470**, 558–564.

[14] Njah, A.N., and Ojo, K.S.(2010), Backstepping control synchronization of parametrically and externally excited ϕ^6 oscillator with application to secure communication, *International Journal of Modern Physics B*, **24**(23), 4581–459.

[15] Ojo, K.S., Njah, A.N., and Adebayo, G.A.(2011), Anti-synchronization of identical and non-identical ϕ^6 van der pol and ϕ^6 duffing oscillator with both parametric and external excitations via backstepping approach, *International Journal of Modern Physics B*, **25**(14), 1957–1969.

[16] Kareem, S.O., Ojo, K.S., and Njah, A.N.(2012), Function projective synchronization of identical and non-identical modified finance and shimizu朴orioka systems, *Pramana*, **79**(1), 71–79.

[17] Ojo, K.S., Njah, A.N., and Ogunjo, S.T. (2013), Comparison of backstepping and modified active control

in projective synchronization of chaos in an extended bonhöffer van der pol oscillator. *Pramana Journal of Physics*, 80(5):825–835, 2013.

[18] Padmanaban, E. ,Hens, C., and Dana, S.K. (2011), Engineering synchronization of chaotic oscillators by controller based coupling design, *Chaos*, **21**, 013110–(10pp).

[19] Njah, A.N. and Ojo, K.S. (2009), Synchronization via backstepping nonlinear control of externally excited ϕ^6 van der pol and ϕ^6 duffing oscillators. *Far East Journal of Dynamical Systems*, **11**(2), 143–159.

[20] Runzi, L. and Yingian, W. (2012), Active backstepping-based combination synchronization of three chaotic systems, *Advanced Science, Engineering and Medicine*, **4**, 142–147.

[21] Sun, J., Shen, Y., Zhang, G., Xu, C., and Cui, G. (2013), Combination-combination synchronization among four identical or different chaotic systems, *Nonlinear Dynamics*, **73**, 1211–1222.

[22] Lin, H., Cai, J., and Wang, J. (2013), Finite-time combination-combination synchronization for hyperchaotic systems, *Journal of Chaos*, **2013**, 304643–(7pp).

[23] Wu, Z. and Fu, X. (2013), Combination synchronization of three different order nonlinear systems using active backstepping design, *Nonlinear Dynamics*, **73**, 1863–1872.

[24] Runzi, L., Yinglan, W., andShucheng, D. (2011), Combination synchronization of three chaotic classic chaotic systems using active backstepping, *Chaos*, **21**, 0431141–0431146.

[25] Runzi, L. and Yingian, W. (2012), Finite-time stochastic combination synchronization of three different chaotic systems and its application in secure communication. *Chaos*, **22**, 02310901–02310910.

[26] Runzi,L. and Yinglan, W.(2012), Finite-time stochastic synchronization of three different chaotic systems and its application in secure communication, *Chaos*, **22**, 023109–(10pp).

Journal of Applied Nonlinear Dynamics 5(1) (2016) 59–64

Journal of Applied Nonlinear Dynamics

https://lhscientificpublishing.com/Journals/JAND-Default.aspx

Paralysis Mechanism of α-Conotoxin SI from Molecular Dynamics Simulations and Free Energy Calculations

Onur Tuna[1†], Serdar Kuyucak[2], Turgut Baştuğ[1]

[1]Department of Material Science and Nanotechnology, TOBB University of Economics and Technology, Ankara, Turkey

[2]School of Physics, University of Sydney, NSW, Australia

Submission Info

Communicated by J.A T. Machado
Received 2 June 2015
Accepted 15 July 2015
Available online 1 January 2016

Keywords

Protein-Ligand Interactions
Molecular Dynamics
Potential of Mean Force
Drug Discovery

Abstract

Peptide toxins offer new avenues for development of novel drugs. α-Conotoxin SI, which binds to neuromuscular Nicotinic Acetylcholine Receptor, is such an analgesic drug candidate. Understanding the mechanism of action is crucial for improving the properties of drug candidates. Here, we use docking and molecular dynamics simulations to propose a model for binding of α-Conotoxin SI to Nicotinic Acetylcholine Receptor and discuss its paralysis effect.

1 Introduction

Through ages, drugs have had an important role in human health. Beside treatment or preventing a disease, drugs are also used for pain relief. Such drugs are called as "pain killers" or "analgesics". Until recently, the most used analgesic is morphine [1]. However morphine has a disadvantage in that it causes addiction when used continuously [2]. New analgesics that do not have such negative effects need to be discovered. In this study, we investigate the binding properties of a toxin peptide, which offers an alternative analgesic to morphine.

Neuromuscular Nicotinic Acetylcholine Receptors (nAChR) are found in most mammalians including humans. nAChRs are responsible for transmitting the signals which cause muscle contraction [3]. If some molecule inhibits such signaling mechanism, then muscle contraction will not occur. Analgesic drugs can be designed on this basis [4], and conotoxins offer promising candidates for this purpose. However, the binding mechanism of Conotoxins to nAChRs is not known. Here we investigate the binding mechanism of α-Conotoxin SI (α-SI) to nAChR using docking and molecular dynamics (MD) simulations [5]. We also determine the binding free energies from the potential of mean force (PMF) using umbrella sampling simulations [6, 7].

†Corresponding author.
Email address: onurtuna@hacettepe.edu.tr

ISSN 2164 – 6457, eISSN 2164 – 6473/$-see front materials
DOI : 10.5890/JAND.2016.03.004

The signaling arise from opening of nAChR channels, which allow Na^+ ions enter into the cell. The opening of nAChRs is triggered by binding of acetylcholine to their C-loops. Previous studies have shown that when two acetylcholines bind to C-loops of two α subunits, they cause a structural change through the α subunit. This structural change is caused by folding in towards the nAChR surface, and results in opening of the channel [8–10]. Here we propose that when α-SI binds to α subunits of nAChRs, it has a reverse effect on this structural change and thus inhibits channel opening.

2 Simulations

In order to obtain complex structures of nAChR and α-SI, we have carried out docking studies using HADDOCK. We have obtained the crystal structure coordinates of these molecules from Protein Data Bank (PDB ID for nAChR is 2BG9 and α-SI is 1HJE). Because HADDOCK is an information-driven docking program, one has to provide information about the potential binding sites [11]. Since the binding site is expected to be near the acetylcholine binding site, we have chosen the amino acid sequences in this region as active sites. These are 1–28, 148–154, and 189–197 numbered amino acids in the 2BG9 structure (see Fig. 1). There is no information on active sites in α-SI, therefore all the amino acids in α-SI are included in docking. From analysis of the docking simulations, we have obtained probabilities for the potential complex structures. The most probable complex structure is shown in Fig. 2. We have performed MD simulations on this structure in order to investigate the dynamics of binding of α-SI to nAChR.

We have performed MD simulations for 20 ns with the NAMD software package [12]. The NPT ensemble is used with the Langevin Piston method, keeping temperature at 298 K and pressure at 1 atm. The box has been created with the dimensions of 95x110x50 $\mathring{A}^3$. We have used PARAM22 version of the CHARMM force field with CMAP correction [13,14]. We have monitored the distance deviation between the center of mass of α-SI and nAChR to check equilibration of the complex structure. As shown in Fig. 3, a stable complex structure emerges after 13 ns.

Analysis of the MD simulations suggests a dynamical mechanism for this binding event. We have investigated the distance between an amino acid on the surface near the C-loop (Thr150) and an amino acid on this C-loop (Cys192). As shown in Fig. 4, the C-loop has moved away from nAChR after α-SI binds to nAChR. As mentioned previously, the signaling system is based on folding of C-loop toward nAChR. The MD simulations indicate that binding of α-SI causes the C-loop to move away from nAChR, which will inhibit opening of the nAChR ion channel. This can cause blocking of the signal transmission needed for muscle contraction.

After the system is equilibrated, one can carry out PMF calculations using the umbrella sampling method. For this purpose, we have created 40 umbrella windows by moving the coordinates of α-SI in the reaction coordinate which is in the y direction. The distance between each window is 0.5 $\mathring{A}$ in the reaction coordinate. For each window, we have carried out 2 ns MD simulations with the same parameters of the equilibrium simulations mentioned previously. The data obtained from the umbrella sampling simulations are unbiased and combined using the weighted histogram analysis method. The final PMF for binding of α-SI (Fig. 5) indicates a free energy well of depth 11 k_BT, which is sufficient to keep α-SI in a stable bound state.

3 Conclusions

In this paper, we have proposed a site on nAChR for binding of α-SI and a binding mechanism. Comparing the docking and MD simulations with PMF calculations, it is clear that the complex structure provides a reasonable model for binding of α-SI to nAChR. The simulations in this study

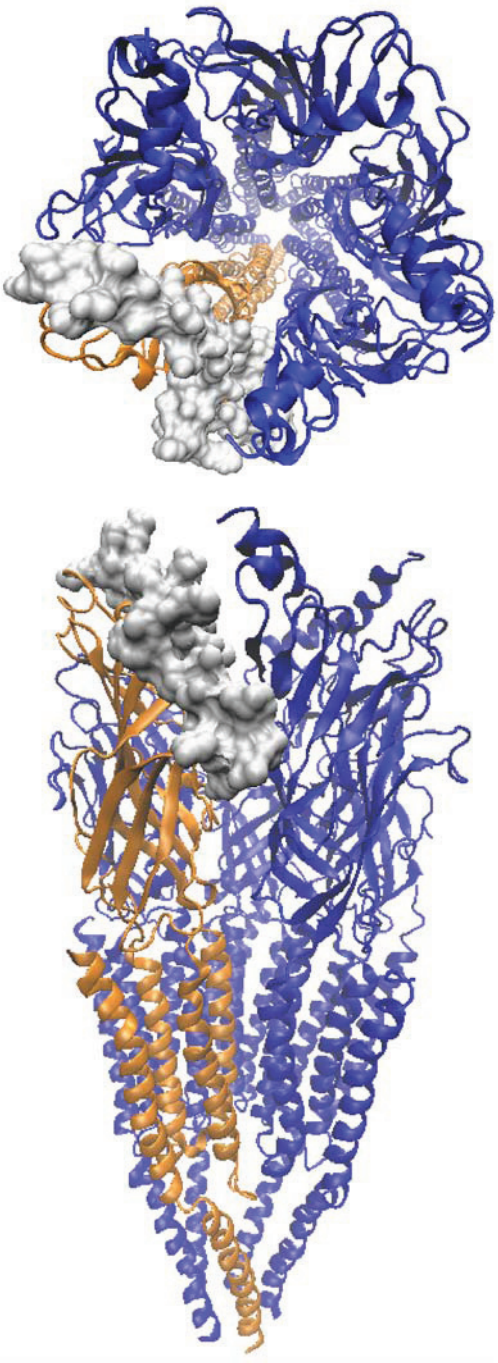

Fig. 1 The active amino acids on nAChR employed in docking calculations are shown as embossed.

reveal the paralysis mechanism caused by the binding of α-SI and how it blocks opening of the channel. Based on the PMF calculations, about 11 kT of energy is needed to dissociate α-SI from nAChR and allow opening of the channel.

For a prospective drug design from α-SI, we need to know the active amino acids involved in binding for both nAChR and α-SI. The active subunit of nAChR was unknown until now. Based on our atomistic level simulations, we propose that the active subunit is the α subunit of nAChR. In future studies, one can carry out mutation simulations in this part of nAChR in order to investigate

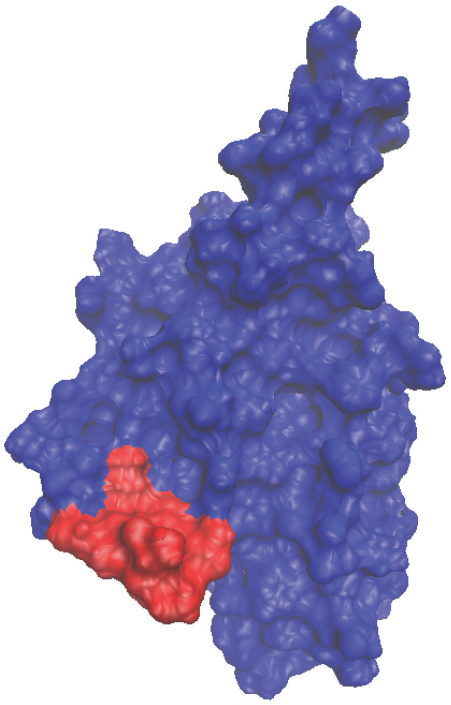

Fig. 2 The most probable complex structure of nAChR and α-SI predicted by HADDOCK. The extracellular part of α subunit of nAChR is shown in blue, and α-SI is shown in red.

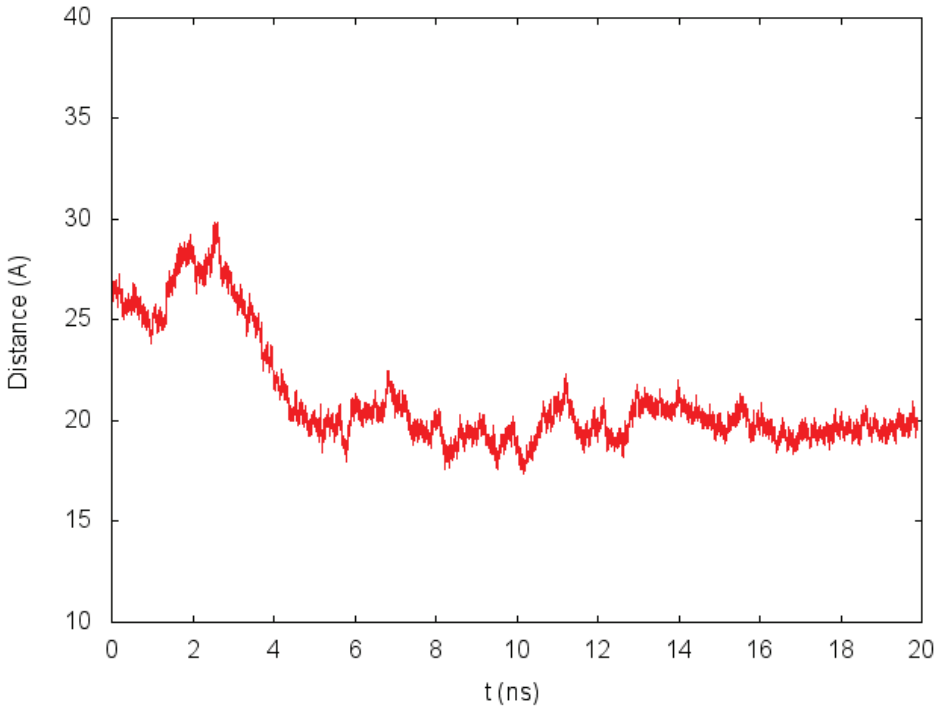

Fig. 3 The distance deviation between the of center of mass of α-SI and nAChR during 20 ns MD simulation.

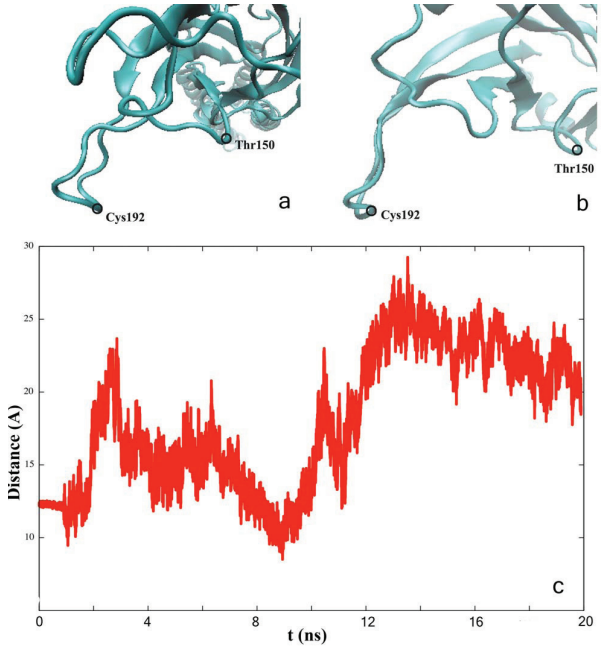

Fig. 4 a) The C-loop of nAChR without a ligand. b) The C-loop of the nAChR after α-SI (not shown) binds. c) The distance change between the α carbons of Cys192 and the Thr150 during 20 ns MD simulations. After the complex is equilibrated, the average distance between the α carbons of Cys192 and the Thr150 has increased by about 10 Å.

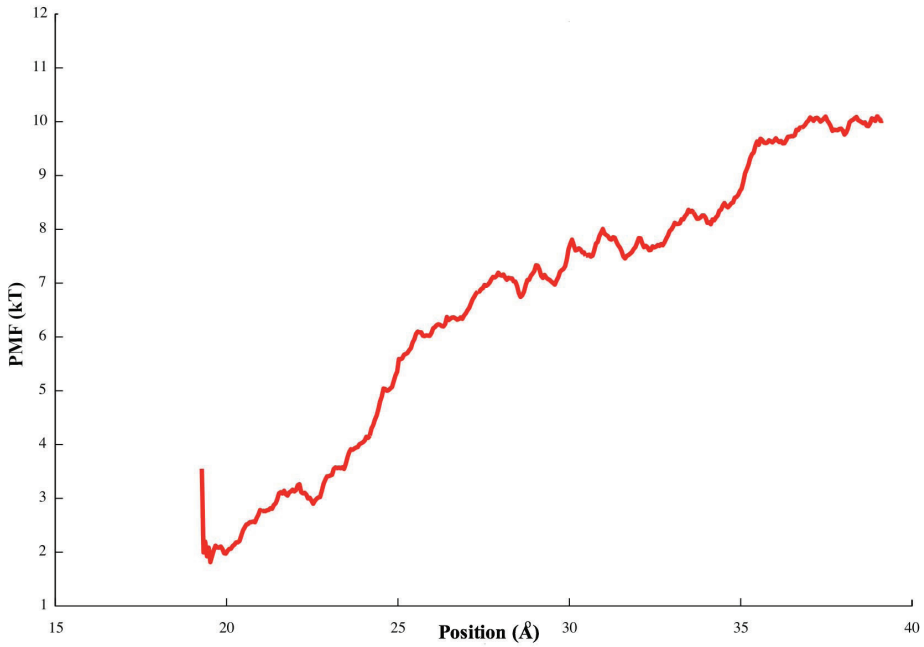

Fig. 5 The potential of mean force curve for the binding of α-SI.

the affinity change due to these mutations. Our study also provides an understanding of the paralysis mechanism of α-SI, which may lead to discovery of new analgesic drugs in future.

References

[1] Jonsson, T., Christensen, C.B., Jordening, H., and Frolund, C. (1988), The bioavailability of rectally administered morphine, *Pharmacological Toxicology*, **62**, 203–205.

[2] Martin, W.R. and Fraser, H.F. (1961), A comparative study of physiological and subjective effects of heroin and morphine administered intravenously in postaddicts, *Journal of Pharmacology and Experimental Therapeutics*, **133**, 388–399.

[3] Karlin, A. (1993), Structure of nicotinic acetylcholine receptors, *Current Opinion in Neurobiology*, **3**, 299–309.

[4] Favreau, P., Le Gall, F., Benoit, E., and Molgo, J. (1999), A review on conotoxins targeting ion channels and acetylcholine receptors of the vertebrate neuromuscular junction, *Acta Physiologica*, **49**, 257–267.

[5] Alder, B.J. and Wainwright, T.E. (1959), Studies in Molecular Dynamics. I. General Method, *The Journal of Chemical Physics*, **31**, 459.

[6] Torrie, G.M. and Valleau, J.P. (1977), Nonphysical sampling distributions in Monte Carlo free-energy estimation: Umbrella sampling, *Journal of Computational Physics*, **23**, 187–199.

[7] Bastug, T. and Kuyucak, S. (2009), Importance of the Peptide Backbone Description in Modeling the Selectivity Filter in Potassium Channels, *Biophysical Journal* **96**, 4006–4012.

[8] Miyazawa, A., Fujiyoshi, Y., and Unwin, N. (2003), Structure and gating mechanism of the acetylcholine receptor pore, *Nature*, **423**, 949–955.

[9] Grosman, C., Zhou, M., and Auerbach, A. (2000), Mapping the conformational wave of acetylcholine receptor channel gating, *Nature*, **403**, 773–776.

[10] Sakmann, B., Methfessel, C., Mishina, M., Takahashi, T., Takai, T., Kurasaki, M., Fukuda, K., and Numa, S. (1985), Role of acetylcholine receptor subunits in gating of the channel, *Nature*, **318**, 538–543.

[11] de Vries, S.J., van Dijk, M., and Bonvin, A.M.J.J. (2010) , The HADDOCK web server for data-driven biomolecular docking *Nature Protocols*, **5**, 883–897.

[12] Kale, L., Skeel, R., Bhandarkar, M., Brunner, R., Gursoy, A., Krawetz, N., Phillips, J., Shinozaki, A., Varadarajan, K., and Schulten, K. (1999) , NAMD2: Greater scalability for parallel molecular dynamics, *Journal of Computational Physics*, **151**, 283–312.

[13] Brooks, B.R., Brooks III, C.L., Mackerell, A.D., Nilsson, L., Petrella, R.J., Roux, B., Won, Y., Archontis, G., Bartels, C., Boresch, S., Caflisch, A., Caves, L., Cui, Q., Dinner, A.R., Feig, M., Fischer, S., Gao, J., Hodoscek, M., Im, W., Kuczera, K., Lazaridis, T., Ma, J., Ovchinnikov, V., Paci, E., Pastor, R.W., Post, C.B., Pu, J.Z., Schaefer, M., Tidor, B., Venable, R.M., Woodcock, H.L., Wu, X., Yang, W, York, D.M., and Karplus, Y. (2009), CHARMM: The Biomolecular simulation Program. *Journal of Computational Chemistry*, **30**, 1545–1615.

[14] Buck, M., Bouguet-Bonnet, S., Pastor, R.W., and MacKerell Jr., A.D. (2006), , Importance of the CMAP Correction to the CHARMM22 Protein Force Field: Dynamics of Hen Lysozyme *Biophysical Journal*, **90**, L36–L38.

Journal of Applied Nonlinear Dynamics 5(1) (2016) 65–71

Journal of Applied Nonlinear Dynamics

https://lhscientificpublishing.com/Journals/JAND-Default.aspx

Numerical Solution of Energy Transmission Lines Equivalent Circuit Equations with Adomian Decomposition Method

N.F.O. Serteller†, D. Ustundag

Marmara University, Electrical-Electronics Engineering, Goztepe, Istanbul
Marmara University, Art and Science Faculty, Mathematics Department, Goztepe, Istanbul

Submission Info

Communicated by J.A T. Machado
Received 9 June 2015
Accepted 15 July 2015
Available online 1 January 2016

Keywords

Adomian decomposition method
Finite difference method
Mathematica
Transmission lines

Abstract

In this paper, analysis for a mathematical model of an equivalent circuit to provide solutions of electrical energy power transmission lines (ETL) with Adomian Decomposition Method (ADM) has been proposed. By using Mathematica program, partial differential equations as a function of voltage (current) forming the model are solved and compared with the finite difference method (FDM). The results of some special examples obtained from ADM and FDM illustrate very good synchronism and show the simplicity and the efficiency of the method.

1 Introduction

The historical development of ETL dates back to first telephone lines with the invention of two simple conductor lines. Since the first development of the transmission lines studies, numerous mathematical and experimental analyses have been done by researchers [1-9]. Especially, various mathematical analysis methods of ETL or telegraph equation are commonly used in the study of wave propagation of electric signals in a cable transmission line and also in wave phenomena by different researchers. Generally in ETL, resistance (R), capacitance (C) and inductance (L) have less impact at low frequencies than high frequencies, but as the frequency goes up, their effect and distribution increase. Therefore, in high frequency devices, resistance, capacitance, inductance and conductance (G) play vital role. This indicates that they are valuable per each unit length and they are called distributed parameters. The electrical equivalent circuits which consist of changeable values of these components schematically represented as in Figure 1. The length of a two conductor ETL is shown in Figure 1(a) and the modelling for components of this circuit type can be seen in Figure 1(b). A lumped parameter of circuit represents a nonlinear differential equation $F(u(z,t)) = f$, where F is a nonlinear differential operator and $u(z,t)$ and f are functions of z and t . Here, to solve the ETL with ADM is used and compared with well-known FDM. The decomposition method ADM by Adomian [1] yields rapidly convergent

†Corresponding author.
Email address: fserteller@marmara.edu.tr

ISSN 2164 – 6457, eISSN 2164 – 6473/$-see front materials
DOI : 10.5890/JAND.2016.03.005

series solutions by using a few iterations for nonlinear partial differential equations. The advantage of this method is that it provides a direct scheme for solving nonlinear equation seen not only in ETL but also transient phenomena in electric machines, wave equations and transient analyses in any other electrical applications. Moreover, there is not any linearization, perturbation and transformation [1-5]. On the other hand, FDM is very old method among numerical methods and lots of researchers have studied it from different aspects. We can refer to the first studies Serteller N.F. [6] and Coggon H. [10] and the references therein. In this paper, the modified FDM is introduced and especially, corners are taken into special consideration unlike others papers.

2 Mathematical methods

In this section, the telegraph equations which are important in electric-electronic engineering are given by using two different methodology (ADM-FDM). Following this, we will give three different non-linear examples graphically.

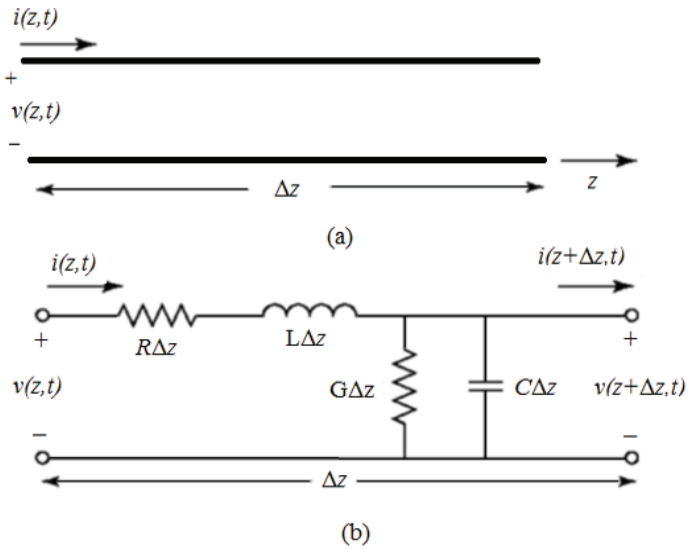

Fig. 1 (a) *Voltage and current formulations in a two-conductor (b) Lossy transmission lines circuit components formulated with distributed parameters.*

To determine the unknown depending on the source connected to transmission line and the effect of the load transmission line in equations, the problems discussed are questioned according to border or initial conditions. In this methodology, the studies are done by approaching the initial conditions. However, for the same mathematical models, with small changes it is also possible to use the boundary conditions. For FDM, grid topology is used to solve system of $(n \times n)$ equations $F(u(z,t)) = f$ for numerical computing. ADM [4-6, 8] does not require grid system but, it requires F to be rewritten in the operator form as follows

$$Lu(z,t) + Ru(z,t) + Nu(z,t) = f, \tag{1}$$

where L is an operator representing the linear portion of F which is easily invertible, R is a linear operator for the reminder of the linear portion and N is a nonlinear operator representing the nonlinear terms of F. Applying the inverse operator L^{-1} to Eq. (1) we obtain

$$u(z,t) = g(z,t) - L^{-1}Ru(z,t) - L^{-1}Nu(z,t), \tag{2}$$

where g represents the function generated by integrating f and using initial conditions. ADM admits linear terms $u(z,t)$ which can be written as an infinite sum of components as follows

$$u(z,t) = \sum_{k=0}^{\infty} u_k(z,t), \tag{3}$$

and identifies the nonlinear terms by decomposition series, that is,

$$Nu = \sum_{k=0}^{\infty} A_k, \tag{4}$$

where A_k is the so called Adomian polynomial, formally determined by a formula[a]. Using this formula and substituting (4) into (2) we get

$$\sum_{k=0}^{\infty} u_k(z,t) = u_0(z,t) - L^{-1} \sum_{k=0}^{\infty} Ru(z,t) - L^{-1} \sum_{k=0}^{\infty} A_k. \tag{5}$$

The recursive relationship is then found as

$$\begin{cases} u_0(z,t) = g \\ u_{k+1}(z,t) = L^{-1} R u_k(z,t) + L^{-1} A_k. \end{cases} \tag{6}$$

After determining components $u_k(z,t)$, $k \geq 0$, the solution $u(z,t)$ turns into a series form immediately. The series may be summed to give the solution in a closed form or used to provide the approximate solution for concrete problems. A general mathematical representation of ETL model in Figure 1 is a partial differential equation below

$$\frac{\partial^2 u(z,t)}{\partial z^2} + CL \frac{\partial^2 u(z,t)}{\partial t^2} + (GL + CR) \frac{\partial u(z,t)}{\partial t} + GR\, u(z,t) = 0. \tag{7}$$

In order to solve it by ADM, leave $\dfrac{\partial^2 u(z,t)}{\partial z^2}$ on the left of equation (7) alone and apply inverse operator $L_{zz}^{-1}(\cdot) = \displaystyle\int_0^z \int_0^z (\cdot) dz dz$ on both sides of this equation. Then, with help of equations (2), (3) and (4) and using the initial conditions the zeroth component $u_0(z,t)$ as $u(z,t) = u(z,0) + t u_t(z,0)$ can be defined by

$$u_0(z,t) = -L_{tt}^{-1}(u(z,t)) - L_{tt}^{-1}(L_{zz}(u(z,t))) - L_{tt}^{-1}(L_t(u(z,t))). \tag{8}$$

If $u(z,t)$ is represented as a series $\displaystyle\sum_{k=0}^{\infty} u_k(z,t)$, where $u_0(z,t)$ is given by Eq. (6), then the rest of components $u_k(z,t)$ $(k \geq 1)$ can be determined recursively as follows

$$\begin{cases} u_1(z,t) = -L_{zz}^{-1}(f(z,t)u_0(z,t)) - L_{zz}^{-1}\left(\frac{\partial^2 u_0(z,t)}{\partial t^2}\right) \\ u_2(z,t) = -L_{zz}^{-1}(f(z,t)u_1(z,t)) - L_{zz}^{-1}\left(\frac{\partial^2 u_1(z,t)}{\partial t^2}\right) \\ \vdots \\ u_k(z,t) = -L_{zz}^{-1}(f(z,t)u_{k-1}(z,t)) - L_{zz}^{-1}\left(\frac{\partial^2 u_{k-1}(z,t)}{\partial t^2}\right). \end{cases} \tag{9}$$

Finally, all of $u_k(z,t)$ are calculable and

$$u(z,t) = \lim_{p \to \infty} \left(\sum_{k=0}^{p-1} u_k(z,t) \right). \tag{10}$$

The discussion of the convergence analysis of this decomposition series is not subject to this paper, but we refer to the work of Ngarhasta et al. [7].

[a] $A_k = \dfrac{1}{k!} \left[\dfrac{d^k}{d\lambda^k} Nu \right]_{\lambda=0}$ can generate Adomian polynomials for all forms of nonlinearity.

3 Numerical results

In this part of the paper we present numerical results to test the efficiency of ADM method for solving the telegraph equations.

Example 1. Let us consider following second order partial differential equation

$$\frac{\partial^2 u(z,t)}{\partial^2 z} - \frac{\partial^2 u(z,t)}{\partial^2 t} - 0.1u(z,t) - 2\frac{\partial u(z,t)}{\partial t} = 0 \tag{11}$$

which is called a Hyperbolic Telegraph Equation with given initial conditions:

$$\begin{aligned} u(z,0) &= \sin(z), \\ u_z(z,0) &= 0. \end{aligned} \tag{12}$$

The formulas found from ADM are:

$$\begin{aligned} u_0(z,t) &= \sin(z), \\ u_1(z,t) &= -0.55t^2 \sin(z), \\ u_2(z,t) &= 0.36667t^3 \sin(z) + 0.050416t^4 \sin(z), \\ &\vdots \end{aligned} \tag{13}$$

Solution is graphically presented in Figure 2(a) and 2(b).

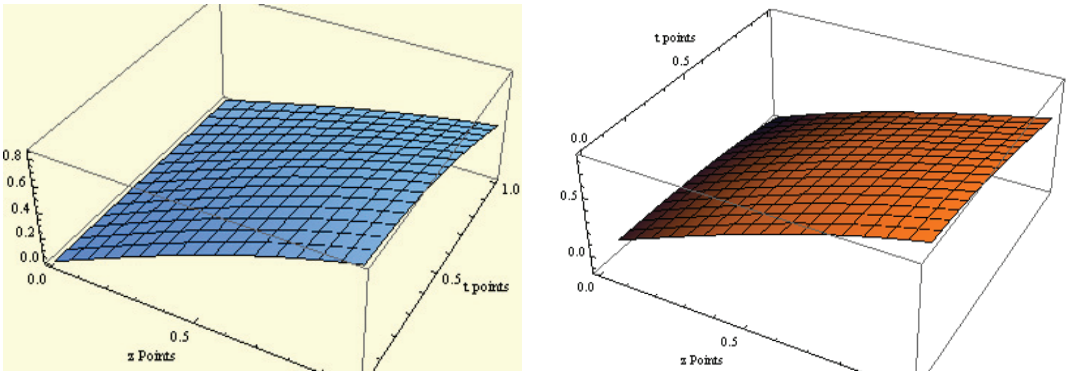

(a) (b)

Fig. 2 Solutions with ADM (a) and FDM (b) for Equation (11).

Example 2. Let us now consider the following equation

$$\frac{\partial^2 u(z,t)}{\partial z^2} - \frac{\partial^2 u(z,t)}{\partial t^2} - (0,01)u(z,t) - (0,2)\frac{\partial u(z,t)}{\partial t} = 0 \tag{14}$$

with initial conditions:

$$\begin{aligned} u(z,0) &= e^z, \\ u_t(z,0) &= z. \end{aligned} \tag{15}$$

Solution with ADM can be found as follows:

$$\begin{aligned} u_0(z,t) &= e^z + zt, \\ u_1(z,t) &= 0.495e^z t^2 - 0,1zt^2 - 0.001666zt^3, \\ u_2(z,t) &= 0.04083e^z t^4 + 0.000083zt^4 + 8,33 \times 10^{-7} zt^5 \\ &\quad -0.2(16499e^z t^3 - 0.0333zt^3 - 0.0004166zt^4), \\ &\vdots \end{aligned} \tag{16}$$

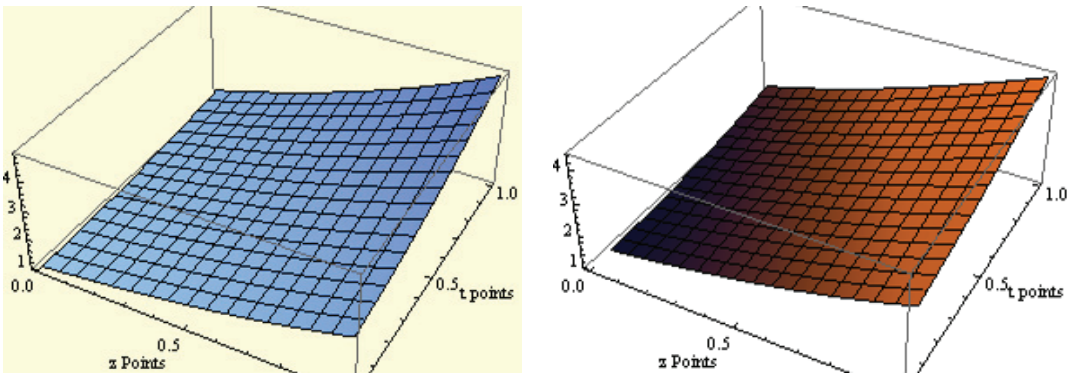

(a) (b)

Fig. 3 (a) Solutions with ADM (a) and FDM (b) for Equation (14).

Example 3. Let us take the following second order partial differential equation

$$\frac{\partial^2 u(z,t)}{\partial z^2} + \frac{\partial^2 u(z,t)}{\partial t^2} - \frac{\partial u(z,t)}{\partial t} + u(z,t) = 0 \tag{17}$$

with the initial conditions:

$$\begin{aligned} u(z,0) &= \sin(z), \\ u_t(z,0) &= -\sin(z). \end{aligned} \tag{18}$$

Solution with ADM could be written as follows:

$$\begin{aligned} u_0 &= \sin(z) - t\sin(z), \\ u_1 &= -\tfrac{1}{2}t^2\sin(z), \\ u_2 &= -\tfrac{1}{6}t^3\sin(z), \\ &\vdots \end{aligned} \tag{19}$$

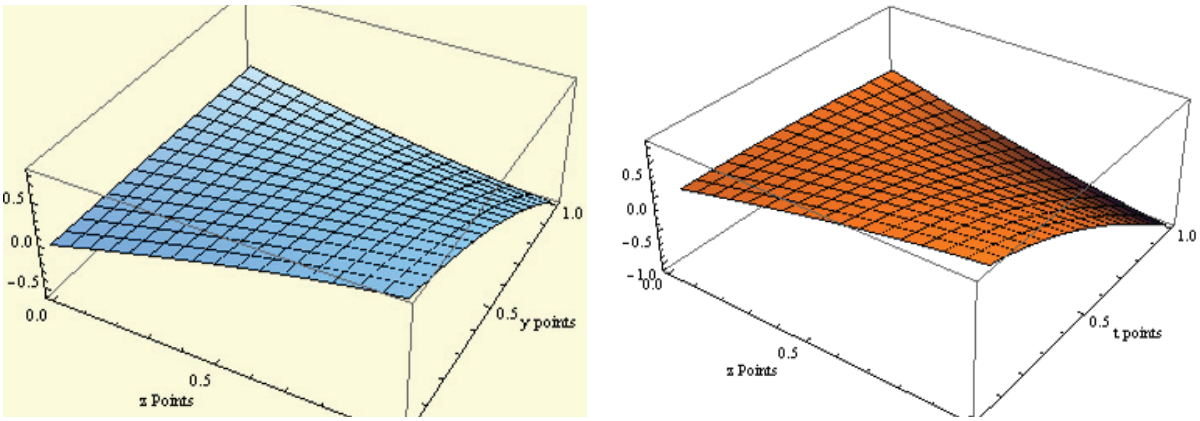

(a) (b)

Fig. 4 (a) ADM and (b) FDM for Example 3.

In Figure 4, one can see the solution of problem (17) with ADM and FDM. As seen in Figure 4 and the others, all three figures are illustrated a good synchronism between the results of FDM and ADM.

It is difficult to give absolute errors for each method because the exact solutions of ETL examples are not known. Therefore, the solutions shown in figures are visually compared. Computer requirements

for storage capacity and CPU time consumption are given in Figure 5 and this indicates that ADM is more advantageous than FDM.

4 Conclusion

In this study, we discussed a second-order hyperbolic telegraph equation including nonlinear initial conditions. We proposed a numerical scheme to solve it with using ADM and FDM techniques. Giving three examples, we have compared the results. As seen in Figure 2-4, ADM methodology has been applied successfully to problems. In electrical engineering, the difficulty of solving higher order partial differential equations is known as very arduous and complex. From this point of view, this study is vital since the solutions could be reduced and simplified with use of ADM. This study could also be extended easily to given boundary conditions or higher order telegraph equations. Moreover, the symbolic implementation ADM code has the flexibility that may easily cover any length of Adomian polynomial for many forms of nonlinear cases.

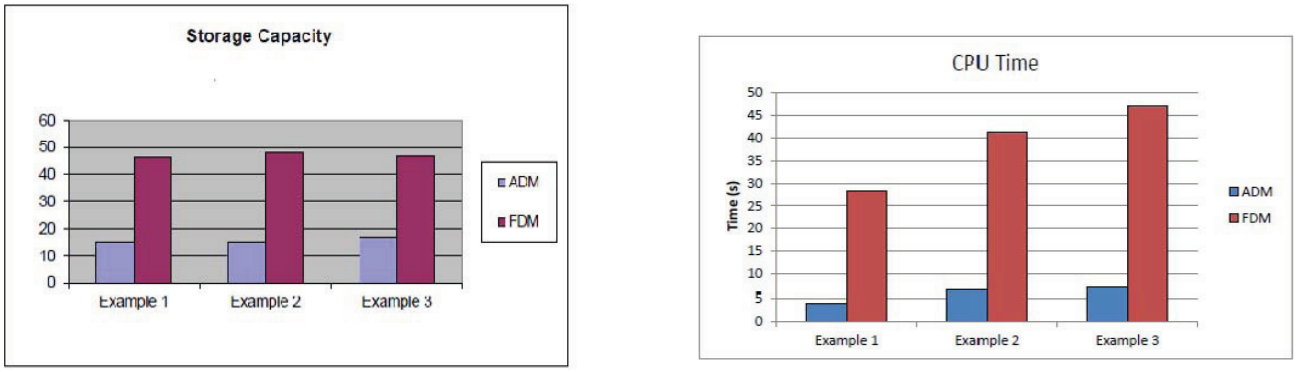

(a) (b)

Fig. 5 Comparison of Methods for consumption of CPU time and memory.

References

[1] Adomian, G. (1998), Solutions of nonlinear PDE, *Appl Math Lett*, **11**, 3, 121–123.
[2] Michalik, M. (2008), Simulation and Analysis of Power System Transients, Lecture Notes.
[3] Lakestani, M. and Saray, B.N., (2010), Numerical Solution of telegraph equation using interpolating scaling functions, *Computers and Appplications*, **60**, 1964–1972.
[4] Srivastava, V.K., Awasthi, M.K., Chaurasia, R.K., and Borenstein, M.T., (2013), The Telegraph Equation and Its Solution by Reduced Differential Transform Method, *Hindawi Publishing Corporation Modelling and Simulation in Engineering*, 1–7.
[5] Biazar, J. and Ebrahimi, H., (2007), An Approximation to the Solution of Telegraph Equation by Adomian Decomposition Method, *International Mathematical Forum*, **2** (45), 2231–2236.
[6] Serteller N.F.O. (2011), Electrostatic Analysis of Transmission Lines to Stimulate Corona Discharge at High Voltage, *Progress in Electromagnetic research M*, 113–117.
[7] Javidi, M. and Nyamoradi, N., (2013), Numerical solution of telegraph equation by using LT inversion Technique, *International Journal of Advanced Mathematical Sciences*, **1** (2), 64-77.
[8] Delghan, M. and Shokri A. (2007), A Numerical Method for Solving the Hyperbolic Telegraph Equation, *Wiley Science*, 1080–1095.

[9] Mittal, R. C. and Bhatia, R. (2014), A Collocation Method for Numerical Solution of Hyperbolic Telegraph Equation with Neumann Boundary Condition, *Hindawi Publishing, International Computational Mathematics*, **2014**.

Journal of Applied Nonlinear Dynamics 5(1) (2016) 73–91

Journal of Applied Nonlinear Dynamics

https://lhscientificpublishing.com/Journals/JAND-Default.aspx

Stability and Hopf Bifurcation of a Predator-Prey Model with Discrete and Distributed Delays

Canan Çelik [1] †, Emine Degirmenci [2]

Department of Mathematical Engineering, Bahçeşehir University, Istanbul, Turkey

Submission Info

Communicated by J.A T. Machado
Received 10 June 2015
Accepted 15 July 2015
Available online 1 January 2016

Keywords

Hopf bifurcation
Predator-prey system
Distributed delay
Discrete delay

Abstract

In this study, a delayed ratio dependent predator-prey model with both discrete and distributed delays is investigated. First, the local stability of a positive equilibrium is studied and then the existence of Hopf bifurcations is established. By using the normal form theory and center manifold theorem, the explicit algorithm determining the stability, direction of the bifurcating periodic solutions are derived. Finally, we perform the numerical simulations for justifying the theoretical results.

1 Introduction

In recent years, dynamical behavior of predator-prey systems have attracted great attention of many theoreticians and experimentalists. (For references see [1]-[28]). Especially incorporating discrete or distributed time delays into these models the authors have observed the effect of the past time of the system. In fact, delay differential equations exhibit more rich and complicated dynamics of stability, periodic structure, bifurcation and so on. For references see [1]-[4], [8], [9], [10]-[33].

In [2], we study the dynamical behavior of the following ratio-dependent delayed predator-prey system with a discrete time delay τ,

$$\begin{aligned} \frac{dN(t)}{dt} &= r_1 N(t) - \varepsilon P(t) N(t), \\ \frac{dP(t)}{dt} &= P(t)(r_2 - \theta \frac{P(t-\tau)}{N(t)}), \end{aligned} \tag{1}$$

where r_1, r_2, ε and θ are positive constants, and $N(t)$ and $P(t)$ can be interpreted as the densities of prey and predator populations at time t, respectively and $\tau \geq 0$ denotes the delay time for the predator density. In this model, predator density is logistic with time delay and the carrying capacity is proportional to prey density. In many of the studies related to stability of predator prey models,

†Corresponding author.
Email address: canan.celik@eng.bahcesehir.edu.tr

ISSN 2164 – 6457, eISSN 2164 – 6473/$-see front materials
DOI : 10.5890/JAND.2016.03.006

authors consider constant carrying capacity, however in this study, we focus on the carrying capacity proportional to prey density which shows really interesting behavior in terms of dynamical structure. However in [1], we moved the discrete time delay into the prey term in the denominator as $\frac{P(t)}{N(t-\tau)}$ and studied the new model with discrete and distributed delay as follows;

$$\begin{aligned} \frac{dN(t)}{dt} &= r_1 N(t) - \varepsilon P(t) N(t) \\ \frac{dP(t)}{dt} &= P(t)[r_2 - \frac{\theta}{N(t-\tau)} \int_{-\infty}^{t} F(t-\tau) P(\tau) d\tau]. \end{aligned} \tag{2}$$

where $F(s)$ is the delay kernel that is a non-negative bounded function defined on $[0,\infty)$ and presents the contribution of the prey population captured by the predator population in the past to the predator population at time t. The reason for introducing a delay into predator-prey models is that the rate of reproduction of predators should depend not just on the rate at which they are consuming prey at the present time, but also on the rate at which they have consumed prey in the past time. Biologically, distributed (continuous) delay is regarded as more realistic than discrete delay since by distributed time delay, we can view the effect of continuous past history of population density.

The model (1) without delay, i.e., $\tau = 0$ was considered by Zhou, et al. [31] in detail. They first studied the stability conditions of the equilibrium points for the system and then by introducing so called Allee effect ([31], [34]) in different forms, the authors investigated the impact of this effect on the dynamics of this predator prey system.

In this paper, we consider the above model (2) by incorporating discrete delay to the predator term in the prey dynamics as,

$$\begin{aligned} \frac{dN(t)}{dt} &= r_1 N(t) - \varepsilon P(t-\tau) N(t), \\ \frac{dP(t)}{dt} &= P(t)[r_2 - \frac{\theta}{N(t-\tau)} \int_{-\infty}^{t} F(t-\tau) P(\tau) d\tau]. \end{aligned} \tag{3}$$

First, by choosing F as the weak kernel, we transform the system into a three dimensional system with discrete time delay and investigate the local stability of the equilibrium point of the associated characteristic equation of the new system and obtain the general stability criteria involving the delay time. Second, we choose time delay τ as bifurcation parameter and show that the positive equilibrium loses its stability and the system exhibits Hopf bifurcation at some critical values. Based on the normal form approach and the center manifold theory introduced by Hassard et. al, [35], we also investigate the direction and the stability of Hopf bifurcation.

The organization of this paper is as follows: In Section 2, we study the local stability of the equilibrium point of the corresponding characteristic equation. In Section 3, we illustrate the existence of Hopf bifurcation. The direction and stability of Hopf bifurcation are investigated in Section 4. Finally in Section 5, numerical simulations are performed to support our results.

2 Equilibrium and local stability analysis

In this section, we first take F as the weak kernel, i.e.,

$$F(s) = \alpha e^{-\alpha s}, \quad \alpha > 0,$$

where $\frac{1}{\alpha}$ presents the mean delay of the weak kernel (the mean delay T is given by $T = \int_0^\infty sF(s)ds = \frac{1}{\alpha}$) and it satisfies $F \geq 0$ for all $t \geq 0$ together with the normalization condition

$$\int_0^\infty F(s)ds = 1.$$

Next, we define a new variable

$$S(t) = \int_{-\infty}^{t} \alpha e^{-\alpha(t-s)} P(s) ds, \tag{4}$$

that transforms system (3) into the following system with discrete time delay;

$$\begin{aligned} \frac{dN(t)}{dt} &= N(t)(r_1 - \varepsilon P(t-\tau)), \\ \frac{dP(t)}{dt} &= P(t)(r_2 - \theta \frac{S(t)}{N(t-\tau)}), \\ \frac{dS(t)}{dt} &= \alpha P(t) - \alpha S(t), \end{aligned} \tag{5}$$

with the equilibrium point $E^* = (N_0^*, P_0^*, S_0^*)$ where $N_0^* = \frac{r_1\theta}{r_2\varepsilon}$, $S_0^* = P_0^* = \frac{r_1}{\varepsilon}$.

To analyze the local stability of the positive equilibrium $E^* = (N_0^*, P_0^*, S_0^*)$, we first use the linear transformation $n(t) = N(t) - N_0^*$, $p(t) = P(t) - P_0^*$ and $s(t) = S(t) - S_0^*$ where $n \ll 1$ and $p \ll 1$ and $s \ll 1$ for which the system (4) turns out to be

$$\begin{aligned} \frac{dn}{dt} &= (N_0^* + n)(r_1 - \varepsilon(P_0^* + p(t-\tau))), \\ \frac{dp}{dt} &= (P_0^* + p)(r_2 - (\frac{\theta(S_0^* + s)}{N_0^* + n(t-\tau)})), \\ \frac{ds}{dt} &= \alpha(P_0^* + p) - \alpha(S_0^* + s). \end{aligned} \tag{6}$$

and using relations $r_1 - \varepsilon P_0^* = 0$, $r_2 - \theta(\frac{S_0^*}{N_0^*}) = 0$ and $P_0^* = S_0^*$, and ignoring the higher order terms yield the following linear system

$$\begin{aligned} \frac{dn}{dt} &= -\varepsilon N_0^* p(t-\tau), \\ \frac{dp}{dt} &= (\frac{r_2 P_0^*}{N_0^*}) n(t-\tau) - \theta(\frac{P_0^*}{N_0^*}) s(t), \\ \frac{ds}{dt} &= \alpha p(t) - \alpha s(t). \end{aligned} \tag{7}$$

whose associated characteristic equation is given by the transcendental equation

$$\lambda^3 + \alpha\lambda^2 + a\lambda + (b + c\lambda)e^{-2\lambda\tau} = 0, \tag{8}$$

where $a = \frac{\alpha\theta P_0^*}{N_0^*}$, $b = \alpha\varepsilon r_2 P_0^*$ and $c = \varepsilon r_2 P_0^*$.

When there is no delay, i.e., $\tau = 0$, the corresponding characteristic equation (7) reduces to

$$\lambda^3 + \alpha\lambda^2 + (a + c)\lambda + b = 0. \tag{9}$$

Since

$$\alpha > 0, \quad b > 0 \quad \texttt{and} \quad \alpha(a + c) > b, \tag{10}$$

by the well-known Routh-Hurwitz criteria, all roots of Eq.(9) are negative or have negative real parts. So if $\tau = 0$, then the equilibrium point E^* is asymptotically stable.

Now we shall consider the distribution of the roots of the transcendental equation (8) since the stability of the point $(0,0,0)$ of linear system (7) depends on the roots of the characteristic equation (8). By the continuous dependence of roots of $\lambda^3 + \alpha\lambda^2 + a\lambda + (b + c\lambda)e^{-2\lambda\tau} = 0$ and the stability result for $\tau = 0$, $\exists \tau_0 > 0$ such that $Re\lambda(\tau) < 0$ for $\tau\varepsilon\ [0, \tau_0)$. Since a loss of asymptotic stability of (N_0^*, P_0^*, S_0^*) will arise when $Re\lambda(\tau) = 0$, we shall examine whether there exists a $\tau^* > 0$ for which $Re\lambda(\tau^*) = 0$. i.e.,

we would like to know when equation (8) has purely imaginary roots. In this section we first obtain the local stability conditions of the equilibrium point.

Suppose for $\tau = \tau^*$ and let $\lambda = i\omega$ be a root of (8) with ω real and without loss of generality, $\omega > 0$. Then ω satisfies

$$(i\omega)^3 + \alpha(i\omega)^2 + a(\omega i) + (b + ic\omega)e^{-2(iw)\tau} = 0.$$

Separating real and imaginary parts, we obtain

$$\begin{aligned} \alpha\omega^2 &= b\cos 2\omega\tau + c\omega\sin 2\omega\tau, \\ -\omega^3 + a\omega &= b\sin 2\omega\tau - c\omega\cos 2\omega\tau, \end{aligned} \tag{11}$$

that is equivalent to

$$\omega^6 + (\alpha^2 - 2a)\omega^4 + (a^2 - c^2)\omega^2 - b^2 = 0.$$

Now let $z = \omega^2$ and denote $p = \alpha^2 - 2a$, $q = (a^2 - c^2)$ and $r = -b^2$ which lead to the equation

$$z^3 + pz^2 + qz + r = 0. \tag{12}$$

Denote

$$g(z) = z^3 + pz^2 + qz + r.$$

Since $\lim_{z\to\infty} g(z) = \infty$ and $r = -b^2 < 0$, we conclude the following result.

Lemma 1. *Since $r < 0$, the polynomial equation (12) has at least one positive root.*

3 Existence of Hopf Bifurcation

By Lemma 1. and without loss of generality, we denote the positive root by z_1 and $\omega_1 = \sqrt{z_1}$.

Solving the equations (11) for τ, we get

$$\tan 2\omega_1\tau = \frac{ab\omega_1 - (b - \alpha c)\omega_1^3}{(\alpha b - ac)\omega_1^2 + c\omega_1^4} + k\pi, k = 0, 1, 2, \ldots$$

which leads to

$$\tau_k = \frac{1}{2\omega_k}\{\arctan(\frac{ab\omega_k - (b - \alpha c)\omega_k^3}{(\alpha b - ac)\omega_k^2 + c\omega_k^4} + k\pi)\}, k = 0, 1, 2, \ldots \tag{13}$$

where $k = 0, 1, 2, \ldots$

Let $\lambda(\tau) = \alpha(\tau) + i\omega(\tau)$ denote the root of (8) near $\tau = \tau_k$ satisfying $\alpha(\tau_k) = 0$ and $\omega(\tau_k) = \omega_{1,}, k = 0, 1, 2, \ldots$ Then we have the following result.

Lemma 2. *Suppose $g'(z_1) \neq 0$, then the following transversality condition is satisfied;*

$$\frac{d\mathrm{Re}\lambda(\tau_k)}{d\tau} \neq 0, \quad \textit{for } k = 0, 1, 2, \ldots$$

and $g'(z_1)$ and $\dfrac{d\mathrm{Re}\lambda(\tau_k)}{d\tau}$ have the same sign.

Proof. Suppose that for $\tau = \tau_k$, let $\lambda = i\omega$ be a root of (8) with ω real and without loss of generality, assume $\omega > 0$. Differentiating the characteristic equation (8) with respect to τ, we get

$$[3\lambda^2 + 2\alpha\lambda + a + ce^{-2\lambda\tau} - 2(b + c\lambda)\tau e^{-2\lambda\tau}]\frac{d\lambda}{d\tau} = 2(b + c\lambda)\lambda e^{-2\lambda\tau},$$

that is

$$\begin{aligned}(\ \frac{d\lambda}{d\tau}\ )^{-1} &= \frac{3\lambda^2+2\alpha\lambda+a+ce^{-2\lambda\tau}-2(b+c\lambda)(\tau e^{-2\lambda\tau})}{2(b+c\lambda)\lambda e^{-2\lambda\tau}}\\ &= .\frac{3\lambda^2+2\alpha\lambda+a+ce^{-2\lambda\tau}}{(b+c\lambda)\lambda e^{-2\lambda\tau}}-\frac{\tau}{\lambda}\\ &= \frac{(3\lambda^2+2\alpha\lambda+a)e^{2\lambda\tau}}{\lambda(b+c\lambda)}+\frac{c}{\lambda(b+c\lambda)}-\frac{\tau}{\lambda}.\end{aligned}$$

Thus we obtain

$$\mathrm{Re}(\ \frac{d\lambda}{d\tau}\ )^{-1}\Big|_{\tau=\tau_k} = \mathrm{Re}[\frac{(3\lambda^2+2\alpha\lambda+a)e^{2\lambda\tau}}{\lambda(b+c\lambda)}]_{\tau=\tau_k}+\mathrm{Re}[\frac{c}{\lambda(b+c\lambda)}]_{\tau=\tau_k}-\mathrm{Re}[\frac{\tau}{\lambda}]_{\tau=\tau_k}.$$

Now, denote

$$\begin{aligned}I &= \mathrm{Re}[\frac{(3\lambda^2+2\alpha\lambda+a)e^{2\lambda\tau}}{\lambda(b+c\lambda)}]_{\tau=\tau_k}\\ J &= \mathrm{Re}[\frac{c}{\lambda(b+c\lambda)}]_{\tau=\tau_k}\\ K &= \mathrm{Re}[\frac{\tau}{\lambda}]_{\tau=\tau_k},\end{aligned}$$

which will be calculated as,

$$I = \mathrm{Re}[\frac{(3\lambda^2+2\alpha\lambda+a)e^{2\lambda\tau}}{\lambda(b+c\lambda)}]_{\tau=\tau_k} = \frac{1}{b^2\omega^2+c^2\omega^4}\{3\omega^6-4a\omega^4+2\alpha^2\omega^4+a^2\}$$

$$J = \mathrm{Re}[\frac{c}{\lambda(b+c\lambda)}]_{\tau=\tau_k} = \frac{-c^2\omega^2}{b^2\omega^2+c^2\omega^4}$$

$$K = \mathrm{Re}[\frac{\tau}{\lambda}]_{\tau=\tau_k} = 0.$$

So we get

$$I+J+K = \frac{1}{b^2\omega^2+c^2\omega^4}\{3\omega^6+2(\alpha^2-2a)\omega^4+(a^2-c^2)\omega^2\} = \frac{1}{b^2\omega^2+c^2\omega^4}\omega^2 g'(z)$$

that is

$$\mathrm{Re}(\ \frac{d\lambda}{d\tau}\ )^{-1}\Big|_{\tau=\tau_k} = \frac{1}{b^2+c^2\omega^2}g'(z).$$

Thus, Lemma 2 follows.

Summarizing the above results, we have the following Theorem on stability and Hopf bifurcation of the system (7).

Theorem 3. *For the system (7) the following results hold,*

i) If $\tau\varepsilon[0,\tau_0)$, *then the equilibrium point* $(0,0,0)$ *of the system (7) is asymptotically stable,*

ii) If $g'(z_1)\neq 0$, *then the system (7) undergoes Hopf bifurcation at the equilibrium point* $(0,0,0)$ *when* $\tau=\tau_k,(k=0,1,2,\ldots)$.

4 Direction and the stability of Hopf bifurcation

In this section we shall determine the direction of Hopf bifurcation and the stability of the bifurcating periodic solutions by applying the normal form theory and the center manifold theorem by Hassard et al. [35].

Throughout this section, we assume that the system (5) undergoes Hopf bifurcations at the positive equilibrium (N_0^*,P_0^*,S_0^*) at $\tau=\tau_k$, and $i\omega_1$ is the corresponding purely imaginary root of the characteristic equation at the positive equilibrium (N_0^*,P_0^*,S_0^*). For the sake of simplicity, we use the notation $i\omega$ for $i\omega_1$.

We first consider the system (5) by the transformation

$$x_1=N-N_0^*,\ x_2=P-P_0^*,\ x_3=S-S_0^*,\ t=\frac{t}{\tau},\ \tau=\tau_k+\mu,$$

which is equivalent to the following Functional Differential Equation(FDE) system in $C=C([-1,0],\mathbb{R}^3)$,

$$\dot{x}(t)=L_\mu(x_t)+f(\mu,x_t), \tag{14}$$

where $x(t)=(x_1(t),x_2(t),x_3(t))^T\in\mathbb{R}^3$, and $L_\mu:C\to\mathbb{R}^3$, $f:\mathbb{R}\times C\to\mathbb{R}^3$ are given respectively, by

$$\begin{aligned}L_\mu(\phi)=\ &(\tau_k+\mu)\begin{bmatrix}0&0&0\\0&0&\dfrac{-\theta P_0^*}{N_0^*}\\0&\alpha&-\alpha\end{bmatrix}\begin{bmatrix}\phi_1(0)\\\phi_2(0)\\\phi_3(0)\end{bmatrix}\\&+(\tau_k+\mu)\begin{bmatrix}0&-\varepsilon N_0&0\\\dfrac{r_2P_0^*}{N_0^*}&0&0\\0&0&0\end{bmatrix}\begin{bmatrix}\phi_1(-1)\\\phi_2(-1)\\\phi_3(-1)\end{bmatrix}\end{aligned}$$

and

$$f(\mu,\phi)=(\tau_k+\mu)\begin{bmatrix}f_{11}\\f_{12}\\0\end{bmatrix}$$

where

$$f_{11}=-\varepsilon\phi_1(0)\phi_2(-1)$$

and

$$f_{12}=-\theta\frac{P_0^*S_0^*}{(N_0^*)^3}\phi_1(-1)\phi_1(-1)+\theta\frac{P_0^*}{(N_0^*)^2}\phi_3(0)\phi_1(-1)+\theta\frac{S_0^*}{(N_0^*)^2}\phi_2(0)\phi_1(-1)-\frac{\theta}{N_0^*}\phi_2(0)\phi_3(0)$$

where $\phi=(\phi_1,\phi_2,\phi_3)\in C$.

By Riesz representation theorem, there exists a function $\eta(\theta,\mu)$ of bounded variation for $\theta\in[-1,0]$, such that

$$L_\mu\phi=\int_{-1}^{0}d\eta(\theta,0)\phi(\theta)\ \text{ for }\ \phi\in C.$$

Indeed we may take

$$\eta(\theta,\mu)=(\tau_k+\mu)\begin{bmatrix}0&0&0\\0&0&\dfrac{-\theta P_0^*}{N_0^*}\\0&\alpha&-\alpha\end{bmatrix}\delta(\theta)-(\tau_k+\mu)\begin{bmatrix}0&-\varepsilon N_0^*&0\\\dfrac{r_2P_0^*}{N_0^*}&0&0\\0&0&0\end{bmatrix}\delta(\theta+1),$$

where δ is the Dirac delta function. For $\phi \in C^1([-1,0],\mathbb{R}^3)$, define

$$A(\mu)\phi = \begin{cases} \dfrac{d\phi(\theta)}{d\theta}, & \theta \in [-1,0) \\ \int_{-1}^{0} d\eta(\mu,s)\phi(s), & \theta = 0. \end{cases}$$

and

$$R(\mu)\phi = \begin{cases} 0, \theta \in [-1,0) \\ f(\mu,\phi), \theta = 0. \end{cases}$$

Then the system (14) is equivalent to

$$\dot{x}_t = A(\mu)x_t + R(\mu)x_t$$

where $x_t(\theta) = x(t+\theta)$ for $\theta \in [-1,0)$. For $\psi \in C^1([-1,0],(\mathbb{R}^3)^*)$, define

$$A^*\psi(s) = \begin{cases} -\dfrac{d\psi(s)}{ds}, & s \in (0,1] \\ \int_{-1}^{0} d\eta^T(t,0)\psi(-t), & s = 0. \end{cases}$$

and a bilinear inner product

$$\langle \psi(s), \phi(\theta) \rangle = \bar{\psi}(0)\phi(0) - \int_{-1}^{0}\int_{\xi=0}^{\theta} \bar{\psi}(\xi-\theta)d\eta(\theta)\phi(\xi)d\xi, \tag{15}$$

where $\eta(\theta) = \eta(\theta,0)$. Then $A(0)$ and A^* are adjoint operators. Suppose that $q(\theta)$ and $q^*(s)$ are eigenvectors of A and A^* corresponding to $i\omega\tau_k$ and $-i\omega\tau_k$, respectively. Then suppose that $q(\theta) = (1,\beta,\gamma)^T e^{i\omega\tau_k\theta}$ is the eigenvector of $A(0)$ corresponding to $i\omega\tau_k$, then $A(0)q(\theta) = i\omega\tau_k q(\theta)$. It follows from the definition of $A(0)$, $L_\mu\phi$ and $\eta(\theta,\mu)$ that

$$\tau_k \begin{pmatrix} i\omega & \varepsilon N_0^* e^{-iw\tau_k} & 0 \\ -\dfrac{r_2 P_0^*}{N_0^*} e^{-i\omega\tau_k} & i\omega & \dfrac{\theta P_0^*}{N_0^*} \\ 0 & \alpha & i\omega+\alpha \end{pmatrix} q(0) = \begin{pmatrix} 0 \\ 0 \\ 0 \end{pmatrix}.$$

Thus we can easily get

$$q(\theta) = (1,\beta,\gamma)^T e^{i\omega\tau_k\theta},$$

where $\beta = -\frac{iw}{\varepsilon N_0^* e^{-iw\tau_k}}$, $\gamma = \frac{S_0^* e^{iw\tau_k}}{N_0^*} - \frac{w^2 e^{iw\tau_k}}{\varepsilon P_0^*\theta}$, $q(0) = (1,\beta,\gamma)^T$.

Similarly, let $q^*(s) = D(1,\beta^*,\gamma^*)e^{i\omega\tau_k s}$ be the eigenvector of A^* corresponding to $-i\omega\tau_k$. By definition of A^*, we get

$$\tau_k \begin{pmatrix} -i\omega & -\dfrac{r_2 P_0^*}{N_0^*} e^{i\omega\tau_k} & 0 \\ \varepsilon N_0^* e^{-iw\tau_k} & -i\omega & \alpha \\ 0 & \dfrac{\theta P_0^*}{N_0^*} & -i\omega+\alpha \end{pmatrix} (q^*(0))^T = \begin{pmatrix} 0 \\ 0 \\ 0 \end{pmatrix}.$$

which leads

$$q^*(0) = D(1, \frac{-iw(N_0^*)^2 e^{iw\tau_k}}{\theta P_0^* S_0^*}, \frac{w^2 (N_0^*)^2 e^{iw\tau_k}}{\theta P_0^* S_0^*} - \frac{\varepsilon N_0^* e^{-iw\tau_k}}{\alpha}).$$

To satisfy that $\langle q^*(s), q(\theta) \rangle = 1$, we evaluate the value of D. By the definition of the bilinear inner product

$$\begin{aligned}\langle q^*(s),q(\theta)\rangle &= \bar{D}(1,\bar{\beta}^*,\bar{\gamma}^*)(1,\beta,\gamma)^T \\ &\quad -\int_{-1}^{0}\int_{\xi=0}^{\theta}\bar{D}(1,\bar{\beta}^*,\bar{\gamma}^*)e^{-i\omega\tau_k(\xi-\theta)}d\eta(\theta)(1,\beta,\gamma)^T e^{i\omega\tau_k\xi}d\xi \\ &= \bar{D}\{1+\beta\bar{\beta}^*+\gamma\bar{\gamma}^* \\ &\quad -\int_{-1}^{O}(1,\bar{\beta}^*,\bar{\gamma}^*)\theta e^{iw\tau_k\theta}d\eta(\theta)(1,\beta,\gamma)^T \\ &= \bar{D}\{1+\beta\bar{\beta}^*+\gamma\bar{\gamma}^* \quad +\tau_k(-\varepsilon N_0^*\beta+\frac{\theta P_0^* S_0^*}{(N_0^*)^2}\bar{\beta}^*)e^{-iw\tau_k}\}.\end{aligned}$$

Thus we can choose $\bar{D}$ as

$$\bar{D}=\frac{1}{1+\beta\bar{\beta}^*+\gamma\bar{\gamma}^* \ +\tau_k(-\varepsilon N_0^*\beta+\frac{\theta P_0^* S_0^*}{(N_0^*)^2}\bar{\beta}^*)e^{-iw\tau_k}},$$

such that $\langle q^*(s),q(\theta)\rangle=1$ and $\langle q^*(s),\bar{q}(\theta)\rangle=0$.

In the following, we use the theory by Hassard et al. [35] to compute the coordinates describing center manifold C_0 at $\mu=0$. Define

$$z(t)=\langle q^*,x_t\rangle, \qquad W(t,\theta)=x_t-2\mathrm{Re}z(t)q(\theta). \tag{16}$$

On the center manifold C_0, we have

$$W(t,\theta)=W(z(t),\bar{z}(t),\theta)=W_{20}(\theta)\frac{z^2}{2}+W_{11}(\theta)z\bar{z}+W_{02}(\theta)\frac{\bar{z}^2}{2}+\cdots,$$

where z and $\bar{z}$ are local coordinates for center manifold C_0 in the direction of q and $\bar{q}^*$. Note that W is real if x_t is real. We consider only real solutions. For the solution $x_t\in C_0$, since $\mu=0$ and (14), we have

$$\begin{aligned}\dot{z} &= i\omega\tau_k z+\langle q^*(\theta),F(0,W(z,\bar{z},\theta)+2Rezq(\theta))\rangle \\ &= i\omega\tau_k z+\bar{q}^*(0)F(0,W(z,\bar{z},0)+2\mathrm{Re}zq(0)) \\ &\overset{def}{=} i\omega\tau_k z+\bar{q}^*(0)F_0(z,\bar{z}) \\ &= i\omega\tau_k z+g(z,\bar{z}),\end{aligned}$$

where

$$g(z,\bar{z})=\bar{q}^*(0)F_0(z,\bar{z})=g_{20}\frac{z^2}{2}+g_{11}z\bar{z}+g_{02}\frac{\bar{z}^2}{2}+g_{21}\frac{z^2\bar{z}}{2}+\cdots, \tag{17}$$

By using (16), we have $x_t(x_{1t}(\theta),x_{2t}(\theta),x_{3t}(\theta))=W(t,\theta)+zq(\theta)+\overline{zq}(\theta)$, $q(\theta)=(1,\beta,\gamma)^T e^{i\omega\tau_k\theta}$, and

$$\begin{aligned}x_{1t}(0) &= z+\bar{z}+W_{20}^{(1)}(0)\frac{z^2}{2}+W_{11}^{(1)}(0)z\bar{z}+W_{02}^{(1)}(0)\frac{\bar{z}^2}{2}+O(|(z,\bar{z})|^3) \\ x_{2t}(0) &= \beta z+\bar{\beta}\bar{z}+W_{20}^{(2)}(0)\frac{z^2}{2}+W_{11}^{(2)}(0)z\bar{z}+W_{02}^{(2)}(0)\frac{\bar{z}^2}{2}+O(|(z,\bar{z})|^3) \\ x_{3t}(0) &= \gamma z+\overline{\gamma\alpha}+W_{20}^{(3)}(0)\frac{z^2}{2}+W_{11}^{(3)}(0)z\bar{z}+W_{02}^{(3)}(0)\frac{\bar{z}^2}{2}+O(|(z,\bar{z})|^3) \\ x_{1t}(-1) &= ze^{-i\omega\tau_k\theta}+\bar{z}e^{i\omega\tau_k\theta}+W_{20}^{(1)}(-1)\frac{z^2}{2}+W_{11}^{(1)}(-1)z\bar{z}+W_{02}^{(1\ )}(-1)\frac{\bar{z}^2}{2}+O(|(z,\bar{z})|^3) \\ x_{2t}(-1) &= z\beta e^{-i\omega\tau_k\theta}+\bar{\beta}\bar{z}e^{i\omega\tau_k\theta}+W_{20}^{(2)}(-1)\frac{z^2}{2}+W_{11}^{(2)}(-1)z\bar{z}+W_{02}^{(2)}(-1)\frac{\bar{z}^2}{2}+O(|(z,\bar{z})|^3)\end{aligned}$$

From the definition of $F(\mu, x_t)$, we have

$$
\begin{aligned}
g(z,\bar{z}) = &\ \bar{q}^*(0) f_0(z,\bar{z}) = \bar{D}\tau_k(1,\bar{\beta}^*,\bar{\gamma}^*)\begin{bmatrix} f_{11}^0 \\ f_{12}^0 \\ 0 \end{bmatrix} \\
f_{11}^0 = &\ -\varepsilon x_{1t}(0)x_{2t}(-1) \\
f_{12}^0 = &\ -\frac{\theta P_0^* S_0^*}{(N_0^*)^3}x_{1t}(-1)x_{1t}(-1) + \frac{\theta P_0^*}{(N_0^*)^2}x_{3t}(0)x_{1t}(-1) + \frac{\theta S_0^*}{(N_0^*)^2}x_{2t}(0)x_{1t}(-1) - \frac{\theta}{N_0^*}x_{2t}(0)x_{3t}(0)
\end{aligned}
$$

Thus

$$
\begin{aligned}
g(z,\bar{z}) = &\ \overline{D}\tau_k[-\varepsilon x_{1t}(0)x_{2t}(-1) + \overline{\beta}^*\{-\frac{\theta P_0^* S_0^*}{(N_0^*)^3}x_{1t}(-1)x_{1t}(-1) + \frac{\theta P_0^*}{(N_0^*)^2}x_{3t}(0)x_{1t}(-1) \\
&+\frac{\theta S_0^*}{(N_0^*)^2}x_{2t}(0)x_{1t}(-1) - \frac{\theta}{N_0^*}x_{2t}(0)x_{3t}(0)\}] \\
= &\ \overline{D}\tau_k\{z^2\begin{bmatrix} -\varepsilon\beta e^{-iw\tau_k\theta} - \overline{\beta}^*\frac{\theta P_0^* S_0^*}{(N_0^*)^3}e^{-2iw\tau_k\theta} + \overline{\beta}^*\frac{\theta P_0^*}{(N_0^*)^2}\gamma e^{-iw\tau_k\theta} + \overline{\beta}^*\frac{\theta S_0^*}{(N_0^*)^2}e^{-iw\tau_k\theta} \\ -\frac{\theta}{N_0^*}\beta\gamma \end{bmatrix} + \\
&z\bar{z}\begin{bmatrix} -\varepsilon\overline{\beta}e^{iw\tau_k\theta} - \varepsilon\beta e^{-iw\tau_k\theta} - \overline{\beta}^*\frac{\theta P_0^* S_0^*}{(N_0^*)^3} \\ -\overline{\beta}^*\frac{\theta P_0^* S_0^*}{(N_0^*)^3} + \overline{\beta}^*\frac{\theta P_0^*}{(N_0^*)^2}\gamma e^{iw\tau_k\theta} + \overline{\beta}^*\frac{\theta P_0^*}{(N_0^*)^2}\overline{\gamma}e \\ -iw\tau_k\theta + \overline{\beta}^*\frac{\theta S_0^*}{(N_0^*)^2}\beta e^{iw\tau_k\theta} + \overline{\beta}^*\frac{\theta S_0^*}{(N_0^*)^2}\overline{\beta}e^{-iw\tau_k\theta} \\ -\overline{\beta}^*\frac{\theta}{N_0^*}\beta\overline{\gamma} - \overline{\beta}^*\frac{\theta}{N_0^*}\overline{\beta}\gamma \end{bmatrix} \\
&+\overline{z}^2\begin{bmatrix} -\varepsilon\overline{\beta}e^{iw\tau_k\theta} - \overline{\beta}^*\frac{\theta P_0^* S_0^*}{(N_0^*)^3}e^{2iw\tau_k\theta} + \overline{\beta}^*\frac{\theta P_0^*}{(N_0^*)^2}\overline{\gamma}e^{iw\tau_k\theta} + \overline{\beta}^*\frac{\theta S_0^*}{(N_0^*)^2}\overline{\beta}e^{iw\tau_k\theta} \\ -\overline{\beta}^*\frac{\theta}{N_0^*}\overline{\beta}\overline{\gamma} \end{bmatrix} \\
&+z^2\overline{z}[\frac{-\varepsilon W_{20}^{(1)}(0)\overline{\beta}e^{iw\tau_k\theta}}{2} - \frac{\overline{\beta}^*\frac{\theta P_0^* S_0^*}{(N_0^*)^3}W_{20}^{(1)}(-1)e^{iw\tau_k\theta}}{2} + \frac{\overline{\beta}^*\frac{\theta P_0^*}{(N_0^*)^2}W_{20}^{(3)}(0)e^{iw\tau_k\theta}}{2} \\
&+\frac{\overline{\beta}^*\frac{\theta S_0^*}{(N_0^*)^2}W_{20}^{(2)}(0)e^{iw\tau_k\theta}}{2} - \frac{\overline{\beta}^*\frac{\theta}{N_0^*}\overline{\gamma}W_{20}^{(2)}(0)}{2} - \frac{\overline{\beta}^*\frac{\theta}{N_0^*}\overline{\beta}W_{20}^{(3)}(0)}{2} + \frac{\overline{\beta}^*\frac{\theta S_0^*}{(N_0^*)^2}\overline{\beta}W_{20}^{(1)}(-1)}{2} \\
&+\frac{\overline{\beta}^*\frac{\theta S_0^*}{(N_0^*)^2}\overline{\gamma}W_{20}^{(1)}(-1)}{2} - \frac{\overline{\beta}^*\frac{\theta P_0^* S_0^*}{(N_0^*)^3}W_{20}^{(1)}(-1)e^{iw\tau_k\theta}}{2} - \frac{\varepsilon W_{20}^{(2)}(-1)}{2}]
\end{aligned}
$$

i.e., By comparing the coefficients with (17), we get

$$g_{20} = 2\overline{D}\tau_k(-\varepsilon\beta e^{-iw\tau_k\theta} - \overline{\beta}^* \frac{\theta P_0 S_0}{N_0^3} e^{-2iw\tau_k\theta} + \overline{\beta}^* \frac{\theta P_0}{N_0^2}\gamma e^{-iw\tau_k\theta} + \overline{\beta}^* \frac{\theta S_0}{N_0^2} e^{-iw\tau_k\theta} - \frac{\theta}{N_0}\beta\gamma)$$

$$g_{11} = (2\overline{D}\tau_k - \varepsilon\overline{\beta}e^{iw\tau_k\theta} - \varepsilon\beta e^{-iw\tau_k\theta} - 2\overline{\beta}^* \frac{\theta P_0 S_0}{N_0^3} + \overline{\beta}^* \frac{\theta P_0}{N_0^2}\gamma e^{iw\tau_k\theta} + \overline{\beta}^* \frac{\theta P_0}{N_0^2}\overline{\gamma} e^{-iw\tau_k\theta}$$

$$g_{02} = 2\overline{D}\tau_k \begin{pmatrix} -\varepsilon\overline{\beta}e^{iw\tau_k\theta} - \overline{\beta}^* \frac{\theta P_0 S_0}{N_0^3} e^{2iw\tau_k\theta} + \overline{\beta}^* \frac{\theta P_0}{N_0^2}\overline{\gamma} e^{iw\tau_k\theta} + \overline{\beta}^* \frac{\theta S_0}{N_0^2}\overline{\beta} e^{iw\tau_k\theta} \\ -\overline{\beta}^* \frac{\theta}{N_0}\overline{\beta}\overline{\gamma} \end{pmatrix}$$

$$\begin{aligned} g_{21} = \ & \overline{D}\tau_k(-\varepsilon W_{20}^{(1)}(0)\overline{\beta}e^{iw\tau_k\theta} - \overline{\beta}^* \frac{\theta P_0^* S_0^*}{(N_0^*)^3} W_{20}^{(1)}(-1)e^{iw\tau_k\theta} + \overline{\beta}^* \frac{\theta P_0^*}{(N_0^*)^2} W_{20}^{(3)}(0)e^{iw\tau_k\theta} \\ & + \overline{\beta}^* \frac{\theta S_0^*}{(N_0^*)^2} W_{20}^{(2)}(0)e^{iw\tau_k\theta} - \overline{\beta}^* \frac{\theta}{N_0^*}\overline{\gamma} W_{20}^{(2)}(0) - \overline{\beta}^* \frac{\theta}{N_0^*}\overline{\beta} W_{20}^{(3)}(0) + \overline{\beta}^* \frac{\theta S_0^*}{(N_0^*)^2}\overline{\beta} W_{20}^{(1)}(-1) \\ & + \overline{\beta}^* \frac{\theta S_0^*}{(N_0^*)^2}\overline{\gamma} W_{20}^{(1)}(-1) - \overline{\beta}^* \frac{\theta P_0^* S_0^*}{(N_0^*)^3} W_{20}^{(1)}(-1)e^{iw\tau_k\theta} - \varepsilon W_{20}^{(2)}(-1) \end{aligned}$$

To determine g_{21},we need to compute $W_{20}(\theta)$ and $W_{11}(\theta)$. By (14) and (17), we have

$$\begin{aligned} \dot{W} \ &= \ \dot{x}_t \ - \dot{z}q + \dot{\overline{z}}\overline{q} \\ &= \begin{cases} AW - 2\mathrm{Re}\{\overline{q}^*(0)f_0 q(\theta)\}, & \theta \in [-1,0) \\ AW - 2Re\{\overline{q}^*(0)f_0 q(\theta)\} + f_0 & \theta = 0, \end{cases} \\ &\overset{def}{=} AW + H(z.\overline{z},\theta), \end{aligned} \tag{18}$$

where

$$H(z.\overline{z},\theta) = H_{20}(\theta)\frac{z^2}{2} + H_{11}(\theta)z\overline{z} + H_{02}(\theta)\frac{\overline{z}^2}{2} + \cdots \tag{19}$$

Note that on the center manifold C_0 near to the origin,

$$\dot{W} = W_z\dot{z} + W_{\overline{z}}\dot{\overline{z}}. \tag{20}$$

Thus we obtain,

$$(A - 2i\omega\tau_k)W_{20}(\theta) = -H_{20}(\theta), \qquad AW_{11}(\theta) = -H_{11}(\theta). \tag{21}$$

By using (18), for $\theta \in [-1,0)$,

$$H(z.\overline{z},\theta) = \overline{q}^*(0)f_0 q(\theta) - q^*(0)f_0(0)\overline{q}(\theta) = -gq(\theta) - \overline{g}\ \overline{q}(\theta). \tag{22}$$

Comparing the coefficients with (19), we obtain the following

$$H_{20}(\theta) = -g_{20}q(\theta) - \overline{g}_{02}\overline{q}(\theta), \qquad H_{11}(\theta) = -g_{11}q(\theta) - \overline{g}_{11}\overline{q}(\theta). \tag{23}$$

From (21) and (23) and the definition of A, we get

$$\dot{W}_{20}(\theta) = 2i\omega\tau_k W_{20}(\theta) - g_{20}q(\theta) - \overline{g}_{02}\overline{q}(\theta).$$

Noticing $q(\theta) = q(0)e^{i\omega\tau_k\theta}$, we have

$$W_{20}(\theta) = \frac{ig_{20}}{\tau_k\omega}q(0)e^{i\omega\tau_k\theta} + \frac{i\overline{g}_{02}}{3\tau_k\omega}\overline{q}(0)e^{-i\omega\tau_k\theta} + E_1 e^{2i\omega\tau_k\theta}, \tag{24}$$

where $E_1 = (E_1^{(1)}, E_1^{(2)}, E_1^{(3)}) \in \mathbb{R}^3$ is a constant vector. Similarly, we have

$$W_{11}(\theta) = -\frac{ig_{11}}{\tau_k\omega}q(0)e^{i\omega\tau_k\theta} + \frac{i\bar{g}_{11}}{\tau_k\omega}\bar{q}(0)e^{-i\omega\tau_k\theta} + E_2, \tag{25}$$

where $E_2 = (E_2^{(1)}, E_2^{(2)}, E_2^{(3)}) \in \mathbb{R}^3$ is a constant vector. Now we will try to find E_1 and E_2. From the definition of A and (21), we obtain

$$\int_{-1}^{0} d\eta(\theta)W_{20}(\theta) = 2i\omega\tau_k W_{20}(0) - H_{20}(0), \tag{26}$$

and

$$\int_{-1}^{0} d\eta(\theta)W_{11}(\theta) = -H_{11}(0), \tag{27}$$

where $d\eta(\theta) = \eta(\theta, 0)$.

By (18) and (19), we have

$$H_{20}(0) = -g_{20}q(0) - \bar{g}_{02}\bar{q}(0) \tag{28}$$

$$+2\tau_k \begin{pmatrix} -\varepsilon\beta e^{-i\omega\tau_k\theta} \\ -\frac{\theta P_0^* S_0^*}{(N_0^*)^3}e^{-2i\omega\tau_k\theta} + \frac{\theta P_0^*\gamma}{(N_0^*)^2}e^{-i\omega\tau_k\theta} + \frac{\theta S_0^*}{(N_0^*)^2}e^{-i\omega\tau_k\theta} - \frac{\theta}{N_0^*}\beta\gamma \\ 0 \end{pmatrix} \tag{29}$$

and

$$H_{11}(0) = -g_{11}q(0) - \bar{g}_{11}\bar{q}(0) \tag{30}$$

$$+2\tau_k \begin{pmatrix} -\varepsilon \mathrm{Re}\left\{\beta e^{-i\omega\tau_k\theta}\right\} \\ -2\frac{\theta P_0^* S_0^*}{(N_0^*)^3} + \frac{\theta P_0^*\gamma}{(N_0^*)^2}\mathrm{Re}\left\{\gamma e^{i\omega\tau_k\theta}\right\} + \frac{\theta S_0^*}{(N_0^*)^2}Re\left\{\beta e^{-i\omega\tau_k\theta}\right\} - \frac{\theta}{N_0^*}\mathrm{Re}\{\beta\overline{\gamma}\} \\ 0 \end{pmatrix}. \tag{31}$$

Substituting (26) and (28) and noticing that

$$\left(i\omega\tau_k I - \int_{-1}^{0} e^{i\omega\tau_k\theta}d\eta(\theta)\right)q(0) = 0$$

$$\left(-i\omega\tau_k I - \int_{-1}^{0} e^{-i\omega\tau_k\theta}d\eta(\theta)\right)q(0) = 0,$$

we obtain

$$(2i\omega\tau_k I - \int_{-1}^{0} e^{2i\omega\tau_k\theta}d\eta(\theta))E_1$$

$$= 2\tau_k \begin{pmatrix} -\varepsilon\beta e^{-i\omega\tau_k\theta} \\ -\frac{\theta P_0^* S_0^*}{(N_0^*)^3}e^{-2i\omega\tau_k\theta} + \frac{\theta P_0^*\gamma}{(N_0^*)^2}e^{-i\omega\tau_k\theta} + \frac{\theta S_0^*}{(N_0^*)^2}e^{-i\omega\tau_k\theta} - \frac{\theta}{N_0^*}\beta\gamma \\ 0 \end{pmatrix}$$

which is

$$\begin{pmatrix} 2i\omega & \varepsilon N_0^* e^{-2i\omega\tau_k\theta} & 0 \\ -\frac{r_2 P_0^*}{N_0^*} e^{-2i\omega\tau_k\theta} & 2i\omega & \frac{\theta P_0^*}{N_0^*} \\ 0 & -\alpha & 2i\omega+\alpha \end{pmatrix} E_1 = 2 \begin{pmatrix} -\varepsilon\beta e^{-i\omega\tau_k\theta} \\ -\frac{\theta P_0^* S_0^*}{(N_0^*)^3} e^{-2i\omega\tau_k\theta} + \frac{\theta P_0^*\gamma}{(N_0^*)^2} e^{-i\omega\tau_k\theta} + \frac{\theta S_0^*}{(N_0^*)^2} e^{-i\omega\tau_k\theta} - \frac{\theta}{N_0^*}\beta\gamma \\ 0 \end{pmatrix}.$$

Now if we solve this system for E_1, we get

$$E_1^{(1)} = \frac{2}{A_1} \begin{vmatrix} -\varepsilon\beta & \varepsilon N_0^* e^{-2i\omega\tau_k\theta} & 0 \\ \frac{-\theta P_0^* S_0^*}{(N_0^*)^3} e^{-2i\omega\tau_k\theta} + \frac{\theta P_0^*\gamma}{(N_0^*)^2} e^{-i\omega\tau_k\theta} + \frac{\theta S_0^*}{(N_0^*)^2} e^{-i\omega\tau_k\theta} - \frac{\theta}{N_0^*}\beta\gamma & 2i\omega & \frac{\theta P_0^*}{N_0^*} \\ 0 & -\alpha & 2i\omega+\alpha \end{vmatrix},$$

$$E_1^{(2)} = \frac{2}{A_1} \begin{vmatrix} 2i\omega & -\varepsilon\beta & 0 \\ -\frac{r_2 P_0^*}{N_0^*} e^{-2i\omega\tau_k\theta} & \frac{-\theta P_0^* S_0^*}{(N_0^*)^3} e^{-2i\omega\tau_k\theta} + \frac{\theta P_0^*\gamma}{(N_0^*)^2} e^{-i\omega\tau_k\theta} + \frac{\theta S_0^*}{(N_0^*)^2} e^{-i\omega\tau_k\theta} - \frac{\theta}{N_0^*}\beta\gamma & \frac{\theta P_0^*}{N_0^*} \\ 0 & 0 & 2i\omega+\alpha \end{vmatrix},$$

$$E_1^{(3)} = \frac{2}{A_1} \begin{vmatrix} 2i\omega & \varepsilon N_0^* e^{-2i\omega\tau_k\theta} & -\varepsilon\beta e^{-i\omega\tau_k\theta} \\ -\frac{r_2 P_0^*}{N_0^*} e^{-2i\omega\tau_k\theta} & 2i\omega & \frac{-\theta P_0^* S_0^*}{(N_0^*)^3} e^{-2i\omega\tau_k\theta} + \frac{\theta P_0^*\gamma}{(N_0^*)^2} e^{-i\omega\tau_k\theta} + \frac{\theta S_0^*}{(N_0^*)^2} e^{-i\omega\tau_k\theta} - \frac{\theta}{N_0^*}\beta\gamma \\ 0 & -\alpha & 0 \end{vmatrix},$$

where

$$A_1 = \begin{vmatrix} 2i\omega & \varepsilon N_0^* e^{-2i\omega\tau_k\theta} & 0 \\ -\frac{r_2 P_0^*}{N_0^*} e^{-2i\omega\tau_k} & 2i\omega & \frac{\theta P_0^*}{N_0^*} \\ 0 & -\alpha & 2i\omega+\alpha \end{vmatrix}.$$

Similarly, substituting (25), (30) and (27), we obtain

$$\begin{pmatrix} 0 & \varepsilon N_0^* e^{-2i\omega\tau_k\theta} & 0 \\ \frac{-\theta P_0^* S_0^*}{(N_0^*)^2} e^{-2i\omega\tau_k\theta} & 0 & \frac{\theta P_0^*}{N_0^*} \\ 0 & -\alpha & \alpha \end{pmatrix} E_2 = 2 \begin{pmatrix} -\varepsilon \mathrm{Re}\left\{\beta e^{-i\omega\tau_k\theta}\right\} \\ K \\ 0 \end{pmatrix}$$

which implies that

$$E_2^{(1)} = \frac{2}{A_2} \begin{vmatrix} -\varepsilon \mathrm{Re}\left\{\beta e^{-i\omega\tau_k\theta}\right\} & \varepsilon N_0^* e^{-2i\omega\tau_k\theta} & 0 \\ K & 0 & \frac{\theta P_0^*}{N_0^*} \\ 0 & -\alpha & \alpha \end{vmatrix},$$

$$E_2^{(2)} = \frac{2}{A_2} \begin{vmatrix} 0 & -\varepsilon \mathrm{Re}\left\{\beta e^{-i\omega\tau_k\theta}\right\} & 0 \\ \frac{-\theta P_0^* S_0^*}{(N_0^*)^2} e^{-2i\omega\tau_k\theta} & K & \frac{\theta P_0^*}{N_0^*} \\ 0 & 0 & \alpha \end{vmatrix},$$

$$E_2^{(3)} = \frac{2}{A_2}\begin{vmatrix} 0 & \varepsilon N_0^* e^{-2i\omega\tau_k\theta} & -\varepsilon \mathrm{Re}\left\{\beta e^{-i\omega\tau_k\theta}\right\} \\ \frac{-\theta P_0 S_0}{N_0^2} e^{-2i\omega\tau_k\theta} & 0 & K \\ 0 & -\alpha & 0 \end{vmatrix},$$

where

$$A_2 = \begin{vmatrix} 0 & \varepsilon N_0^* e^{-2i\omega\tau_k\theta} & 0 \\ -\frac{\theta P_0^* S_0^*}{(N_0^*)^2} e^{-2i\omega\tau_k\theta} & 0 & \frac{\theta P_0^*}{N_0^*} \\ 0 & -\alpha & \alpha \end{vmatrix}.$$

$$K = \frac{-2\theta P_0^* S_0^*}{(N_0^*)^3} + \frac{\theta P_0^* \gamma}{(N_0^*)^2}\mathrm{Re}\left\{\gamma e^{i\omega\tau_k\theta}\right\} + \frac{\theta S_0^*}{(N_0^*)^2}\mathrm{Re}\left\{\beta e^{-i\omega\tau_k\theta}\right\} - \frac{\theta}{N_0^*} Re\{\beta\overline{\gamma}\}$$

Thus we can compute $W_{20}(\theta)$ and $W_{11}(\theta)$ from (24) and (25) and determine the following values to investigate the qualities of bifurcating periodic solution in the center manifold at the critical value τ_k. For this purpose, we express $g'_{ij}s$ in terms of the parameters and delay. And then we can evaluate the following values;

$$\begin{aligned} c_1(0) &= \frac{i}{2\omega\tau_k}(g_{20}g_{11} - 2|g_{11}|^2 - \frac{|g_{02}|^2}{3}) + \frac{g_{21}}{2}, \\ \mu_2 &= -\frac{\mathrm{Re}\{c_1(0)\}}{\mathrm{Re}\{\lambda'(\tau_k)\}}, \\ \beta_2 &= 2\mathrm{Re}\{c_1(0)\}, \\ T_2 &= -\frac{\mathrm{Im}\{c_1(0)\} + \mu_2 \mathrm{Im}\{\lambda'(\tau_k)\}}{\omega\tau_k}. \end{aligned} \tag{32}$$

Theorem 4. *The ratio μ_2 determines the direction of Hopf bifurcation; if $\mu_2 > 0$, then the Hopf bifurcation is supercritical and the bifurcating periodic solutions exist for $\tau > \tau_0$, if $\mu_2 < 0$, then the Hopf bifurcation is subcritical and the bifurcating periodic solutions exist for $\tau < \tau_0$. β_2 determines the stability of the bifurcating periodic solutions; bifurcating periodic solutions are stable if $\beta_2 < 0$, unstable if $\beta_2 > 0$.T_2 determines the period of the bifurcating solution; the period increases if $T_2 > 0$, decreases if $T_2 < 0$.*

In the following section, we shall give a numerical example to verify the theoretical results.

5 A numerical example

In this section, we present some numerical simulations to verify the results in Lemma 1., Lemma 2., Theorem 3. and Theorem 4. by using MATLAB(7.6.0) programming. We simulate the predator-prey system (5) by choosing the parameters $r_1 = 0.45$, $r_2 = 0.1$, $\theta = 0.05$, $\varepsilon = 0.03$, and $\alpha = 1$, we obtain the following linearized system

$$\begin{aligned} \frac{dN(t)}{dt} &= 0.45N(t) - 0.03P(t-\tau)N(t) \\ \frac{dP(t)}{dt} &= P(t)(0.1 - 0.05\frac{S(t)}{N(t-\tau)}) \\ \frac{dS(t)}{dt} &= P(t) - S(t) \end{aligned} \tag{33}$$

which has only one positive equilibrium $E^* = (N_0^*, P_0^*, S_0^*) = (7.5, 15, 15)$. By algorithms in the previous sections, we obtain $\tau_0 = 1.1094$, $\omega_1 = 0.2103$, $z_1 = \omega_1^2$ and $g'(z_1) = 0.0845 > 0$. So by Theorem 3., the

equilibrium point E^* is asymptotically stable when $\tau \in [0, \tau_0) = [0, 1.1094)$ and unstable when $\tau > 1.1094$ and also Hopf bifurcation occurs at $\tau = \tau_0 = 1.1094$ as it is illustrated by computer simulations.

By the theory of Hassard et al. [35], as it is discussed in previous section, we also determine the direction of Hopf bifurcation and the other properties of bifurcating periodic solutions. From the formulaes in Section 3, we evaluate the values of μ_2, β_2 and T_2 as

$$\mu_2 = -0.5050 < 0, \ \beta_2 = 0.0502 > 0, \ T_2 = 0.0253 > 0$$

from which we conclude that Hopf bifurcation of system (33) occurring at $\tau_0 = 1.1094$ is supercritical and the bifurcating periodic solution exists when τ crosses τ_0 to the right, and also the bifurcating periodic solution is stable.

In computer simulations, the initial conditions are taken as $(N_0, P_0, S_0) = (50, 25, 25)$ and MATLAB DDE (Delay Differential Equations) solver is used to simulate the system (33). We first take $\tau = 0.009 < \tau_0$ and plot the density functions $N(t)$, $P(t)$ and $S(t)$ in Fig-1,2,3 respectively which shows that the positive equilibrium is asymptotically stable for $\tau < \tau_{0.}$. Moreover in Fig-4, we illustrate the asymptotic stability in three dimensions.

However in Figures 5,6,7 and 8 below, we take $\tau = 1.0002$ sufficiently close to τ_0 which illustrates the existence of bifurcating periodic solutions from the equilibrium point E^*.

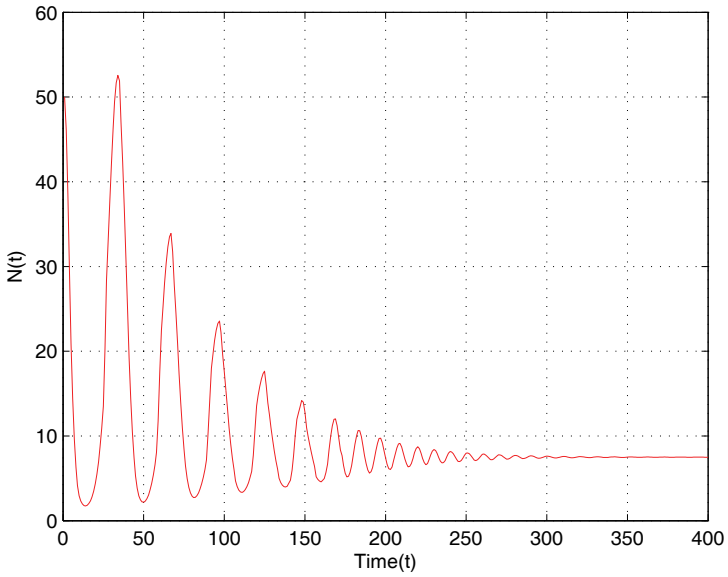

Fig. 1 The trajectory of predator density versus time with the initial condition $N_0 = 50$. The graph of solutions of model (33) when $\tau = 0.0009 < \tau_0$ where the equilibrium point E^* is asymptotically stable.

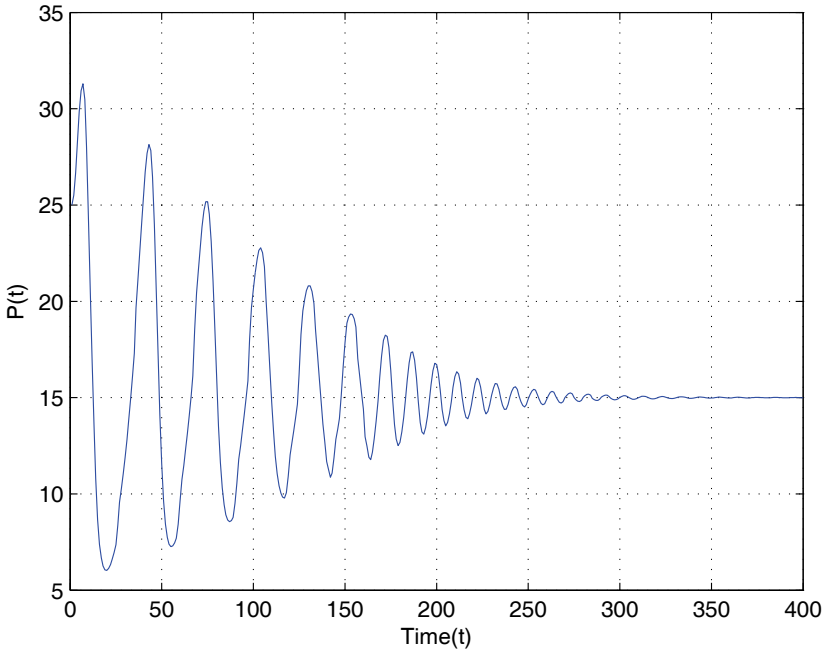

Fig. 2 The trajectory of prey density versus time with the initial condition $P_0 = 25$. The graph of solutions of model (33) when $\tau = 0.0009 < \tau_0$ where the equilibrium point E^* is asymptotically stable.

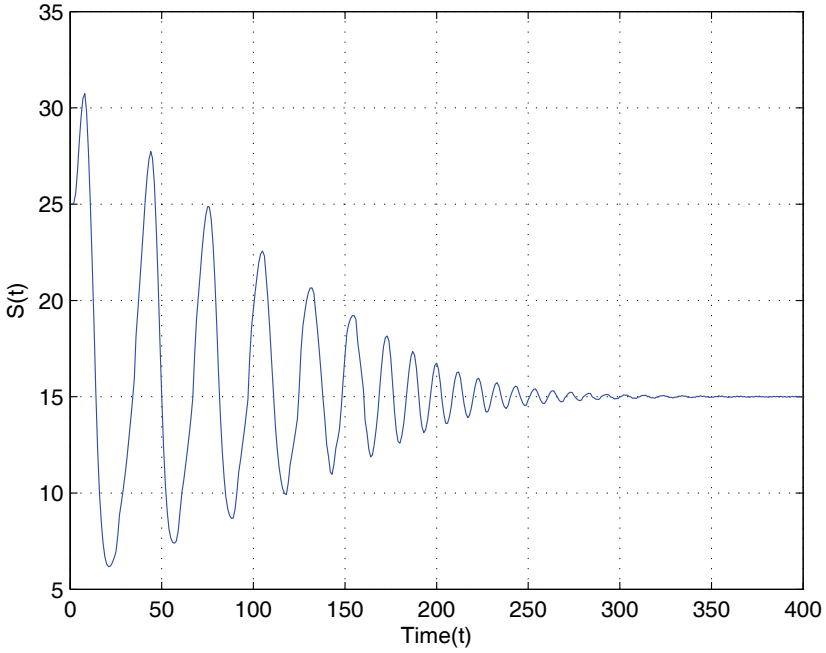

Fig. 3 The trajectories of S(t) versus time with the initial condition $S_0 = 25$. The graph of solutions of model (33) when $\tau = 0.0009 < \tau_0$ where the equilibrium point E^* is asymptotically stable.

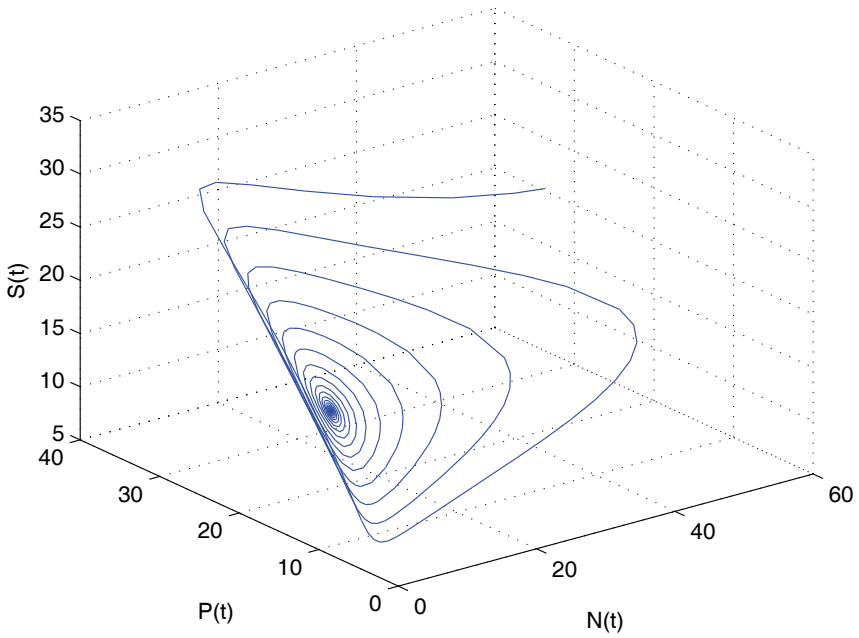

Fig. 4 The trajectory of N, P, S in three dimension with the initial condition $(50,25,25)$ when $\tau = 0.0009$ for which the equilibrium point E^* is asymptotically stable.

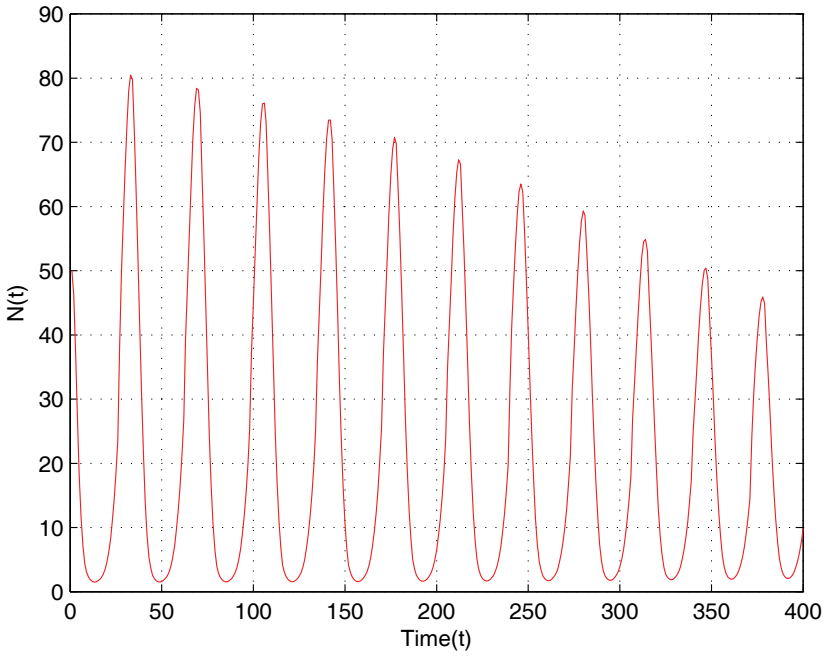

Fig. 5 The trajectory of N(t) when $\tau = 1.002$.

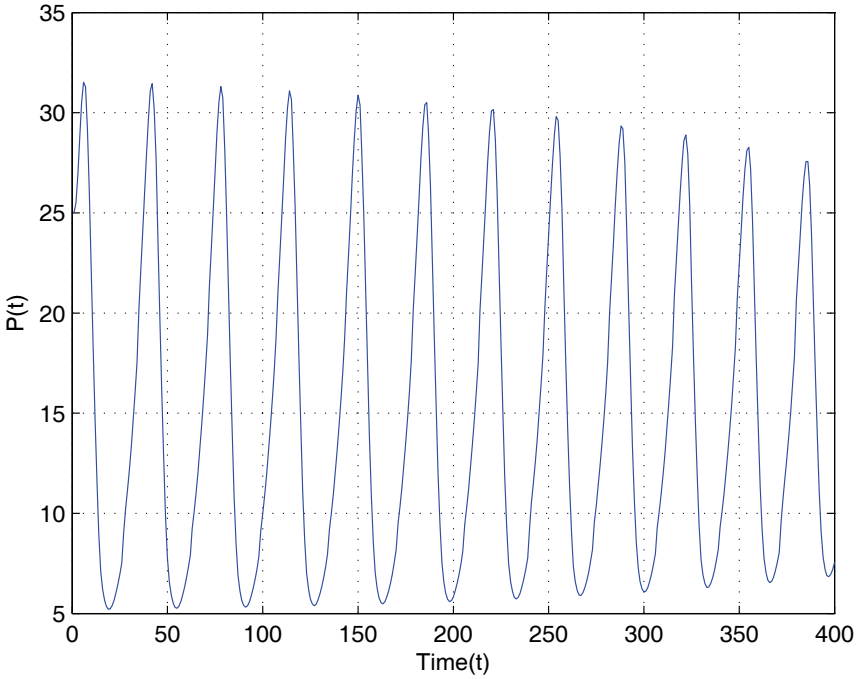

Fig. 6 The trajectory of P(t) when $\tau = 1.002$.

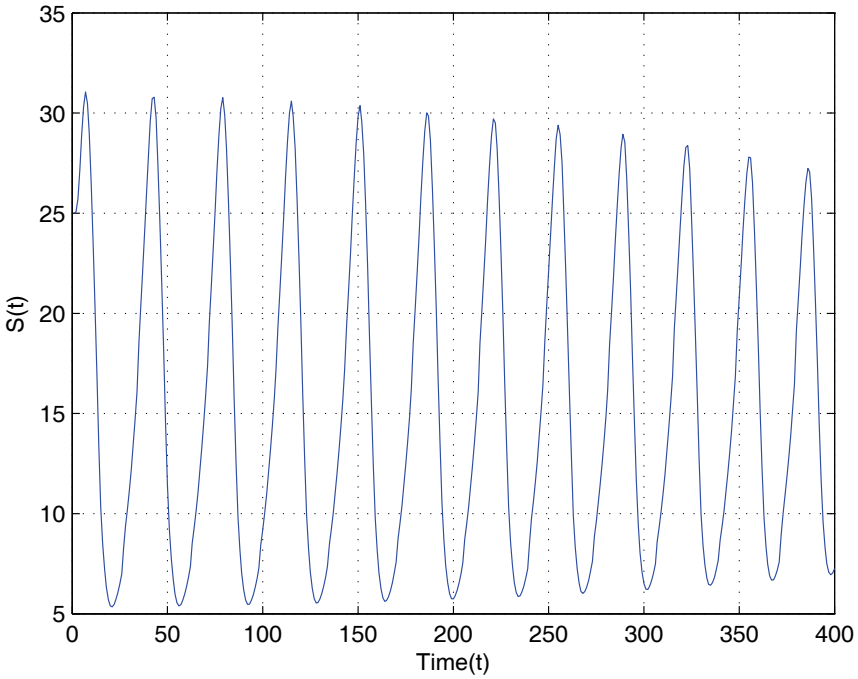

Fig. 7 The trajectory of S(t) when $\tau = 1.002$.

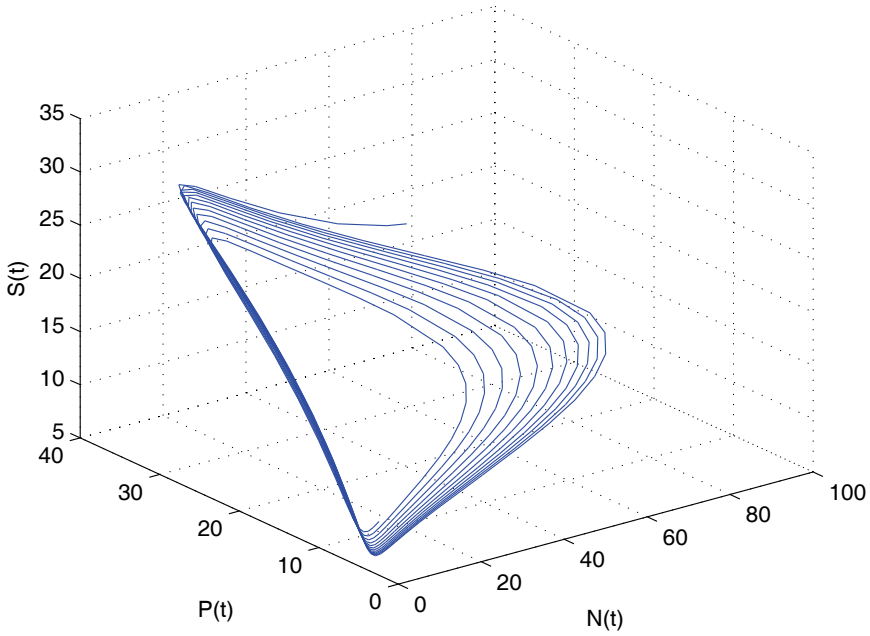

Fig. 8 When $\tau = 1.002$ a stable periodic orbit bifurcates from the equilibrium point E^*.

References

[1] Çelik, C. (2011), Dynamical Behavior of a ratio dependent predator-prey system with distributed delay. Discrete and Cont. Dynam. Systems-Series B, **16**, No.3, 719-738.
[2] Çelik, C. (2008), The stability and Hopf bifurcation for a predator-prey system with time delay. Chaos, Solitons & Fractals, **37**, 87-99.
[3] Çelik, C. (2009), Hopf bifurcation of a ratio-dependent predator-prey system with time delay. Chaos, Solitons & Fractals, **42**, 1474-1484.
[4] Çelik, C. Merdan H., (2013), Hopf bifurcation analysis of a system of coupled delayed-differential equations. Applied Mathematics and Computation, **219**, 6605-6617.
[5] Chen, X. (2007), Periodicity in a nonlinear disrete predator-prey system with state dependent delays. Nonlinear Anal. RWA **8**, 435-446.
[6] Hale, J. (1977), Theory of functional differential equations. Springer Verlag, New York Heidelberg Berlin.
[7] He, X. (1996), Stability and delays in a predator–prey system. J. Math. Anal. Appl. **198** 355-370.
[8] Gopalsamy, K. (1980), Time lags and global stability in two species competition. Bull Math Biol, **42**, 728-737.
[9] Huo, H.-F., Li, W.-T. (2004), Existence and global stability of periodic solutions of a discrete predator-prey system with delays. Appl. Math. Comput. **153** 337-351.
[10] Jiang, G., Lu, Q. (2007), Impulsive state feedback of a predator-prey model. J. Comput. Appl. Math. **200** 193-207.
[11] Karaoglu, E., Merdan, H. (2014), Hopf bifurcations of a ratio-dependent predator-prey model involving two discrete maturation time delays. Chaos, Solitons & Fractals, **68** 159-168.
[12] Karaoglu, E., Merdan, H. (2014), Hopf bifurcations Analysis for a ratio-dependent predator prey system involving two delays. Anziam Journal, **56** Issue 3, 214-231.
[13] Krise, S., Choudhury, SR. (2003), Bifurcations and chaos in a predator–prey model with delay and a laser-diode system with self-sustained pulsations. Chaos, Solitons & Fractals **16** 59-77.
[14] Leung, A. (1977), Periodic solutions for a prey–predator differential delay equation. J. Differential Equations **26** 391-403.
[15] Liu, Z., Yuan, R. (2006), Stability and bifurcation in a harvested one-predator–two-prey model with delays. Chaos, Solitons & Fractals, **27**, Issue 5 1395-1407.
[16] Liu, B., Teng, Z., Chen, L. (2006), Analysis of a predator-prey model with Holling II functional response

concerning impulsive control strategy. J. Comput. Appl. Math. **193** 347-362.
[17] Liu, X., Xiao, D. (2007), Complex dynamic behaviors of a discrete-time predator-prey system. Chaos, Solitons & Fractals **32** 80-94.
[18] Ma, W., Takeuchi, Y. (1998), Stability analysis on a predator-prey system with disributed delays. J. Comput. Appl. Math. **88** 79-94.
[19] Ruan, S. (2001), Absolute stability, conditional stability and bifurcation in Kolmogorov-type predator–prey systems with discrete delays. Quart Appl Math **59**, 159-173.
[20] Ruan, S., Wei, J. (1999), Periodic solutions of planar systems with two delays. Proc. Roy. Soc. Edinburgh Sect. A **129** 1017-1032.
[21] Sun, C., Han, M., Lin, Y., Chen, Y. (2007), Global qualitative analysis for a predator-prey system with delay. Chaos, Solitons & Fractals **32** 1582-1596.
[22] Teng, Z., Rehim, M. (2006), Persistence in nonautonomous predator-prey systems with infinite delays. J. Comput. Appl. Math. **197** 302-321.
[23] L.-L. Wang, L.-L., Li, W.-T., Zhao, P.-H. (2004), Existence and global stability of positive periodic solutions of a discrete predator-prey system with delays. Adv. Difference Equ. **4** 321-336.
[24] Wang, F., Zeng, G. (2007), Chaos in Lotka-Volterra predator-prey system with periodically impulsive ratio-harvesting the prey and time delays. Chaos, Solitons & Fractals. **32** 1499-1512.
[25] Wen, X., Wang, Z. (2002), The existence of periodic solutions for some models with delay. Nonlinear Anal. RWA **3** 567-581.
[26] Xu, R., Wang, Z. (2006), Periodic solutions of a nonautonomous predator-prey system with stage structure and time delays. J. Comput. Appl. Math. **196** 70-86.
[27] Yafia, R. (2007), Hopf bifurcation in differential equations with delay for tumor immune system competition model. SIAM J. Appl.Math. **67**, no 6,1693-1703.
[28] Yafia, R.(2007), Hopf bifurcation analysis and numerical simulations in an ODE model of the immune system with positive immune response. Nonlinear Anal. Real World Appl, no 5, 1359–1369.
[29] Yan, X.P., Chu, Y.D. (2006), Stability and bifurcation analysis for a delayed Lotka Volterra predator-prey system. J. Comput. Appl. Math. **196** 198-210.
[30] Yu, J., Zhang, K., Fei, S., Li, T. (2008), Simplified exponential stability analysis for recurrent neural networks with discrete and distributed time-varying delays, Applied Mathematics and Computation, **205** 465-474.
[31] Zhou, S.R., Liu, Y.F., Wang, G. (2005), The stability of predator-prey systems subject to the Allee effects. Theor. Population Biol. **67** 23-31.
[32] Zhou, L., Tang, Y. (2002), Stability and Hopf bifurcation for a delay competition diffusion system. Chaos, Solitons & Fractals **14** 1201-1225.
[33] Zhou, X., Wu, Y., Li, Y., Yau, X. (2009), Stability and Hopf Bifurcation analysis on a two neuron network with discrete and distributed delays. Chaos, Solitons & Fractals **40** 1493-1505.
[34] Çelik, C., Duman, O. (2009), Allee effect in a discrete-time predator-prey system. Chaos, Solitons & Fractals, **40** Issue 4 1956-1962.
[35] Hassard, N.D., Kazarinoff, Y.H. (1981), Theory and Applications of Hopf Bifurcation. Cambridge University Press, Cambridge.

Journal of Applied Nonlinear Dynamics 5(1) (2016) 93–104

Journal of Applied Nonlinear Dynamics

https://lhscientificpublishing.com/Journals/JAND-Default.aspx

Global Dynamics of a Three Species Predator-Prey Competition Model with Holling type *II* Functional Response on a Circular Domain

Walid Abid[1], R. Yafia[2] †, M.A. Aziz-Alaoui[3], H. Bouhafa[1] and A. Abichou[1]

[1]Université de Carthage, Laboratoire d'ingenierie Mathématique EPT, Tunisia
[2]Ibn Zohr University, Polydisciplinary Faculty of Ouarzazate, B.P: 638, Ouarzazate, Morocco
[3]Laboratoire de Mathématiques Appliquées, 25 Rue Ph. Lebon, BP 540, 76058Le Havre Cedex, France

Submission Info

Communicated by J.A T. Machado
Received 10 June 2015
Accepted 15 July 2015
Available online 1 January 2016

Keywords

Predator-prey
Top predator
Local and global stability
Pattern formation
Circular domain

Abstract

This paper is devoted to the study of a three species ecosystem model consisting of a prey, a predator and a top predator. This model is given by a reaction diffusion system defined on a circular spatial domain and incorporates the Holling type *II* and a modified Leslie-Gower functional response. The aim of this paper is to investigate theoretically and numerically the asymptotic behavior of the interior equilibrium of the model. The conditions of boundedness, existence of a positively invariant and attracting set are proved. Sufficient conditions of local/global stability of the positive steady state are established. In the end, we present a numerical evidence of time evolution of the pattern formation.

1 Introduction and Mathematical Model

In the last few decades, the dynamic relationship between predator and its prey has long been and will continue to be one of the dominant themes in both ecology and mathematical modeling. One of the oldest and well known mathematical model which describing the interaction between predator and prey populations was introduced by A. Lotka 1925 [1] and V. Volterra 1927 [2], governed by the following differential equations

$$\begin{cases} \dot{u}(t) = u(t)(m_1 - n_1 v(t)), \\ \dot{v}(t) = v(t)(-m_2 + n_2 u(t)), \end{cases} \tag{1}$$

where u and v represent the population densities of prey and predator at time t, respectively, m_1, n_1, m_2 and n_2 are positive constants, which stand for the prey growth rate in the absence of the predators, the capture rate of prey by per predator, the constant death rate in the absence of prey and the rate at which each predator converts captured prey into predator births, respectively. They showed that, predator-prey systems permanently oscillate for any initial condition if the prey growth rate is constant and

†Corresponding author.
Email address: yafia1@yahoo.fr

ISSN 2164 – 6457, eISSN 2164 – 6473/$-see front materials
DOI : 10.5890/JAND.2016.03.007

the predator functional response is linear. The dynamical behavior of interacting species with different functional response has been extensively investigated in terms of boundedness of solutions, existence of an attracting set, local/global stability of equilibria and bifurcations (see, for example, [3–6]).

In [4], the authors considered a reaction diffusion predator-prey model defined on a square domain which incorporates Holling type II and a modified Leslie-Gower functional response. They have proved the local/global stability, occurrence of bifurcations and patterns formations. In [7], the authors considered the same model defined on a circular domain which is given by

$$\begin{cases} \dfrac{\partial u}{\partial t} = \Delta_{r\theta} u + u(1-u) - \dfrac{av}{u+e_1}u = \Delta_{r\theta} u + f(u,v) & (r,\theta) \in \Omega,\ t>0, \\ \dfrac{\partial v}{\partial t} = \delta \Delta_{r\theta} v + b(1 - \dfrac{v}{u+e_2})v = \delta \Delta_{r\theta} v + g(u,v) & (r,\theta) \in \Omega,\ t>0, \\ \partial_r u(.,r,\theta) = \partial_r v(.,r,\theta) = 0 \text{ for } r = R \text{ (radial derivative)}. \end{cases} \tag{2}$$

This two species food chain model describes a prey population u which serves as food for a predator v, where $f(u,v)$ and $g(u,v)$ are the local activity (in the absence of diffusion), Ω is a disc domain and $\Delta_{r\theta}$ is the Laplacian operator in polar coordinates. The parameters a, b, e_1 and e_2 are assumed positive values. Boundedness of the system, existence of an attracting set, local/global stability, occurrence of Hopf and Turing bifurcations and patterns formation are studied.

In [8], the authors studied a reaction diffusion system of predator-prey model which is based on the modified Leslie-Gower model with Beddington-DeAngelis functional responses on a circular domain below

$$\begin{cases} \dfrac{\partial u}{\partial t} = D_1 \Delta_{r\theta} u + (a_1 - b_1 u - \dfrac{c_1 v}{d_1 u + d_2 v + k_1})u & (r,\theta) \in \Omega,\ t>0, \\ \dfrac{\partial v}{\partial t} = D_2 \Delta_{r\theta} v + (a_2 - \dfrac{c_2 v}{u+k_2})v & (r,\theta) \in \Omega,\ t>0. \end{cases} \tag{3}$$

Recently, many researchers have studied the pattern formation for different models of three interacting species in discrete and continuous cases and most of them have considered a food chain model with diffusion and have investigated the local/global stability in the spatio-temporal system defined on a square domain (see [9–13]).

In the present paper, we consider a three-species food chain model consisting of prey, intermediate predator and top-predator, modeled by a reaction-diffusion system defined on a circular spatial domain and incorporates the Holling type *II* and a modified Leslie-Gower functional response. One of the well known methods in biology or ecology plays a crucial role in regulating the balance of the ecosystem and controlling the dynamics of species is the introduction of a population further called "top-predator". However, the impact of this introduction should previously be studied in order to minimize adverse effects. The first species denoted by U is the only food source of the second V. As well, intermediate predator V is the only prey of a top-predator W. Local interactions between species U and V are modeled by Lotka-Volterra type scheme and the interactions between species W and V has been modeled by Leslie-Gower scheme [14, 15]. The spatio-temporal system for the three components species can be written as follows (see [16]):

$$\begin{cases} \dfrac{\partial U(T,x,y)}{\partial T} = D_1 \Delta U(T,x,y) + (a_0 - b_0 U(T,x,y) - \dfrac{v_0 V(T,x,y)}{U(T,x,y)+d_0})U(T,x,y), \\ \dfrac{\partial V(T,x,y)}{\partial T} = D_2 \Delta V(T,x,y) + (-a_1 + \dfrac{v_1 U(T,x,y)}{U(T,x,y)+d_0} - \dfrac{v_2 W(T,x,y)}{V(T,x,y)+d_2})V(T,x,y), \end{cases} \tag{4}$$

$$\begin{cases} \dfrac{\partial W(T,x,y)}{\partial T} = D_3 \Delta W(T,x,y) + (c_3 - \dfrac{v_3 W(T,x,y)}{V(T,x,y)+d_3}) W(T,x,y), \\ \dfrac{\partial U}{\partial n} = \dfrac{\partial V}{\partial n} = \dfrac{\partial W}{\partial n} = 0, \\ U(0,x,y) = U_0(x,y) \geq 0,\ V(0,x,y) = V_0(x,y) \geq 0,\ W(0,x,y) = W_0(x,y) \geq 0, \end{cases}$$

where $U(T,x,y)$, $V(T,x,y)$ and $W(T,x,y)$ are the densities of prey, intermediate predator and top-predator, respectively, at time T and position (x,y) defined on a circular domain Ω with radius R (i.e. $\Omega = \{(x,y) \in \mathbf{R}^2 / x^2 + y^2 < R^2\}$. The three species are assumed to diffuse at rates D_i (i = 1, 2, 3). The parameters a_0, b_0, v_0, d_0, a_1, v_1, v_2, d_2, c_3, v_3 and d_3 are assumed to be positive constants and are defined as follows: a_0 is the growth rate of the prey U, b_0 measures the mortality due to the competition between individuals of the species U, v_0 is the maximum extent that the rate of reduction by individual U can reach, d_0 measures the protection that the species U and V benefit through the environment, a_1 represents the death rate of V in the absence of U, v_1, v_2 and v_3 are the the maximum value that the rate of reduction by the individual of U, V and W can reach respectively, d_2 is the value of V for which the rate of elimination by individual V becomes $\frac{v_2}{2}$, c_3 describes the growth rate of W, assuming that there is the same number of males and females and d_3 represents the residual loss caused by high scarcity of prey V of the specie W. The vector n is an outward unit normal vector to the smooth boundary $\partial\Omega$. The homogeneous Neumann boundary conditions mean that the system is self contained and there is no flux across the boundary $\partial\Omega$.

The first model proposed in this topic is given by a system of ordinary differential equations as follows (see [17]):

$$\begin{cases} \dfrac{\partial U}{\partial T} = a_0 U - b_0 U^2 - \dfrac{v_0 V U}{U + d_0}, \\ \dfrac{\partial V}{\partial T} = -a_1 V + \dfrac{v_1 U V}{U + d_1} - \dfrac{v_2 W V}{V + d_2}, \\ \dfrac{\partial W}{\partial T} = c_3 W^2 - \dfrac{v_3 W^2}{V + d_3}, \end{cases} \tag{5}$$

where U, V and W represent the population densities at time T, a_0, b_0, v_0, d_0, a_1, v_1, d_1, v_2, d_2, c_3, v_3 and d_3 are model parameters assumed to be positive. Based on the studies presented in [17, 18], our main contribution in this paper is to generalize the results presented in [7, 8] for two species to three-species reaction-diffusion system defined on a circular domain.

The organization of the remaining part of this work is as follows. In Section 2, we show the boundedness of solutions. In section 3, we prove the existence of the equilibrium points and their stability. Section 4 is devoted to the global stability of the nontrivial steady state. In section 5, we give some numerical simulations and we end our work by a conclusion.

2 Boundedness of solutions

Considering system (4) and writing x and y in polar coordinates $x = r\cos\theta$ and $y = r\sin\theta$, we get $\Gamma = \{(r,\theta) : 0 < r < R, 0 \leq \theta < 2\pi\}$ (R is the radius of the disc), $r = \sqrt{x^2+y^2}$ and $\theta = \tan^{-1}(\frac{y}{x})$.
Without loss of generalities we denote also $u(t,x,y) = u(t, r\cos(\theta), r\sin(\theta)) = u(t,r,\theta)$,
$v(t,x,y) = v(t, r\cos(\theta), r\sin(\theta)) = v(t,r,\theta)$ and $w(t,x,y) = w(t, r\cos(\theta), r\sin(\theta)) = w(t,r,\theta)$ as the densities of prey, predator and top predator in polar coordinates, respectively. Therefore, the Laplacian operator in polar coordinates is given by

$$\Delta_{r\theta} u = \frac{\partial^2 u}{\partial r^2} + \frac{1}{r}\frac{\partial u}{\partial r} + \frac{1}{r^2}\frac{\partial^2 u}{\partial \theta^2}. \tag{6}$$

To simplify system (4) we introduce the following transformations:

$$U=\frac{a_0}{b_0}u,\ V=\frac{a_0^2}{b_0v_0}v,\ W=\frac{a_0^3}{b_0v_0v_2}w,\ T=\frac{t}{a_0},\ r=\frac{r^{'}}{a_0},\ \theta=\theta^{'},$$

and

$$a=\frac{b_0d_0}{a_0},\ b=\frac{a_1}{a_0},\ c=\frac{v_1}{a_0},\ d=\frac{d_2v_0b_0}{a_0^2},\ p=\frac{c_3a_0^2}{v_0b_0v_2},\ q=\frac{v_3}{v_2},\ s=\frac{d_3v_0b_0}{a_0^2},\ \delta_1=\frac{D_1}{a_0},\ \delta_2=\frac{D_2}{a_0},\ \delta_3=\frac{D_3}{a_0}.$$

In polar coordinates, the spatio-temporal system (4) is written as follows:

$$\begin{cases}\dfrac{\partial u(t,r,\theta)}{\partial t}=\delta_1\Delta_{r\theta}u(t,r,\theta)+(1-u(t,r,\theta)-\dfrac{v(t,r,\theta)}{u(t,r,\theta)+a})u(t,r,\theta), & \forall(r,\theta)\in\Gamma,\ t>0\\ \dfrac{\partial v(t,r,\theta)}{\partial t}=\delta_2\Delta_{r\theta}v(t,r,\theta)+(-b+\dfrac{cu(t,r,\theta)}{u(t,r,\theta)+a}-\dfrac{w(t,r,\theta)}{v(t,r,\theta)+d})v(t,r,\theta), & \forall(r,\theta)\in\Gamma,\ t>0\\ \dfrac{\partial w(t,r,\theta)}{\partial t}=\delta_3\Delta_{r\theta}w(t,r,\theta)+(p-\dfrac{qw(t,r,\theta)}{v(t,r,\theta)+s})w(t,r,\theta) & \forall(r,\theta)\in\Gamma,\ t>0\\ \partial_ru(.,r,\theta)=\partial_rv(.,r,\theta)=\partial_rw(.,r,\theta)=0 \text{ for } r=R \text{ (radial derivative)}\\ u(0,r,\theta)=u_0(r,\theta)\geq 0,\ v(0,r,\theta)=v_0(r,\theta)\geq 0,\ w(0,r,\theta)=w_0(r,\theta)\geq 0.\end{cases}\tag{7}$$

The following result gives the boundedness of solutions for system (7).

Theorem 1. *Let* Θ *be a set defined as follows:*

$$\Theta\equiv[0,1]\times[0,1+a]\times[0,\frac{p}{q}(1+a+s)].\tag{8}$$

Then,
i) Θ *is positively invariant region,*
ii) *All solutions of (7) starting in* Θ *are ultimately bounded and eventually enter the attracting set* Θ.

Proof: From equation (7), we have

$$\begin{cases}\dfrac{\partial u(t,r,\theta)}{\partial t}=\delta_1\Delta_{r\theta}u(t,r,\theta)+(1-u(t,r,\theta))u(t,r,\theta)\leq(1-u)u,\\ \dfrac{\partial u(0,r,\theta)}{\partial n}=0,\\ u(0,r,\theta)=u_0(r,\theta)\leq u_{01}=\max\limits_{(r,\theta)\in\overline{\Gamma}}u_0(r,\theta),\end{cases}\tag{9}$$

and

$$\begin{cases}\dfrac{\partial v(t,r,\theta)}{\partial t}=\delta_2\Delta_{r\theta}v+(-b+\dfrac{cu}{u+a}-\dfrac{w}{v+d})v\leq(\dfrac{c}{1+a}-b)v,\\ \dfrac{\partial v(0,r,\theta)}{\partial n}=0,\\ v(0,r,\theta)=v_0(r,\theta)\leq v_{01}=\max\limits_{(r,\theta)\in\overline{\Gamma}}v_0(r,\theta),\end{cases}\tag{10}$$

and

$$\begin{cases}\dfrac{\partial w(t,r,\theta)}{\partial t}=\delta_3\Delta_{r\theta}w+(p-\dfrac{qw}{v+s})w\leq p(1-\dfrac{w}{\dfrac{p}{q}(1+a+s)})w,\\ \dfrac{\partial w(0,r,\theta)}{\partial n}=0,\\ w(0,r,\theta)=w_0(r,\theta)\leq w_{01}=\max\limits_{(r,\theta)\in\overline{\Gamma}}w_0(r,\theta).\end{cases}\tag{11}$$

From equations (9)-(11) and by applying the comparison principle, we have $u(t,r,\theta) \leq u_1 \leq 1$, $v(t,r,\theta) \leq v_1 \leq 1$ and $w(t,r,\theta) \leq w_1 \leq 1$ such that: $\limsup_{t\to+\infty} u_1(t) = 1$, $\limsup_{t\to+\infty} v_1(t) = 1+a$ and $\limsup_{t\to+\infty} w_1(t) = \frac{p}{q}(1+a+s)$, where u_1, v_1 and w_1 are solutions of the following equations, respectively,

$$\begin{cases} \dfrac{du(t,r,\theta)}{dt} = (1-u_1)u_1, \\ u_1(0) = u_{01} = \max\limits_{(r,\theta)\in\overline{\Gamma}} u_0(r,\theta) \leq 1, \end{cases} \tag{12}$$

$$\begin{cases} \dfrac{dv(t,r,\theta)}{dt} = (\dfrac{c}{1+a} - b)v_1, \\ v_1(0) = v_{01} = \max\limits_{(r,\theta)\in\overline{\Gamma}} v_0(r,\theta) \leq 1, \end{cases} \tag{13}$$

and

$$\begin{cases} \dfrac{dw(t,r,\theta)}{dt} = p(1 - \dfrac{w}{\frac{p}{q}(1+a+s)})w, \\ w_1(0) = w_{01} = \max\limits_{(r,\theta)\in\overline{\Gamma}} w_0(r,\theta) \leq 1. \end{cases} \tag{14}$$

Then, we deduce the result.

3 Analysis of Temporal System

In this section, we will study the behavior of system (7) in the absence of diffusion, (i.e., $\delta_1 = \delta_2 = \delta_3 = 0$).

3.1 Equilibria and Local Stability

Without diffusion, system (7) becomes

$$\begin{cases} \dfrac{du(t)}{dt} = (1 - u(t) - \dfrac{v(t)}{u(t)+a})u(t), \\ \dfrac{dv(t)}{dt} = (-b + \dfrac{cu(t)}{u(t)+a} - \dfrac{w(t)}{v(t)+d})v(t), \\ \dfrac{dw(t)}{dt} = (p - \dfrac{qw(t)}{v(t)+s})w(t). \end{cases} \tag{15}$$

Let $E = (u,v,w)^T$ and

$$F(E) = \begin{pmatrix} f(u,v,w) \\ g(u,v,w) \\ h(u,v,w) \end{pmatrix} = \begin{pmatrix} (1 - u - \dfrac{v}{u+a})u \\ (-b + \dfrac{cu}{u+a} - \dfrac{w}{v+d})v \\ (p - \dfrac{qw}{v+s})w \end{pmatrix}.$$

Then, system (15) takes the following form:

$$\frac{dE}{dt} = F(E). \tag{16}$$

By computation, system (16) has four trivial equilibrium points $E_0 = (0,0,0)$, $E_1 = (1,0,0)$, $E_2 = (0,0,\frac{sp}{q})$, $E_3 = (1,0,\frac{sp}{q})$ and a positive nontrivial one $E^* = (u^*,v^*,w^*)$ which exists if and only if the following inequality is satisfied

$$qc > bq + p \text{ and } qc - bq - p > a(bq+p) \tag{17}$$

such that

$$u^* = \frac{a(bq+p)}{qc-bq-p},\ v^* = (1-u^*)(u^*+a) \text{ and } w^* = \frac{p(v^*+s)}{q}. \tag{18}$$

By linearizing system (16) around the equilibrium point E^*, we obtain the associated Jacobian Matrix J defined by

$$J(E^*) = \begin{pmatrix} 1-2u^* - \dfrac{av^*}{(u^*+a)^2} & -\dfrac{u^*}{u^*+a} & 0 \\ \dfrac{acv^*}{(u^*+a)^2} & \dfrac{cu^*}{u^*+a} - b - \dfrac{dw^*}{(v^*+d)^2} & -\dfrac{v^*}{v^*+d} \\ 0 & \dfrac{q(w^*)^2}{u^*+a} - b - \dfrac{dw^*}{(v^*+d)^2} & -\dfrac{2qw^*}{v^*+d} \end{pmatrix}. \tag{19}$$

Evaluating the Jacobian Matrix J at E_0, E_1, E_2 and E_3 and calculating the corresponding eigenvalues, we have the following result:

Theorem 2. i) *The steady state E_0 is unstable,*
ii) *If $ab > c-b$, then the steady state E_1 is asymptotically stable and it is unstable elsewhere,*
iii) *The steady state E_2 is a saddle point,*
iv) *If $b + \frac{sp}{qd} > \frac{c}{1+a}$, then the equilibrium point $E_3 = (1,0,\frac{sp}{q})$ is asymptotically stable and is a saddle point elsewhere.*

In the following, we prove the stability of the positive equilibrium $E^* = (u^*, v^*, w^*)$.

Theorem 3. *If the condition (17) holds and the following inequalities are satisfied*

$$\frac{a+1}{qc} > \frac{2a}{qc-bq-p}$$

and

$$b + \frac{dp((1-u^*)(u^*+a)+s)}{q((1-u^*)(u^*+a)+d)^2} > \frac{cu^*}{u^*+a} \tag{20}$$

and

$$\frac{p^2((1-u^*)(u^*+a)+s)^2}{q(u^*+a)} > b + \frac{dp((1-u^*)(u^*+a)+s)}{q((1-u^*)(u^*+a)+d)^2},$$

then, the nontrivial equilibrium point $E^* = (u^*, v^*, w^*)$ is asymptotically stable.

Proof: Writing $F_E(E^*)$ as

$$F_E(E^*) = J(E^*) = \begin{pmatrix} a_{11} & a_{12} & a_{13} \\ a_{21} & a_{22} & a_{23} \\ a_{31} & a_{32} & a_{33} \end{pmatrix}.$$

According to (18), a direct computation yields

$$\begin{cases} a_{11} = 1-2u^* - \dfrac{a(1-u^*)}{(u^*+a)},\ a_{12} = -\dfrac{u^*}{u^*+a}, a_{13} = 0, \\ a_{21} = \dfrac{ac(1-u^*)}{(u^*+a)},\ a_{22} = \dfrac{cu^*}{u^*+a} - b - \dfrac{\frac{dp}{q}((1-u^*)(u^*+a)+s)}{((1-u^*)(u^*+a)+d)^2},\ a_{23} = -\dfrac{(1-u^*)(u^*+a)}{(1-u^*)(u^*+a)+d}, \\ a_{31} = 0,\ a_{32} = \dfrac{\frac{p^2}{q}((1-u^*)(u^*+a)+s)^2}{u^*+a} - b - \dfrac{\frac{dp}{q}((1-u^*)(u^*+a)+s)}{((1-u^*)(u^*+a)+d)^2},\ a_{33} = -\dfrac{2p((1-u^*)(u^*+a)+s)}{(1-u^*)(u^*+a)+d}, \end{cases} \tag{21}$$

where

$$u^* = \frac{a(bq+p)}{qc-bq-p}.$$

The characteristic polynomial of $F_E(E^*)$ can be written as:

$$\varphi(\lambda) = \lambda^3 + B_1\lambda^2 + B_2\lambda + B_3, \tag{22}$$

where

$(1-u^*)(u^*+a) = \frac{aqc(qc-(bq+p)(a+1))}{(qc-bq-p)^2}$, $\frac{(1-u^*)}{(u^*+a)} = \frac{qc-(bq+p)(a+1)}{aqc}$ and $\frac{u^*}{(u^*+a)} = \frac{bq+p}{qc}$.

Hence

$$\begin{aligned}
B_1 =& -\mathrm{tr}(L_E(E^*)) \\
=& -(a_{11}+a_{22}+a_{33}) \\
=& u^*(2-\frac{a}{u^*+a})+b+\frac{dp(qc-bq-p)^2(aqc(qc-(bq+p)(a+1))+s(qc-bq-p)^2)}{q(aqc(qc-(bq+p)(a+1))+d(qc-bq-p)^2)} \\
&+\frac{2paqc(qc-(bq+p)(a+1))}{aqc(qc-(bq+p)(a+1))+d(qc-bq-p)^2} > 0, \\
B_2 =& a_{11}a_{22}+a_{11}a_{33}+a_{22}a_{33}-a_{23}a_{32}-a_{12}a_{21} \\
=& (-\frac{cu^*}{u^*+a}+b+\frac{\frac{dp}{q}((1-u^*)(u^*+a)+s)}{((1-u^*)(u^*+a)+d)^2})(2u^*-\frac{(bq+p)(a+1)}{qc}+\frac{2p((1-u^*)(u^*+a)+s)}{(1-u^*)(u^*+a)+d}) \\
&+(\frac{2p((1-u^*)(u^*+a)+s)}{(1-u^*)(u^*+a)+d})(2u^*-\frac{(bq+p)(a+1)}{qc})+(\frac{ac(1-u^*)u^*}{(u^*+a)^2}) \\
&+(\frac{\frac{p^2}{q}((1-u^*)(u^*+a)+s)^2}{u^*+a}-b-\frac{\frac{dp}{q}((1-u^*)(u^*+a)+s)}{((1-u^*)(u^*+a)+d)^2})(\frac{(1-u^*)(u^*+a)}{(1-u^*)(u^*+a)+d}) > 0, \\
B_3 =& -\det(L_E(E^*)) \\
=& a_{12}a_{21}a_{33}+a_{11}a_{23}a_{32}-a_{11}a_{22}a_{33} \\
=& (\frac{ac(1-u^*)u^*}{(u^*+a)^2})(\frac{2p((1-u^*)(u^*+a)+s)}{(1-u^*)(u^*+a)+d}) \\
&+(\frac{\frac{p^2}{q}((1-u^*)(u^*+a)+s)^2}{u^*+a}-b-\frac{\frac{dp}{q}((1-u^*)(u^*+a)+s)}{((1-u^*)(u^*+a)+d)^2}) \\
&\times(2u^*-\frac{(bq+p)(a+1)}{qc})(\frac{(1-u^*)(u^*+a)}{(1-u^*)(u^*+a)+d})+(-\frac{cu^*}{u^*+a}+b+\frac{\frac{dp}{q}((1-u^*)(u^*+a)+s)}{((1-u^*)(u^*+a)+d)^2}) \\
&\times(2u^*-\frac{(bq+p)(a+1)}{qc})(\frac{2p((1-u^*)(u^*+a)+s)}{(1-u^*)(u^*+a)+d}) > 0,
\end{aligned}$$

$$\begin{aligned}
B_1B_2-B_3 =& a_{11}^2(-a_{22}-a_{33})+a_{22}^2(-a_{11}-a_{33})+a_{33}^2(-a_{11}-a_{22}) \\
&+a_{12}a_{21}(a_{11}+a_{22})+a_{32}a_{23}(a_{33}+a_{22})-2a_{11}a_{22}a_{33} \\
=& [a_{11}^2-a_{32}a_{23}](-a_{22}-a_{33})+[a_{33}^2-a_{12}a_{21}](-a_{11}-a_{22})+a_{22}^2(-a_{11}-a_{33})-2a_{11}a_{22}a_{33} \\
=& (-\frac{cu^*}{u^*+a}+b+\frac{\frac{dp}{q}((1-u^*)(u^*+a)+s)}{((1-u^*)(u^*+a)+d)^2}+\frac{2p((1-u^*)(u^*+a)+s)}{(1-u^*)(u^*+a)+d}) \\
&[a_{11}^2+(\frac{(1-u^*)(u^*+a)}{(1-u^*)(u^*+a)+d})\times(\frac{\frac{p^2}{q}((1-u^*)(u^*+a)+s)^2}{u^*+a}-b-\frac{\frac{dp}{q}((1-u^*)(u^*+a)+s)}{((1-u^*)(u^*+a)+d)^2})] \\
&+a_{22}^2(2u^*-\frac{(bq+p)(a+1)}{qc}+\frac{2p((1-u^*)(u^*+a)+s)}{(1-u^*)(u^*+a)+d})
\end{aligned}$$

$$+[a_{33}^2+(\frac{acu^*(1-u^*)}{(u^*+a)^2})](2u^*-\frac{(bq+p)(a+1)}{qc}-\frac{cu^*}{u^*+a}+b+\frac{\frac{dp}{q}((1-u^*)(u^*+a)+s)}{((1-u^*)(u^*+a)+d)^2})$$
$$+2(2u^*-\frac{(bq+p)(a+1)}{qc})(-\frac{cu^*}{u^*+a}+b+\frac{\frac{dp}{q}((1-u^*)(u^*+a)+s)}{((1-u^*)(u^*+a)+d)^2})(\frac{2p((1-u^*)(u^*+a)+s)}{(1-u^*)(u^*+a)+d})$$
$$> 0.$$

Using the condition (20), we have $B_1B_2-B_3>0$. By applying the Routh-Hurwitz criteria, we deduce the result.

4 Global Stability of the Nontrivial Steady State with Diffusion

In this section, we study the global stability of the homogeneous non-trivial equilibrium $E^*=(u^*,v^*,w^*)$ with diffusion terms.

Theorem 4. *Suppose that the condition (17) holds and the following inequalities are satisfied*

$$b<c,\ 1-a<u^*<\frac{ab}{c-b}\ \ and\ \ v^*<d(c-b). \tag{23}$$

Then, the homogeneous non-trivial steady state (u^*,v^*,w^*) is globally asymptotically stable for system (7).

Proof: The proof is based on the positive definite Lyapunov function. Let

$$\int_\Gamma f(\rho)d\rho=\int_0^R\int_0^{2\pi}f(r,\theta)d\theta dr$$

and

$$Z(u,v,w)=z_1(u)+z_2(v)+z_3(w),$$

where

$$z_1(u)=\int_{u^*}^{u}\frac{\eta-u^*}{\eta}d\eta,\ z_2(v)=\int_{v^*}^{v}\frac{(\eta-v^*)(\eta+d)}{\eta}d\eta \text{ and } z_3(w)=\int_{w^*}^{w}\frac{\eta-w^*}{\eta}d\eta. \tag{24}$$

Let

$$\begin{aligned}\Psi(u,v,w)&=\int_\Gamma Z(u(t,\rho),v(t,\rho),w(t,\rho))d\rho \\ &=\int_\Gamma z_1(u(t,\rho))d\rho+\int_\Gamma z_2(v(t,\rho))d\rho+\int_\Gamma z_3(w(t,\rho))d\rho \\ &=\int_\Gamma z_1(u(t,\rho))d\rho+\int_\Gamma z_2(v(t,\rho))d\rho+\int_\Gamma z_3(w(t,\rho))d\rho,\end{aligned} \tag{25}$$

where Ψ is positive for all $(u,v,w) \in \mathbb{R}^3_{*+}$ and $\Psi(u^*,v^*,w^*)= 0$.By differentiating Ψ with respect to time t, we have

$$\begin{aligned}
\frac{d\Psi}{dt} &= \int_\Gamma (\frac{\partial Z}{\partial u}\frac{\partial u}{\partial t} + \frac{\partial Z}{\partial v}\frac{\partial v}{\partial t} + \frac{\partial Z}{\partial w}\frac{\partial w}{\partial t})d\rho \\
&= \int_\Gamma (\frac{\partial Z}{\partial u}(\delta_1\Delta u + f(u,v,w)) + \frac{\partial Z}{\partial v}(\delta_2\Delta v + g(u,v,w)) + \frac{\partial Z}{\partial w}(\delta_3\Delta w + h(u,v,w)))d\rho \\
&= \int_\Gamma (\delta_1\frac{\partial Z}{\partial u}\Delta u + \delta_2\frac{\partial Z}{\partial v}\Delta v + \delta_3\frac{\partial Z}{\partial w}\Delta w)d\rho + \int_\Gamma (\frac{\partial Z}{\partial u}f(u,v,w) + \frac{\partial Z}{\partial v}g(u,v,w) + \frac{\partial Z}{\partial w}h(u,v,w))d\rho \\
&= \int_\Gamma (\delta_1\frac{\partial Z}{\partial u}\Delta u + \delta_2\frac{\partial Z}{\partial v}\Delta v + \delta_3\frac{\partial Z}{\partial w}\Delta w)d\rho + \int_\Gamma \dot{Z}d\rho,
\end{aligned}$$

where $\dot{Z} = \frac{\partial Z}{\partial t}$. From Green's identity we get

$$\begin{aligned}
\int_\Gamma \frac{\partial Z}{\partial u}\Delta u d\rho &= \int_{\partial\Gamma} \frac{\partial Z}{\partial u}\frac{\partial u}{\partial \eta} - \int_\Gamma \nabla\frac{\partial Z}{\partial u}\nabla u d\rho \\
&= -\int_\Gamma \nabla\frac{\partial Z}{\partial u}\nabla u d\rho,
\end{aligned}$$

$$\begin{aligned}
\int_\Gamma \frac{\partial Z}{\partial v}\Delta v d\rho &= \int_{\partial\Gamma} \frac{\partial Z}{\partial v}\frac{\partial v}{\partial \eta} - \int_\Gamma \nabla\frac{\partial Z}{\partial v}\nabla v d\rho \\
&= -\int_\Gamma \nabla\frac{\partial Z}{\partial v}\nabla v d\rho
\end{aligned}$$

and

$$\begin{aligned}
\int_\Gamma \frac{\partial Z}{\partial w}\Delta w d\rho &= \int_{\partial\Gamma} \frac{\partial Z}{\partial w}\frac{\partial w}{\partial \eta} - \int_\Gamma \nabla\frac{\partial Z}{\partial w}\nabla w d\rho \\
&= -\int_\Gamma \nabla\frac{\partial Z}{\partial w}\nabla w d\rho,
\end{aligned}$$

where $\nabla_{r\theta}u = (\frac{\partial u}{\partial r}, \frac{1}{r}\frac{\partial u}{\partial \theta})$.
As $Z(u,v,w) = z_1(u) + z_2(v) + z_3(w)$ is written in a separable form, we have

$$z_1''(u) = \frac{u^*}{u} \geq 0,\ z_2''(v) = \frac{v + dv^*}{v} \geq 0 \text{ and } z_3''(v) = \frac{w^*}{w} \geq 0.$$

Therefore, the matrix

$$\begin{pmatrix}
\frac{\partial^2 Z}{(\partial u)^2} & \frac{\partial^2 Z}{\partial u \partial v} & \frac{\partial^2 Z}{\partial u \partial w} \\
\frac{\partial^2 Z}{\partial v \partial u} & \frac{\partial^2 Z}{(\partial v)^2} & \frac{\partial^2 Z}{\partial v \partial w} \\
\frac{\partial^2 Z}{\partial w \partial u} & \frac{\partial^2 Z}{\partial w \partial v} & \frac{\partial^2 Z}{(\partial w)^2}
\end{pmatrix}$$

is positive definite and we have

$$\int_\Gamma (\frac{\partial Z}{\partial u}\delta_1\Delta u + \delta_2\frac{\partial Z}{\partial v}\Delta v + \delta_3\frac{\partial Z}{\partial w}\Delta w)d\rho \leq 0.$$

As $\dot{Z} \leq 0$, we deduce that

$$\frac{d\Psi}{dt} \leq 0 \text{ for } b < c,\ 1 - a < u^* < \frac{ab}{c-b} \text{ and } v^* < d(c-b).$$

Then, we have the result.

5 Numerical simulations

In this section, we give some numerical simulations of pattern formation resulting from spatial distribution of system (7) on the disc $\Gamma = \{(r,\theta) : 0 < r < R, 0 \leq \theta < 2\pi\}$. The Laplacian describing diffusion is calculated using finite difference schemes, that is, the derivatives are approached by differences over space steps (Δr) and an explicit Euler's method for the time integration with a time step size (Δt) with zero-flux on the boundary. In order to avoid numerical artifacts, the values of time (Δt) and space steps (Δr and $\Delta\theta$) have been chosen sufficiently small satisfying the CFL (Courant-Friedrichs-Levy) stability criterion for diffusion equation. For numerical simulations, the initial condition is a small perturbation in the vicinity of equilibrium point (u^*, v^*, w^*). These initial conditions have been chosen as:

$$\begin{aligned} u(0,r,\theta) &= u^*((r\cos\theta)^2 + (r\sin\theta)^2) < 50, \\ v(0,r,\theta) &= v^*((r\cos\theta)^2 + (r\sin\theta)^2) < 50, \\ w(0,r,\theta) &= w^*((r\cos\theta)^2 + (r\sin\theta)^2) < 50. \end{aligned}$$

The used parameters are summarized in Table 1. The time evolution of spatial distributions is observed

Table 1 Table of the used parameters and the corresponding pictures of patterns formations

	t	a_0	a_1	b_0	c_3	d_0	d_2	d_3	v_0	v_1	v_2	v_3
Fig.1(a)	0	0.5	0.4	0.36	0.2	0.3	0.4	0.4	0.4	0.8	0.4	0.6
Fig.1(b)	1200	0.5	0.4	0.36	0.2	0.3	0.4	0.4	0.4	0.8	0.4	0.6
Fig.1(c)	20000	0.5	0.4	0.36	0.2	0.3	0.4	0.4	0.4	0.8	0.4	0.6

in Fig.1, where the left figures are the evolution of the prey spatial distribution and the right figures are the top predators and the center ones are the predators. We observe that, for $t = 0$ we have spots patterns over the whole domain (see Fig.1 (a)). If we increase time t, these spots burst leading to an aperiodic spatial distribution of some domain. Then this aperiodicity spreads throughout the area and remains in time. After a while, the patterns exhibit a behavior that does not seem to change its characteristics anymore and the labyrinth spatial pattern arise and we obtain the spatio-temporal chaos. Thus, we have observed the patterns formation with respect to time (see Fig.1).

6 Conclusion

In this paper, we have considered a three-species food chain, namely, prey, predator and top predator, given by a reaction diffusion system incorporating Holling type II and a modified Leslie-Gower functional response defined in a circular domain. We have proved the conditions for boundedness, existence of a positively invariant and attracting set. By using Routh-Hurwitz criterion, we have showed that E^* is locally asymptotically stable for system (15) if some conditions are satisfied. By constructing a Lyapunov function, we have obtained a sufficient conditions for global stability of the positive equilibrium for system (7). By numerical simulations, we have plotted the nature of spatial patterns with respect to time (see Fig.1) which leads to the formation of the labyrinth spatial patterns (the formation of spatio-temporal chaos).

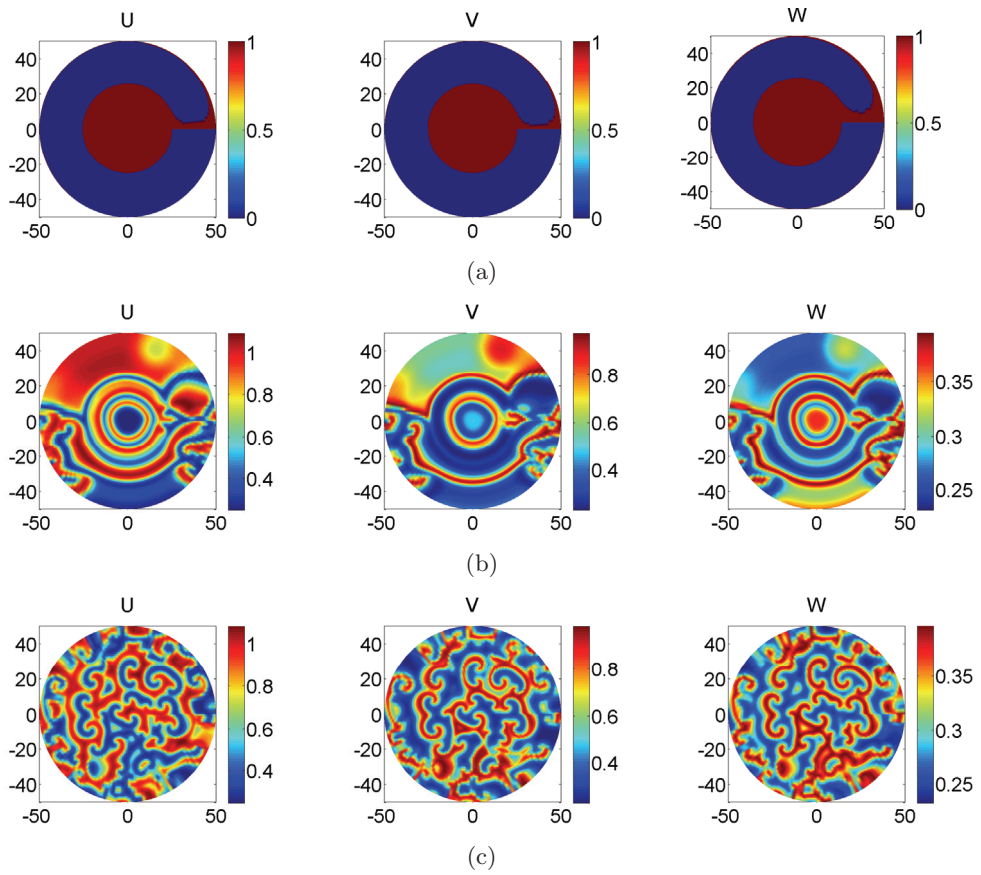

Fig. 1 Spatial distribution of prey (first column), predator (second column) and top predator (third column) are population densities of the spatial system (7). Spatial patterns are obtained with diffusivity coefficients $\delta_1 = 0.02$, $\delta_2 = 0.01$ and $\delta_3 = 0.05$.

References

[1] Lotka, A.J. (1925), *Elements of Physical Biology*, Williams and Wilkins, Baltimore, New York.

[2] Volterra, V. (1926), Variation and fluctuations of the number of individuals of animal species living together. In Animal Ecology. McGraw-Hill.

[3] Aziz-Alaoui, M.A. and Daher, O.M. (2003), Boundedness and global stability for a predator-prey model with modified Leslie-Gower and Holling type II schemes, *Applied Mathematics Letters*, **16**, 1069-1075.

[4] Camara, B.I. and Aziz-Alaoui, M.A. (2008), Dynamics of predator-prey model with diffusion, *Dynamics of Continuous, Discrete and Impulsive System, series A*, **15**, 897-906.

[5] Letellier, C. and Aziz-Alaoui, M.A. (2002), Analysis of the dynamics of a realistic ecological model, *Chaos Solitons Fractals,* **13**, 95-107.

[6] Chunyan, J. and Jiang, D. (2011), A note on a predator-prey model with modified Leslie-Gower and Holling-type *II* schemes with stochastic perturbation, *Journal of Mathematical Analysis and Applications*, **377**, 435-440.

[7] Abid, W., Yafia, R., Aziz-Alaoui, M.A., Bouhafa, H. and Abichou, A. (2015), Diffusion Driven Instability and Hopf Bifurcation in Spatial Predator-Prey Model on a Circular Domain, *Applied Mathematics and Computation*, **260**, 292-313.

[8] Abid, W., Yafia, R., Aziz-Alaoui, M.A., Bouhafa, H. and Abichou, A. (2015), Global Dynamics on a Circular Domain of a Diffusion Predator-Prey Model with Modified Leslie-Gower and Beddington-DeAngelis Functional Type, *Evolution Equations and Control Theory*, **4**, 115-129.

[9] Maionchi, D.O., dos Reis, S.F. and de Aguiar, M.A.M. (2006), Chaos and pattern formation in a spatial tritrophic food chain, *Ecological Modelling,* **191**, 291-303.

[10] Upadhyay, R.K. and Sharada, N.R. (2011), Complex dynamics of a three species food-chain model with Holling type IV functional response, *Nonlinear Analysis: Modelling and Control,* **16**, 353-374.
[11] Dubey, B. and Upadhyay, R. K. (2004), Persistence and extinction of one-prey and two-predator system, *Nonlinear Analysis,* **9**, 307-329.
[12] Shuwen, Z. and Dejun, T. (2009), Permanence in a food chain system with impulsive perturbations, *Chaos, Solitons and Fractals*, **40**, 392-400.
[13] Mada Sanjaya, W.S., Mamat, M., Salleh, Z. and Mohamad, N. (2011), Numerical simulation dynamical model of three species food chain with Holling type-II functional response, *Malaysian Journal of Mathematical Sciences*, **5**, 1-12.
[14] Leslie, P. H. (1948), Some further notes on the use of matrices in population mathematics, *Biometrica*, **35**, 213-245.
[15] Leslie, P.H. and Gower, J.C. (1960), The properties of a stochastic model for the predator-prey type of interaction between two species, *Biometrica*, **47**, 219-234.
[16] Camara, B.I. (2009), *Complexité de dynamiques de modèles proie-prédateur avec diffusion et applications*, Ph.D. thesis, Université du Havre.
[17] Aziz-Alaoui, M.A. (2002), Study of a Leslie-Gower-type tritrophic population model Chaos, *Solitons and Fractals*, **14**, 1275-1293.
[18] Nindjin, A.F. and Aziz-Alaoui, M.A. (2008), Persistence and global stability in a delayed Leslie-Gower type three species food chain, *Journal Mathematical Analysis and Applications*, **340**, 340-355.

Journal of Applied Nonlinear Dynamics 5(1) (2016) 105–115

Journal of Applied Nonlinear Dynamics

https://lhscientificpublishing.com/Journals/JAND-Default.aspx

A Bayesian Random Walk Approach for Mapping Dynamic Quantitative Trait

Burak Karacaören†

Department of Animal Science, Faculty of Agriculture, Akdeniz University Antalya, 07059, TURKEY

Submission Info

Communicated by J.A T. Machado
Received 10 June 2015
Accepted 16 July 2015
Available online 1 January 2016

Keywords

Association Mapping
Random Walk
Gibbs Sampling
State Space model

Abstract

Analyzing longitudinal observations with an appropriate methodology is important for detecting significant single nucleotide polymorphisms (SNPs) for complex traits in genome wide association studies (GWAS). Here we assumed that genomic signal over time could be traced by a Bayesian random walk- Kalman filter model in state space form to obtain longitudinal residuals. The Kalman filter removes the requirement for collecting the whole data set before making estimations, thus estimates are immediately available. For example, with the functional mapping approach, whole sets of observations must to be collected in advance. This may include months (if not years) of waiting time depending on the nature of the phenotypes and the experimental design. Whereas, because of the longitudinal residuals used in association mapping, biological reasoning can be easily applied given that the signal is genuine. The advantages of our method are demonstrated by both simulated and real datasets.

1 Introduction

Most complex traits can be measured longitudinally over time, which is advantageous compared to cross sectional observations. Key advantages of longitudinal approaches including control of measurements and associated retrospective factors, exploration of individual trajectories, and larger power for prediction of model parameters [1]. It is therefore important to select the correct methodology when analyzing longitudinal observations to detect significant single nucleotide polymorphisms (SNPs) for complex traits in genome wide association studies (GWAS).

It has been suggested that a random regression methodology could be use to detect quantitative trait loci (QTL) by longitudinal measurements [2]. However, a random regression methodology may fail to follow the underling pattern of longitudinal observations at the beginning and end of the time course [3]. A functional mapping approach by analyzing fitted curves to detect QTL for dynamic association studies has been proposed [4]. However, interpreting the results of functional mapping may not always be biologically meaningful [5]. Additional details on the literature of dynamic association mapping could be found in [5], [6].

†Corresponding author.
Email address: burakkaracaoren@akdeniz.edu.tr

ISSN 2164 – 6457, eISSN 2164 – 6473/$-see front materials
DOI : 10.5890/JAND.2016.03.008

In addition, both of the above mentioned models (and others) require whole sets of observations in order to generate predictions. This may result in delays of months (if not years) before obtaining predictions. Here we assumed that the genomic signal over time could be traced by a random walk-Kalman filter model in state space form to obtain longitudinal residuals. Use of the Kalman filter eliminates the need for the entire data set for making estimations, so that estimates are available immediately. Moreover, because of the available longitudinal residuals to employ in association mapping, and given that the signal is genuine, biological reasoning can also be easily deduced.

Recently, we extended the GRAMMAR model of [7] in the Bayesian context of [8]. Here we extended our model for dynamic association mapping [8] by including dynamic components using a random walk-Kalman filter approach to analyze a mouse behavioral [9] and simulated QTL-MAS [10] datasets.

2 Material and Methods

We used both simulated and real datasets to evaluate our model. QTLMAS Data were simulated for 5 time-points using the pedigree including 1,000 individuals with 453 SNPs [10]. Measurements were taken on days 1, 132, 265, 397 and 530. In total 18 QTLs were simulated. Phenotypes were simulated using a logistic growth curve. There was a population structure due to full sib families reflected by the pedigree pattern. True positives were detected if SNPs were found within 10 cM from true QTLs.

We used a mouse behavioral data set [9] for application of the random walk model. The mouse behavior data set was obtained using an automated home cage monitoring system (for 222 time points). A backcross population (n=89) was obtained to measure active state probabilities (ASP). The genotype data included 233 informative SNPs from 19 chromosomes. The average distance was 9.7 Mb.

2.1 Statistical Methods

We will use the notation and results of [8], [12]. For genetic analyses of traits following mixed model is normally used

$$\mathbf{y} = \mathbf{X}\beta + \mathbf{Z_a}\mathbf{a} + \mathbf{Z_p}\mathbf{p} + \mathbf{e}, \tag{1}$$

where $\mathbf{y}$ is the vector of observations $(y_1, \ldots, y_n)$, β is the vector of fixed effects, $\mathbf{a}$ $(a_1 \ldots, a_n)$, is the vector of random effects, $\mathbf{p}$ $(p_1 \ldots, p_n)$, is the vector of random permanent environmental effects, $\mathbf{X}$, $\mathbf{Z_a}$ and $\mathbf{Z_p}$ are design matrices and $\mathbf{e}$ is the vector of random residual effects. For the random effects it was assumed that

$$\begin{pmatrix} \mathbf{a}_t \\ \mathbf{p}_t \\ \mathbf{e}_t \end{pmatrix} \sim \mathscr{N} \left(\begin{matrix} \mathbf{a}_{t-1} \\ \mathbf{p}_{t-1}; \\ \mathbf{e}_{t-1} \end{matrix} \begin{bmatrix} \mathbf{A}\sigma_a^2 & \mathbf{0} & \mathbf{0} \\ \mathbf{0} & \mathbf{I}\sigma_p^2 & \mathbf{0} \\ \mathbf{0} & \mathbf{0} & \mathbf{I}\sigma_e^2 \end{bmatrix} \right),$$

where σ_a^2, σ_p^2 and σ_e^2 are genetic, permanent environment and error variances. We used diffuse (0) starting values for random effects, permanent environmental effects, and error terms. $\mathbf{A}$ is the additive genetic relationship matrix for the individuals; $\mathbf{I}$ is an identity matrix. $\mathbf{A}$ was obtained by the coefficient of coancestry matrix using both the genotype and pedigree of individuals. In the following, we show general assumptions used in KF-RW method, based on Bayesian principles. Proportional joint posterior distribution without constant terms could be written using (1) based on following smoother recursive relationship [13]

$$P(\theta_\mathbf{t}|\theta_{-\mathbf{t}}, Y_n) \propto P(\theta_\mathbf{t}|\theta_{\mathbf{t-1}}, Y_{t-1})\, P(\theta_{\mathbf{t+1}}|\theta_\mathbf{t}, Y_{t-1})\, P(Y_t|\theta_\mathbf{t}, Y_{t-1}),$$

$$
\begin{aligned}
& f(y|\beta,a,p,\sigma_a^2,\sigma_p^2,\sigma_e^2) \\
\propto\ & (\sigma_e^2)^{-0.5N}\exp(0.5(\mathbf{y}-\mathbf{X}\beta-\mathbf{Z_a}\mathbf{a}-\mathbf{Z_p}\mathbf{p})'(\mathbf{y}-\mathbf{X}\beta-\mathbf{Z_a}\mathbf{a}-\mathbf{Z_p}\mathbf{p})/\sigma_e^2) \\
& \times(\sigma_a^2)^{-0.5N_a}\exp(0.5(\mathbf{a_1'}\mathbf{A^{-1}}\mathbf{a_1}\sigma_a^2))[\prod_{t=2}^{T}(\sigma_a^2)^{-0.5N_a}((\mathbf{a_t}-\mathbf{a_{t-1}})'\mathbf{A^{-1}}(\mathbf{a_t}-\mathbf{a_{t-1}})/\sigma_a^2)] \\
& \times(\sigma_p^2)^{-0.5N_p}\exp(0.5(\mathbf{p_1'}\mathbf{I^{-1}}\mathbf{p_1}/\sigma_p^2))[\prod_{t=2}^{T}(\sigma_p^2)^{-0.5N_p}((\mathbf{p_t}-\mathbf{p_{t-1}})'\mathbf{I^{-1}}(\mathbf{p_t}-\mathbf{p_{t-1}})/\sigma_p^2)] \\
& \times(\sigma_a^2)^{-\frac{v_a}{2}-1}\exp[-\frac{v_aS_a}{2\sigma_a^2}](\sigma_p^2)^{-\frac{v_p}{2}-1}\exp[-\frac{v_pS_p}{2\sigma_p^2}](\sigma_e^2)^{-\frac{v_e}{2}-1}\exp[-\frac{v_eS_e}{2\sigma_e^2}]
\end{aligned}
$$

After algebraic manipulations conditional distributions could be written as following,

$$
\begin{aligned}
& \mathbf{b_t}|\sigma_a^2,\sigma_p^2,\sigma_e^2,a_t,p_t,y_t \sim \mathscr{N}((\mathbf{X'X})\mathbf{X'}(\mathbf{y}-\mathbf{Z_a}\mathbf{a}-\mathbf{Z_p}\mathbf{p}),(\mathbf{X'X})^{-1}\sigma_e^2), \\
& \mathbf{a_t}|\sigma_a^2,\sigma_p^2,\sigma_e^2,b_t,p_t,y_t \sim \mathscr{N}((\frac{\mathbf{Z'_{a_t}}\mathbf{Z_{a_t}}}{\sigma_e^2}+\frac{2\mathbf{A^{-1}}}{\sigma_a^2})^{-1}(\frac{\mathbf{Z'}(\mathbf{y_t}-\mathbf{X_a}\mathbf{b_t}-\mathbf{p_t}\mathbf{Z_{p_t}})}{\sigma_e^2}+\frac{a_{t+1}\mathbf{A^{-1}}}{\sigma_a^2}),(\frac{\mathbf{Z'_{a_t}}\mathbf{Z_{a_t}}}{\sigma_e^2}+\frac{2\mathbf{A^{-1}}}{\sigma_a^2})^{-1}) \\
& \mathbf{p_t}|\sigma_a^2,\sigma_p^2,\sigma_e^2,b_t,a_t,y_t \sim \mathscr{N}((\frac{\mathbf{Z'_{p_t}}\mathbf{Z_{p_t}}}{\sigma_e^2}+\frac{2\mathbf{A^{-1}}}{\sigma_p^2})^{-1}(\frac{\mathbf{Z'}(\mathbf{y_t}-\mathbf{X_a}\mathbf{b_t}-\mathbf{a_t}\mathbf{Z_{p_t}})}{\sigma_e^2}+\frac{p_{t+1}\mathbf{A^{-1}}}{\sigma_p^2}),(\frac{\mathbf{Z'_{p_t}}\mathbf{Z_{p_t}}}{\sigma_e^2}+\frac{2\mathbf{A^{-1}}}{\sigma_p^2})^{-1}), \\
& \sigma_a^2|\,\sigma_p^2,\sigma_e^2,b_t,a_t,p_t,y_t \sim \frac{(Q_a+v_aS_a)}{\chi^2_{DF}}, \\
& \sigma_p^2|\,\sigma_a^2,\sigma_e^2,b_t,a_t,p_t,y_t \sim \frac{(Q_p+v_pS_p)}{\chi^2_{DF}}, \\
& \sigma_e^2|\,\sigma_a^2,\sigma_p^2,b_t,a_t,p_t,y_t \sim \frac{(Q_e+v_eS_e)}{\chi^2_{DF}},
\end{aligned}
$$

where in the last three line Q_a, Q_p and Q_e stands for quadratic form of the respective error terms and DF degrees of freedoms. We ran the model with 20,000 iterations using a 1000-iteration burn-in period. To reduce auto-correlation, we sampled every tenth iteration. We tried different parameters of inverse Wishart prior distributions to obtain residuals. For mouse data set we used genomic relationship matrix [14] to take into account of backcross structure: $\mathbf{A} = WW'/c$ where c is a normalizing constant and $W_{ik} = X_{ik} + 1 - 2_{pk}$ where p_k is the frequency of the 1 allele at marker k [14].Time points and square of the time points was used as explanatory variables in the mouse behavioral data set. We used a single SNP model to perform genome-wide association analyses [8], [15];

$$\mathbf{y}=\mathbf{X}\mathbf{b}+\mathbf{e},$$

where $\mathbf{y}$ contains the residuals or random effects from (1), $\mathbf{b}$ designates the fixed effects (single or whole SNP), $\mathbf{X}$ is incidence matrices, and $\mathbf{e}$ is a vector containing residuals and assumed normally distributed with $\mathbf{I}\sigma_e^2$. Here $\mathbf{I}$ is an identity matrix and σ_e^2 is the residual variance. We used a false discovery threshold of 5% to detect a genomic signal in association mapping.

3 Results

3.1 Analyses of QTLMAS Dataset

Residual, genetic and permanent environment variances predicted as 34.46, 24.55, and 26.52 respectively. Correlations between observations and predictions were found to be about 0.85. Heritability were found to be around 0.29. In Table 1 the number of correctly identified SNPs were given for two different random walk approaches using 5 time points. We used residuals with single SNP regression

model,(RANDOM WALK-1), and random effects, $(\mathbf{a_t}|\sigma_a^2, \sigma_p^2, \sigma_e^2, b_t, p_t, y_t)$, with single regression model (RANDOM WALK-2),. Manhattan plots for RANDOM WALK-1 shown in Figure 1 [16].

3.2 Analyses of Mouse Behavioral Data Set

Residual, genetic and permanent environment variances were predicted as 14.51, 6.49, and 9.01 respectively. Correlations between observations and predictions were found to be around 0.20. In order to account for backcross structure, we employed a genomic kinship matrix. Heritabilities were found to be around 0.21. The strongest genomic signals (0.11 FDR [17]) were observed for mCV22849619 and rs3689947 at chromosome 1 by adjacent positions (Table 2) from time-points 65, 80, 88, 94 and 96. The next strongest signal was detected from chromosome 9 at marker rs13480208. For both markers longitudinal p-values were found to be higher around time-points 57 to 89 (Figure 2 and Figure 3). Longitudinal permanent environmental effects (Figure 5) were found to have less autocorrelation $(-0.17 < \hat{\rho} < 0.19)$ compared with longitudinal gene effects $(-0.07 < \hat{\rho} < 0.29)$. However, the average phenotypic trajectory showed strong autocorrelation $(-0.25 < \hat{\rho} < 0.98)$, and hence was found to be non-stationary.

4 Discussion

As the cost of sequencing a genome becomes cheaper, we expect that; genomic and phenotypic information will be available for a number of time points for both agricultural species and humans. The current practice of GWAS uses only cross sectional experimental designs. Collecting longitudinal phenotypes for each individual may increase the statistical power for detecting genomic associations. Since gene expression may change over time; failing to take longitudinal gene effects into account might lead to erroneous conclusions. Here we proposed the use a random walk model for dynamic association studies. We assumed that gene and environmental effects change (slightly) over time, similar to a random walk model. However, random walk is a non-stationary process and, therefore, stationary assumptions could be evaluated empirically. For example, [17] used daily means and variances from various datasets and concluded that most experimental circadian rhythm data sets are non-stationary. This was also the case for our mouse behavioral data set, as autocorrelations of the mean phenotype among each time-point were found to be $(-0.25 < \hat{\rho} < 0.98)$. Random walk is a discrete stochastic process. Since our random walk model was based on a non-stationary assumption, it may have wide applicability for longitudinal genetic and genomic studies.

Correlations between predictions and observations were found to be around 0.85 for the QTLMAS data set. We did not employ any parametric function (e.g., logistic growth curve) in the model (1). Only time and its square were used as explanatory variables in the model. Employing random effects (RANDOM-WALK 2, Table 1) in the association model increased the false positives (430 SNPs reported at 5% false discovery rate). When genetics effects were taken into account (RANDOM WALK-1) we detected 104 SNPs, of which 77 were considered to be true signals. This was not surprising since the population structure could lead to false positives. The number of true positives was increased by collecting more longitudinal observations. Similarly significance levels were also found to be increased by collecting more longitudinal observations (Figure 1). In that regard, predictions from the initial time-points of random walk models should be interpreted carefully as they may lead to false positives due to a lack of information.

As pointed out in [9], the mouse behavioral data set has unique features, as such: the number of longitudinal observations (222) was larger than the number of mice (89); there was a large mice specific variation; and the correlation structure from 222 time-points was distinctive. Correlations between observations and predictions were found to be around 0.20. The differences between the predicted and

observed trajectories can probably be explained by the huge variation within and between mice and the small number of individuals. Both [9] and [6] detected genomic signals from marker rs3689947, similar to our results (Table 2). The next strongest signal was detected from Chromosome 9 (rs13480208) at 0.15 FDR. [9] and [6] detected strong signals from Chromosome 9, which is again in line with our results (Table 2).

The model given in this paper is novel and distinct from other previously reported models in that our model predicts time-specific genomic signals, and hence associated SNPs. For instance, we detected rs3689947 at chromosome 1 (Table 2) from time-points 65, 80, 88, 94 and 96 using the mouse behavioral dataset. Although [18] have criticized (uncorrected) time-specific approaches since interpretation of the appearing and disappearing of QTLs could be considered as speculative, our approach readily corrected the phenotypes by taking into account both longitudinal gene and environmental effects. We analyzed the average phenotypes for 222 time-points and detected 23 SNPs at FDR 15% (results not shown). By using this cross sectional approach the aforementioned SNPs were detected from Chromosome 1 and Chromosome 9, although false positives were also detected. In that respect [5] noted the failure to take into account the smoothing structures across time-points, which might lead to reduced power to QTL detection. Again, our model handles smoothing structures for different time-points via the random walk model. It has been suggested that combining the results of time-specific analyses may lead to inconsistent interpretations [5]. However, we could also hypothesize that biologically meaningful patterns might be observable since gene effects are also changing over time, and may subject to certain types of longitudinal structures. Although we do not expect that every fluctuation in time should lead to genomic associations, as would be compatible with the neutral theory of molecular evaluation.

Automated measurements may also be important in longitudinal studies [9]. Due to the Kalman Filter recursive structure given in (2); filtering version of our model could give on-line predictions of longitudinal residuals. Hence, biological reasoning could be made as soon as longitudinal measurements are collected. To our knowledge, there is no such model currently reported in the literature of dynamic association studies. For example, in order to use a functional mapping [4] approach, whole sets of observations must to be collected in advance. This may include months (if not years) of waiting time depending on the nature of the phenotypes and experimental designs. Again, compared with other available models, our model generates understandable and easy to interpretable results. Since longitudinal residuals detrended for both genetic and environmental effects, they could be employed with more complex models, as such genomic prediction, epistatic, or haplotype based models. Although we used single SNP model for detecting potential gene and SNP associations using simulated and the mice data sets; area of interest could easily be extended for whole genome using genomic selection models [19] or dynamic gene networks [20] based on residuals of each time point.

Random walk is a non stationary process and the model could be extended for stationary case by introducing autoregressive parameter in equation (1). However theoretical and empirical dynamic association studies are needed if non stationary assumption is useful or not for dynamics of gene and permanent environmental effects.

5 Acknowledgements

The author wishes to acknowledge useful discussions with Dr Li Zitong on mouse behavioral data set. The author wishes to acknowledge useful discussions with Dr Sitki Çağdaş İnam on LaTeX typesettings. This work was supported by Research Fund of the Akdeniz University Project Number 106.

zaman1. png (750x300x24b png)

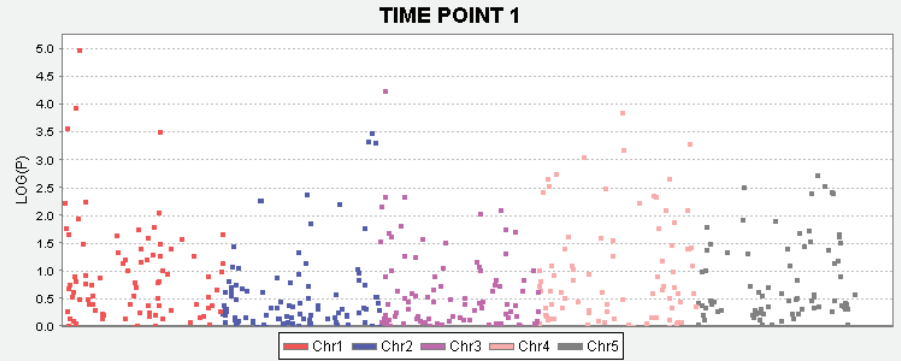

Fig. 1

zaman2. png (750x300x24b png)

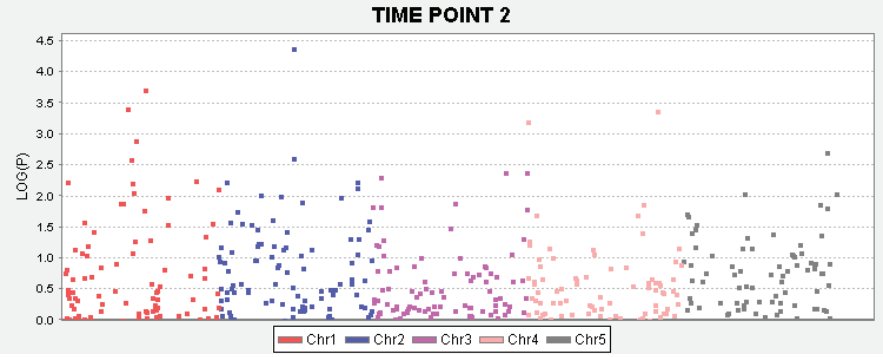

Fig. 2

zaman3. png (750x300x24b png)

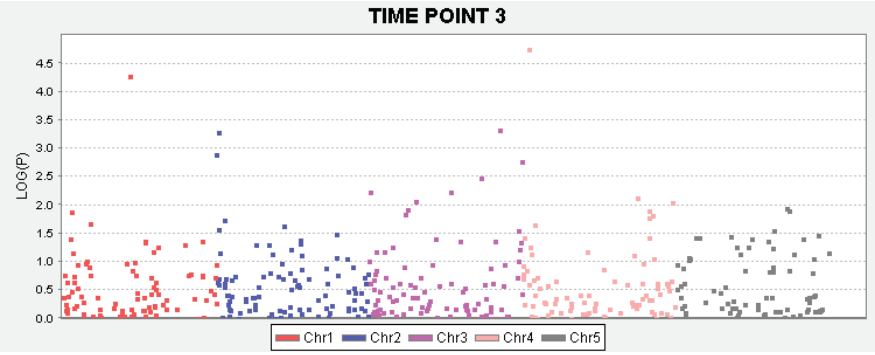

Fig. 3

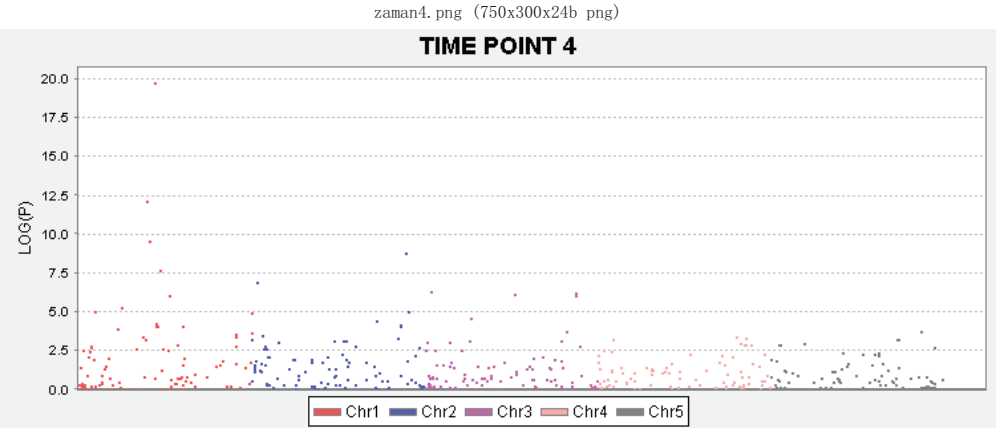

Fig. 4

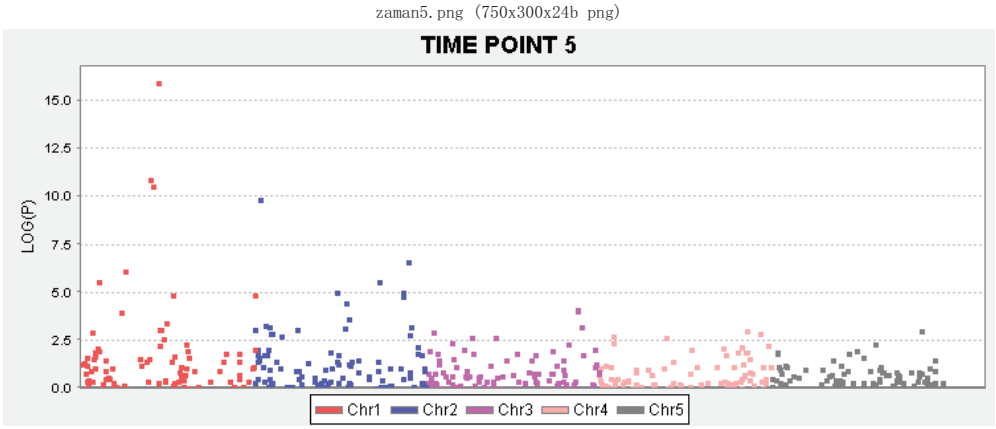

Fig. 5 Manhattan plots for 5 time points using random walk residuals and single marker regression.

Table 1 Number of total (#REPORTED) and correct SNPs detected using QTLMAS dataset for time points 1, 2, 3,4 and 5 (RANDOM WALK-1: residuals with single SNPs; RANDOM WALK-2: random effects with single SNPs)

MODEL	#REPORTED	#CORRECT	#T 1	#T 2	#T 3	#T 4	#T 5
RANDOM WALK-1	104	77	1/4	1/1	2/2	18/26	55/71
RANDOM WALK-2	430	370	9/18	145/196	126/179	6/9	84/110

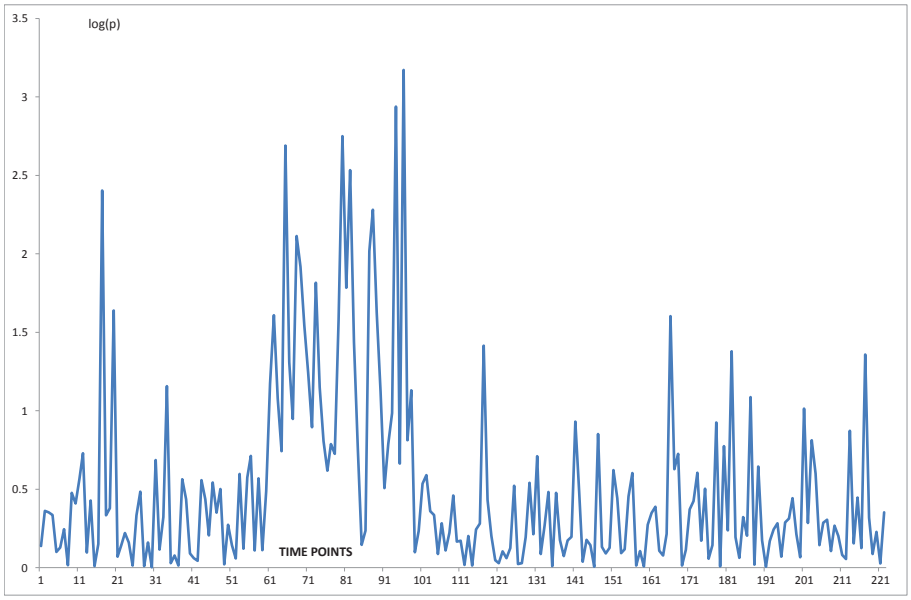

Fig. 6 Longitudinal (-logarithmic) p values for marker rs3689947 over 222 time points.

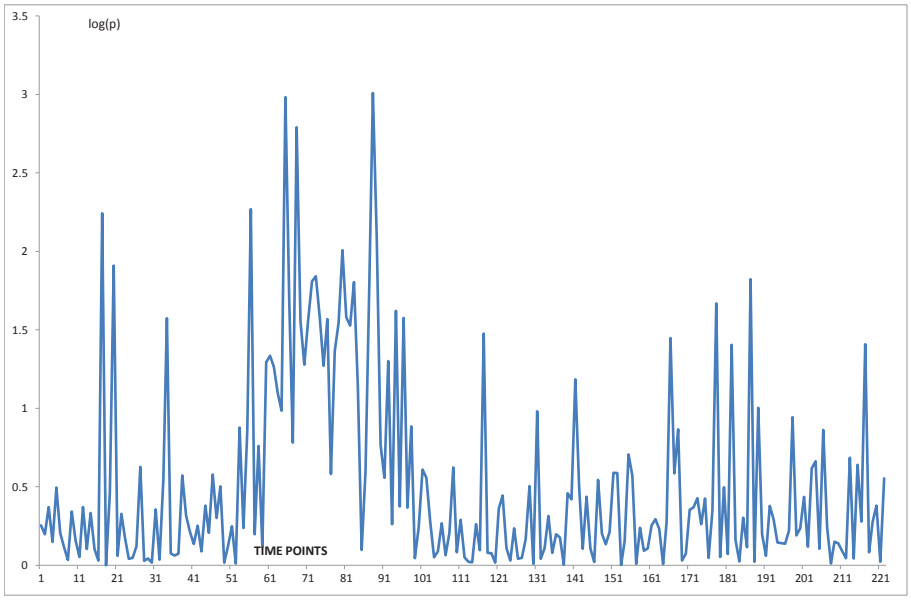

Fig. 7 Longitudinal (-logarithmic) p values for marker mCV22849619 over 222 time points.

Table 2 The results of mouse behavioral data analysis by using a random walk model

Marker	Chromosome	Location	P value	False Discovery Rate	Time Point
mCV22849619	1	186531848	0.00098	0.11	88
rs3689947	1	192397145	0.001776	0.11	80
rs3689947	1	192397145	0.001154	0.11	94
rs3689947	1	192397145	0.000674	0.11	96
mCV22849619	1	186531848	0.00104	0.12	65
rs13480208	9	55395056	0.001325	0.15	86

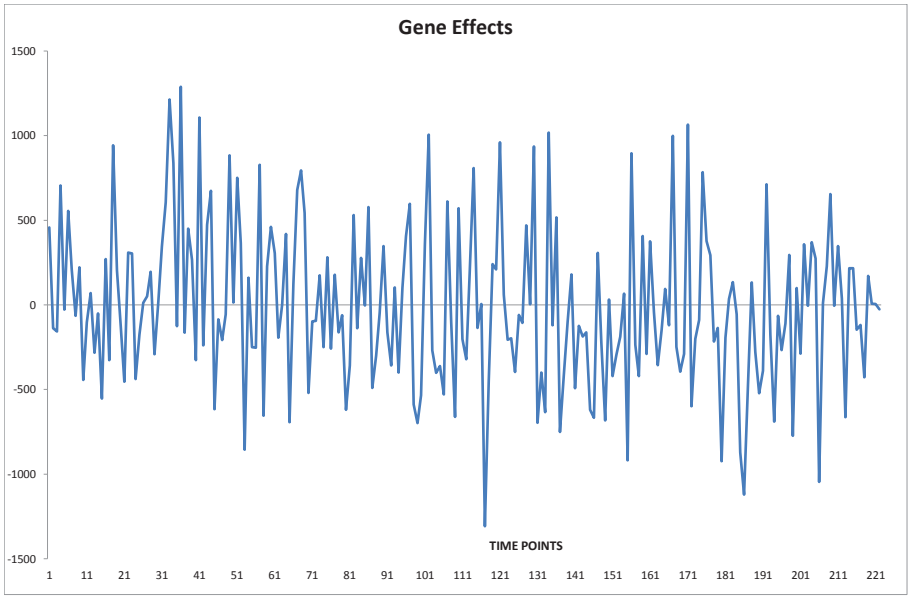

Fig. 8 Proportional average posterior distributions of longitudinal average gene effects over 222 time points.

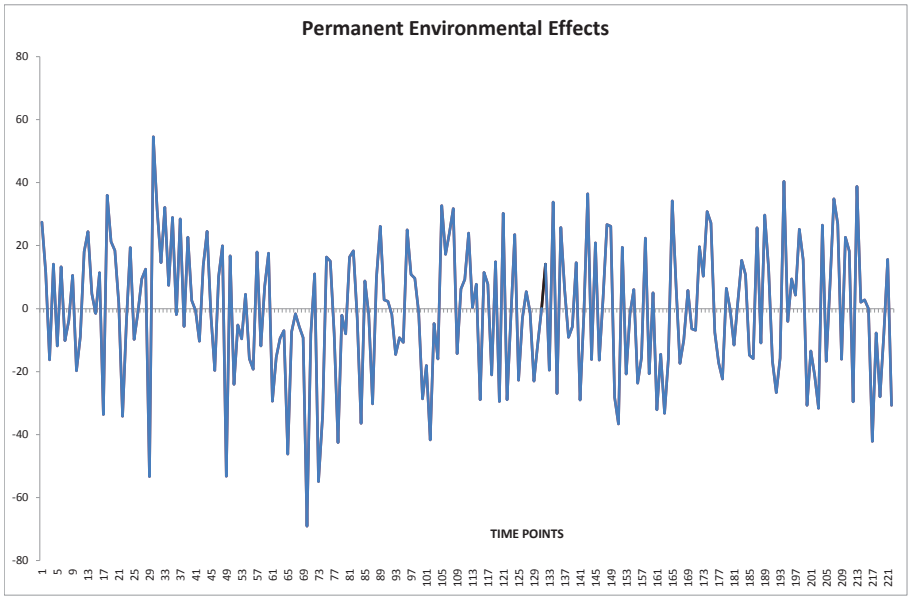

Fig. 9 Proportional average posterior distributions of longitudinal average environmental effects over 222 time points.

References

[1] Ware, J.H. (1985), Linear models for the analysis of longitudinal studies, *American Statistician*, **39**, 95-101.
[2] Macgregor, S. Knott, S.A. White, I. and Visscher, P.M. (2005), Quantitative trait locus analysis of longitudinal quantitative trait data in complex pedigrees, *Genetics*, **171**, 1365-1376.
[3] El Faro, L. Cardoso, V.L. and Albuquerque, L.G. (2008), Variance component estimates applying random regression models for test-day milk yield in caracu heifers, *Genetics and Molecular Biology*, **31**, 665-673.
[4] Wu, R.L. and Lin, M. (2006), Functional mapping-how to map and study the genetic architecture of dynamic complex traits, *Nature Review Genetics*, **7**, 229-237.
[5] Kwak, Y.I. Moore, R.C. Spalding, P.E. and Broman, W.K. (2014), A Simple regression method to map quantitative trait loci underlying function-valued phenotypes, *Genetics*, **197**, 1409-1416.
[6] Li, Z. Sillanpa and ää, JM. (2013), A bayesian nonparametric approach for mapping dynamic quantitative traits, *Genetics*, **194**, 997-1016.
[7] Aulchenko, S.Y. de Koning, D.J. and Haley, C.S. (2007), Genomewide rapid association using mixed model and regression: a fast and simple method for genomewide pedigree-based quantitative trait loci association analysis, *Genetics*, **177**, 577-585.
[8] Karacaören, B. (2014), Admixture mapping of growth related traits in F2 mice dataset using ancestry informative markers *Journal of Bioinformatics and Computational Biology*, **2**(doi: 10.1142/S0219720014410108).
[9] Xiong, H. Goulding, E.H. Carlson, E.J. Tecott, L.H. McCulloch, C.E. and Sen, Ś. (2011), A flexible estimating equations approach for mapping function-valued traits, *Genetics*, **189**, 305-316.
[10] Coster, A. Bastiaansen, J.W. Calus, M.P. Maliepaard, C. and Bink, M.C. (2010), QTLMAS 2009: Simulated dataset. *BMC proceedings*, **4**, 1(doi:10.1186/1753-6561-4-S1-S3).
[11] R Development Core Team, (2007), R: A language and environmental for statistical computing Vienna: R Foundation for statistical computing.
[12] Karacaören, B. Janss, L.L.G, Kadarmideen, H.N. (2012), Predicting Breeding Values In Animals By Kalman Filter: Application To Body Condition Scores In Dairy Cattle, *Journal of the Faculty of Veterinary Medicine, Kafkas University*, **18**, 627-632.

[13] West, M. and Harrison, J. (1997), *Bayesian Forecasting and Dynamic Models* Springer: New York
[14] Endelman, J.B. (2011), Ridge regression and other kernels for genomic selection with R package rrBLUP, *Plant Genomics*, **4**, 250-255.
[15] Purcell, S. Neale, B. Todd-Brown, K. Thomas, L. Ferreira, M.A.R. Bender, D. Maller, J. Sklar, P. de Bakker, P.I.W. Daly, M.J. and Sham, P.C. (2007), PLINK: a toolset for whole-genome association and population-based linkage analysis, *American Journal of Human Genetics*, **81**, 559-575.
[16] Barrett, J.C. Fry, B. Maller, J. Daly, and M.J. (2005), Haploview: analysis and visualization of LD and haplotype maps, *Bioinformatics*, **21**, 263-265.
[17] Refinetti, R. (2004), Non-stationary time series and the robustness of circadian rhythms, *Journal of Theoretical Biology*, **21**, 571-581.
[18] Maliepaard, C. Bastiaansen, J.W. Calus, M.P, Coster, A. (2010), Comparison of analyses of the QTLMAS XIII common dataset II: QTL analysis, *BMC proceedings*, **4**, 2(doi:10.1186/1753-6561-4-S1-S2).
[19] Meuwissen, T.H.E. Hayes, B.J. Goddard, M.E. (2001), Prediction of total genetic value using genome wide dense marker maps, *Genetics*,**157**,1819-1829.
[20] Weber, G.W. Alparslan, Gök.S.Z. Söyler, B. (2009a), A new mathematical approach in environmental and life sciences: gene-environment networks and their dynamics, *Environmental Modeling and Assessment*, **14**, 267-288.

Journal of Applied Nonlinear Dynamics 5(1) (2016) 117–125

Journal of Applied Nonlinear Dynamics

https://lhscientificpublishing.com/Journals/JAND-Default.aspx

Numerical Modeling of Photon Migration in Human Neck Based on the Radiative Transport Equation

Hiroyuki Fujii [1†], Shinpei Okawa [2], Ken Nadamoto[3], Eiji Okada[3], Yukio Yamada[4], Yoko Hoshi[5], and Masao Watanabe[1]

[1] Division of Space and Mechanical Engineering, Faculty of Engineering, Hokkaido University, Kita 13 Nishi 8, Kita-ku, Sapporo, Japan

[2] National Defense Medical College, 3-2 Namiki, Tokorozawa, Saitama, Japan

[3] Department of Electronics and Electrical Engineering, Faculty of Science and Technology, Keio University, 3-14-1 Hiyoshi, Kohoku-ku, Yokohama, Kanagawa, Japan

[4]Brain Science Inspired Life Support Research Center, University of Electro-Communications, 1-5-1 Chofugaoka, Chofu, Japan

[5]Tokyo Metropolitan Institute of Medical Science, 2-1-6 Kamikitazawa, Setagaya, Tokyo, Japan

Submission Info

Communicated by J.A T. Machado
Received 17 June 2015
Accepted 21 August 2015
Available online 1 January 2016

Keywords

Biomedical optical imaging
Photon migration in biological tissue
Radiative transport equation
Diffusion approximation

Abstract

Biomedical optical imaging has a possibility of a comprehensive diagnosis of thyroid cancer in conjunction with ultrasound imaging. For improvement of the optical imaging, this study develops a higher order scheme for solving the time-dependent radiative transport equation (RTE) by use of the finite-difference and discrete-ordinate methods. The accuracy and efficiency of the developed scheme are examined by comparison with the analytical solutions of the RTE in homogeneous media. Then, the developed scheme is applied to describing photon migration in the human neck model. The numerical simulations show complex behaviors of photon migration in the human neck model due to multiple diffusive reflection near the trachea.

1 Introduction

Thyroid cancer is one of common cancers, whose incidence increases in accordance with developments of biomedical imaging modalities [1]. There are several kinds of thyroid cancers, and most of them can be accurately diagnosed by using the ultrasound tomography and fine needle aspiration cytology to examine the cellular structures [2]. Nevertheless, diagnosis of follicular thyroid carcinoma is still difficult, because neither the ultrasound tomography nor the needle aspiration cytology can differentiate between them. Hence, other imaging modality is essential for comprehensive diagnosis of thyroid cancer.

†Corresponding author.
Email address: fujii-hr@eng.hokudai.ac.jp

ISSN 2164 – 6457, eISSN 2164 – 6473/$-see front materials
DOI : 10.5890/JAND.2016.03.009

Diffuse optical tomography (DOT) has a potential to accurately and non-invasively diagnose whether the tumor is benign or malignant based on the difference in optical properties [3,4]. The optical properties (e.g. the absorption and scattering coefficients, and anisotropic factor) characterize the strength of absorption and scattering of light by a turbid medium such as biological tissue. Unlike a conventional image reconstruction algorithm for X-ray computed tomography, of which fundamentals are measuring line integrals of the attenuation coefficients and solving a set of integral equations for the attenuation coefficients, DOT needs an inversion process to reconstruct a distribution of tomographic image of the optical properties inside the tissues based on a mathematical model describing the diffusive nature of photon migration in scattering media [5]. Hence, for obtaining a high quality image of DOT, an accurate photon migration model is essential, and an efficient scheme for solving the model is required.

Mainly, two types of the governing equations for photon migration have been used: the radiative transport equation (RTE) and the diffusion equation (DE). The RTE can accurately describe photon migration in wide ranges of time-length scales, and numerical schemes for solving the RTE have extensively been developed by using the finite-difference [6, 7], finite-element [8], and finite-volume methods [9].

However, their computational loads for solving the RTE are heavy because the RTE is an integro-differential equation with many independent variables. Due to this reason, the RTE has usually been applied to small-sized media such as human fingers and rats. Meanwhile, the DE can be applied to large-sized media (e.g. the human brain) [10–12] because the approximation can decrease the number of the independent variables to reduce the computational loads. However, it is well understood the DE is valid in spatial and temporal regions after photons undergo a sufficient number of scattering events. In non-scattering or void regions, the DE is invalid and fails to describe photon migration [13–15].

The human neck is a large-sized and inhomogeneous medium consisting of the trachea, arteries, veins, muscles, bones, adipose tissue, and so on. The trachea is a void region where photons travel straight without being absorbed and scattered. Also, the arteries and veins are highly absorbing regions, where photons are totally absorbed before photons undergo a sufficient number of scattering events for the DE to be valid. Considering the above-mentioned characteristics of the human neck, an efficient scheme for solving the RTE is still in need of further development.

This paper develops the numerical scheme for solving the RTE using the finite-difference and discrete-ordinate methods (the 3rd order upwind and the 4th order Runge-Kutta methods). At first, the validity of the developed scheme is confirmed for homogeneous media by comparison with analytical solutions. After the validation, the developed scheme is applied to investigation of photon migration in the human neck.

The following section provides an explanation of the numerical method based on the RTE. Section 3 provides the numerical results for a 2D homogeneous square medium and an inhomogeneous medium modeled from an MR image of the human neck. Finally, conclusions are given in section 4.

2 Numerical method

2.1 Radiative transport equation and numerical scheme

2D photon migration in turbid media such as biological tissues is accurately formulated by the RTE [16],

$$[\frac{\partial}{v\partial t}+\mathbf{\Omega}\cdot\nabla+\mu_a(\boldsymbol{r})+\mu_s(\boldsymbol{r})]I(\boldsymbol{r},\mathbf{\Omega},t)=\mu_s(\boldsymbol{r})\int_{2\pi}d\mathbf{\Omega}'P(\boldsymbol{r},\mathbf{\Omega}\cdot\mathbf{\Omega}')I(\boldsymbol{r},\mathbf{\Omega}',t)+q(\boldsymbol{r},\mathbf{\Omega},t), \tag{1}$$

where $I(\boldsymbol{r},\mathbf{\Omega},t)$ [W/cm rad] represents the intensity, which describes the photon energy flow as a function of position, $\boldsymbol{r}=(x,y)$ [cm], angular direction, $\mathbf{\Omega}=(\Omega_x,\Omega_y)=(\cos\theta,\sin\theta)$ with angle, θ [rad], and time, t [ps]. $\mu_a(\boldsymbol{r})$ [1/cm] and $\mu_s(\boldsymbol{r})$ [1/cm] are the absorption and scattering coefficients, respectively, v [cm/ps]

is the velocity of light in the turbid medium, $P(\boldsymbol{r},\boldsymbol{\Omega}\cdot\boldsymbol{\Omega}')$ [1/rad] is the scattering phase function with $\boldsymbol{\Omega}$ and $\boldsymbol{\Omega}'$ denoting the scattered and incident directions, respectively, and $q(\boldsymbol{r},\boldsymbol{\Omega},t)$ [W/cm^2 rad] is a source. In this study, $P(\boldsymbol{r},\boldsymbol{\Omega}\cdot\boldsymbol{\Omega}')$ is given by the Henyey-Greenstein function [17] in two dimensions [18],

$$P(\boldsymbol{r},\boldsymbol{\Omega}\cdot\boldsymbol{\Omega}') = \frac{1}{2\pi}\frac{1-\{g(\boldsymbol{r})\}^2}{1+\{g(\boldsymbol{r})\}^2-2g(\boldsymbol{r})\boldsymbol{\Omega}\cdot\boldsymbol{\Omega}'}, \tag{2}$$

where $g(\boldsymbol{r})$ represents the anisotropic factor defined as the average cosine of $P(\boldsymbol{r},\boldsymbol{\Omega}\cdot\boldsymbol{\Omega}')$. For simplicity, $q(\boldsymbol{r},\boldsymbol{\Omega},t)$ is given by an isotropic delta function. The boundary condition under the refractive-index mismatching is employed with the reflectivity, $R(n,\boldsymbol{\Omega}\cdot\hat{\boldsymbol{e}}_n(\boldsymbol{r}_b))$, calculated by the Fresnel's law and Snell's law, where n denotes the refractive index of the medium and $\hat{\boldsymbol{e}}_n(\boldsymbol{r}_b)$ denotes the outward normal vector at the boundary position, $\boldsymbol{r}_b$ [7].

In this study, the RTE is numerically solved based on the finite-difference and discrete-ordinate methods. For numerical discretization, x, y, θ, and t are divided into $x_i = i\Delta x$ $(i\in\{0,\cdots,N_x\})$, $y_j = j\Delta y$ $(j\in\{0,\cdots,N_y\})$, $\theta_k = k\Delta\theta$ $(k\in\{0,\cdots,N_\theta\})$, and $t_m = m\Delta t$ $(m\in\{0,\cdots,N_t\})$ with constant step sizes of Δx, Δy, $\Delta\theta$, and Δt, respectively, and numbers of grid nodes and timesteps, N_x, N_y, N_θ, and N_t, respectively. In the same manner, $\boldsymbol{\Omega}$ is discretized as $(\Omega_{kx},\Omega_{ky}) = (\cos\theta_k,\sin\theta_k)$, and $I(\boldsymbol{r},\boldsymbol{\Omega},t)$ at the grid node and timestep is expressed as I^m_{ijk}.

For the finite-difference discrete-ordinate methods, previous papers mostly employ the 1st order scheme: the 1st order upwind (1UW) scheme for $\boldsymbol{r}$, the extended trapezoidal rule for $\boldsymbol{\Omega}$, and the forward Euler method (FE) for t [19,20]. The 1st order scheme is stable and accurate if the spatial and temporal step sizes, Δx and Δt, are sufficiently fine, but the fine step sizes result in heavy computational loads. To reduce the computational loads, this study employs the 3rd order upwind (3UW) scheme and 4th order Runge-Kutta (4RK) method.

In the 3UW, the advection term in the x-direction, $\Omega_x\partial I(\boldsymbol{r},\boldsymbol{\Omega})/\partial x$, is discretized as

$$\Omega_x\partial I(\boldsymbol{r},\boldsymbol{\Omega})/\partial x \sim \begin{cases} \dfrac{\Omega_{kx}}{6\Delta x}\left[2I_{i+1jk}+3I_{ijk}-6I_{i-1jk}+I_{i-2jk}\right] & \Omega_{kx}\geq 0 \\ \dfrac{\Omega_{kx}}{6\Delta x}\left[-I_{i+2jk}+6I_{i+1jk}-3I_{ijk}-2I_{i-1jk}\right] & \Omega_{kx}<0 \end{cases}, \tag{3}$$

for the internal nodes. For the grids near the boundary, the 1UW scheme is employed. The advection term in the y-direction, $\Omega_y\partial I(\boldsymbol{r},\boldsymbol{\Omega})/\partial y$, is also discretized in the same manner as in the x-direction. The 3UW is slightly unstable compared to the 1st order scheme, and oscillations appear at early arriving times and at positions very close to the source. In this study, the media is so large that the oscillations are negligibly small.

Based on the extended trapezoidal rule, the scattering integral is calculated as

$$\int_{2\pi} d\boldsymbol{\Omega}' P(\boldsymbol{r},\boldsymbol{\Omega}\cdot\boldsymbol{\Omega}')I(\boldsymbol{r},\boldsymbol{\Omega}') \sim \sum_{k'=1}^{N_\theta} w_{k'}f_{k'}P_{kk'}I_{ijk'}, \tag{4}$$

where $w_{k'} = 2\pi/N_\theta$ is a weight and $f_{k'}$ is a renormalizing factor. To satisfy the normalization of the scattering phase function $\int_{2\pi} d\boldsymbol{\Omega}' P = 1$, $f_{k'}$ is formulated with a slight modification of the Liu's renormalization [21], $1/f_{k'} = \sum_{k'=1}^{N_\theta} w_{k'}P_{kk'}$.

In the matrix notation, the discretized RTE except for the time variable, t, is given as an algebraic equation,

$$\frac{\partial}{v\partial t}\boldsymbol{I} + \boldsymbol{A}\boldsymbol{I} = \boldsymbol{P}\boldsymbol{I} + \boldsymbol{Q}, \tag{5}$$

where a matrix $\boldsymbol{A}$ represents the second, third, and fourth terms in the left-hand side of Eq. (1), a matrix $\boldsymbol{P}$ represents the scattering integral (Eq. (4)) multiplied by $\mu_s(\boldsymbol{r})$, vectors $\boldsymbol{I}$ and $\boldsymbol{Q}$ are the intensity and source, respectively.

Based on the 4RK, the temporal change in the intensity is calculated as

$$\boldsymbol{I}^{m+1} \sim \boldsymbol{I}^m + \frac{1}{6}(\boldsymbol{k}_1 + 2\boldsymbol{k}_2 + 2\boldsymbol{k}_3 + \boldsymbol{k}_4), \tag{6}$$

where $\boldsymbol{k}_l (l = 1, 2, 3, 4)$ are given by the following equations,

$$\begin{aligned}
\boldsymbol{k}_1 &= v\Delta t(-\boldsymbol{A} + \boldsymbol{P})\boldsymbol{I}^m, \\
\boldsymbol{k}_2 &= v\Delta t(-\boldsymbol{A} + \boldsymbol{P})(\boldsymbol{I}^m + 0.5\boldsymbol{k}_1), \\
\boldsymbol{k}_3 &= v\Delta t(-\boldsymbol{A} + \boldsymbol{P})(\boldsymbol{I}^m + 0.5\boldsymbol{k}_2), \\
\boldsymbol{k}_4 &= v\Delta t(-\boldsymbol{A} + \boldsymbol{P})(\boldsymbol{I}^m + \boldsymbol{k}_3).
\end{aligned} \tag{7}$$

Because the explicit method is used for the 4RK, it should satisfy the Courant-Friedrichs-Lewy (CFL) condition, $\Delta t \leq \Delta x/2v$, for stable solutions [20, 22].

In this study, parallel programming is implemented with a 24 threads computer (Intel Xeon X5690 @3.47GHz) by using OpenMP, which is a portable and shared-memory programming scheme.

2.2 Geometry, optical properties, and step sizes in discretization

To construct the human neck model, the study uses an MR image of the human neck as shown in Fig. 1 (a). Segmentation of the MR image is performed, and primary organs in the human neck such as common carotid artery, internal jugular vein, trachea, spinal cord, and spine are extracted as shown in Fig. 1 (b). Other organs such as human muscle, bone, and adipose tissue are collected to form a homogeneous background. Then, irregular boundaries of the organs and background in the image are mapped with regular grids for numerical calculations. At the surface of the human neck, the Fresnel's law is employed for the boundary condition which describes the reflection and refraction at the boundary due to the difference in the refractive index between the medium and surrounding air. Meanwhile, we assume that the refractive index inside the medium is homogeneous. So neither reflection nor refraction takes places at the interfaces between different organs, and no boundary condition is used at the interfaces. The optical properties of the organs and background tissues in the human neck in the near-infrared wavelength range are listed in Table 1, referring to [23, 24], and the properties of the thyroid gland is considered to be the same as those of the background. Strictly speaking, the arteries have different values of the properties from the veins, but it is simply assumed that the both have the same optical properties. Except the trachea, the tissues are assumed to have a constant value of $g = 0.9$, corresponding to highly forward-peaked scattering.

Appropriate values of the step sizes are dependent on the optical properties; Δx and Δt are inversely proportional to $\mu_s' = \mu_s(1-g)$ and μ_a, and $\Delta\theta$ should be smaller when g approaches to one. In each case, we set the appropriate values of the step sizes.

Table 1 Optical properties of the primary organs and background in the human neck [23, 24]

	μ_a[1/cm]	μ_s[1/cm]	g
Artery and vein	4.76	675	0.9
Trachea	0.0001	0.0001	0.0
Spinal cord	0.17	882	0.9
Spine	0.25	148	0.9
Background	0.30	80.0	0.9

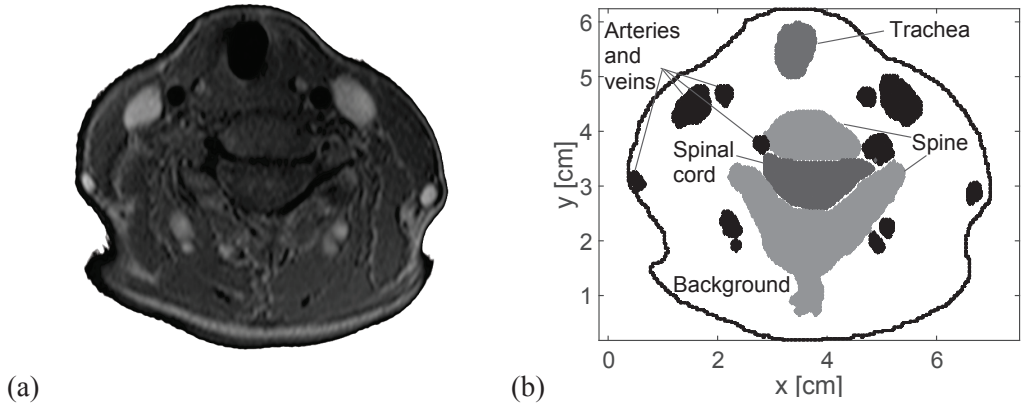

Fig. 1 (a) MR image of the human neck, (b) primary organs after the segmentation.

3 Numerical results

3.1 Validation of the developed numerical scheme

Before a discussion on the results of photon migration in the human neck model, the developed numerical scheme is validated for the case of a homogeneous 2D square medium with a side of 4.0 cm by comparison with analytical solutions for infinite media. When the source is located inside the medium far from the boundary, the numerical solutions of the intensities at the positions far from the boundary are less influenced by the boundary. Then, the comparisons of the numerical solutions for finite media with the analytical solutions for infinite media are reasonable. In this subsection, an isotropic impulse point source is incident at $(x, y) = (1.5\text{ cm}, 2.0\text{ cm})$, and the intensities at (2.5 cm, 2.0 cm) are calculated.

At first, the case of isotropic scattering ($g = 0.0$) is examined because the exact analytical solution of the RTE has been given by Paasschens [25] as follows,

$$\Phi_{ER}(\rho,t) = v\frac{\delta(vt-\rho)}{2\pi\rho}e^{-\mu_t vt} + \frac{v\mu_s}{2\pi}\frac{\exp(\mu_s\sqrt{(vt)^2-\rho^2})}{\sqrt{(vt)^2-\rho^2}}e^{-\mu_t vt}\Theta(vt-\rho), \tag{8}$$

where Φ is the fluence rate defined as $\int_{2\pi} d\boldsymbol{\Omega} I$, Θ is the Heaviside step function, $\mu_t = \mu_a + \mu_s$, and ρ is the distance from the source. Also, the analytical solution of the DE [26], Φ_{DE}, is given as,

$$\Phi_{DE}(\rho,t) = \frac{1}{4\pi Dt}e^{-\mu_a vt}e^{-\frac{\rho^2}{4Dvt}}, \tag{9}$$

where the diffusion coefficient D is given as $[2(1-g)\mu_s]^{-1}$ for the 2D time-dependent case [27,28]. The absorption and scattering coefficients are given as the same as those of either (a) the background: $\mu_a = 0.30\text{ cm}^{-1}$ and $\mu_s = 80.0\text{ cm}^{-1}$, or (b) the artery: $\mu_a = 4.76\text{ cm}^{-1}$ and $\mu_s' = 67.5\text{ cm}^{-1}$ as listed in Table 1. The former and latter cases correspond to weakly and strongly absorbing media, respectively. The step sizes are given as (a) $\Delta x = \Delta y = 0.02$ cm, $\Delta\theta = 0.13$ rad, and $\Delta t = 0.3$ ps, and (b) $\Delta x = \Delta y = 0.005$ cm, $\Delta\theta = 0.13$ rad, and $\Delta t = 0.07$ ps, respectively.

Figure 2 shows the time-resolved profiles of Φ calculated numerically and analytically at $\rho = 1.0$ cm. As shown in Fig. 2 (a), the numerical solution of the RTE based on the 3UW+4RK agrees very well with the analytical solutions in the case of the weakly absorbing medium. Meanwhile, the numerical solution based on the 1UW+FE deviates from the analytical solutions. This result indicates that in the case of the 1st order scheme, the current values of Δx and Δt are inappropriate, and smaller values of

them are necessary to obtain good agreement with the analytical solutions. Note that Φ_{DE} is in good agreement with Φ_{ER} and the numerical solution based on the higher order scheme. This is because ρ is sufficiently long for the DE to hold.

The results of the case of the strongly absorbing medium are shown in Fig. 2 (b), where Φ has sharp peaks at earlier times than in Fig. 2 (a) due to stronger absorption. Similarly to the case of the weakly absorbing medium (Fig. 2 (a)), the numerical solution based on the 3UW+4RK agrees very well with Φ_{ER}, meanwhile the solution based on the 1UW+FE deviates from Φ_{ER}. It is seen that the curve of Φ_{DE} has a similar shape to that of Φ_{ER} even for the strongly absorbing medium, although the peak time and width of the curve of Φ_{DE} are slightly different from those of Φ_{ER}.

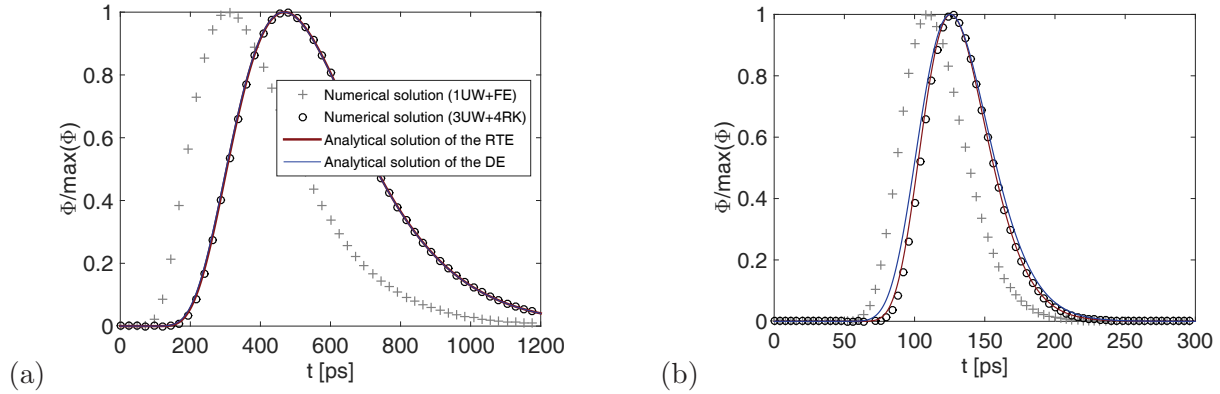

Fig. 2 Normalized time-resolved profiles of Φ for the RTE and the DE in the case of the isotropic scattering ($g = 0.0$) at $\rho = 1.0$ cm: pluses and circles represent the numerical solution based on the 1UW+FE, and the 3UW+4RK, respectively, and red and blue solid curves the analytical solutions, Φ_{ER} and Φ_{DE}, respectively. The optical properties are given as (a) $\mu_a = 0.30\,\mathrm{cm}^{-1}$, $\mu_s = 80.0\,\mathrm{cm}^{-1}$, and $g = 0.0$ and (b) $\mu_a = 4.76\,\mathrm{cm}^{-1}$, $\mu_s = 67.5\,\mathrm{cm}^{-1}$, and $g = 0.0$.

In the case of anisotropic scattering media ($g \neq 0$), a derivation of exact analytical solutions of the RTE is still a difficult problem even in infinite homogeneous media. In this study, an approximate RTE solution, Φ_{AR}, proposed by Martelli [29] is used to be compared with the numerical solutions. The basic assumption for Φ_{AR} is that μ_s and μ_t in Eq. (8) can be replaced by $\mu_s' = \mu_s(1-g)$ and $\mu_t' = \mu_s' + \mu_a$, respectively. Again, two sets of the optical properties of the medium are considered: (a) $\mu_a = 0.30$ cm^{-1}, $\mu_s = 80.0$ cm^{-1}, and $g = 0.9$ of the background, and (b) $\mu_a = 4.76$ cm^{-1}, $\mu_s = 675$ cm^{-1}, and $g = 0.9$ of the artery. Other conditions are the same as those in the case with the isotropic scattering media. As shown in Fig. 3 (a) in the case of the weak absorption, the numerical solution of the RTE based on the 3UW+4RK agree well with Φ_{AR}. However, in details, a small difference between them is seen during the period from about 100 ps to 400 ps. Even if the step sizes are finer, the numerical solution is found to be unchanged. Thus, this small difference could be the error in Φ_{AR} due to the approximation. In Fig. 3 (a), the deviations of the numerical solution based on the 1UW+FE are small compared with that in the case of isotropic scattering. Because the appropriate value of Δx is inversely proportional to μ_s', it is much larger in the anisotropic scattering case with $\mu_s' = 8.0\,\mathrm{cm}^{-1}$ than in the isotropic scattering case with $\mu_s' = 80\,\mathrm{cm}^{-1}$. This is the reason why the 1UW+FE performs better in the anisotropic scattering case.

Figure 3 (a) shows that Φ_{DE} is in agreement with the approximate RTE solution at the peak time ($t \sim$100 ps) and the decay period ($t > 100$ ps). At early arriving time ($t < 100$ ps), meanwhile, Φ_{DE} deviates from the approximate RTE solution. This deviation comes from the difference in the speed of light between the RTE and the DE. In the RTE, the speed of light is given as v, while in the DE it is infinite [22].

The strongly absorbing and anisotropic scattering case is shown in Fig. 3 (b). The curves of Φ in the case of anisotropic scattering are the same as those in the case of isotropic scattering (Fig. 2 (b)). This is maybe because the curves are mostly determined by μ_s', and the values of μ_s' are the same for the two cases.

From the results shown in Figs. 2 and 3, the developed schemes is validated.

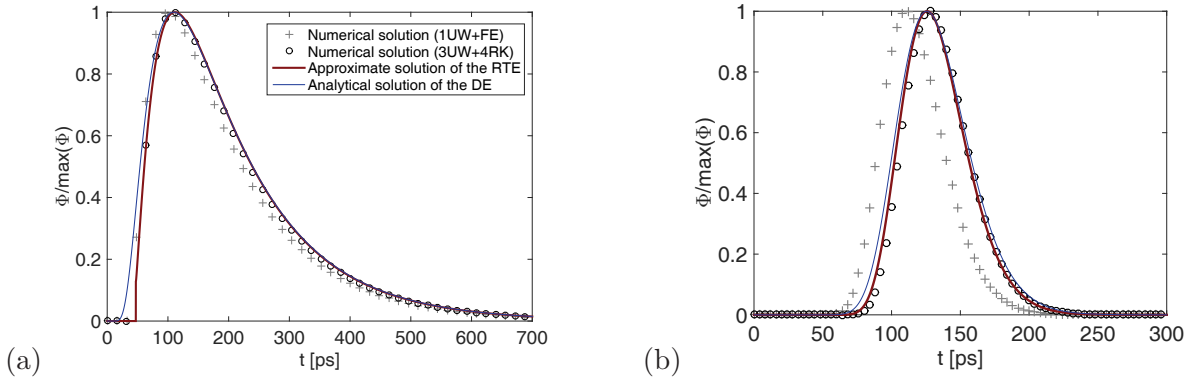

Fig. 3 Anisotropic scattering case ($g = 0.9$) of Φ at $\rho = 1.0$ cm: a red solid curve represents the approximate solution of the RTE, Φ_{AR}. (a) $\mu_a = 0.30\,\mathrm{cm}^{-1}$, $\mu_s = 80.0\,\mathrm{cm}^{-1}$, and $g = 0.9$ and (b) $\mu_a = 4.76\,\mathrm{cm}^{-1}$, $\mu_s = 675\,\mathrm{cm}^{-1}$, and $g = 0.9$. Other details are the same as in Fig. 2.

3.2 Photon migration in the human neck model

The developed numerical scheme of the 3UW+4RK is used to describe photon migration in the human neck model shown in Fig. 1 (b). Figure 4 shows the snapshots of Φ-distributions at fixed times in the human neck model, where light is incident on the front surface of the human neck at the position of $(x, y) = (3.5\text{ cm}, 6.3\text{ cm})$.

As listed in Table 1, the trachea is a void region indicated by a white solid curve in each figure of Fig. 4. Therefore, at the early time of 46.2 ps shown in Fig. 4 (a), photons propagate without being scattered or absorbed inside the trachea. At the time of 79.9 ps shown in Fig. 4 (b), the photons reach the trachea boundary far from the source position, and migrate diffusively in the background tissue where they are scattered in all directions, and some portion of the scattered photons return back to the trachea as the diffusive reflection. Then, the reflected photons travel back to the trachea boundary near the source position as shown in Fig. 4 (c), repeat diffusive reflections back and forth inside the trachea, and gradually migrate into the tissue outside the trachea as diffusive propagation as shown in Fig. 4 (d) to (f). It looks as if the void region of the trachea acts as a light source.

Note that the magnitudes of Φ indicated by the color bars rapidly decay as time goes and photons migrate into the tissue. Also note that photons are absorbed especially by veins and arteries having large μ_a which appear as dark blue spots in all of Fig. 4 (a) to (f). Thus, few photons reach the backside of the human neck. In fact, it is confirmed that at the backside position, $(x, y) = (3.5\text{ cm}, 0.0\text{ cm})$, the magnitude of Φ is kept at less than 10^{-10} during the time period from 0 ps to 800 ps.

These results suggest that near the light source, the accurate scheme for solving the RTE is necessary, while far from the light source, the approximate and efficient scheme is good enough to describe photon migration in the human neck model.

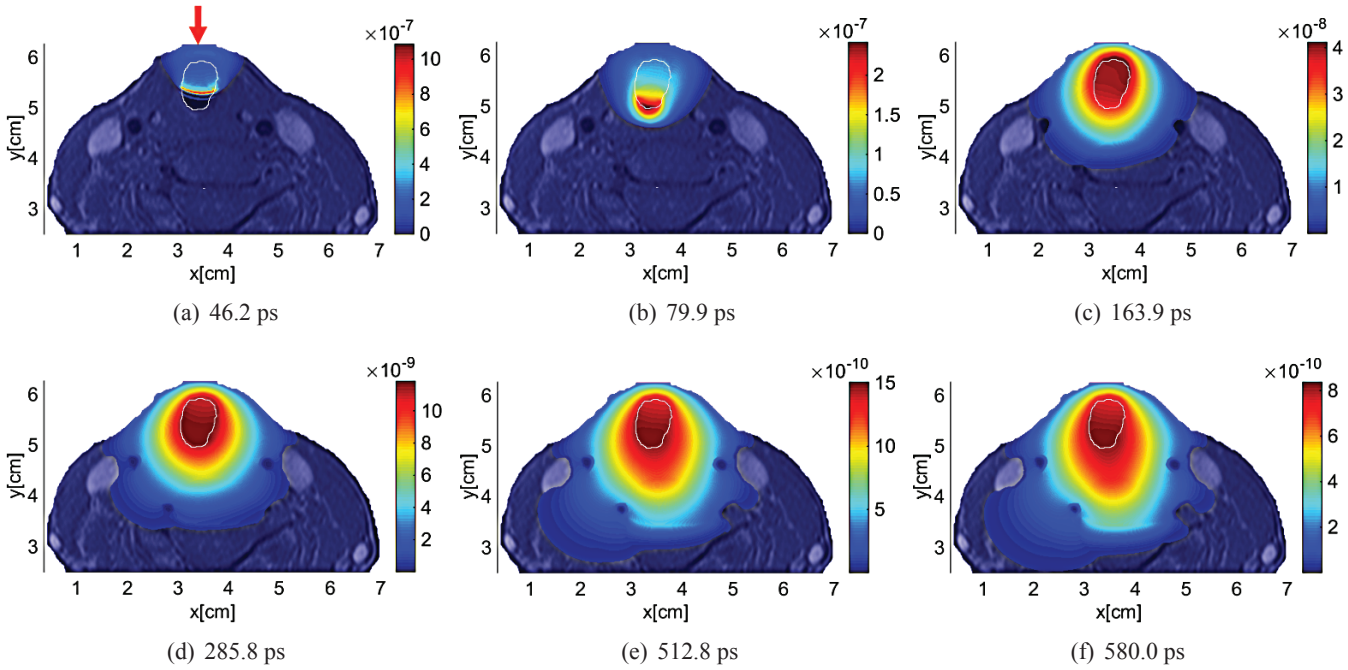

(a) 46.2 ps (b) 79.9 ps (c) 163.9 ps

(d) 285.8 ps (e) 512.8 ps (f) 580.0 ps

Fig. 4 Spatial distributions of Φ calculated from the RTE in the human neck model (Fig. 1 (b)) at fixed times. Unit of the color bar is [W/cm]. The light source is represented by a red arrow in (a), and the boundary of the trachea is denoted by a white solid curve in each figure.

4 Conclusions

To describe photon migration in the human neck, we have developed the accurate and efficient numerical scheme to solve the RTE based on the 3rd order upwind and 4th order Runge-Kutta methods for the purpose of comprehensive diagnose of thyroid cancer by optical imaging. We have confirmed the validity of the developed scheme by comparison with the analytical solutions in homogeneous media. Numerical simulations of photon migration in the human neck model have shown a complicated pattern of photon migration, arising from multiple diffusive reflection near the trachea.

Acknowledgments

This work is supported in part by Grants-in-Aid for Regional R&D Proposal-Based Program from Northern Advancement Center for Science & Technology of Hokkaido Japan, and the Japan Science and Technology Agency. We would like to express appreciation to Dr. Kazumichi Kobayashi for fruitful discussions.

References

[1] Wartofsky, L., (2010), Increasing world incidence of thyroid cancer : Increased detection or higher radiation exposure ?. *HORMONES,* **9**, 103–108.
[2] Levi, J., Kothapalli, S.-R., Bohndiek, S., Yoon, J.-K., Dragulescu-Andrasi, A., Nielsen, C., Aleksandra, T., Bodapati, S., Gowrishankar, G., Yan, X., Chan, C., Starcevic, D., and Gambhir, Sam, S., (2013), Molecular Photoacoustic Imaging of Follicular Thyroid Carcinoma. *Clin. Cancer Res.,* **19**, 1494–1502.
[3] Yamada, Y., and Okawa, S., (2014), Diffuse Optical Tomography : Present Status and Its Future. *Opt. Rev.,*

21, 185–205.
[4] Gibson, A. P., Hebden, J. C., and Arridge, S. R., (2005), Recent advances in diffuse optical imaging. *Phys. Med. Biol.,* **50**, R1–R43.
[5] Arridge, S. R., (1999), Optical tomography in medical imaging. *Inverse Prob.,* **15**, R41-R93.
[6] Klose, A. D., Netz, U., Beuthan, J., and Hielscher, A. H., (2002), Optical tomography using the time-independent equation of radiative transfer - Part 1 : forward model. *J. Quant. Spectrosc. Radiat. Transfer,* **72**, 691–713.
[7] Klose, A. D., Ntziachristos, V., and Hielscher, A. H., (2005), The inverse source problem based on the radiative transfer equation in optical molecular imaging. *J. Comput. Phys.,* **202**, 323–345.
[8] Abdoulaev, G. S., and Hielscher, A. H., (2003), Three-dimensional optical tomography with the equation of radiative transfer. *J. Electron. Imaging.,* **12**, 594–601.
[9] Marin, M., Asllanaj, F., and Maillet, D., (2014), Sensitivity analysis to optical properties of biological tissues subjected to a short-pulsed laser using the time-dependent radiative transfer equation. *J. Quant. Spectrosc. Radiat. Transfer,* **133**, 117–127.
[10] Schweiger, M., Arridge, S. R., and Delpy, D. T., (1993), Application of the Finite-Element Method for the Forward and Inverse Models in Optical Tomography, *J. Math. Imag. Vision,* **3**, 263–283.
[11] Gao, F., Zhao, H., and Yamada, Y., (2002), Improvement of Image Quality in Diffuse Optical Tomography by use of Full Time-Resolved Data. *Appl. Opt.,* **41**, 778–791.
[12] Okawa, S., Hoshi, Y., and Yamada, Y., (2011), Improvement of image quality of time-domain diffuse optical tomography with lp sparsity regularization. *Biomed. Opt. Express,* **2**, 3334–3348.
[13] Yoo, K. M., Liu, F., and Alfano, R. R., (1990), When does the diffusion approximation fail to describe photon transport in random media?. *Phys. Rev. Lett.,* **64**, 2647–2650.
[14] Hielscher, A. H., Alcouffe, R. E., and Barbour, R. L., (1998), Comparison of finite-difference transport and diffusion calculations for photon migration in homogeneous and heterogeneous tissues. *Phys. Med. Biol.,* **43**, 1285–1302.
[15] Yuan, Z., Hu, X.-H., and Jiang, H., (2009), A higher order diffusion model for three-dimensional photon migration and image reconstruction in optical tomography. *Phys. Med. Biol.,* **54**, 65–88.
[16] Chandrasekhar, S., (1960), *Radiative Transfer.* Dover, New York.
[17] Henyey, L. G., and Greenstein, L. J., (1941), Diffuse radiation in the galaxy. *J. Astrophys.,* **93**, 70–83.
[18] Heino, J., Arridge, S., Sikora, J., and Somersalo, E., (2003), Anisotropic effects in highly scattering media. *Phys. Rev. E,* **68**, 031908 1–8.
[19] Fujii, H., Okawa, S., Yamada, Y., and Hoshi, Y., (2014), Hybrid model of light propagation in random media based on the time-dependent radiative transfer and diffusion equations. *J. Quant. Spectrosc. Radiat. Transfer,* **147**, 145–154.
[20] Klose, A. D., and Hielscher, A. H., (1999), Iterative reconstruction scheme for optical tomography based on the equation of radiative transfer. *Med. Phys.,* **26**, 1698–1707.
[21] Liu, L., Ruan, L., and Tan, H., (2002), On the discrete ordinates method for radiative heat transfer in anisotropically scattering media. *Int. J. Heat Mass Transfer,* **45**, 3259–3262.
[22] Guo, Z., and Kumar, S., (2001), Discrete-ordinates solution of short-pulsed laser transport in two-dimensional turbid media. *Appl. Opt.,* **40**, 3156–3163.
[23] Bashkatov, A. N., Genina, E. A., and Tuchin, V. V., (2011), OPTICAL PROPERTIES OF SKIN , SUBCUTANEOUS , AND MUSCLE TISSUES : A REVIEW. *J. Innovative Opt. Heanlth Sci.,* **4**, 9–38.
[24] Dehaes, M., Gagnon, L., Vignaud, A., Valabr, R., Grebe, R., Wallois, F., and Benali, H., (2011), Quantitative investigation of the effect of the extra-cerebral vasculature in diffuse optical imaging : a simulation study. *Biomed. Opt. Express,* **2**, 680–695.
[25] Paasschens, J. C. J., (1997), Solution of the time-dependent Boltzmann equation. *Phys. Rev. E,* **56**, 1135–1141.
[26] Chandrasekhar, S., (1943), Stochastic Problems in Physics and Astronomy. *Rev. Mod. Phys.,* **15**, 1–88.
[27] Furutsu, K., and Yamada, Y., (1994), Diffusion approximation for a dissipative random medium and the applications. *Phys. Rev. E,* **50**, 3634–3640.
[28] Pierrat, R., Greffet, J.-j., and Carminati, R., (2006), Photon diffusion coefficient in scattering and absorbing media. *J. Opt. Soc. Am. A,* **23**, 1106–1110.
[29] Martelli, F., Sassaroli, A., Pifferi, A., Torricelli, A., Spinelli, L., and Zaccanti, G., (2007), Heuristic Green's function of the time dependent radiative transfer equation for a semi-infinite medium. *Opt. Express,* **15**, 18168–18175.

2016 ORDER FORM

This subscription is ◯ New ◯ A renewal

Please choose one subscription	Price (US$)	Required	Shipping price (US$)
USA	◯ $300.00	Ground Shipping-USA	◯ Free
Canada	◯ $300.00	Ground Shipping- Canada	◯ $30.00
Mexico	◯ $300.00	Ground Shipping- Mexico	◯ $30.00
All Other Countries	◯ $300.00	Airmail -not available for USA and Canada	◯ $60.00

For e-copy subscription, no shipping fee is required.

Title Selection

No	TITLE	ISSN	QTY	PRICE(US$)
1				
2				
3				
4				

Methods Of Payment

Please Make Check/Bank Draft Payable to: L&H Scientific Publishing

Methods of Payment ◯Check/Bank Draft Enclosed _____ US$ ◯Master Card ◯Visa

Card No ☐☐☐☐ ☐☐☐☐ ☐☐☐☐ ☐☐☐☐ Exp. Date ☐☐☐☐

Contact Information

Organization:

Name:

Street Address:

(sorry, we cannot deliver to P.O. Box)

City/State/Zip

Country:

Email:

Phone/ Fax:

Date **X**	Signature **X**

L&H Scientific Publishing P.O. Box 99 Glen Carbon IL 62034 USA

Please complete the order form with payment to

L&H Scientific Publishing
P.O. Box 99
Glen Carbon, IL 62034, USA
Tel: 1-618-402-2267
Fax:1-618-545-9338
Email: lhscientificpublishing@gmail.com

Aims and Scope

The interdisciplinary journal publishes original and new research results on applied nonlinear dynamics in science and engineering. The aim of the journal is to stimulate more research interest and attention for nonlinear dynamics and application. The manuscripts in complicated dynamical systems with nonlinearity and chaos are solicited, which includes mathematical theories and methods, physical principles and laws, and computational techniques. The journal provides a place to researchers for the rapid exchange of ideas and techniques in nonlinear dynamics and engineering nonlinearity. Topics of interest include but not limited to

- Complex dynamics in engineering
- Nonlinear vibration and control
- Nonlinear dynamical systems and control
- Fractional dynamics and control
- Dynamical systems in chemical and bio-systems
- Economic dynamics and predictions
- Dynamical systems synchronization
- Bio-mechanical systems
- Nonlinear structural dynamics
- Nonlinear multi-body dynamics
- Multiscale wave propagation in materials
- Nonlinear rotor dynamics

No length limitations for contributions are set, but only concisely written manuscripts are published. Brief papers are published on the basis of Technical Notes. Discussions of previous published papers are welcome.

Peer Review

Journal of Applied Nonlinear Dynamics adopts the traditional blind-review policy in which the reviewers' names are concealed for submission author(s) for free submission. Each submitted manuscript is reviewed at least two referees in appropriate fields. In addition, the editorial board members' recommendation or established experts' recommendation publication are welcome.

Manuscript Submission Guidelines

For manuscript submission, authors can directly contact Editors-in-Chief. Manuscript preparation can follow the sample papers and journal manuscript templates (word file and Latex files), which can be found from the website at https://lhscientificpublishing.com/Journals/JAND-Default.aspx

Proofs and Electronic Offprints

Authors will receive a PDF proof of their articles and, on publication, electronic offprints of the article.

Open Access

After manuscripts were accepted, author(s) have a right to request the accepted manuscripts published by L&H Scientific publishing with open access, and the author(s) have a responsibility to paying the open access publication fee with US$30 per page. The copyright is still held by the Publisher. Without any request of the open access publication, the accepted manuscripts are assumed to be published traditionally.

Continued from inside front cover

Journal of Applied Nonlinear Dynamics

Volume 5, Issue 1 March 2016

Contents

Available online at https://lhscientificpublishing.com/Journals/JAND-Download.aspx

L&H

Printed in USA